COMPOSITE BEAMS WITH WEB OPENINGS

by

William C. Clawson

David Darwin

A Report on Research Sponsored by

THE NATIONAL SCIENCE FOUNDATION

Research Grant ENG 76-19045

UNIVERSITY OF KANSAS

LAWRENCE, KANSAS

October 1980

ABSTRACT

COMPOSITE BEAMS WITH WEB OPENINGS

The purpose of this investigation was to study the behavior and develop an ultimate strength model for composite beams with rectangular web openings.

Six composite beams with concentric rectangular web openings were tested to failure. Varying moment to shear ratios were used to help develop and verify the ultimate strength model. One steel beam was tested to demonstrate the contribution of the concrete to the capacity of composite beams. Two steel sections were used, while the concrete slab size was held constant for all beams. Three elastic tests were performed on each beam before it was tested to failure.

An ultimate strength model was developed to predict the strength of composite beams at the web openings in the form of moment-shear interaction diagrams. The steel is modeled as an elastic-perfectly plastic material. The yield stress of the steel is defined as a function of the assigned shear stress according to the von Mises yield criterion. The concrete is modeled for ultimate strength behavior. Concrete compressive strength is also defined as a function of the assigned shear stress, based on experimental results. Strain compatibility between the concrete and steel is assumed. The model is compared with experimental results and is used to study the effect of key parameters (material properties, opening size, and opening eccentricity) affecting the strength of composite beams with web openings. A simplified design interaction procedure is presented to conservatively guide the placement of web openings in composite beams.

Based on the experimental study, it is clear that web openings

can greatly reduce the strength of composite beams. It appears that the secondary bending has a sizable effect on beam behavior. The concrete in composite beams contributes, not only, to the flexural strength, but, also, to the shear capacity of the beams at web openings. The ultimate strength of composite beams at web openings is governed by the failure of the concrete.

The ultimate strength model satisfactorily predicts the strength of the experimental beams.

ACKNOWLEDGEMENTS

This report is based on a thesis presented by William C. Clawson in partial fulfillment of the requirements for the Ph.D. degree. The research was supported by the National Science Foundation under NSF Grant No. ENG 76-19045 through a sub-contract from Kansas State University.

Additional support was provided by University of Kansas General Research Allocation #3128-XO-0038.

Numerical calculations were preformed on the Honeywell 66/60 computer system of the Academic Computer Center of the University of Kansas.

TABLE OF CONTENTS

TABLE OF CONTENTS (continued)

LIST OF TABLES

LIST OF FIGURES

LIST OF FIGURES (continued)

LIST OF FIGURES (continued)

LIST OF FIGURES (continued)

LIST OF FIGURES (continued)

CHAPTER 1

INTRODUCTION

1.1 General

Composite construction has become an important method of building for both bridges and commercial structures. Composite construction is a technique in which a rolled steel member (usually a wide-flange beam) is mechanically connected to a concrete slab by shear studs. The shear studs are designed to transmit the horizontal shear force between the steel and the concrete slab. The two materials act as a homogeneous unit when subjected to loading.

The use of composite construction has increased, because it allows more efficient use of construction materials. Savings in steel costs of 20 to 30% can be achieved. Additional benefits of this construction method are reduction in the depth of flexural members, increased stiffness of floor systems, and increased overload capacity (20).

The demand for more economical and efficient structures has led designers to reduce or eliminate the space below beams and girders in buildings provided for utility passage. The use of web openings (holes in the vertical portion of the steel section) will allow the passage of utilities through beams, thereby eliminating the need for space beneath them. The total height of a building can be reduced, resulting in a substantial reduction in material costs.

Numerous analytical and experimental investigations have been undertaken to study web openings in steel beams. However, only a limited effort has been made to analyze web openings in composite beams. The large differences in material properties of steel and concrete suggest

that analytical and experimental investigations of composite beams with web openings are necessary to fully understand their behavior.

1.2 Previous Work

Since the early 1960's, many investigators have studied web openings in steel beams (Fig. 1.1). Segner (26) tested a series of I-beams with reinforced rectangular web openings to determine the applicability of the Vierendeel truss analogy to members having web openings located on the neutral axis of the beam. Opening depths ranged from 0.4 to 0.7 of the total beam depths. This analysis includes the assumption that points of contraflexure occur both above and below the opening at the opening centerline (Fig. 1.2). Segner found that the Vierendeel method underestimates the stresses in the vicinity of the opening. The secondary moments due to the shear transfer through the opening are critical for large openings.

Bower (7, 9) presents an analytical method, based on the theory of elasticity, to determine the elastic stress distribution around rectangular and elliptical openings. The analysis accurately predicts bending and tangential stresses. His results show that the Vierendeel method predicts the bending stresses with reasonable accuracy, for rectangular openings not exceeding half of the beam depth, but neglects stress concentrations near the edges of the openings. Bower indicates, however, that the assumption that points of contraflexure occur at the opening centerline in the Vierendeel analysis does not provide accurate results in all cases.

Redwood and McCutcheon (22) note that the presence of shear forces at an opening reduce the plastic moment capacity of steel beams.

Under pure bending, the presence of an opening reduces the plastic moment capacity to the predicted plastic moment capacity based on the net section. A lower-bound strength solution presented by Bower (8) neglects local bending caused by the Vierendeel action. This method predicts higher ultimate loads than actual experimental loads for steel beams with web openings.

Congdon and Redwood (13) present an ultimate strength analysis for beams with concentric rectanglar reinforced openings. The shear force is assumed to be carried, uniformly, by the web, and the yield stress of the web is reduced using the von Mises yield criterion. This analysis is conservative in predicting the ultimate strength of beams with rectangular web openings. Moment-shear interaction curves are presented to represent the failure of a beam with varying combinations of moment and shear (Fig. 1.3).

Design guides have been developed (10, 23, 28) to aid designers in the placement of web openings in steel beams. The guides may be used for the design of concentric and eccentric, rectangular and circular, and reinforced and unreinforced openings using both working stress and plastic design methods.

Later investigations (12, 14, 18, 31) present more general methods of analysis, primarily for eccentric circular openings and eccentric reinforced rectangular openings. Wang, Snell, and Cooper (31) propose an ultimate strength method for rectangular openings, which assumes a four-hinge failure mechanism (Fig. 1.4). The points of contraflexure are not fixed at the opening centerline. Experimental and finite element results (14) indicate reasonable agreement with this theory. Redwood, et al (24, 25) have studied the effects of web slenderness in

steel beams with web openings. They conclude that both web slenderness and opening length are critical factors for web stability.

For most ultimate strength analyses, the shear force is assumed to be carried by the web of the steel section. Shrivastava and Redwood (27) present a method that allows part of the shear force to be carried by the flanges. This tends to expand the moment-shear interaction curve outward, as the theoretical shear strength of the members is increased.

The large amount of research conducted on steel beams with web openings has helped to identify the critical factors involved and has enabled designers to place web openings in steel beams with suitable factors of safety. However, this research is only indirectly applicable to composite beams. Composite beams are composed of both steel and concrete. The properties of steel and concrete are vastly different. Concrete is a highly non-linear material with reasonably good compressive strength, but very low tensile strength. Steel, on the other hand, is a linear elastic material, when stressed below its proportional limit, and exhibits high tensile and compressive strength.

In the United States, composite beams are usually designed in accordance with the AISC specifications for composite construction (5). The shear force is assumed to be carried solely by the web of the steel beam, and the concrete is assumed to contribute only to the flexural strength.

Granade (16) tested 2 composite beams with rectangular web openings and attempted to predict the experimental stresses using the Vierendeel method. In his analysis, the points of contraflexure were assumed to be located above and below at the centerline of the opening.

The Vierendeel estimates of the experimental stresses were found to be inaccurate.

Todd and Cooper (30) present an ultimate strength method for composite beams with web openings and assume that the shear force is carried only by the steel web. Based on the experimental results obtained by Granade, the model greatly underestimates the shear strength of composite beams (Fig. 1.5). Todd and Cooper indicate that beam strength will decrease with increasing opening size and that the effect of both positive or negative opening eccentricities is to increase the strength of the sections under high shear. Under high moment, positive eccentricities (raised openings) increase the beam capacity, while negative eccentricities decrease the capacity.

Swartz and Eluifoo (29) present a method for determining the neutral axis of the section in composite beams with web openings using the Vierendeel method and considering the cracked section. This method compares reasonably well with finite element solutions.

1.3 Object and Scope

The purpose of this investigation is to study the behavior and develop an ultimate strength model for composite beams with rectangular web openings.

Six composite beams were tested to failure. Varying moment to shear ratios were used to help develop and verify the ultimate strength model. One steel beam was also tested. Two different steel sections were used, while the concrete slab size was held constant for all beams. The beams were designed in accordance with the AISC specifications for composite construction (5) using standard wide-flange

sections. The concrete slabs were reinforced according to ACI recommendations (4). Three elastic tests were performed on each beam before it was tested to failure.

The ultimate strength model includes the contribution of the concrete to shear strength. The model is compared to experimental test results and is used to study the effects of key parameters that control the strength of composite beams with web openings. Design procedures are proposed for the sizing and placement of web openings in composite beams.

CHAPTER 2

EXPERIMENTAL INVESTIGATION

2.1 General

The purpose of the experimental work is to study the behavior of composite beams with web openings and to aid in the development and verification of the proposed failure model.

The goal of the experimental investigation is to develop reasonably complete moment-shear interaction curves for particular beam sizes and opening configurations. To achieve this goal, it is necessary to test beams with openings located at points with differing moment-shear ratios. Of the six beams tested, two steel sections were used. This not only enables comparisons to be made with the proposed failure model, but provides information on the effect of beam geometry. Four of the tests used one size cross-section (although one beam was slightly different from the others due to changes in the AISC beam shapes). The other two beams used a smaller cross-section.

In addition to the composite beam tests, one steel beam was tested. The steel beam utilized the same steel section and had the same moment-shear ratio at the opening as one of the composite beams. The two tests provided a good illustration of the effect of the concrete slab on the shear strength at the opening.

Concentric rectangular openings were used in all tests. Opening sizes were fixed with depth equal to 60% of the steel beam depth and lengths equal to twice the opening depth. The concrete slab dimensions were identical in all six beams.

2.2 Beam Design

The six composite beams were designed following the AISC Design Specifications (5) and the ACI Building Code (4), with certain limitations. The AISC Design Specifications (5) are based on elastic design methods, in which the concrete slab is transformed to an equivalent area of steel. Allowable stresses are given for the concrete and steel. The AASHTO Specifications for Highway Bridges (1) and foreign codes (11) are based on ultimate strength. Since the beams were to be loaded to failure, ultimate strength design methods were used. The shear stud design method recommended by the AISC specifications was utilized, since it is based on ultimate strength criteria.

In designing beams with web openings to be used in an experimental study, it is important to size the beams so that they will fail at the web opening. A long span in a high shear test can result in flexural failure at an interior high moment location, while the area around the opening is relatively unaffected. Unnecessarily long spans are not economical. The spans of the six test beams were selected with these points in mind. The opening locations, load configurations, and span lengths for all beams are shown in Figs. 2.1 to 2.3.

In composite beams, the effective width of the concrete slab is based on several requirements specified by the AISC Design Specifications. For full, symmetrical slabs, the effective width, b_{eff}, of the concrete flange must be less than

$$(1) \quad L/4 \tag{2.1a}$$

$$(2) \quad 16t_s + b_f \tag{2.1b}$$

in which L = span of the beam, t_s = depth of the concrete slab, and b_f = width of the compression steel flange.

For these tests, the conditions were met with a slab width of 48" and a thickness of 4", except for the 2 beams with 15' spans in which the slabs were 3" wider than b_{eff}.

In composite beams, it is desirable to size the slab to be "adequate". This requires that the steel yield in tension prior to failure of the concrete at ultimate strength. Therefore, the neutral axis must lie somewhere in the concrete. Failure of the beam is preceeded by large deformations, as the steel yields. At the ultimate load, the Whitney stress block (32) with a concrete stress equal to 0.85 f'_c is used for the concrete. The concrete tensile strength is disregarded. The steel stress is limited to the yield stress, F_y. No strain hardening is assumed.

For the neutral axis to lie in the slab at collapse, the axial capacity of the slab, C'_c, must exceed the axial capacity of the steel, T'.

$$C'_c > T' \tag{2.2a}$$

$$C'_c = 0.85\, f'_c\, A_c \tag{2.2b}$$

$$T' = F_y\, A_s \tag{2.2c}$$

in which f'_c = concrete compressive strength, A_c = area of slab, and A_s = area of steel beam.

These conditions were met in all experimental beams.

The steel beams were chosen based on their availability as well as the desire to work with realistic cross-sections. The steel beams were hot-rolled A36 structural steel wide-flange sections. The concrete was normal-weight, Portland cement concrete using 3/4" maximum size aggregate. Minimum concrete design strength was 3500 psi. The concrete reinforcing steel was standard Grade 40 deformed reinforcing steel. Standard headed concrete shear studs were used.

Shear studs in composite beams are designed to carry the entire horizontal shear force at the steel-concrete interface. The horizontal shear is assumed to be acting between the maximum and the zero moment locations. Using AISC procedures (5), the horizontal shear is assumed to be the smaller of the following values.

$$(1) \quad V_h = \frac{0.85\ f'_c\ A_c}{2} \tag{2.3a}$$

$$(2) \quad V_h = \frac{A_s\ F_y}{2} \tag{2.3b}$$

For an allowable horizontal shear load per stud, q, the number of studs required on each side of the point of maximum moment, assuming double rows, is

$$N = \frac{V_h}{2q} \tag{2.4}$$

Shear connectors or shear studs must have at least 1" of concrete cover, and the diameter of the stud must not be greater than 2.5 times the thickness of the flange to which it is welded. The 3/4 inch diameter, 3 inch headed stud was chosen, since it was the largest stud

which conformed to these requirements. For f'_c = 3500 psi, q = 12.5 kips (5). Shear stud loctions and spacings are shown in Fig. 2.4.

Pairs of bearing stiffeners were provided at points of concentrated load (supports and load points). The stiffeners were hot-rolled flat bars and were designed in accordance with the AISC Design Specifications (5). The stiffeners were continuously welded to the web, with close contact against the flanges on the top and bottom.

Bearing plates were provided for the steel beam at the supports and the concrete at the load points. All bearing plates were cold-rolled, high-strength steel. The bearing surfaces were designed according to the AISC Specifications and were sized very conservatively.

The concrete slabs were designed based on ultimate strength criteria and effective width requirements and were reinforced following the ACI Building Code (4). In the longitudinal direction, minimum temperature and shrinkage reinforcement was provided using No. 3 bars at 14" spacing (4 bars). In the transverse direction, an increased reinforcing ratio was used to reduce the possibility of longitudinal splitting (15), with No. 4 bars placed at 6". The longitudinal reinforcing was placed at the mid-depth of the 4" concrete slab. Reinforcing steel placement is shown in Fig. 2.5.

2.3 Materials

2.3.1 Concrete

The concrete was normal weight, Portland cement concrete using 3/4" maximum size aggregate (locally described as 1/2" rock). The concrete was ordered with a 3500 psi nominal compressive strength, 3" slump, and 6% entrained air. The cement factor of the mixes were varied

depending on the desired rate of concrete strength gain. If a rapid strength gain was desired, a cement factor of 5½-6 sacks per cubic yard was specified. Design strength was usually attained in 1 week. If a more moderate strength gain was desired, a cement factor of 5 sacks per cubic yard was used, in which case the design strength was attained in about 2 weeks.

Concrete properties were tested in accordance with ASTM procedures (6). Six standard 6" diameter cylinders, 3 standard 3" diameter cylinders, and 2 flexure beams were cast for each slab. The slab and the test specimens were cured in the same manner. The formwork was removed from the slab and the test specimens were stripped at the same time. The 3" cylinders were instrumented with paper-backed strain gages to obtain stress-strain data.

The 6" diameter cylinders were tested on the day of the ultimate strength test. The results were used to obtain the average compressive strength, f'_c. The flexural beams were tested to determine the modulus of rupture. The concrete properties are listed in Table 2.1.

2.3.2 Structural Steel

The steel sections were hot-rolled, A36 wide-flange beams. Tensile tests were run on coupons cut from the beams. Longitudinal coupons were cut from the top and bottom flanges and the web using a band saw. Vertical coupons were also taken from the web for some beams to determine the effect of rolling direction on the tensile properties. The coupons were machined to standard 12" ASTM tensile coupons using a horizontal milling machine.

Tensile tests were run on a screw-type testing machine. The cross-sectional dimensions were measured using dial-gage calipers

graduated in 0.001". The coupons were fitted with an extensometer to obtain load-deflection plots during the test. The tests were designed to measure the "static" yield strength of the material, so the specimens were loaded slowly. After the steel began to yield, the displacement was stopped. The load would drop and usually stabilize (at the static yield load) within 10 minutes. Loading was continued and stopped again to obtain a second static yield load. For most specimens, this was done 3 times to get an average static yield load. Careful control was required so that the steel did not begin to strain-harden before the static yield test was completed. The loading was continued until the coupons reached the ultimate tensile strength. The results of a typical test is illustrated in Fig. 2.6. Table 2.2 lists the steel properties for the 6 beams.

2.3.3 Reinforcing Steel

The concrete reinforcing steel was standard Grade 40 deformed reinforcing steel. The longitudinal and transverse reinforcement consisted of No. 3 bars and No. 4 bars, respectively. The reinforcing steel was tested for yield strength and tensile strength. An extensometer was fitted to a 18" length of reinforcing steel to monitor the deflection. The bars were loaded slowly and when yielding began, the yield load was recorded. Loading was continued until the tensile strength of the bar has been reached. Material strengths of the reinforcing are shown in Table 2.2.

2.4 Beam Fabrication

The steel beams were purchased locally from a structural steel fabrication company. An 18" section was cut from each beam to provide

coupons for determining the material properties of the steel. The shear studs were hand-welded to the top flange of the beam by the steel fabricator, and the beams were delivered to the University of Kansas Structural Testing Laboratory.

The beams were measured and marked for stiffener location. The stiffeners were flame-cut to size and welded to the web of the steel beam using 6011 3/16" welding rods. The stiffeners were clamped into position using C-clamps and continuously welded to the web using an AC-DC electric welder (Fig. 2.7). The stiffeners were not welded to the flanges, but were in close contact with them. Double stiffeners were used at all locations.

After stiffener welding was completed, the web opening was measured and marked in the desired location. At the corners of the opening, 3/4" diameter holes were drilled to reduce stress concentrations. The opening was flame-cut using an oxy-acetylene torch. Little cosmetic work was done on the edges of the opening. Grinding of the flame-cut surfaces was restricted to the strain gage locations.

Bearing plates were welded to the bottom flange using an electric welder (Fig. 2.8). Prior to welding, the bearing plates were clamped into place with C-clamps to insure uniform bearing on the bottom flange.

The beams were supported on 15" square concrete pedestals poured directly on the structural floor (Fig. 2.9). A pin and a roller were used to provide the simple supports. The pinned support consisted of a 5" diameter cold-rolled bar welded to a 1" thick, 12" square cold-rolled plate grouted to one pedestal. End plates were used to hold the bar in position on the plate. The roller support consisted of another

5" diameter bar resting on a 1" thick, 12" square plate grouted to the other concrete pedestal. Since the concrete formwork was fixed in height, the pedestal heights were varied as the beam depths were altered.

The concrete formwork was constructed using structural grade lumber and plyform. Rectangular frames with diagonal braces were placed transverse to the steel beam on 4' centers to support the 3/4" plyform. The frames were then braced together both transversely and longitudinally. This resulted in a very stiff formwork which could be moved as a unit on either side of the beam.

After the steel beam was placed on the supports and instrumented with strain gages, the formwork was moved into position with the top of the plyform in close contact and flush with the top flange of the steel beam. All joints in the formwork were chaulked, and the formwork was oiled. The reinforcing steel was flame-cut to length using an oxy-acetylene torch. The longitudinal reinforcing was placed on 1½" reinforcing chairs and tied to the formwork using soft wire. The transverse reinforcing steel was placed on the longitudinal reinforcing bars and wired to it. Splices in the longitudinal steel were designed in accordance with the ACI Building Code (4) and were not placed in the vicinity of the opening.

The concrete was obtained from a local ready-mix company and trucked to the laboratory for placement. Concrete was placed in the formwork using a 1 cubic yard bucket operated by an electric hoist. After the concrete was placed, it was vibrated using a high-frequency flexible tube vibrator. The slab was screeded and bull-floated. Standard concrete test cylinders (3" and 6" diameter) and flexure beams were

cast as the beam was poured. Slump and air tests were performed prior to the cylinder and beam casting.

After the concrete surface had begun to set, the slab was covered with a plastic sheet. The concrete test specimens were covered and placed under the beam. As the concrete cured, the slab and test cylinders were kept continuously moist by spraying with water several times each day. Concrete strength was monitored by testing the standard 6" diameter cylinders at regular intervals after the slab was cast. The formwork was removed and the concrete allowed to dry after the concrete had reached a compressive strength of 3500 psi.

The dimensions of the steel section and the opening were obtained before the concrete was placed. The concrete dimensions were obtained after the formwork was removed. The beam dimensions are listed in Table 2.3.

2.5 Instrumentation

Each of the six beams were instrumented with electrical resistance strain gages on the concrete and steel. The number and location of the gages varied. The later beams were instrumented more thoroughly to obtain more information.

The gages were placed around the opening. Gages were placed on the steel, both below (bottom tee) and above (top tee) the opening. Gages were, also, placed on the top and bottom surfaces of the slab. The gages were placed longitudinally on the beams (except for 1 transverse gage placed on the top of the concrete slab in 3 beams) and were recessed in from the edge of the opening to avoid regions of stress

CHAPTER 3

EXPERIMENTAL RESULTS

3.1 General

Three elastic tests and one ultimate strength test constituted the experimental investigation for each of the six beams. One elastic test was selected for each beam, as being representative of the other two elastic tests, for presentation and evaluation. The results from the six ultimate strength tests are also included. Load-strain and load-deflection diagrams are presented in Figs. 3.1 to 3.30 (see Figs. 2.10 to 2.15 for strain gage locations). Load slip diagrams are not presented for the elastic tests due to the negligible values recorded. The strain, deflection, and load data for the tests are tabulated in Appendix C. The behavior of the six beams is discussed in the following sections.

3.2 Test Results

The six composite beams were tested to provide information on the effect of a web opening on beam behavior. The moment-shear ratio was varied by changing the location of the opening and proved to be critical in determining the mode of failure of the beams. The moment-shear ratios varied from 3', for Beams No. 4 and 6, to 33', for Beam No. 3.

The Vierendeel action of beams with web openings can be described in terms of the relative vertical displacement of the ends of the opening, δ_r, due to the presence of secondary bending moments. For an accurate comparison, the values of δ_r are normalized with respect to the centerline deflection, δ_c, to take into account the varying stiffnesses of the sections ($\overline{\delta} = \delta_r/\delta_c$).

Secondary bending moments are produced by the transfer of shear force through the opening by the top and bottom tees. The lower the moment-shear ratio (more shear transferred through the opening at failure), the more pronounced is the Vierendeel effect. The test beams demonstrated this Vierendeel action. Beam No. 3, with a high moment-shear ratio* (33') showed little Vierendeel action. At failure, the relative displacement of the ends of the opening was small (less than 0.5") compared to the centerline deflection, δ_c, at failure (4.3"). $\overline{\delta}$ was only 0.12. The beams with lower moment-shear ratios showed this Vierendeel action to a greater degree, as more shear was transferred through the opening at failure. Beams No. 1, 2, and 5 with moment-shear ratios of 7', 9', and 6' showed larger relative displacements at failure (0.8", 0.9", and 0.7"), with $\overline{\delta}$ equal to 0.16, 0.30, and 0.63, respectively. The beams with the lowest moment-shear ratios, Beams No. 4 and 6, showed smaller relative displacements between the opening edges, both at about 0.5", but large values of $\overline{\delta}$, 0.66, and 0.50, respectively.

The strain readings, also, show the effect of the moment-shear ratio. The high moment, low shear test (Beam No. 3) had strain readings (Figs. 3.11 to 3.15) that showed the Vierendeel effect was minimal. The bottom tee acted as a tension member, while the neutral axis of primary bending was in the top tee. Failure of the beam was flexural in nature. The beams with lower moment-shear ratios, however,

---

* It may be more general to express the moment-shear ratio, M/V, as a normalized shear-span to depth ratio, M/Vd, as done for reinforced concrete. This point needs careful consideration for composite beams, but for the purposes of this report, the actual values of M/V will be used.

showed that secondary bending was more important. The presence of compressive, as well as tensile, strains in the bottom tee indicates the presence of Vierendeel action. As the moment-shear ratio decreased, the zones of compression in the bottom tee increased correspondingly.

Cracking of the concrete slab occurred in the vicinity of the opening and, in some beams (Beams No. 1, 2, and 3), in the high moment regions near the interior load points. Critical cracking regions were the top of the slab at the low moment end of the opening, the bottom of the slab at the high moment end of the opening, and the bottom of the slab near the center of the opening.

The cracking in the concrete in the high moment, low shear beam (Beam No. 3) was due to the primary bending moment. As the steel in the bottom tee began to yield, the neutral axis began to shift upward. Tensile cracks in the bottom of the slab occurred as the tensile stress exceeded the tensile strength of the concrete. Tensile cracks were also present near the load points in the bottom of the slab. A slight separation between the slab and the steel occurred at a load of about one-half of the ultimate load. At the ultimate load, the concrete at the top of the slab failed by crushing (Fig. 3.31).

In the beams with lower moment-shear ratios, the concrete cracking patterns were more complex (Fig. 3.32). Cracking occurred first at the top of the slab at the low moment end of the opening (due to the Vierendeel effect). This cracking occurred at a load equal to one-half to three-quarters of the ultimate load. Cracking of the bottom of the slab at the high moment end of the opening began slightly after cracks began to develop at the low moment end. A longitudinal crack in the center of the upper surface of the slab began to develop as cracks

developed at the low moment end. The crack began near the low moment end of the opening and propagated toward the high moment end as the load increased. The most significant cracking began at about three-quarters of the ultimate load, near the center of the opening on the bottom of the slab. The slab separated slightly from the steel flange, and cracks propagated at about 45° across the bottom slab surface, moving toward the high moment end of the opening (Fig. 3.32). At the ultimate load, these cracks extended to the edge and propagated diagonally to the top of the slab. This shear-type failure in the slab appeared to be due to the prying action caused by the large relative displacement between the ends of the opening.

In all cases, the compressive strains in the concrete remained low until well after the steel had begun to yield. The ultimate failure of all beams was due to the failure (crushing or cracking) of the concrete. Strain hardening of the steel in the bottom and top tees occurred prior to ultimate load.

Due to the nature of the loading procedure (see section 2.7), some beams (Nos. 1, 2, 3, and 4) failed during loading, at the maximum load attained, while others (Beams No. 5 and 6) failed at a fixed deflection (and a load less than the maximum attained during the test), while data readings were being taken. For the purposes of this report, the maximum load attained is considered to be the ultimate load.

Table 3.1 presents a summary of the test results including load at first yielding, maximum load, and mode of failure.

3.3 Evaluation of Results

The strain distributions at the end of the bottom and top tees

are plotted for each beam at 4 stages of load (elastic, first yield, late yield, and collapse) (Figs. 3.33 to 3.38).

On each beam (except Beam No. 1), strain gages were placed on the top flange of the steel under the slab and the bottom of the slab at the high moment end of the opening. This was done to assess the degree of strain compatibility between the concrete and the steel. The concrete gages on the bottom of the slab were placed toward the outside edge. The strain readings from these gages during loading indicated a lack of compatibility between the concrete and steel; the concrete gages read tension, while the steel gages read compression. This effect was observed for all load stages in the beams, except for Beam No. 2, in which the steel gage on the top flange showed this effect until the ultimate load was approached, when it went into tension. The probable cause of the incompatibility of strains at the interface is slip between the steel and concrete, although some transverse bending in the slab may have contributed to the difference in readings. The presence of slip at the concrete-steel interface is substantiated by the values of slip measured at the supports (Figs. 3.4, 3.9, 3.14, 3.19, 3.24, and 3.29). Concrete gages should be placed close to the steel section to improve the accuracy of the strain readings in future tests.

Many analytical models using the Vierendeel method of analysis assume that the point of contraflexure is located at the center of the opening in both the top and bottom tees. The experimental results (Figs. 3.33 to 3.38) indicate that this is reasonably correct for the elastic case, but that this is not the case near the ultimate load. Once general yielding is underway, the point of contraflexure is nearer to the low moment end of the opening. The movement is greatest in the

high moment, low shear cases. At collapse in Beam No. 2 (Fig. 3.35), the low moment end of the bottom tee had yielded completely in tension, while the high moment end had compressive strains at the top of the web. At collapse, Beams No. 4, 5, and 6 (Figs. 3.37, 3.38, and 3.34) seem to be effected less. Any movement of the point of contraflexure toward the low moment end will tend to lessen the secondary bending effects at the low moment end, while increasing the secondary bending effects at the high moment end.

Beam No. 1 was constructed using the smaller size steel section (W14 x 34). Due to problems with the load system, the beam was not tested until 180 days after the concrete was cast. This resulted in a concrete compressive strength of 7000 psi. This is considered a high moment - high shear test with a "medium" moment-shear ratio at the opening of 7'. This beam was instrumented less thoroughly than the following tests, with strain gages only on the bottom tee in the vicinity of the opening. Where the gages were placed, however, both sides of the web and flange were strain-gaged to verify the advisability of gaging only one side of the beam in later tests. First yield occurred in tension at the edge of the opening at the low moment end of the bottom tee (Fig. 3.33). At first yield, small compressive strains were present at the top of the web at the high moment end of the bottom tee. At ultimate load, the entire tee yielded in tension. The collapse condition was reached when the cracks in the concrete at the center of the opening had propagated completely through the slab. The ultimate shear at the opening was 32.2 kips, with a primary moment of 2710 in-kips.

Beam No. 6 was a low moment - high shear test. It was constructed using the W14 x 34 section and served as a companion test to

Beam No. 1. The moment-shear ratio was 3', and the behavior of the beam was completely dominated by the effects of the secondary bending moments. As shown in Fig. 3.34, at elastic loads the low moment end of the bottom tee was in tension, while the top of the web at the high moment end was in compression. First yield occurred at the high moment end of the top tee. At the ultimate load, the low moment end of the bottom tee had developed a compressive region in the flange (unyielded), while the web and the remainder of the flange yielded in tension. At the high moment end of the bottom tee, the compressive region increased in size until, at the ultimate load, the entire web and the top part of the flange yielded in compression. The bottom part of the flange yielded in tension. The top tee showed the secondary effects, also. At the high moment end, the steel yielded in tension, while, at the low moment end, the steel yielded in compression. The strain readings were inconsistent across the steel-concrete interface at both the low and high moment ends. A large separation near the center of the opening between the steel and concrete occurred at high loads (3/4 of ultimate load). The diagonal tension-type cracks began propagating from this area on both sides of the slab. At the ultimate load, the cracks had propagated outward toward the high moment end and through the slab. The ultimate shear through the section was 39.4 kips, with a primary moment of 1420 in-kips. Fig. 3.39 shows the shear strains ($\varepsilon_{sh} = \varepsilon_{+45} - \varepsilon_{-45}$) obtained from the rosettes at the end of each tee. The results show that the shear strains began as expected, with the low moment ends of both tees and the high moment end of the top tee reversing the trend as yielding began. The shear strains at the high moment end of the top tee reversed the trend again at the

The bottom tee cross-section is shown in Fig. 4.9. The plastic centroid, PC, is defined as the point of application of an axial force which will cause no moment to develop when the section is fully plastic (analagous to the center of gravity for elastic behavior). The equal area axis, EAA, is the neutral axis, assuming perfect plasticity in the steel. The location of the PC and EAA, with respect to the bottom of the tee, are $\bar{y}$ and y^*, respectively.

$$y^* = \frac{s_b t_w r}{2b_f} + \frac{t_f}{2} \tag{4.8}$$

$$\bar{y} = \frac{\frac{b_f t_f^2}{2} + s_b t_w r(t_f + \frac{s_b}{2})}{b_f t_f + s_b t_w r} \tag{4.9}$$

in which, $r = F_{yw}/F_{yf}$, F_{yw} = yield stress of web, F_{yf} = yield stress of flange, s_b = web stub length, t_w = web thickness, t_f = flange thickness, and b_f = flange width.

For a specific location of the neutral axis, the axial force is found by integrating the stresses on the cross-section of the tee ($P = \int \sigma dA$). The secondary bending moment is found by taking the moment of these stresses about the plastic centroid ($M = \int \sigma y dA$).

4.3.1 Low Moment End

A negative secondary bending moment will result at the low moment end of the bottom tee, if a positive bending moment is applied to the beam. The negative secondary moment will create tensile stresses in the top of the tee and compressive stresses in the bottom of the tee. The neutral axis will always be in the flange, providing that the area of the web is not greater than the area of the flange (which is rarely

encountered in wide-flange beams with reasonably sized web openings). The neutral axis will be at the EAA when no axial force is present. As the axial force increases to the maximum tensile force, P_u, which is equal to $s_b t_w F_{yw} + b_f t_f F_{yf}$, the neutral axis shifts downward toward the bottom of the flange.

The location of the neutral axis with respect to the plastic centroid is designated as g (Fig. 4.10). The ratio of the axial force for a specific stress distribution, P'_u, is designated by n (17). Fig. 4.10 shows the stress distribution for a given neutral axis location. Equations of equilibrium can be written for the moment and axial force for a given neutral axis location, g.

$$\underline{F = 0:} \quad (A_w r + A_f)\, n = s_b t_w r + b_f(g - y_b) - b_f(\bar{y} - g) \tag{4.10}$$

$$\underline{M = 0:} \quad M_{bl} = s_b t_w F_{yw}\left(y_t - \frac{s_b}{2}\right) - b_f F_{yf} g^2 + \frac{b_f F_{yf}}{2}\left(y_b^2 + \bar{y}^2\right) \tag{4.11}$$

in which, $y_b = \bar{y} - t_f$ and $y_t = s_b - y_b$. Eqs. (4.10) and (4.11) may be combined to obtain a single equation in terms of n.

$$M_{bl} = -b_f F_{yf} C_1^2 n^2 - 2C_1 C_2 b_f F_{yf} n - b_f F_{yf} C_2^2 + Z_1 + Z_2 \tag{4.12}$$

in which $$C_1 = \frac{A_w r + A_f}{2b_f}$$

$$C_2 = \frac{b_f(y_b + \bar{y}) - s_b t_w r}{2b_f}$$

$$A_w = s_b t_w$$

$$A_f = b_f t_f$$

$$Z_1 = s_b t_w F_{yw}(y_t - \frac{s_b}{2})$$

$$Z_2 = \tfrac{1}{2} b_f F_{yf}(y_b^2 + \bar{y}^2)$$

The result is a quadratic equation from which the tensile force ($P'_u = nP_u$) can be found, if the secondary moment, M_{b1}, is known.

4.3.2 High Moment End

The high moment end of the bottom tee is subjected to a positive secondary bending moment and a tensile axial force when the beam is subjected to a positive primary bending moment (Fig. 4.8). The positive secondary moment will create tensile stresses in the bottom of the tee and compressive stresses in the top of the tee. The equal area axis, EAA, and plastic centroid, PC, are obtained from Eqs. (4.8) and (4.9). The neutral axis under plastic bending is located at the EAA. As the tensile force is increased in the tee, the neutral axis shifts upward into the web. Two cases must be considered in order to develop the moment-axial force equations: (1) neutral axis in the web and (2) neutral axis in the flange. Fig. 4.11 shows these two cases.

When the neutral axis is in the web, the resulting moment-axial force equation is

$$M_{bh}(1) = -t_w F_{yw} C_3^2 n^2 - 2t_w F_{yw} C_3 C_4 n + Z_3 + Z_4 - t_w F_{yw} C_4^2 \qquad (4.13)$$

in which $C_3 = \dfrac{A_w r + A_f}{2t_w r}$

$$C_4 = \frac{(y_t - y_b)\, t_w r - b_f t_f}{2 t_w r}$$

$$Z_3 = b_f t_f F_{yf} \left(\frac{t_f}{2} + y_b\right)$$

$$Z_4 = \tfrac{1}{2} t_w F_{yw} (y_b^2 + y_t^2)$$

When the neutral axis is in the flange, the moment-axial force equations can be reduced to

$$M_{bh}(2) = -b_f F_{yf} C_6^2 n^2 - 2 b_f F_{yf} C_5 C_6 n - b_f F_{yf} C_5^2 + Z_5 + Z_6 \qquad (4.14)$$

in which

$$C_5 = \frac{b_f(\bar{y} + y_b) - s_b t_w r}{2 b_f}$$

$$C_6 = -\frac{(A_w r + A_f)}{2 b_f}$$

$$Z_5 = \tfrac{1}{2} b_f F_{yf} (\bar{y}^2 + y_b^2)$$

$$Z_6 = s_b t_w F_{yw} \left(y_t - \frac{s_b}{2}\right)$$

4.3.3 Total Capacity

From the moment equilibrium equation, Eq. (4.7), the secondary moments at both ends of the bottom tee must equal the bottom shear force (V_b) times the opening length (2a). Using the moment-axial force equations developed for the bottom tee, Eq. (4.7) can be expressed as

Neutral Axis in Web at High Moment End

$$2V_b a = M_{bl} + M_{bh}(1)$$

$$= (- b_f F_{yf} C_1^2 n^2 - 2C_1 C_2 b_f F_{yf} n - b_f F_{yf} C_2^2 + Z_1 + Z_2)$$

$$+ (- t_w F_{yw} C_3^2 n^2 - 2t_w F_{yw} C_3 C_4 n + Z_3 + Z_4 - t_w F_{yw} C_4^2) \quad (4.15)$$

Neutral Axis in Flange at High Moment End

$$2V_b a = M_{bl} + M_{bh}(2)$$

$$= (- b_f F_{yf} C_1^2 n^2 - 2C_1 C_2 b_f F_{yf} n - b_f F_{yf} C_2^2 + Z_1 + Z_2)$$

$$+ (- b_f F_{yf} C_6^2 n^2 - 2b_f F_{yf} C_5 C_6 n - b_f F_{yf} C_5^2 - Z_5 + Z_6) \quad (4.16)$$

The web-flange crossover point for the high moment end equations will occur when $g = - y_b$ at the high moment end. At this neutral axis location,

$$n = \frac{b_f t_f - 2y_b t_w r + (y_b - y_t)\, t_w r}{(A_w r + A_f)} \quad (4.17)$$

The axial force ratio at the crossover point is designated n_c. By substituting n_c into either Eq. (4.15) or Eq. (4.16), the crossover shear force can be found.

$$V_{bc} = \frac{M_{bl}(n_c) + M_{bh}(1 \text{ or } 2)(n_c)}{2a} \quad (4.18)$$

If the applied shear force, V_b, is less than V_{bc}, Eq. (4.15) is used. Eq. (4.16) is used if the shear force is greater than V_{bc}.

The moment-axial force equations, Eqs. (4.15) and (4.16), are of the form $2V_b a = K_1 n^2 + K_2 n + K_3$. For a specific shear force, V_b, transferred through the tee, the equation is solved for n (positive root). The axial force is found by $P'_u = nP_u$, where $P_u = s_b t_w F_{yw} + b_f t_f F_{yf}$. The secondary moments can be found by substituting n into the moment-axial force equations for the low and high moment ends of the tee, Eqs. (4.12), (4.13), and (4.14).

The moment-axial force equations for the bottom tee determine the combination of axial forces and moments that the tee can carry, assuming that the steel is yielding. The equations are presented for a tensile axial force in the bottom tee. These equations can be adapted for a compressive axial force by applying the high moment end equations to the low moment end, and vice versa. The interaction diagram for moment and axial force in the bottom tee is shown in Fig. 4.12a for both tensile and compressive axial forces. Note that the negative bending moment in Fig. 4.12a represents a counterclockwise moment applied at the low moment end of the tee (i.e., a positive M_{bl} in Fig. 4.8). Fig. 4.12b shows the interaction diagram in terms of total secondary moment versus axial force.

The shear force that is transferred through the bottom tee decreases the capacity of the tee. Within the model, this shear is assigned to the web of the tee. The web is assumed to extend through the flange. The average shear stress for the web is

$$\tau_b = \frac{V_b}{(s_b + t_f)\, t_w} \tag{4.19}$$

Using the von Mises yield criterion, Eq. (4.1), the reduced longitudinal

yield strength of the web is

$$F_{ywr} = (F_{yw}^2 - 3\tau_b^2)^{\frac{1}{2}} \tag{4.20}$$

F_{ywr} is used in place of F_{yw} in Eqs. (4.11) - (4.16). The maximum axial capacity of the bottom tee, P_u, is fixed by virtue of the material strength and the tee size. P_u occurs only when the beam is in pure bending. Since no shear is transferred through the tee in the pure bending case, the axial strength is not reduced.

Secondary moments develop as shear is transferred through the tee. As more shear is transferred, the capacity is reduced due to the reduced yield stress of the web, F_{ywr}. From the moment equilibrium equation, Eq. (4.7), the sum of the secondary moments is equal to the product of the bottom shear force times the opening length. For a particular value of the secondary moments, as the opening length decreases, the capacity of the tee (as represented by the axial force-moment interactions) decreases because the higher shear causes a greater reduction in the web yield strength. Fig. 4.13 shows the effect of opening length on the bottom tee axial force-moment interaction diagram. The results illustrated in Fig. 4.13 may seem contradictory, since a shorter opening can carry a greater shear. The shorter opening carries a greater shear, because the reduction in the secondary moments obtained with the shorter opening more than compensates for the reduction in the secondary moment capacity.

4.4 Top Tee

The top tee is subjected to an axial force, a shear force, and secondary moments similar to the bottom tee. Under a positive primary bending moment, the top tee carries an axial compressive force, equal in magnitude to the tensile force in the bottom tee (Fig. 4.14). The equilibrium equations for the top tee are

$$(1) \quad P_{tl} = P_{th} \tag{4.21}$$

$$(2) \quad V_{tl} = V_{th} \tag{4.22}$$

$$(3) \quad M_{tl} + M_{th} = 2V_t a \tag{4.23}$$

in which, P_{tl} = axial force at the low moment end, P_{th} = axial force at the high moment end, V_{tl} = shear force at the low moment end, V_{th} = shear force at the high moment end, M_{tl} = secondary moment at the low moment end, and M_{th} = secondary moment at the high moment end.

The equilibrium forces are shown in Fig. 4.15. Since the axial and shear forces at the ends of the tee are equal, they will be referred to as P_t and V_t, respectively.

The two failure modes described in section 4.1 are controlled by the top tee. A "mechanism" failure corresponds with the formation of plastic hinges (one or two) at the ends of the tee. A "shear" failure is governed by the strength of the top tee at the point of contraflexure.

4.4.1 Mechanism Failure

Under pure bending, it is assumed that failure of the top tee will occur by crushing in the concrete in compression and yielding of the steel in tension below the neutral axis. The stress distributions at the

low and high moment ends of the top tee are assumed to be identical. As shear force is added to the top tee, a negative secondary moment is induced at the low moment end and a positive secondary moment is induced at the high moment end (Fig. 4.15). At the low moment end, the secondary moment tends to counter the effect of the primary moment, as tensile stresses are created at the top of the slab and compressive stresses are added at the bottom of the tee. At the high moment end, the secondary moment adds to the stresses caused by the primary bending moment. Therefore, as shear is first added to the top tee, a plastic hinge occurs only at the high moment end. As the moment-shear ratio at the opening is further reduced, the shear increases, and the primary bending moment decreases. This results in a negative secondary bending moment at the low moment end, which produces a plastic hinge. The shear force in the top tee which corresponds to two plastic hinges and zero axial force is called the "mechanism" shear strength of the top tee, $V_{tmax}(mech)$.

High Moment End

The secondary moment at the high moment end is positive under a positive primary moment, as shown in Fig. 4.15. The concrete at the top of the slab is in compression, while the bottom of the steel is in tension.

Failure of the high moment end is assumed to occur when the strain at the top of the concrete slab reaches -0.003. Strain compatibility across the concrete-steel interface is assumed (plane sections remain plane). This assumption does not match the experimental observations but proves to be satisfactory for the model. The plastic centroid is defined as the point of application of an axial force which will cause no moment when the concrete and steel are at their maximum

stresses in compression. All secondary moments are calculated with respect to the plastic centroid (Fig. 4.16). The location of the plastic centroid with respect to the bottom of the tee is calculated by

$$x_c = \frac{.85f'_c t_s b_{eff} x_r + A_r F_{yr} x_r}{.85f'_c t_s b_{eff} + A_r F_{yr} + A_f F_{yf} + A_w F_{yw}} + x_s \qquad (4.24)$$

$$x_s = \frac{\frac{1}{2} s_t^2 t_w r + b_f t_f (s_t + \frac{1}{2} t_f)}{b_f t_f + s_t t_w r}$$

$$x_r = s_t + t_f - x_s + \frac{1}{2} t_s$$

in which, f'_c = compressive strength of concrete, s_t = web stub length, t_s = slab thickness, b_{eff} = slab width, A_r = area of longitudinal reinforcing steel, F_{yr} = yield strength of reinforcing steel, A_f = area of top tee steel flange, and A_w = area of top tee steel web.

Since the top tee consists of two different materials, it is necessary to utilize strain-compatibility and stress-strain relations to determine the strength of the section. For each strain distribution, there is a corresponding stress distribution. The stress distribution determines the secondary moments and axial force. The requirement for failure is that the concrete "crush" at the top of the slab (strain = -0.003). The steel is elastic-plastic. Fig. 4.17 shows strain distributions, and the corresponding stress distributions, for different locations of the neutral axis. At failure, the concrete is assumed to have a depth of stress block equal to 0.85 times the depth to the neutral axis. The concrete stress within the stress block is 0.85 times the

the reduced strength, f, obtained using Eq. (4.3). The effective width of the concrete in compression is limited by the AISC restrictions (5).

Both the concrete and the steel can carry shear. The concrete carries shear above the neutral axis, in a width, $3t_s$, equal to three times the slab thickness. This effective width for shear is based on experience with reinforced concrete T-beams in which a portion of the flange is shown to participate in carrying shear (3).

The steel carries shear in both the web and the flange. However, the flange is allowed to carry shear only if both the web and the slab are at full capacity.

During the solution process, all of the shear force is first assigned to the concrete. The concrete compressive strength is reduced using Eq. (4.3). The shear stress in the concrete is

$$\tau_c = \frac{V_{hc}}{3t_s c} \tag{4.25}$$

in which, V_{hc} = shear force assigned to the concrete, and c = depth to the neutral axis from the top of the slab.

The strain distribution is varied (the strain in the top of the slab is held constant at -0.003) until the desired axial force is found (within .01% in this study). The shear stress in the concrete is rechecked, since the value changes as the depth of the neutral axis changes. The concrete strength is readjusted until the calculated shear stress is equal to the assumed shear stress.

The steel is assigned a shear force, V_s, in increasing increments to determine the distribution of shear within the top tee that will result in the highest value for the primary moment. The concrete

is assigned the remainder of the shear ($V_{hc} = V_t - V_s$). The shear stress in the steel is taken to be

$$\tau_s = \frac{V_s}{(s_t + t_f)\ t_w} \tag{4.26}$$

The steel yield strength is reduced for the shear using Eq. (4.2).

For each distribution of shear, the strain distribution is again varied to obtain the required axial force. The stresses in the steel are found by transforming the assumed strain distribution to a stress distribution ($\sigma = \varepsilon E$). The stress in the steel may not exceed the reduced yield stress. From the stress distribution, the axial force and secondary moment are calculated. A moment-axial force interaction diagram for the high moment end of the top tee is shown in Fig. 4.18.

The maximum axial force that the top tee will carry is equal to the maximum axial force for the bottom tee. As the opening length decreases, the shear in the tees increases for a given secondary moment. This increased shear reduces the capacity of the top tee. Fig. 4.19 shows the reduction in capacity due to the decrease in opening length. As explained in section 4.3.3, this is somewhat misleading, since the overall shear capacity of the tee will increase as the opening is shortened due to the reduction in the secondary moments.

Low Moment End

A hinge will form at the low moment end of the top tee in the "pure shear case", that is when no axial force is present in the top tee. The negative secondary moment will create a tensile stress in the top of the slab which causes the concrete to crack. Since the neutral

axis is normally in the steel section, the concrete is fully cracked and is assigned no shear.

The web of the steel is assigned all of the shear force until the web yield strength is reduced to zero. The shear stress in the web is

$$\tau = \frac{V_t}{(s_f + t_f)\ t_w} \tag{4.27}$$

The steel strength is reduced using Eq. (4.2), and the maximum shear that can be carried by the web is

$$V_{wmax} = \frac{F_{yw}(s_t + t_f)\ t_w}{\sqrt{3}} \tag{4.28}$$

If the shear in the top tee is greater than V_{wmax}, the flange carries $V_t - V_{wmax}$, and the flange yield stress is reduced accordingly.

When the beam is subjected to zero primary moment at the opening (pure shear case), a closed-form solution is obtained for the low moment end of the top tee by assuming that the steel is fully plastic. The secondary moment is calculated with respect to the plastic centroid of the top tee (see Eq. (4.24)).

For normal amounts of reinforcing steel, the neutral axis is not in the slab, but in the steel section. The neutral axis is in the flange (Fig. 4.20a) if

$$A_r F_{yr} + b_f t_f F_{yfr} > s_t t_w F_{ywr} \tag{4.29}$$

in which, A_r = area of the reinforcing steel, and F_{yr} = yield stress of

the reinforcing steel. In this case, the neutral axis is a distance, y_1, from the top of the flange.

$$y_1 = \frac{b_f t_f F_{yfr} + s_t t_w F_{ywr} - A_r F_{yr}}{2 b_f F_{yfr}} \tag{4.30}$$

and the secondary moment at the low moment end is

$$M_{tl} = s_t t_w F_{ywr}(h_r + t_f + \tfrac{1}{2}s_t) + b_f(t_f - y_1)\, F_{yfr}(h_r + \tfrac{1}{2}y_1 + \tfrac{1}{2}t_f) - b_f y_1 F_{yfr}(h_r + \tfrac{1}{2}y_1) \tag{4.31}$$

in which, h_r = the height of the reinforcing steel above the steel flange.

The neutral axis is in the web (Fig. 4.20b) if

$$A_r F_{yr} + b_f t_f F_{yfr} < s_t t_w F_{twr} \ . \tag{4.32}$$

In this case, the neutral axis is a distance, y_2, from the bottom of the web

$$y_2 = \frac{A_r F_{yr} + b_f t_f F_{yfr} + s_t t_w F_{ywr}}{2 t_w F_{ywr}} \tag{4.33}$$

and the secondary moment at the low moment end is

$$M_{tl} = A_r F_{yr}(h_r + t_f + s_t - \tfrac{1}{2}y_2) + b_f t_f F_{yfr}(\tfrac{1}{2}t_f + s_t - \tfrac{1}{2}y_2) + \tfrac{1}{2}t_w F_{ywr} s_t(s_t - y_2) \ . \tag{4.34}$$

For a "mechanism" failure, the low moment end of the top tee is critical only in the "pure shear" case. With the application of a primary bending moment at the opening, the addition of an axial force and the reduction in the shear stress serve to strengthen the low moment end. Under increasing moment, the low moment end become critical, again, only under pure bending, when the entire top tee is subjected to the same stress distribution.

4.4.2 Shear Failure

A shear failure can occur in the concrete and steel at the point of contraflexure, where no secondary bending stresses are present (only axial forces). In the "pure shear case", no axial forces are present. The concrete and the steel are subjected only to shear stresses at this location. The shear strength of the top tee at the point of contraflexure is

$$V_{tmax}(sh) = 3.5\sqrt{f'_c}\, 3t_s^2 + \frac{(s_t + t_f)\, t_w F_{yw}}{\sqrt{3}} \qquad (4.35)$$

4.5 Summary of Interaction Procedure

The initial step in developing an interaction curve is to determine the maximum shear strength of the top and bottom tees:

The bottom tee shear strength, V_{bmax}, is calculated by varying the shear force assigned to the tee until a shear force is found that corresponds to zero axial force.

The maximum shear strength of the top tee for a "shear" failure, $V_{tmax}(sh)$, is calculated using Eq. (4.35). The maximum shear for a "mechanism" failure, $V_{tmax}(mech)$, is calculated by varying the shear force assigned to the top tee

until the moment equilibrium equation, Eq. (4.23), is satisfied. The shear strength of the top tee, V_{tmax}, is assumed to be the smaller of the two values. The total shear strength of the beam at the opening, V_{max}, is the sum of V_{tmax} and V_{bmax}.

To develop an interaction curve, values of shear, between 0 and V_{max}, are assigned to the opening. For a specific value of shear, V_{total}, the amount assigned to the bottom is

$$V_b = V_{total} \left(\frac{V_{bmax}}{V_{max}}\right) \tag{4.36}$$

while top tee carries

$$V_t = V_{total} - V_b = V_{total} \left(\frac{V_{tmax}}{V_{max}}\right) \tag{4.37}$$

This method of assigning the shear to the top and bottom tees is used for convenience. It is on the safe side, because the overall procedure is an equilibrium method and produces a lower bound solution.

In distributing the shear force to the tees, two cases must be considered. When $V_{tmax}(mech) < V_{tmax}(sh)$, the shear force in the bottom and top tees vary linearly from 0 to V_{bmax} and $V_{tmax}(mech)$, respectively as shown in Fig. 4.21.

When $V_{tmax}(sh) < V_{tmax}(mech)$, the shear in the bottom tee varies linearly from 0 to V_{bmax}, while the shear in the top tee varies linearly from 0 to $V_{tmax}(mech)$, until it reaches 95% of $V_{tmax}(sh)$. Then the top shear varies linearly from 95 to 100% of $V_{tmax}(sh)$, as the shear in the bottom tee continures to increase (Fig. 4.22).

The axial force in the tees is controlled by the bottom tee. As the shear in the bottom tee is varied from 0 to V_{bmax}, the axial

force and secondary moments are calculated. The axial force in the top tee is equal to the axial force in the bottom tee. The primary moment at the centerline of the opening is

$$M_{primary} = P\ z + M_{th} + M_{bh} - V_{total}\ a \qquad (4.38)$$

in which, P = axial force, z = distance between the plastic centroids in the top and bottom tee, a = half of the opening length, and V_{total} = the total shear at the opening at a given increment.

The primary moment is calculated at each increment as the total shear on the section varies from 0 to V_{max} and is maximized for each value of V_{total} by adjusting the shear distribution within the high moment end of the top tee. Fig. 4.23 shows an example of an interaction curve in which a "mechanism" failure controls under high shear for the top tee. Fig. 4.24 shows an example of an interaction curve in which a "shear" failure controls.

The "pure shear" case discussed previously does not, in fact, represent pure shear. This is due to the fact that although the axial forces (and therefore Pz) are zero, the points of contraflexure are not in the center of the opening and $M_{primary}$ is greater than zero (see Eq. (4.38)). To obtain a zero primary moment, it is necessary to apply a compressive axial force to the bottom tee and a tensile axial force to the top tee such that

$$P\ z = - M_{th} - M_{bh} + V_{total}\ a \qquad (4.39)$$

For this calculation, the shear force on the top tee, V_{tmax}, is held

constant, and the bottom shear is decreased slightly until the primary moment drops to zero. Holding V_{tmax} constant is justified since the effect of a small tensile force is small. The effect on V_b is also small, so that, in practice, the difference in V_{max} for the "pure shear" case and the case in which $M_{primary} = 0$ is negligible.

CHAPTER 5

APPLICATION OF ULTIMATE STRENGTH MODEL

5.1 General

To determine the applicability of the proposed ultimate strength model for composite beams with web openings, comparisons with experimental tests are required. Interaction diagrams are developed using the geometric and material properties for each of the six beams tested (Tables 2.1 to 2.3). Average yield stresses for the bottom and top flanges and the horizontal yield stress for the web are used. Further comparisons are made to the two beams tested by Granade (16) using nominal beam dimensions and his reported values for the material properties.

The effect of opening length, opening eccentricity, and material properties on the predicted strength of composite beams with web openings is, also, investigated.

5.2 Comparison with Test Results

5.2.1 Current Tests

The moment-shear interaction diagrams for the six beams in the current study are shown in Figs. 5.1 to 5.6. Table 5.1 presents the predicted and observed ultimate shear strengths and primary moments for the beams at the opening. The experimental ultimate shear and primary moment is plotted on the interaction diagram. The origin and the experimental data point are connected with a straight line. The point at which the line crosses the interaction curve represents the predicted ultimate shear and primary moment at the moment-shear ratio. The slope of the line represents the moment-shear ratio. Table 5.2 summarizes

the interaction results for the pure shear and pure moment cases.

With the exception of Beam No. 4, the model conservatively predicts the ultimate strength at the opening. The results for Beams No. 2, 3, 4, and 5 (larger steel sections) indicate that as the moment-shear ratio of the opening increases, the ratio of the difference in experimental and predicted strength to predicted strength, R, increases. Beam No. 3, with a moment-shear ratio of 33', failed at an ultimate shear (13.3 kips) that was 27% higher than predicted (11 kips).* The tests with the lower moment-shear ratios, Beams No. 2 and 5, failed at shears 16% and 14%, respectively, higher than predicted. The low moment-shear ratio test (Beam No. 4) failed at a shear that was 4.0% below the predicted shear strength. The low strength of Beam No. 4 is consistent with the trend of the test results, when compared with the ultimate strength model. However, the fact that this test result is <u>below</u> the predicted value is <u>not</u> consistent with the rest of the results and may be due to a variability in material properties within the beam. The results for Beams 1 and 6 (smaller steel section) also show the increase in experimental over predicted strength as the moment-shear ratio increases. Beam No. 1, with a 7' moment-shear ratio, failed at a shear 24% higher than the predicted shear. Beam No. 6, with a moment-shear ratio of 3', failed at a shear 7% higher than predicted.

A large part of the difference in the predicted and the experimental strength of the beams can be attributed to the material representation in the model. The steel is assumed to behave in an elasto-plastic manner. No strain hardening was assumed. However, the recorded strains in some beams were very high (over 0.02).

---

* Comparisons based on applied load. See Table 5.1b for comparisons including dead load.

In the high-moment beams, the strain hardening effect is greater, due to the high tensile strains throughout the steel section. The effect of strain hardening in high-shear beams will be smaller because of the high strain gradient present in the tees due to the large secondary bending moments. These effects can be seen in the 6 test beams. The high moment, low shear beam (Beam No. 3) had the largest value of R. The low moment, high shear beams (Beams No. 4 and 6) showed the smallest values of R.

One method that can be used to include the effect of strain hardening is to increase the yield stress of the steel in the model. The material and geometric properties of Beam No. 2 are used to generate an interaction curve, in which the yield stress of the steel is increased (Fig. 5.7). For the pure moment case, the steel yield stress is increased by 20%. As the total shear on the section is increased to V_{max} (pure shear case), the steel yield stress is reduced, linearly, to the original value. The curve is normalized with respect to the pure shear and moment capacities* of Beam No. 2. The four data points, representing the test beams (large steel sections), are, also, normalized with respect to the pure shear and moment strengths of the beams. The interaction curve for Beam No. 2 with a constant yield strength is shown for comparison.

Table 5.1 shows the predicted points of contraflexure in the bottom tee for the test beams at failure. The model predicts, in every case, that the point of contraflexure will occur near the low moment end

---

* A zero length opening is used to normalize the pure shear capacity. $V_{max_{a=0}} = 3.5\sqrt{f'_c}\, 3t_s^2 + \dfrac{(s_t + s_b + 2t_f)\, t_w F_y}{\sqrt{3}}$.

of the opening. Under pure shear, the model predicts that the point of contraflexure will occur in the center of the opening in the bottom tee at failure. As the moment is increased on the section, the point of contraflexure shifts toward the low moment end. In the pure moment case, no point of contraflexure is located in the opening. At failure, the point of contraflexure in the top tee will never occur at the center of the opening due to the cracked low moment end's reduced flexural capacity.

Slip between the concrete and the steel is not considered in the model. Based on the experimental evidence, however, slip does occur. This lack of agreement does not seem to be of great importance for the beams in this study.

The model is based on two possible modes of failure in the top tee, "shear" and "mechanism" failure. Beam No. 3 failed primarily in flexure as predicted by the model ("mechanism" failure in the top tee). Beams No. 1, 2, 4, 5, and 6 failed in the diagonal tension-type (shear) mode. The model predicts "mechanism" failures for these beams. However, the difference in the predicted "shear" and "mechanism" strengths is small for these beams. In all of the higher shear tests (Beams No. 1, 2, 4, 5, and 6), the behavior supported the "mechanism" failure, cracking at the top of the slab at the low moment end and cracking at the bottom of the slab at the high moment end. However, before the hinges could fully develop for a "mechanism" failure, the concrete failed in shear.

5.2.2 Granade Tests

Two small (W8 x 28) composite beams with web openings were tested by Granade (16) (see Fig. 5.8). Each beam had a 3½" thick, 24" wide concrete slab and was supported on a 10' span. The opening height

was 4.8", with a length of 7.2", 0.6 and 0.9 of the depth of the steel section, compared to 0.6 and 1.2 for the current tests. The concrete strength was 3980 psi and the steel strength was 43.8 ksi for the flanges and 47.9 ksi for the web. The moment-shear ratios of the openings were 2' and 4', respectively. The interaction diagram for the beams is shown in Fig. 5.9. The results are summarized in Tables 5.1 and 5.2. A shear type failure occurred in both beams as predicted by the model. The experimental ultimate strength of the high moment beam was 3% higher than the predicted value. The experimental strength of the high shear beam was 16% higher than the predicted strength. The test with the moment-shear ratio of 4' had a value of R (3%) that was consistent with the current tests. The high shear test, however, does not show the decrease in R observed for the current tests for lower moment-shear ratios. Detail is lacking on the test procedures and material properties for these beams. Clearly, more study is needed for short openings.

5.3 Effects of Geometry

5.3.1 Opening Length

The length of a web opening affects the strength of a beam at the web opening. The pure moment capacity is not affected. As seen in Chapter 4, the sum of the secondary moments must be equal to the product of the shear force in the tee times the opening length. Since the secondary moment capacity of the tees is largely fixed (although some reduction occurs due to shear stress), the shear strength of both the top and bottom tees decrease as the opening length increases. On the other hand, if the opening length is reduced sufficiently so that a "shear" failure controls in the top tee, the shear strength of the top

tee is fixed and the strength varies only with the strength increase in the bottom tee. Fig. 5.10 shows the predicted effects of doubling the opening length and reducing the opening length by one-half in Beam No. 2.

5.3.2 Eccentricity

The location of the opening in the steel beam has an effect on the moment and shear capacity at the opening. As the opening is shifted upward from the centerline of the steel beam (positive eccentricity), the area of the bottom tee increases. The larger bottom tee develops a greater axial force, and the primary moment capacity in pure bending increases. As the opening is shifted downward from the centerline of the steel beam, the primary moment capacity in pure bending decreases (Fig. 5.11 and 5.12).

The type of failure that occurs in the top tee has a large effect on the behavior of openings with varying eccentricites, E. If a "mechanism" failure controls, the concentric opening will produce a lower pure shear strength, while the positive and negative eccentricities will increase the shear strength. Fig. 5.11 shows the effect of eccentricities of -1.5", 0", and 1.5" with a "mechanism" failure controlling in the top tee. The highest shear strength occurs at E = -1.5" and the lowest at E = 0". If a "shear" failure controls in the top tee, positive eccentricities produce lower shear strengths, while negative eccentricities produce higher shear strengths. Fig. 5.12 shows the effect of eccentricities of -1.5", 0", and 1.5" with a "shear" failure controlling in the top tee. The model exhibits this behavior because of the manner in which the tee shear strengths are calculated when a "shear" failure controls. As the opening is shifted upward or downward, the top tee responds with a linear decrease or increase in its shear

capacity. The bottom tee, however, does not respond with a proportional increase or decrease. Thus in this case, the shear capacity increases when more web area is given to the top tee and vice versa. The results obtained for high shear are in conflict with the model proposed by Todd and Cooper (30) who suggest that both positive and negative eccentricities increase the pure shear strength of composite beams equally at the opening. These interaction diagrams raise an important area for further validation of the model.

5.4 Material Properties

5.4.1 Steel

The steel yield strength affects the moment and shear capacity of a composite beam at a web opening. An increase in steel strength tends to expand the interaction curve as the moment and shear capacities of the section increase. Fig. 5.13 shows the effect of increasing the steel strength of Beam No. 2 by 10%. The pure shear strength of the beam at the opening is increased by 7% and the pure flexural capacity is increased by 9%. A "mechanism" failure in the top tee controls at high shears in both diagrams; however, the "mechanism" strength and the "shear" strength are nearly equal.

5.4.2 Concrete

Concrete strength also affects the strength of composite beams with web openings. An increase in concrete strength tends to expand the interaction curve, as does the steel, but to a lesser degree. Fig. 5.14 shows the interaction curves for Beam No. 2 with concrete strengths of 2000, 4000 and 6000 psi. A 200% increase in concrete strength results in a predicted increase in the pure shear strength of

the section of only 16% while the predicted increase in the pure moment capacity is only 13%. The predicted mode of failure for all three beams is a "mechanism" failure.

CHAPTER 6

DESIGN OF WEB OPENINGS IN COMPOSITE BEAMS

6.1 General

A simplified method for constructing moment-shear interaction diagrams is presented to aid designers in the placement of rectangular web openings in composite beams. The approach is based on the existing experimental evidence and the analytical results obtained in the current study.

The procedure is based on a number of simplifying assumptions: The steel will yield in compression or tension. The shear force in the top tee is carried by both the concrete and the steel at the high moment end, but only by the steel at the low moment end. At the high moment end of the top tee, the concrete is at its maximum shear stress (0.21 f'_c), which corresponds to a compressive stress of $0.73f'_c$ (see Section 4.2). The steel yield stresses are reduced according to the von Mises yield criterion. The bottom tee carries shear only in the web. "Shear" and "mechanism" failure criteria are utilized for the top tee to determine its shear capacity.

Due to the iterative nature of this procedure, it is well suited for use with a mini-computer.

6.2 Analysis Procedure

6.2.1 Simplified Interaction Curve

The interaction between moment and shear in composite beams with web openings is weak; that is, the moment capacity at a web opening is relatively unaffected by the shear force, until the shear

approaches V_{max}. Due to this weak interaction, a circular interaction curve satisfactorily represents the moment-shear interaction. The circular interaction curve is represented by

$$\left(\frac{M}{M_{max}}\right)^2 + \left(\frac{V}{V_{max}}\right)^2 = 1 \qquad (6.1)$$

in which, M_{max} = the maximum moment capacity of the beam at the web opening and V_{max} = the maximum shear capacity of the beam at the web opening.

Eq. (6.1) is plotted in Fig. 6.1 for Beam No. 4. The interaction diagram generated by the proposed ultimate strength model is also shown. The two curves match quite well. The circular interaction curve slightly overestimates the moment capacity in the high moment region of the curve and slightly underestimates the moment capacity in the high shear region of the curve. However, in the high moment region, the effect of strain hardening is more pronounced and results in higher safety factors.

The current tests, as well as the two beams tested by Granade (16), are safely represented by Eq. (6.1).

The moment and shear strengths of the beam at the opening must be known in order to use the circular interaction equation. The following sections describe procedures to obtain M_{max} and V_{max}.

6.2.2 Maximum Moment Capacity

The maximum moment capacity of a composite beam at a web opening is based on the usual ultimate strength procedures, using the net steel section at the opening. The steel yields and the concrete crushes at failure. The neutral axis will be in the slab, provided that the

slab is "adequate". The concrete stress within the stress block is fixed at $0.85f'_c$. The strength contribution of the reinforcing steel in the slab is neglected because it is generally near the location of the neutral axis. Assuming that the slab is adequate (see Eq. (2.1)), the maximum moment capacity of the beam at the web opening is

$$M_{max} = T' \left(\frac{d}{2} + t_s - \frac{\bar{a}}{2}\right) \tag{6.2}$$

in which $T' = A_{net} F_y = t_w(s_t + s_b)F_y + 2t_f b_f F_y$

$$\bar{a} = \frac{T'}{0.85f'_c b_{eff}}$$

d = depth of steel section.

6.2.3 Maximum Shear Capacity

6.2.3a Maximum Shear Capacity of the Bottom Tee

The shear capacity of the bottom tee is determined by calculating the plastic moment and accompanying shear force that satisfy the moment equilibrium equation for the bottom tee (Eq. (4.7)). The shear force is assigned to the web, and the web yield stress is reduced using the von Mises yield criterion. The flange carries shear, only if the web has yielded in shear. Initially, the web yield stress is not reduced ($F_{ywr} = F_{yw}$). The following steps show the procedure used to calculate the bottom tee shear capacity:

Step No. 1

Calculate the location of the EAA.

$$y^* = \frac{s_b t_w F_{ywr} + t_f b_f F_{yf}}{2 b_f F_{yf}} \tag{6.3}$$

Step No. 2

Calculate the plastic moment for the bottom tee.

$$M_b = s_b t_w F_{ywr}\left(\frac{s_b}{2} + t_f - \frac{y^*}{2}\right) + b_f F_{yf}(t_f - y^*)\frac{t_f}{2} \tag{6.4}$$

Step No. 3

Calculate the shear force, V_b, that satisfies the moment equilibrium equation.

$$V_b = \frac{2M_b}{2a} = \frac{M_b}{a} \tag{6.5}$$

in which, 2a is the opening length.

Step No. 4

Assign V_b to the web, and reduce the web yield strength.

$$F_{ywr} = \left[F_{yw}^2 - 3\left[\frac{V_b}{(s_t + t_f)\, t_w}\right]^2\right]^{\frac{1}{2}} \tag{6.6}$$

Step No. 5

Using the reduced web yield strength, return to Step No. 1, and iterate until V_b converges. The result is V_{bmax}. Convergence usually occurs within a few iterations.

6.2.3b Maximum Shear Capacity of the Top Tee

The shear capacity of the top tee is governed by the smaller of the "mechanism" and "shear" failure loads.

"Shear" Failure

For a "shear" failure, the maximum capacity of the top tee is

$$V_{tmax}(sh) = \frac{3.5\sqrt{f'_c}\ 3t_s^2}{1000} + \frac{(s_t + t_f)\ t_w F_{yw}}{\sqrt{3}}\ , \text{ kips}, \qquad (6.7)$$

f'_c in psi.

"Mechanism" Failure

To determine the "mechanism" shear strength, $V_{tmax}(mech)$, it is necessary to vary the shear force in the top tee until the moment equilibrium equation for the top tee, Eq. (4.23), is satisfied. The concrete compressive strength is fixed at $0.73f'_c$. This corresponds to its maximum shear carrying capacity, $0.21f'_c$. This is a conservative assumption with respect to the ultimate strength model and will, generally, result in a lower value for $V_{tmax}(mech)$ than will be obtained using the procedures presented in Chapter 4. The shear in the concrete is carried only in the uncracked portion of the slab. Therefore, shear is assigned to the concrete at the high moment end of the top tee only. In the steel, the yield stress is reduced separately at the low and high moment ends of the tee. The flange is assigned shear only if the web has completely yielded in shear ($F_{ywr} = 0$). To obtain rapid convergence, the web at the low moment end is initially assumed to be yielding in shear ($F_{ywr} = 0$).

Step No. 1

With the concrete strength fixed at $0.73f'_c$, calculate the depth of the stress block, $\bar{a}$, at the high moment end.

$$\bar{a} = \frac{b_f t_f F_{yfr} + t_w s_t F_{ywr}}{0.85(0.73)f'_c b_{eff}} \qquad (6.8)$$

Step No. 2

Calculate the secondary moment at the high moment end.

$$M_{th} = b_f t_f F_{yfr} \left(\frac{t_f}{2} + t_s - \frac{\bar{a}}{2}\right) + t_w s_t F_{ywr} \left(\frac{s_t}{2} + t_f + t_s - \frac{\bar{a}}{2}\right) \quad (6.9)$$

Step No. 3

Calculate the depth of the neutral axis at the low moment end, using Eq. (4.30) or Eq. (4.33).

If $A_r F_{yr} + b_f t_f F_{yfr} > s_t t_w F_{ywr}$, then

$$y_1 = \frac{b_f t_f F_{yfr} + s_t t_w F_{ywr} - A_r F_{yr}}{2 b_f F_{yfr}} \quad (4.30)$$

If $A_r F_{yr} + b_f t_f F_{yfr} < s_t t_w F_{ywr}$, then

$$y_2 = \frac{A_r F_{yr} + b_f t_f F_{yfr} + s_t t_w F_{ywr}}{2 t_w F_{ywr}} \quad (4.33)$$

Step. No. 4

Calculate the moment at the low moment end, using Eq. (4.31) or Eq. (4.34).

If y_1 controls, then

$$M_{tl} = s_t t_w F_{ywr}\left(h_r + t_f + \frac{s_t}{2}\right) + b_f (t_f - y_1) F_{yfr}\left(h_r + \frac{y_1}{2} + \frac{t_f}{2}\right)$$

$$- b_f y_1 F_{yfr}\left(h_r + \frac{y_1}{2}\right) \quad (4.31)$$

If y_2 controls, then

$$M_{tl} = A_r F_{yr}(h_r + t_f + s_t - \frac{y_2}{2}) + b_f t_f F_{yfr}(\frac{t_f}{2} + s_t - \frac{y_2}{2})$$

$$+ \tfrac{1}{2} t_w F_{ywr} s_t (s_t - y_2) \qquad (4.34)$$

Step No. 5

Calculate the shear force that satisfies the moment equilibrium equation.

$$V_t = \frac{M_{tl} + M_{th}}{2a} \qquad (6.10)$$

Step No. 6

Adjust the yield stresses for the steel at the low and high moment ends based on V_t:

High Moment End

The concrete shear capacity is based on the previously calculated stress block depth, $\bar{a}$.

$$V_{conc} = 0.21 f'_c \bar{a}\, 3 t_s \qquad (6.11)$$

Calculate the maximum web shear.

$$V_{wmax} = (s_t + t_f) t_w F_{yw} / \sqrt{3} \qquad (6.12)$$

Calculate the shear assigned to steel.

$$V_s = V_t - V_{conc} \tag{6.13}$$

If $V_s < V_{wmax}$, reduce web yield strength

$$F_{ywr} = \left[F_{yw}^2 - 3\left[\frac{V_s}{(s_t + t_f)\ t_w}\right]^2\right]^{\frac{1}{2}} \tag{6.14}$$

If $V_s > V_{wmax}$, $F_{ywr} = 0$ and flange yield stress is reduced by

$$F_{yfr} = \left[F_{yf}^2 - 3\left[\frac{V_s - V_{wmax}}{(b_f - t_w)\ t_f}\right]^2\right]^{\frac{1}{2}} \tag{6.15}$$

Low Moment End

The steel at the low moment end carries all of the shear force, V_t. All of the shear is assigned to the web until it yields. The remainder is assigned to the flange. The web capacity is calculated by using Eq. (6.12). If $V_t < V_{wmax}$, use Eq. (6.14) replacing V_s with V_t. If $V_t > V_{wmax}$, use Eq. (6.15) replacing V_s with V_t.

Step No. 7

Using the reduced yield stresses for the low and high moment ends of the top tee, repeat the sequence beginning with Step No. 1. The solution will converge rapidly (a few iterations) to V_{tmax}(mech).

6.2.3c Total Shear Strength

The total shear strength, V_{max}, is calculated by adding the bottom tee shear strength, V_{bmax}, to the smaller of the top tee shear strengths, V_{tmax}(sh) or V_{tmax}(mech).

6.3 Design Example

A simply-supported composite beam is part of a floor system in which the center-to-center beam spacing is 10' (Fig. 6.2). The span is 40'. The composite beam is composed of a W18 x 45 steel section with a 4" thick concrete slab. The beam is designed for full composite action. A concentric opening with a 12" height and 24" length is to be placed in the beam. The steel has a minimum yield strength of 36 ksi, and the concrete has a nominal compressive strength of 4000 psi. The reinforcing consists of Grade 40 #3 bars placed at 18" at mid-depth in the slab. The live load is 50 lbs/ft^2. For simplicity, a load factor of 1.7 is used for both dead and live loads.

Solution:

For the W18 x 45 steel section with a 12" x 24" opening at mid-height in the steel beam, the section properties are

b_f = 7.477" $\quad$ s_t = 2.431"

t_f = 0.499" $\quad$ s_b = 2.431"

t_w = 0.335" $\quad$ t_s = 4"

d = 17.86" $\quad$ A_r = (71.5/18) x .11 = .44 sq. in.

The cross-sectional dimensions are shown in Fig. 6.3.

The material properties are $F_{yw} = F_{yf}$ = 36 ksi, f'_c = 4000 psi, and F_{yr} = 40 ksi.

The effective slab width must be calculated using AISC (5) requirements.

(1) Span/4 = 40'x 12/4 = 120"

(2) Beam Spacing = 10' = 120"

(3) $16t_s + b_f$ = 16 x 4 + 7.477 = 71.5" ← controls

Therefore, b_{eff} = 71.5"

Load Analysis

Dead Load

Steel Beam	.045 kips/ft
Concrete Slab $\frac{120x4}{144}$ x .15	.500 kips/ft
Total Dead Load	.545 kips/ft

Live Load

$\frac{50 \times 10}{1000}$	.500 kips/ft
Total Load	1.045 kips/ft

Factored Load, w = 1.045 x 1.7 = 1.777 kips/ft.

$$M_{max}(\text{Design}) = \frac{wl^2}{8} = \frac{1.777(40)^2}{8}(12) = 4265 \text{ in-kips}$$

$$V_{max}(\text{Design}) = \frac{wl}{2} = \frac{1.777(40)}{2} = 35.54 \text{ kips}$$

Maximum Moment Capacity

Using Eq. (6.2),

$$T' = 0.335(2.431 + 2.431)36 + 2 \times 36 \times 0.499 \times 7.477$$

$$= 327.3 \text{ kips}$$

$$\bar{a} = 327.3/(0.85 \times 4 \times 71.5) = 1.346"$$

$$M_{max} = 327.3\left(\frac{17.86}{2} + 4 - \frac{1.346}{2}\right) = 4012 \text{ in-kips}$$

Bottom Tee Shear Capacity

Step No. 1

$$y^* = \frac{2.431(0.335)36 + 7.477(0.499)36}{2(7.477)36} = 0.304"$$

Step No. 2

$$M_b = (2.431 \times 0.335 \times 36) \times (\frac{2.431}{2} + 0.499 - \frac{0.304}{2})$$

$$+ (7.477 \times 36 \times 0.499/2) \times (0.499 - 0.304)$$

$$= 58.91 \text{ in-kips}$$

Step No. 3

$$V_b = \frac{2(58.91)}{24} = 4.91 \text{ kips}$$

Step No. 4

$$F_{ywr} = \left[(36)^2 - 3\left[\frac{4.91}{(2.431 + 0.499)0.335}\right]^2\right]^{\frac{1}{2}} = 34.94 \text{ ksi}$$

Step No. 5

Using F_{ywr} and continuing the sequence at Step No. 1, V_b converges to V_{bmax} = 4.82 kips, on the third iteration.

Top Tee Shear Capacity

"Shear" Failure

$$V_{tmax(sh)} = \frac{3.5\sqrt{4000}\ 3(4)^2}{1000} + \frac{(2.431 + 0.499) \times 0.335 \times 36}{\sqrt{3}}$$

$$= 31.02 \text{ kips}$$

"Mechanism" Failure

Step No. 1

$$a = \frac{7.477 \times 0.499 \times 36 + 0.355 \times 2.431 \times 36}{0.85 \times 0.73 \times 4 \times 71.5} = 0.922"$$

Step No. 2

$$M_{th} = 7.477 \times 0.499 \times 36 \times \left(\frac{0.499}{2} + 4 - \frac{0.922}{2}\right)$$

$$+ 0.335 \times 2.431 \times 36 \times \left(\frac{2.431}{2} + 0.499 + 4 - \frac{0.922}{2}\right)$$

$$= 662.9 \text{ in-kips}$$

Step No. 3

$$A_r F_{yr} + b_f t_f F_{yfr} = 0.44 \times 40 + 7.477 \times 0.499 \times 36 =$$

$$= 151.9 \text{ kips}$$

$$s_t t_w F_{ywr} = 2.431 \times 0.335 \times 36 = 29.3 \text{ kips} < 151.9 \text{ kips}$$

Therefore, use Eq. (4.30), (for first iteration, assume web yielded)

$$y_1 = \frac{7.477 \times 0.499 \times 36 - 0.44 \times 40}{2 \times 7.477 \times 36} = 0.217"$$

Step No. 4

$$M_{t1} = 7.477 \times (0.499 - 0.217) \times 36 \times \left(2 + \frac{0.217}{2} + \frac{0.499}{2}\right)$$

$$- 7.477 \times 0.217 \times 36 \times \left(2 + \frac{0.217}{2}\right) = 55.83 \text{ in-kips}$$

Step No. 5

$$V_t = \frac{55.83 + 662.9}{24} = 29.95 \text{ kips}$$

Step No. 6

High Moment End

$$V_{conc} = 0.21 \times 4 \times 0.922 \times 3 \times 4 = 9.29 \text{ kips}$$

$$V_{wmax} = (2.431 \times 0.499) \times 0.335 \times 36/\sqrt{3} = 20.40 \text{ kips}$$

V_s = 29.95 - 9.29 = 20.66 > 20.40, therefore, the web has yielded, and

$F_{ywr} = 0$

Since V_{wmax} is very close to V_s, $F_{yfr} = F_{yf} = 36$ ksi.

Low Moment End

$$V_{wmax} = 20.40 \text{ kips}$$

$V_t > V_{wmax}$, therefore $F_{ywr} = 0$

$$F_{yfr} = \left[(36)^2 - 3\left[\frac{(29.95 - 20.40)}{(7.477 - 0.335)0.499}\right]^2\right]^{\frac{1}{2}} = 35.70 \text{ ksi}$$

Beginning the sequence again at Step No. 1 with the readjusted yield stresses, the calculated shear is on the low side for the second iteration. After 8 iterations, V_t converges to $V_{tmax}(mech)$ = 26.64 kips. However, after 4 iterations, V_t was within 2% of $V_{tmax}(mech)$.

Total Shear Strength

$$V_{bmax} = 4.82 \text{ kips}$$

$$V_{tmax}(sh) = 31.02 \text{ kips}$$

$$V_{tmax}(mech) = 26.64 \text{ kips}$$

$$V_{max} = 4.82 + 26.64 = 31.46 \text{ kips}$$

Using M_{max} = 4012 in-kips and V_{max} = 31.46 kips in Eq. (6.1), the circular interaction curve is calculated, as shown in Fig. 6.4. Fig. 6.4 also shows a curve representing the values of factored moment and shear along the span.

Since the loading on the beam is symmetrical, only one half of the beam needs to be considered. The beam moment-shear diagram crosses the interaction diagram at two points. Between these two points, the combination of moment and shear in the beam is less than the predicted capacity at the web opening. The opening may be placed between the points on the beam represented by the points of intersection of the two curves. For this problem, the points are located 3.3' and 12.05' from the supports. Fig. 6.5 shows the allowable opening locations.

It is interesting to note that if the span of the beam had been 5' shorter, the opening could have been placed anywhere in the beam. Stronger concrete and steel would have increased the strength of the section and increased the allowable locations for the opening. A smaller opening would, also, have increased the capacity at the opening. On the other hand, a slightly higher load would have prohibited the use of such a large opening in the beam.

6.4 Design Interaction Summary

The proposed method for obtaining design interaction curves is simple in concept and can be easily adapted to computer use.

This method can be utilized to determine interaction curves for all sizes and locations of rectangular openings. However, the amount of experimental data substantiating the method is very low. Particularly, further testing is necessary to determine the validity of the method for eccentric openings and different size steel sections. However, for beams with concentric openings, it appears that this procedure provides a conservative prediction of beam capacity.

CHAPTER 7

SUMMARY AND CONCLUSIONS

7.1 Summary

The purpose of this investigation was to study the effects of web openings on composite beams through experimental testing and to develop an ultimate strength model. Six composite beams with concentric rectangular web openings were tested to failure. Varying moment-shear ratios were used to help develop and verify the model. One non-composite steel beam was tested to demonstrate the contribution of the concrete to the capacity of composite beams with web openings. Two steel sections were used, while the concrete slab size was held constant for all beams. Three elastic tests were performed on each beam before it was tested to failure.

The model was developed to predict the ultimate strength of composite beams at the web openings with varying amounts of moment and shear. The model is compared with experimental results and is used to study the effects of key parameters (material strength, opening size and eccentricity) that affect the strength of composite beams with web openings.

A simplified design interaction procedure is presented to conservatively guide the placement of web openings in composite beams.

7.2 Conclusions

1. Based on the experimental study, it is clear that web openings can greatly reduce the strength of composite beams.
2. In the vicinity of the opening, the compressive strains in the concrete remain low, long after the steel begins to yield.

3. The load, at first yield in the steel near the openings, is not representative of the ultimate strength of the beam.
4. The nature of failure in composite beams with web openings is ductile. Concrete failure is preceeded by general yielding of the steel in the vicinity of the opening.
5. The ultimate strength of composite beams at web openings is governed by the failure of the concrete.
6. The concrete and steel exhibit large values of slip prior to failure at the web opening. It is not clear that this has an important effect on strength.
7. The concrete in composite beams contributes, not only, to the flexural strength, but also to the shear strength of the beams at web openings.
8. The moment-shear ratio at an opening has a pronounced effect on ultimate behavior. Beams with high moment-shear ratios fail by general yielding in the steel below the neutral axis and crushing in the concrete. Beams with medium to low moment-shear ratios fail by the formation of plastic hinges in the bottom tee accompanied by a diagonal tension-type failure in the concrete.
9. The contribution of the concrete to shear strength must be considered to obtain an adequate analytical model.
10. The proposed ultimate strength model provides satisfactory predictions of the strength and failure mode of composite beams with web openings. With the exception of one beam, the model conservatively predicts the ultimate strength of the test beams.

11. The ultimate strength model shows that the flexural and shear capacities of beams at web openings are increased as the strengths of the concrete and steel are increased. Increasing the steel strength provides a relatively greater increase in capacity than increasing the concrete strength.
12. Increasing the opening length decreases the shear capacity of a beam, while decreasing the opening length increases the capacity.
13. The eccentricity of an opening affects the flexural and shear capacity of a composite beam. The model predicts that raising an opening will increase the flexural capacity, while lowering an opening will reduce the flexural capacity. The effect on shear capacity depends on the predicted failure mode. If a "mechanism" failure is predicted, raising or lowering an opening will increase the shear strength. If a "shear" failure is predicted, raising an opening will decrease the shear strength, while lowering an opening will increase the shear strength.
14. The simplified interaction curve provides reasonably good agreement with the interaction diagrams developed using the ultimate strength model and will provide designers with a suitable method to assist in the placement of web openings in composite beams.

7.3 Recommendations for Further Study

The use of web openings in composite beams is a design tool with important engineering and economic potential. The ultimate strength

model presented in this report was developed and verified using the results obtained from just eight beams with rectangular concentric web openings. This is too little verification to allow the procedure to be applied to more than a narrow range of applications. The effect of additional variables must be studied. To test the validity of the model for beams with eccentric openings, further experimental testing is required. Only a single slab size was used. The opening sizes in the current tests were limited to 0.6 times the steel beam depth, with an opening length equal to twice the opening depth. Further tests are needed for beams with varying opening sizes and cross-sectional geometries. The finite element technique should prove useful in assisting in the development of an adequate testing program.

Further improvement may be possible in the analytical model by including strain hardening in the steel and the incompatibility of the strains at the steel-concrete interface.

REFERENCES

1. AASHTO, Standard Specifications for Highway Bridges, 12th ed., American Association of State Highway and Transportation Officials, Washington, D.C., 1977.

2. ACI-ASCE Committee 326, "Shear and Diagonal Tension," Journal of the American Concrete Institute, Proc. Vol. 59, No. 1, Jan., 1962, pp. 1-30, No. 2, Feb., 1962, pp. 277-333, No. 3, March, 1962, pp. 353-395.

3. ACI-ASCE Committee 426, "The Shear Strength of Reinforced Concrete Members," Journal of the Structural Division, ASCE, Vol. 99, No. ST6, Proc. Paper 9791, June, 1973, pp. 1091-1187.

4. ACI, Building Code Requirements for Reinforced Concrete (ACI 318-77), American Concrete Institute, Detroit, Michigan, 1977.

5. AISC, Manual of Steel Construction, American Institute of Steel Construction, Inc., New York, 1973, pp. 5-32 - 5-35.

6. ASTM, 1979 Annual Book of ASTM Standards, American Society for Testing and Materials, Philadelphia, Pa., Vol. 14.

7. Bower, John E., "Elastic Stresses Around Holes in Wide-Flange Beams," Journal of the Structural Division, ASCE, Vol. 92, No. ST2, Proc. Paper 4773, April, 1966, pp. 85-101.

8. Bower, John E., "Ultimate Strength of Beams With Rectangular Holes," Journal of the Structural Division, ASCE, Vol. 94, No. ST6, Proc. Paper 5982, June, 1968, pp. 1315-1337.

9. Bower, John E., "Experimental Stresses in Wide-Flange Beams With Holes," Journal of the Structural Division, ASCE, Vol. 92, No. ST5, Proc. Paper 4945, October, 1966, pp. 167-186.

10. Bower, John E., "Design of Beams With Web Openings," Journal of the Structural Division, ASCE, Vol. 94, No. ST3, Proc. Paper 5869, March, 1968, pp. 783-807.

11. British Standards Institution, Composite Construction in Structural Steel and Concrete, British Standard Code of Practice, CP117, Part 2, "Beams for Bridges."

12. Chan, P. W., and Redwood, R. G., "Stresses in Beams With Circular Eccentric Web Holes," Journal of the Structural Division, ASCE, Vol. 100, No. ST1, Proc. Paper 10291, January, 1974, pp. 231-248.

13. Congdon, J. G., and Redwood, R. G., "Plastic Behavior of Beams With Reinforced Holes," Journal of the Structural Division, ASCE, Vol. 96, No. ST9, Proc. Paper 7561, September, 1970, pp. 1933-1955.

14. Cooper, P. B., Snell, R. R., and Knostman, H. D., "Failure Tests on Beams With Eccentric Web Holes," Journal of the Structural Division, ASCE, Vol. 103, No. ST9, Proc. Paper 13202, September, 1977, pp. 1731-1737.

15. Davies, C., "Steel-Concrete Composite T-beams With Welded Stud Connectors," thesis presented to the University of London, in 1966, in partial fulfillment of the requirements for the degree of Master of Science (Eng).

16. Granade, C. J., "An Investigation of Composite Beams Having Large Rectangular Openings in Their Webs," thesis presented to the University of Alabama, at University, Ala., in 1968, in partial fulfillment of the requirements for the degree of Master of Science.

17. Horne, M. R., Plastic Theory of Structures, The M.I.T. Press, Cambridge, Mass., 1971.

18. Knostman, H. D., Cooper, P. B., and Snell, R. R., "Shear Force Distribution at Eccentric Web Openings," Journal of the Structural Division, ASCE, Vol. 103, No. ST6, Proc. Paper 12999, June 1977, pp. 1207-1221.

19. Kupfer, H., Hilsdorf, H. K., and Rusch, H., "Behavior of Concrete Under Biaxial Stress," Journal of the American Concrete Institute, Proc. V. 66, No. 8, Aug., 1969, pp. 656-666.

20. Kuzmanovic, B. O. and Willems, N., Steel Design for Structural Engineers, Prentice-Hall, New Jersey, 1977, pp. 370-371.

21. Neal, B. G., The Plastic Method of Structural Analysis, Halsted Press, New York, 1977, pp. 48.

22. Redwood, R. G., and McCutcheon, J. O., "Beam Tests With Unreinforced Web Openings," Journal of the Structural Division, ASCE, Vol. 94, No. ST1, Proc. Paper 5706, January, 1968, pp. 1-17.

23. Redwood, R. G., "Tables for Plastic Design of Beams With Rectangular Holes," Engineering Journal, AISC, Vol. 9, No. 1, January, 1972.

24. Redwood, R. G., Baranda, H., and Daly, M. J., "Tests of Thin-Webbed Beams With Unreinforced Holes," Journal of the Structural Division, ASCE, Vol. 104, No. ST3, Proc. Paper 13624, March, 1978, pp. 577-595.

25. Redwood, R. G., and Uenoya, M., "Critical Loads for Webs With Holes," Journal of the Structural Division, ASCE, Vol. 105, No. ST10, Proc. Paper 14925, October, 1979, pp. 2053-2076.

26. Segner, Edmund P., "Reinforcement Requirements for Girder Web Openings," Journal of the Structural Division, ASCE, Vol. 90, No. ST3, Proc. Paper 3919, June, 1964, pp. 147-164.

27. Shrivastava, S. C., and Redwood, R. G., "Shear Carried by Flanges at Unreinforced Web Holes," Journal of the Structural Division, ASCE, Vol. 105, No. ST8, Tech. Note, August, 1979, pp. 1706-1711.

28. "Suggested Design Guides for Beams With Web Holes," by the Subcommittee on Beams with Web Openings of the Task Committee on Flexure Members of the Structural Division, John E. Bower, Chmn., Journal of the Structural Division, ASCE, Vol. 97, No. ST11, Proc. Paper 8536, November, 1971, pp. 2707-2728.

29. Swartz, S. E., and Eliufoo, K. S., "Composite Beams With Web Openings," Journal of the Structural Division, ASCE, Vol. 106, No. ST5, Tech. Note, pp. 1203-1208.

30. Todd, D. M., and Cooper, P. B., "Strength of Composite Beams With Web Openings," Journal of the Structural Division, ASCE, Vol. 106, No. ST2, Proc. Paper 15179, February, 1980, pp. 431-444.

31. Wang, T-M, Snell, R. R., and Cooper, P. B., "Strength of Beams With Eccentric Reinforced Holes," Journal of the Structural Division, ASCE, Vol. 101, No. ST9, Proc. Paper 11540, September, 1975, pp. 1783-1799.

32. Winter, George, and Nilson, Arthur H., Design of Concrete Structures, 9th ed., McGraw-Hill, 1979, pp. 60.

TABLE 2.1

CONCRETE PROPERTIES

	Slump (in)	Cement Factor (sacks/yd^3)	Age at Test (days)	f'_c (psi)	f_r (psi)	% Air
Beam No. 1	1½	5½	180	7000	---	5.0
Beam No. 2	5½	5½	13	4200	675	4.8
Beam No. 3	½	5	21	4930	600	6.0
Beam No. 4	1¼	5	10	4460	470	3.2
Beam No. 5	2	6	8	4680	590	2.5
Beam No. 6	1½	6	14	4020	510	4.0

TABLE 2.2

STEEL PROPERTIES

	TOP FLANGE			BOTTOM FLANGE			WEB (HORIZ.)			WEB (VERT.)			REINFORCING STEEL	
	Yield (ksi)	Static Yield (ksi)	Tensile (ksi)	Yield (ksi)	Static Yield (ksi)	Tensile (ksi)	Yield (ksi)	Static Yield (ksi)	Tensile (ksi)	Yield (ksi)	Static Yield (ksi)	Tensile (ksi)	Yield (ksi)	Tensile (ksi)
Beam No. 1	39.37	34.92	61.33	40.39	35.84	61.85	38.54	34.57	60.93	-----	-----	-----	-----	-----
Beam No. 2	39.27	38.88	68.84	39.88	38.97	69.39	42.44	40.58	70.55	-----	-----	-----	54.50	82.00
Beam No. 3	39.27	38.88	68.84	39.88	38.97	69.39	42.44	40.58	70.55	-----	-----	-----	54.50	82.00
Beam No. 4	46.39	44.38	73.28	44.89	41.24	71.42	52.00	48.71	74.86	-----	50.81	74.67	54.50	82.00
Beam No. 5	43.88	40.93	65.40	45.10	41.86	67.05	44.23	39.47	63.70	43.62	40.77	63.94	59.10	87.20
Beam No. 6	42.94	39.44	67.11	43.47	39.57	66.61	49.80	43.76	67.05	48.12	43.67	67.79	59.10	87.20

TABLE 2.3

BEAM GEOMETRIC PROPERTIES

	Steel Section	d (in)	b_f (Top) (in)	t_f (Top) (in)	t_w (in)	s_t (in)	s_b (in)
Beam No. 1	W14 x 34	14	6.75	0.453	0.287	2.55	2.55
Beam No. 2	W18 x 45	$17^7/_8$	7.50	0.475	0.356	3.00	3.25
Beam No. 3	W18 x 45	$17^7/_8$	7.50	0.475	0.356	3.13	3.13
Beam No. 4	W18 x 45	$17^7/_8$	7.50	0.485	0.343	3.00	3.06
Beam No. 5	W18 x 46	$18^1/_8$	6.00	0.623	0.380	3.06	3.13
Beam No. 6	W14 x 34	14	6.69	0.475	0.296	2.38	2.38

	b_f (Bot.) (in)	t_f (Bot.) (in)	$b_{conc.}$ (in)	M/V (ft)	t_s (in)	Opening Size (in)
Beam No. 1	6.75	0.453	48.0	7	4	8 x 16
Beam No. 2	7.50	0.520	48.0	9	4	$10^{13}/_{16}$ x $21^5/_8$
Beam No. 3	7.50	0.520	48.0	33	4	$10^{13}/_{16}$ x $21^5/_8$
Beam No. 4	7.50	0.495	48.0	3	4	$10^{13}/_{16}$ x $21^5/_8$
Beam No. 5	6.00	0.615	48.0	6	4	$10^{13}/_{16}$ x $21^5/_8$
Beam No. 6	6.69	0.423	48.0	3	4	8 x 16

TABLE 3.1

TEST RESULTS

	FIRST YIELD				
	$\frac{M}{V}$ at Opening (ft)	P_{total} (P_{1y})* (kips)	M at Opening (in-kips)	V at Opening (kips)	Location
Beam No. 1	7	26.5	1110	13.3	B. Tee
Beam No. 2	9	16.8	680	6.30	T. Tee
Beam No. 3	33	31.7	1570	3.96	B. Tee
Beam No. 4	3	42.4	763	21.2	T. Tee
Beam No. 5	6	20.7	745	10.4	B. Tee
Beam No. 6	3	16.1	290	8.05	T. Tee

	MAXIMUM LOAD				
	P_{total} (P_{ult}) (kips)	M at Opening (in-kips)	V at Opening (kips)	$\frac{P_{1y}}{P_{ult}}$	Mode of Failure
Beam No. 1	64.5	2710	32.2	0.41	Shear Failure in Concrete Over Opening
Beam No. 2	96.2	3900	36.1	0.17	Shear Failure in Concrete Over Opening
Beam No. 3	106.5	5270	13.3	0.30	Crushing in Concrete Above Opening
Beam No. 4	93.0	1670	46.5	0.46	Shear Failure in Concrete Over Opening
Beam No. 5	94.0	3380	47.0	0.22	Shear Failure in Concrete Over Opening
Beam No. 6	77.8	1420	39.4	0.21	Shear Failure in Concrete Over Opening

* Applied load including load system

TABLE 5.1a

COMPARISON OF PROPOSED MODEL WITH EXPERIMENTAL TESTS
(BASED ON APPLIED LOAD)

CURRENT TESTS	M/V (ft)	PREDICTED V_t/V	PREDICTED V (kips)	PREDICTED M (in-kips)	PREDICTED "Mode" of Failure[t]
Beam No. 1	7	0.84	25.9	2180	Mech.
Beam No. 2	9	0.79	31.2	3370	Mech.
Beam No. 3	33	0.81	11.0	4300	Mech.
Beam No. 4	3	0.81	48.8	1860	Mech.
Beam No. 5	6	0.80	41.2	2970	Mech.
Beam No. 6	3	0.82	36.7	1320	Mech.
GRANADE TESTS					
No. 1	2	0.74	28.0	672	Shear
No. 2	4	0.74	25.6	1230	Shear

CURRENT TESTS	OBSERVED V (kips)	OBSERVED M (in-kips)	OBSERVED "Mode" of Failure[t]	% Diff. R	Predicted Point of Contraflexure (Bottom Tee) (in)	Opening Length (in)
Beam No. 1	32.2	2710	Shear	24.0	4.74(L)	16.0
Beam No. 2	36.1	3900	Shear	16.0	5.93(L)	21.625
Beam No. 3	13.3	5270	Mech.	27.0	6.63(L)	21.625
Beam No. 4	46.5	1670	Shear	-4.0	3.44(L)	21.625
Beam No. 5	47.0	3380	Shear	14.0	4.89(L)	21.625
Beam No. 6	39.4	1420	Shear	7.0	2.98(L)	10.00
GRANADE TESTS						
No. 1	32.4	780	Shear	16.0	.22(L)	7.2
No. 2	26.4	1270	Shear	3.0	1.19(L)	7.2

t - See Sections 4.4 and 5.2.1 for an explanation.
(L) - Measured from the opening centerline toward the Low Moment End.

TABLE 5.1b

COMPARISON OF PROPOSED MODEL WITH EXPERIMENTAL TESTS

(BASED ON APPLIED LOAD PLUS DEAD LOAD)

CURRENT TESTS	PREDICTED $\frac{V_t}{V}$	V (kips)	M (in-kips)
Beam No. 1	0.84	25.8	2230
Beam No. 2	0.79	31.0	3460
Beam No. 3	0.81	11.2	4370
Beam No. 4	0.81	48.8	1860
Beam No. 5	0.80	41.1	3010
Beam No. 6	0.82	36.7	1320
GRANADE TESTS			
No. 1	0.74	28.0	672
No. 2	0.74	25.6	1230

CURRENT TESTS	OBSERVED $\frac{M}{V}$	V (kips)	M (in-kips)	% Diff. R
Beam No. 1	7.2	33.4	2887	29.3
Beam No. 2	9.3	36.8	4099	18.7
Beam No. 3	32.5	14.0	5468	25.0
Beam No. 4	3.0	47.6	1723	-2.5
Beam No. 5	6.1	48.1	3513	17.0
Beam No. 6	3.0	40.4	1470	10.0
GRANADE TESTS				
No. 1	2.0	32.7	790	16.8
No. 2	4.1	26.5	1295	3.5

TABLE 5.2

PREDICTED PURE SHEAR AND MOMENT STRENGTHS FOR TEST BEAMS

CURRENT TESTS	V_{tmax}(mech) (kips)	V_{tmax}(sh) (kips)	V_{bmax} (kips)	V_{max} (kips)	M_{max} (in-kips)
Beam No. 1	33.0	31.3	6.0	27.2	2878
Beam No. 2	36.3	40.1	9.4	45.6	4630
Beam No. 3	37.6	37.8	8.7	46.3	4660
Beam No. 4	40.1	40.2	9.7	49.7	7040
Beam No. 5	39.1	43.4	9.8	48.9	4930
Beam No. 6	34.1	31.8	6.8	38.5	2990
GRANADE TEST					
No. 1 + No. 2	56.9	21.0	7.2	28.2	1740

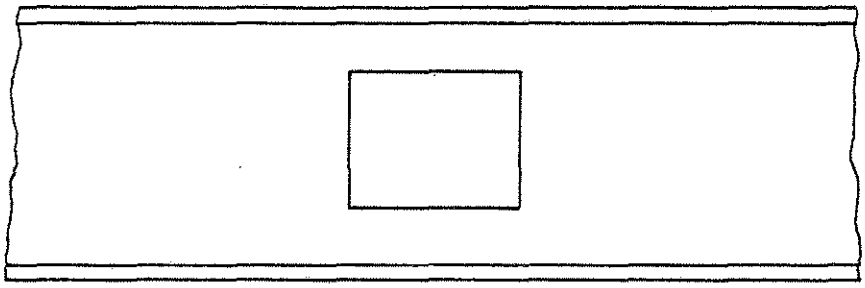

Fig. 1.1 Web Opening in Steel Beam

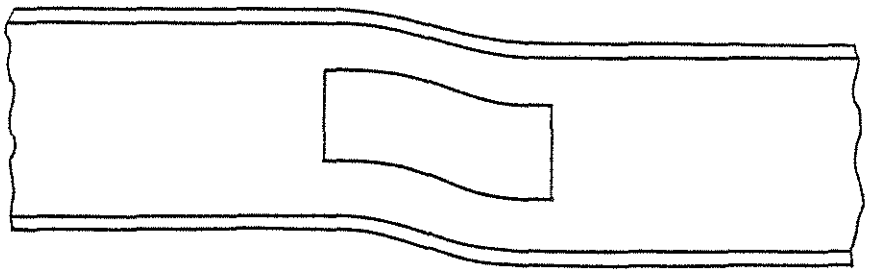

Fig. 1.2 Web Opening with Points of Contraflexure at Opening Centerline

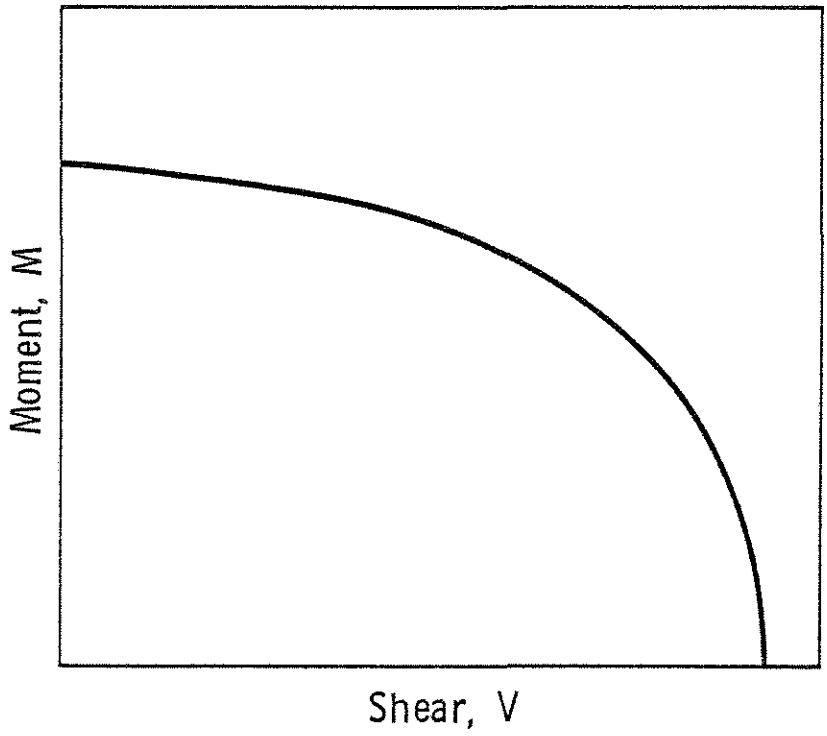

Fig. 1.3 Moment-Shear Interaction Diagram

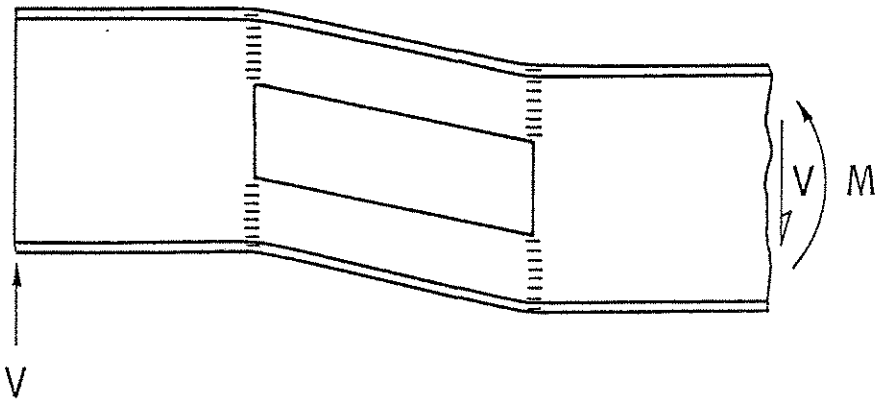

Fig. 1.4 Four-Hinge Failure Mechanism at Web Opening

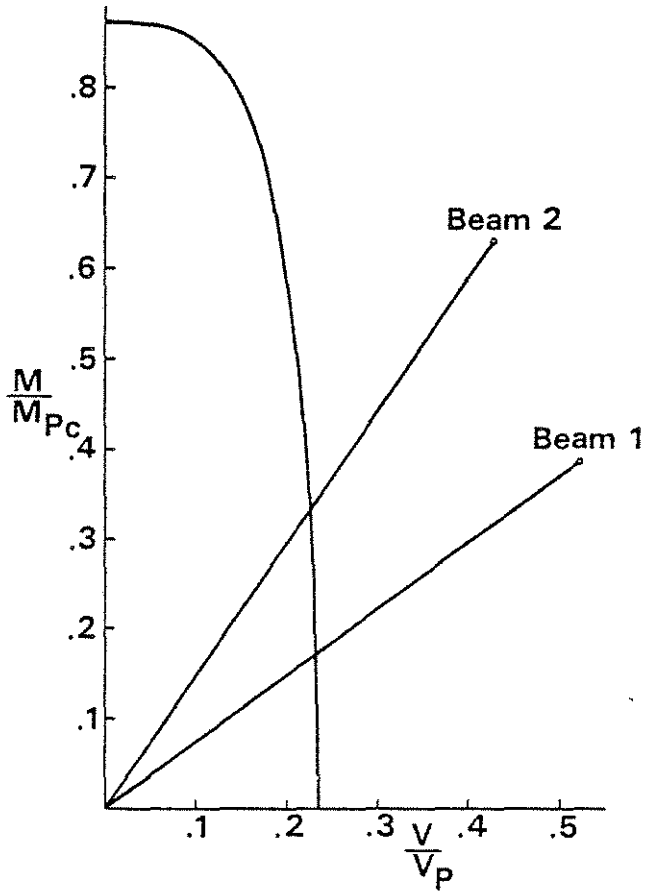

Fig. 1.5 Comparison of Todd-Cooper Model with Granade's Beams (30)

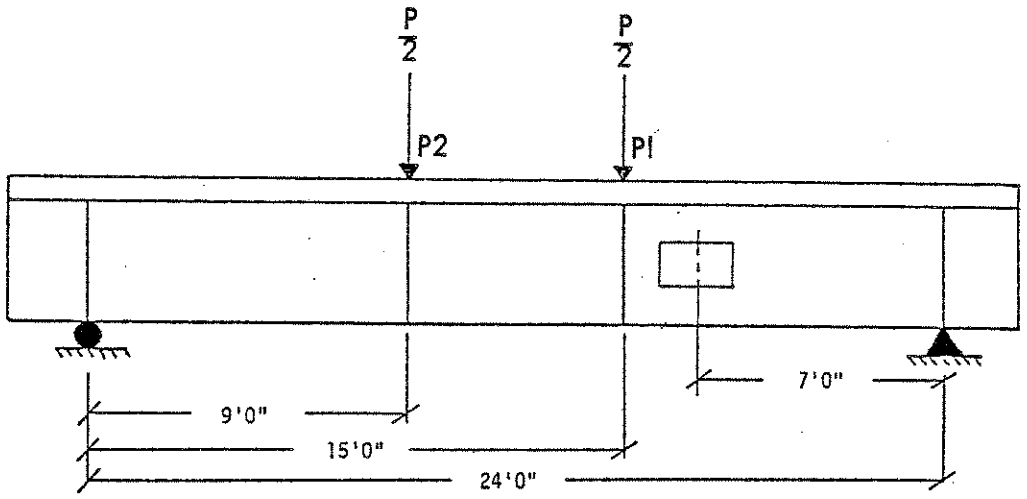

Beam No. 1

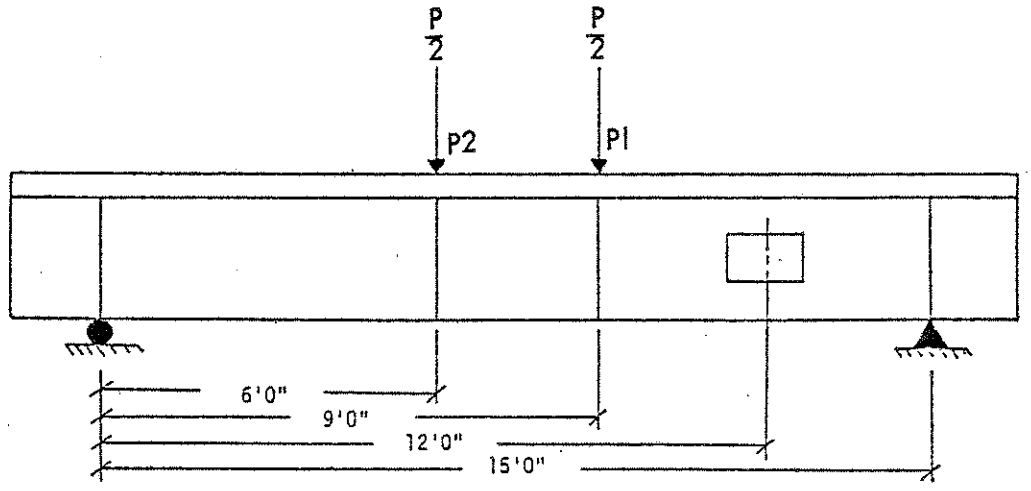

Beam No. 6

Fig. 2.1 Test Layouts for Beams No. 1 and 6

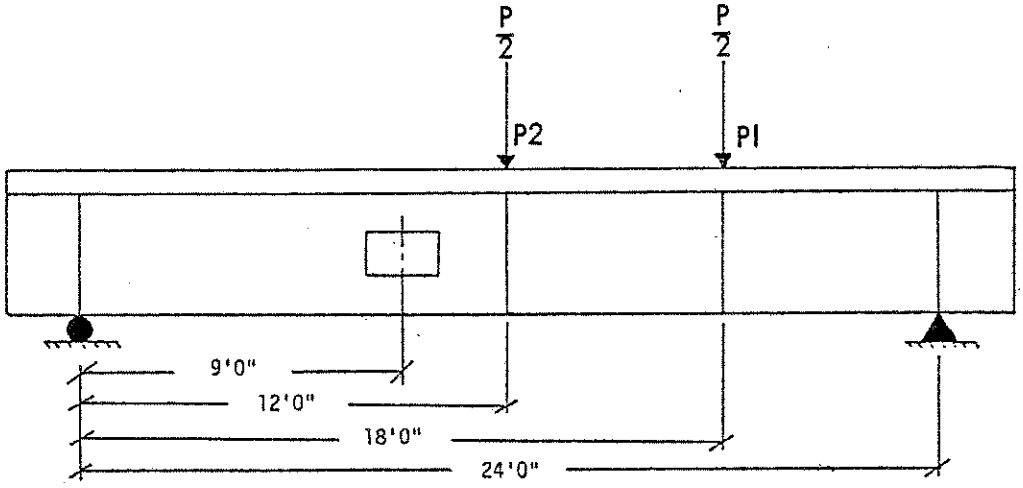

Beam No. 2

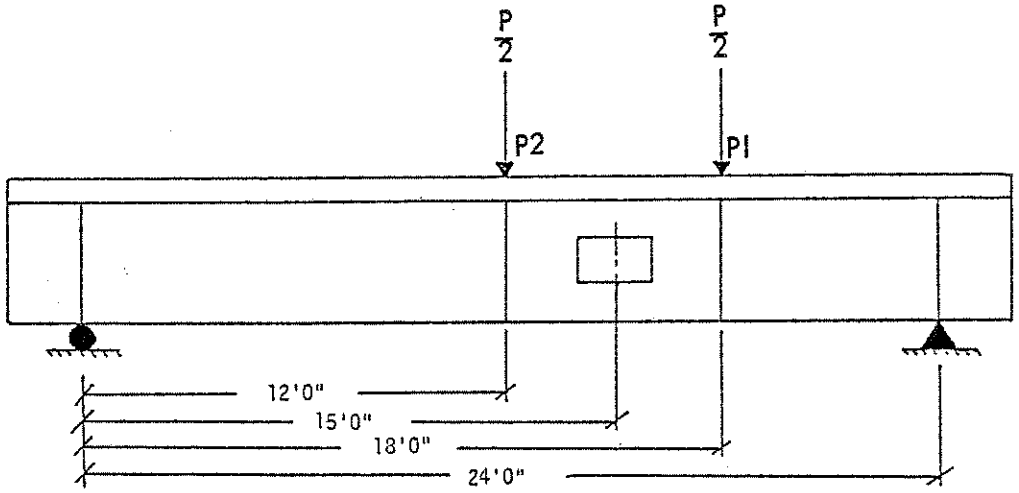

Beam No. 3

Fig. 2.2 Test Layouts for Beams No. 2 and 3

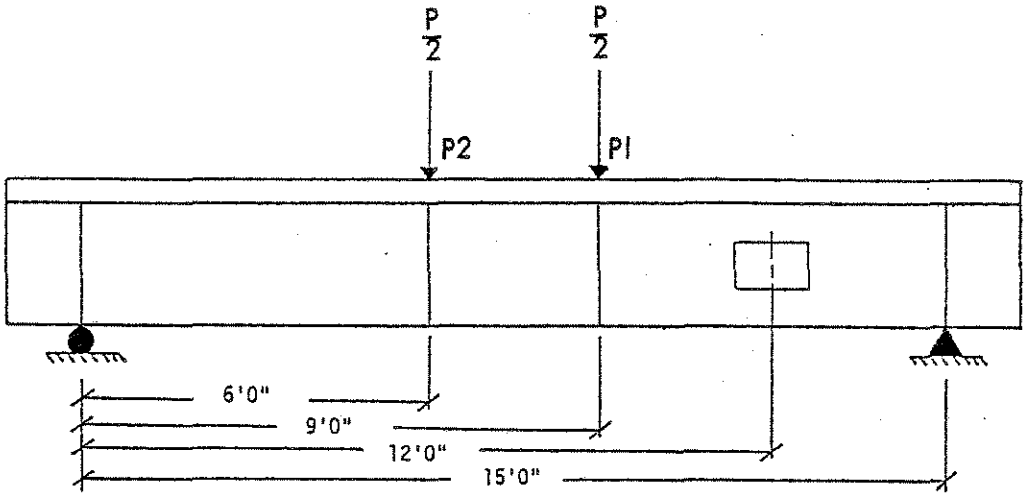

Beam No. 4

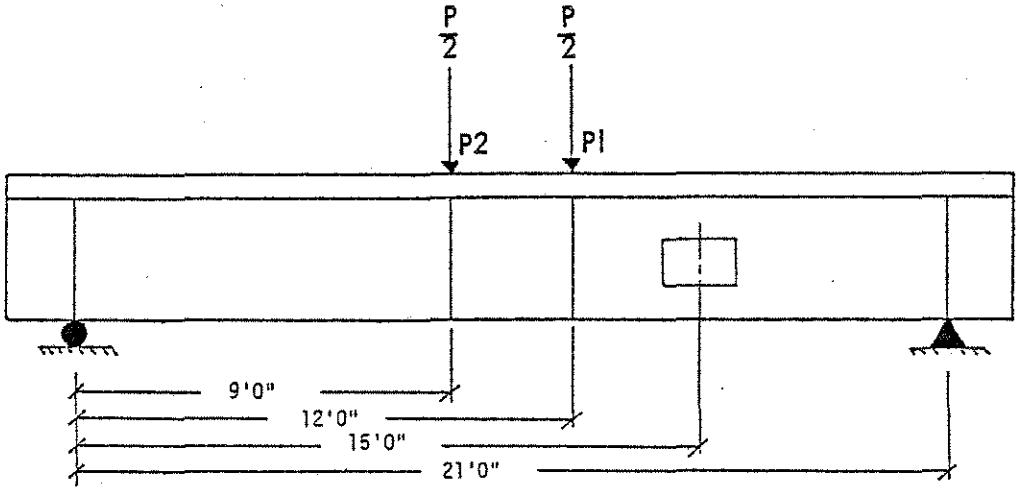

Beam No. 5

Fig. 2.3 Test Layouts for Beams No. 4 and 5

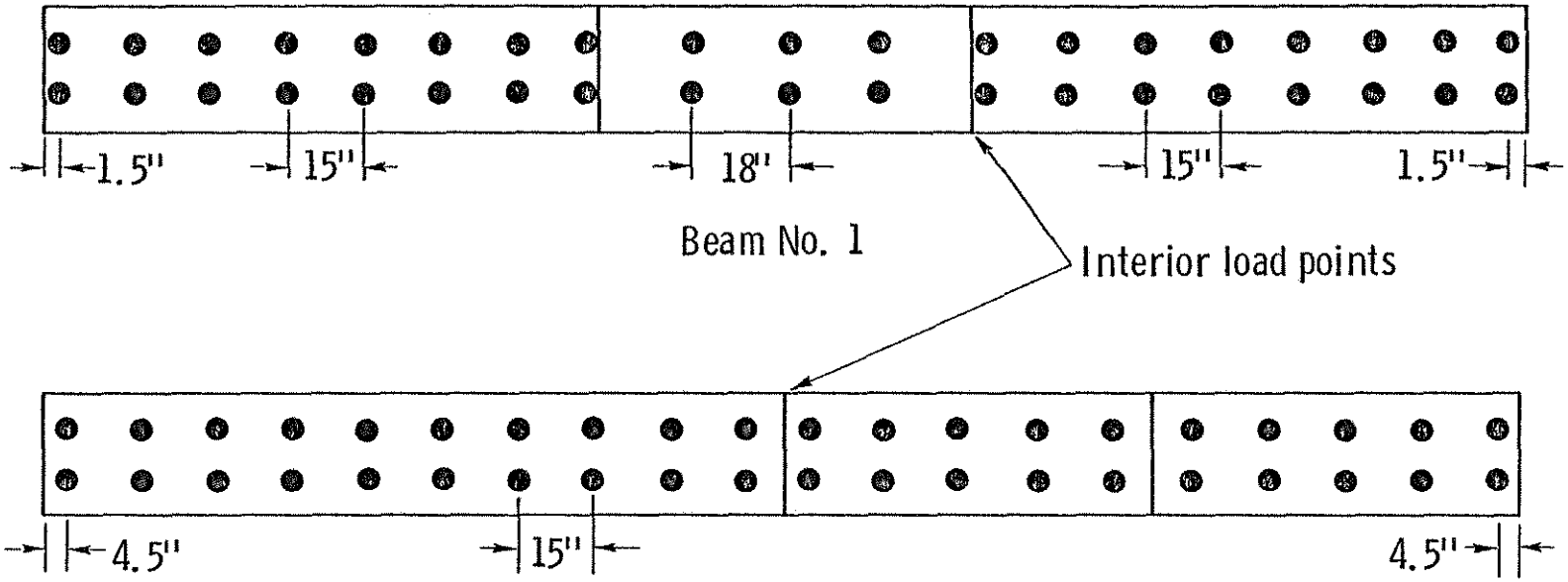

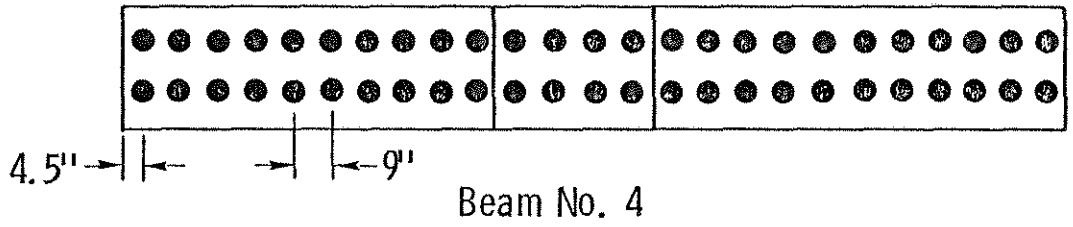

Fig. 2.4 Shear Stud Locations

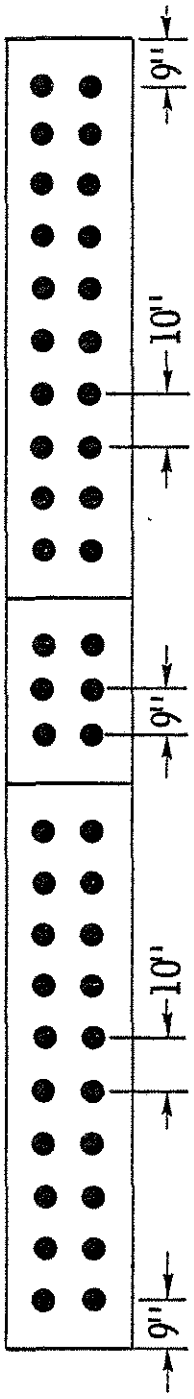

Beam No. 5

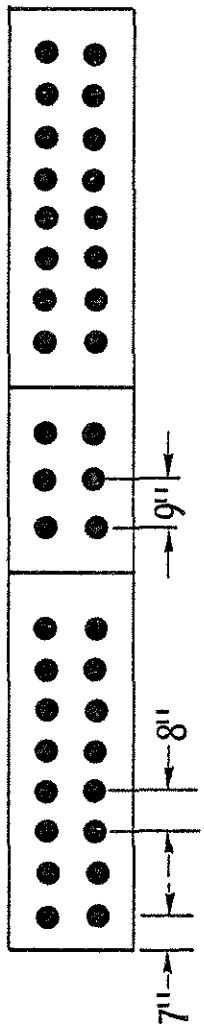

Beam No. 6

Fig. 2.4 Shear Stud Locations (cont'd)

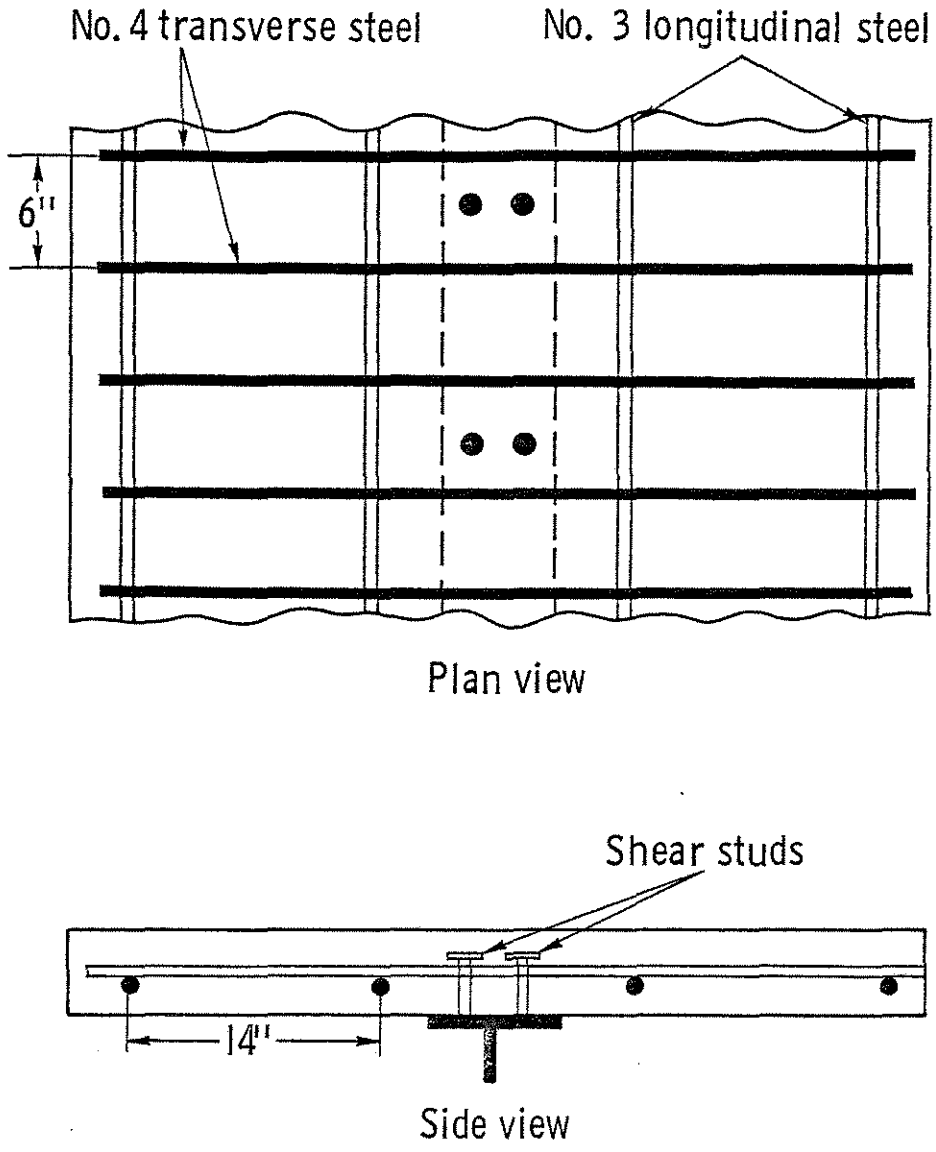

Fig. 2.5 Reinforcing Steel

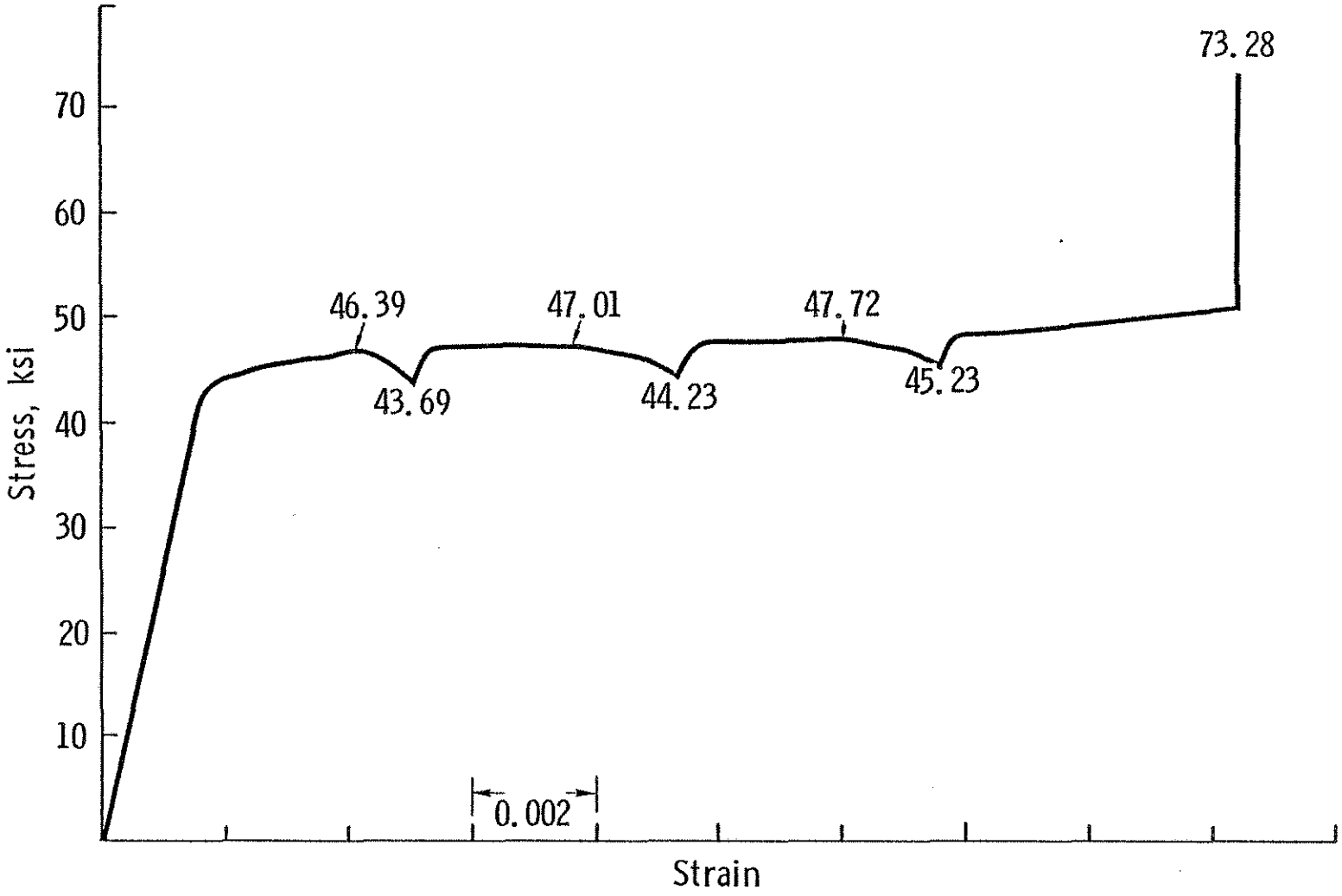

Fig. 2.6 Typical Stress-Strain Curve for Structural Steel

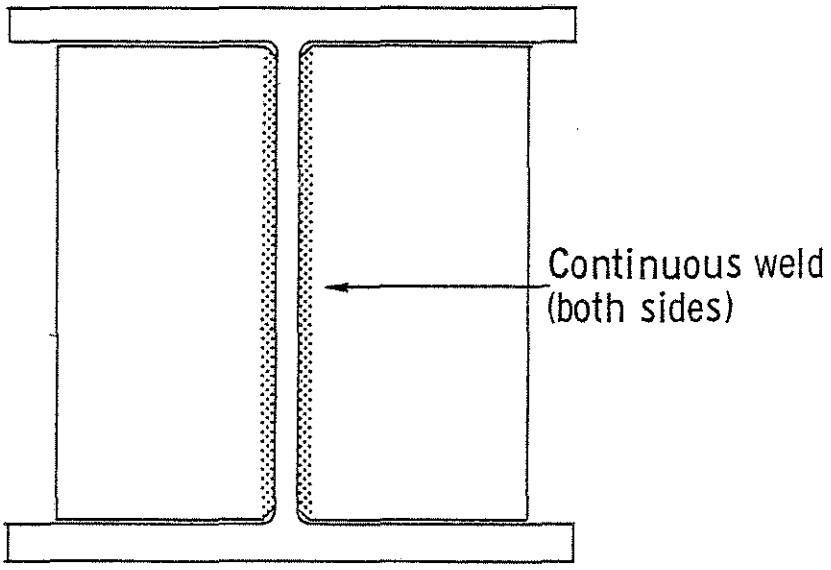

Fig. 2.7 Stiffener Detail

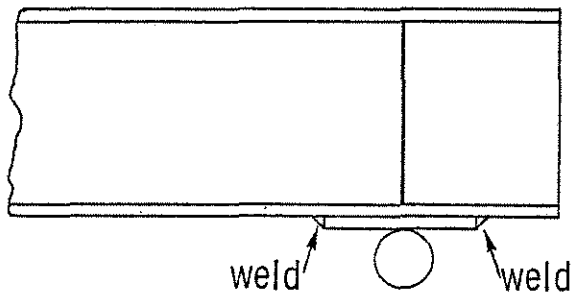

Fig. 2.8 Bearing Plate Detail

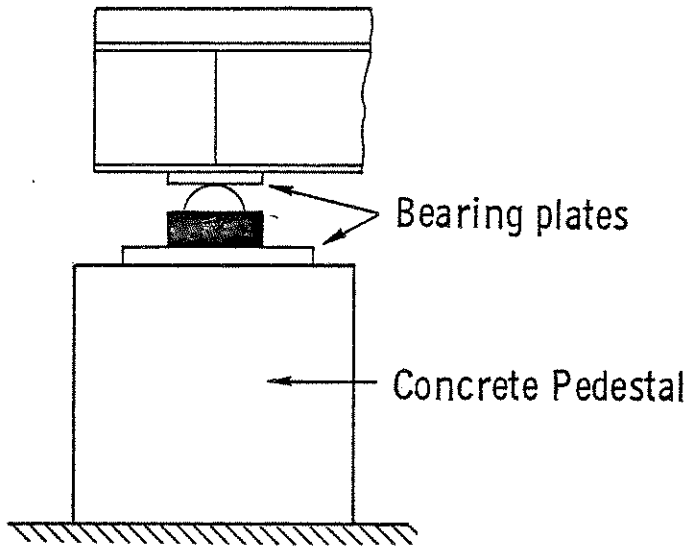

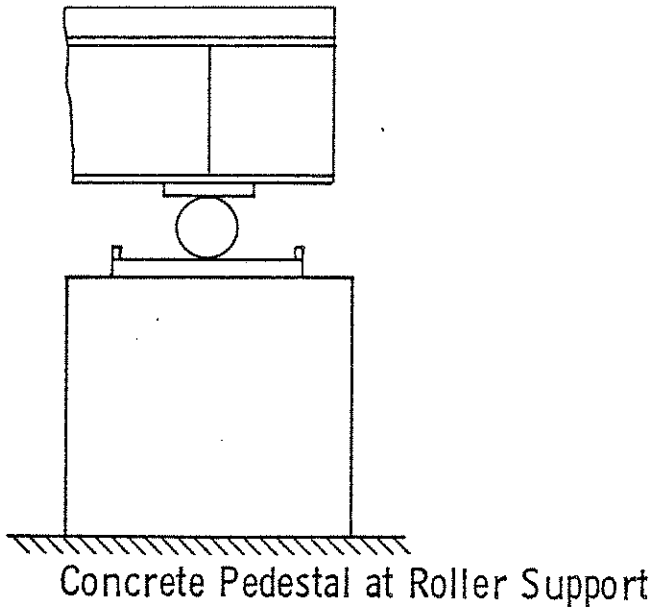

Fig. 2.9 Concrete Support Pedestals

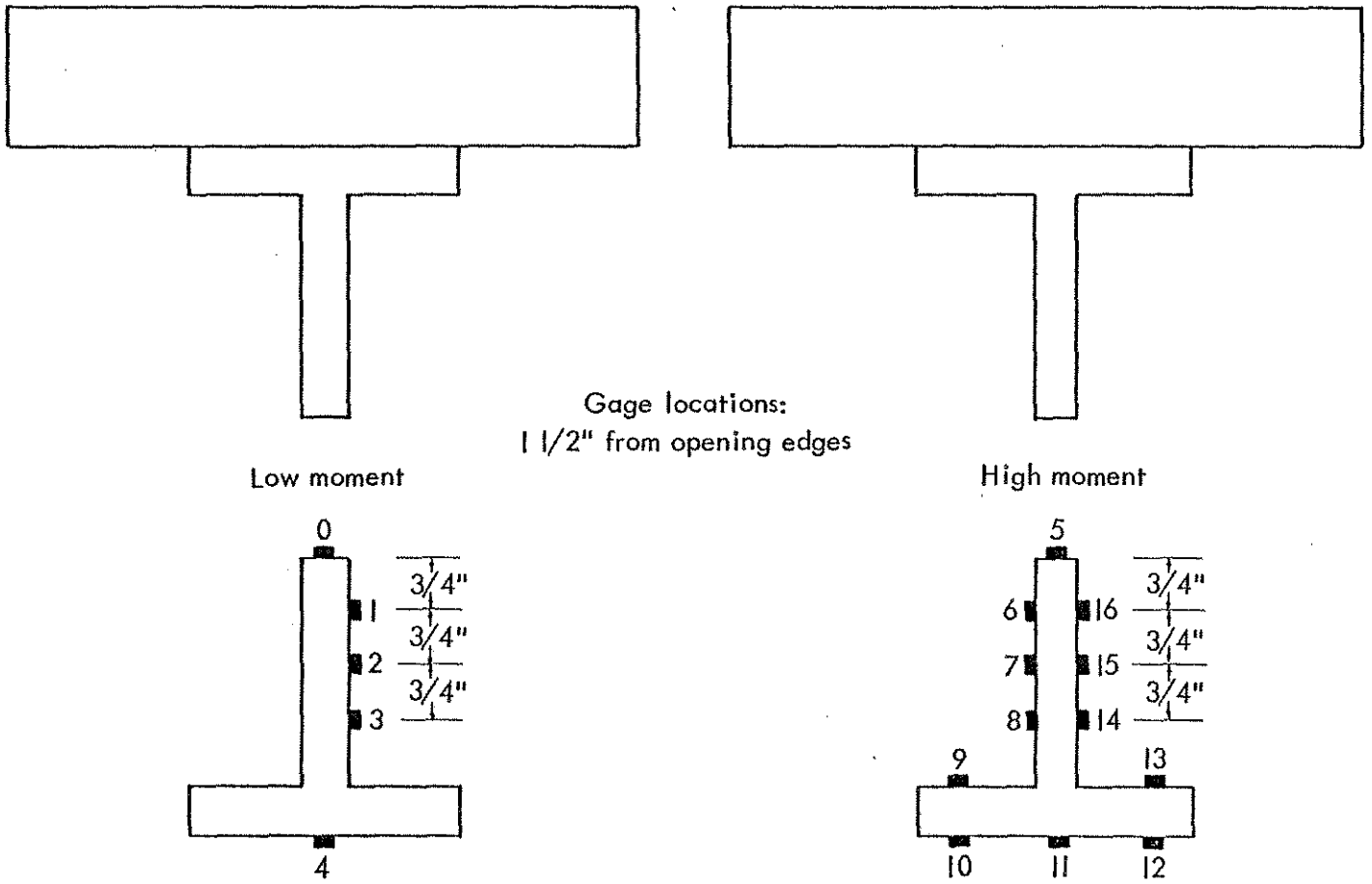

Fig. 2.10 Strain Gage Locations for Beam No. 1

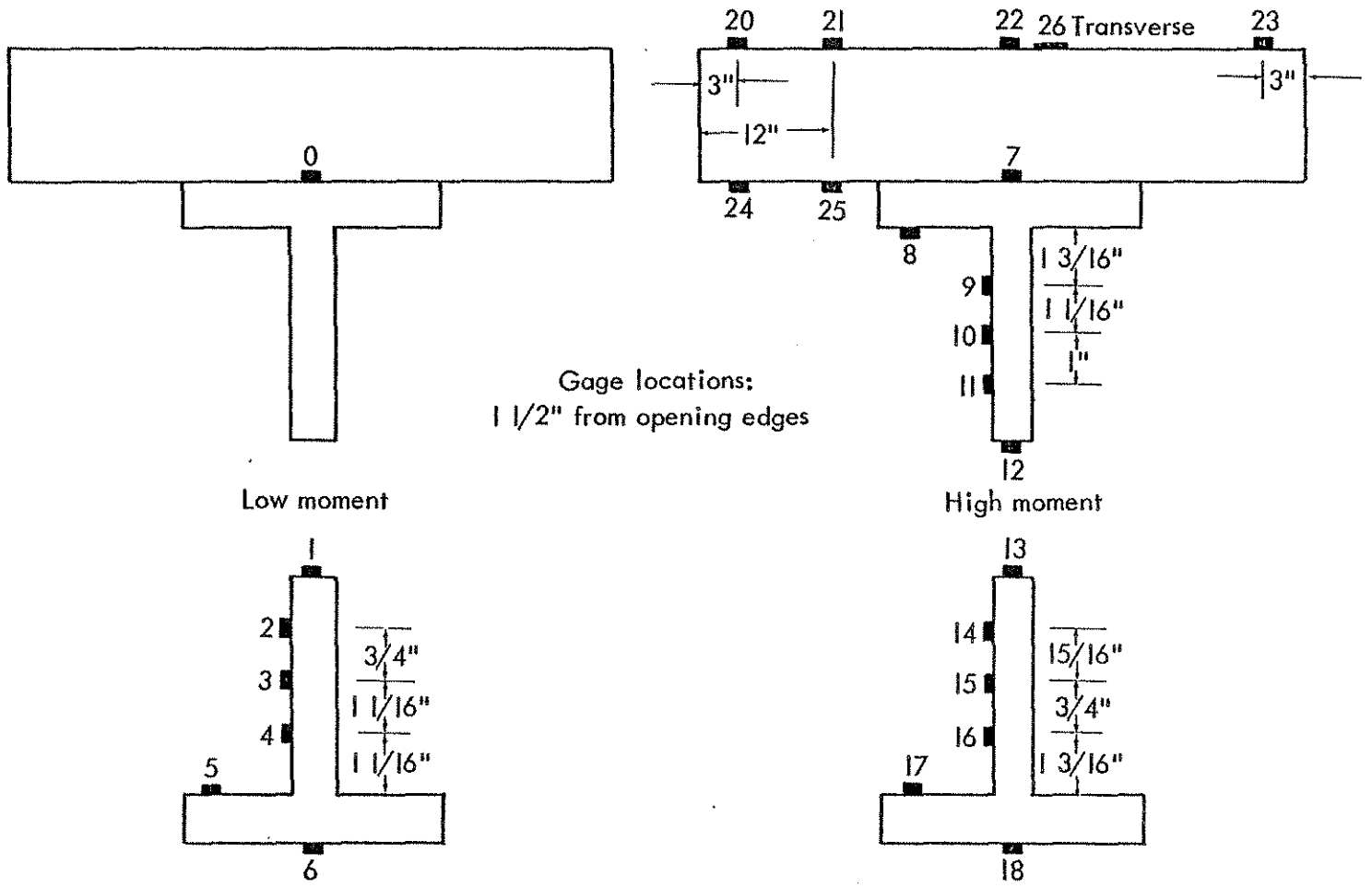

Fig. 2.11 Strain Gage Locations for Beam No. 2

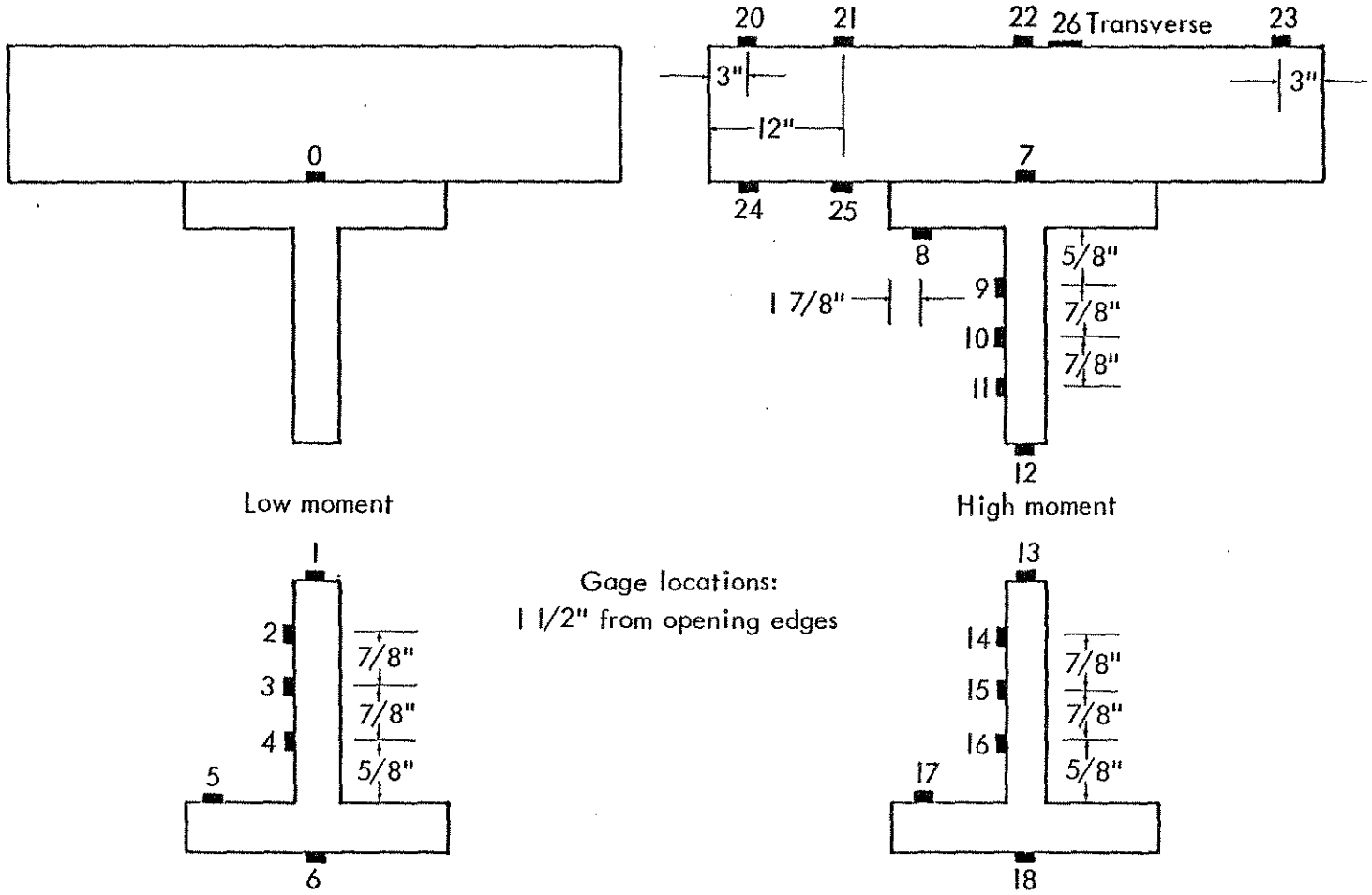

Fig. 2.12 Strain Gage Locations for Beam No. 3

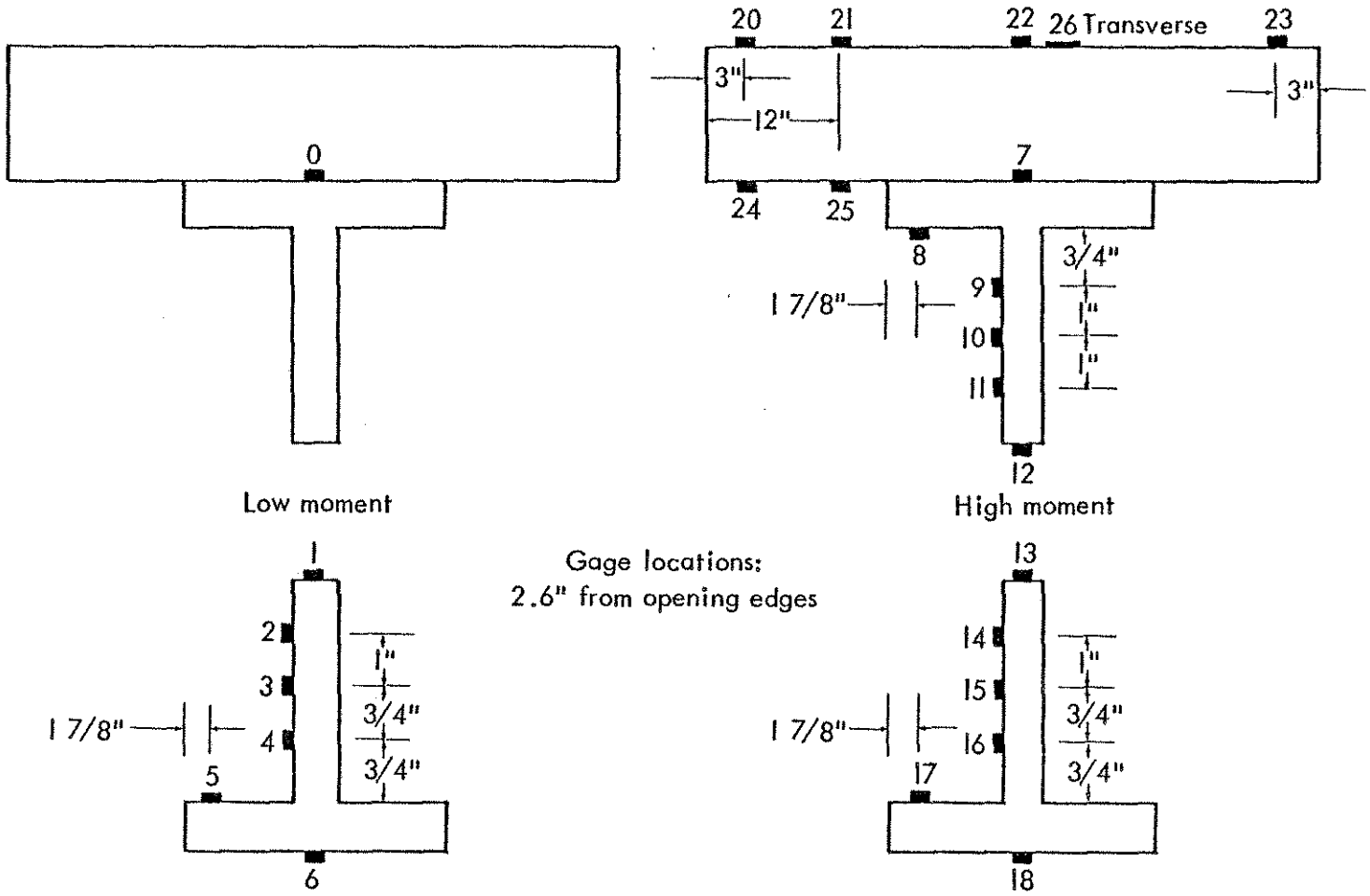

Fig. 2.13 Strain Gage Locations for Beam No. 4

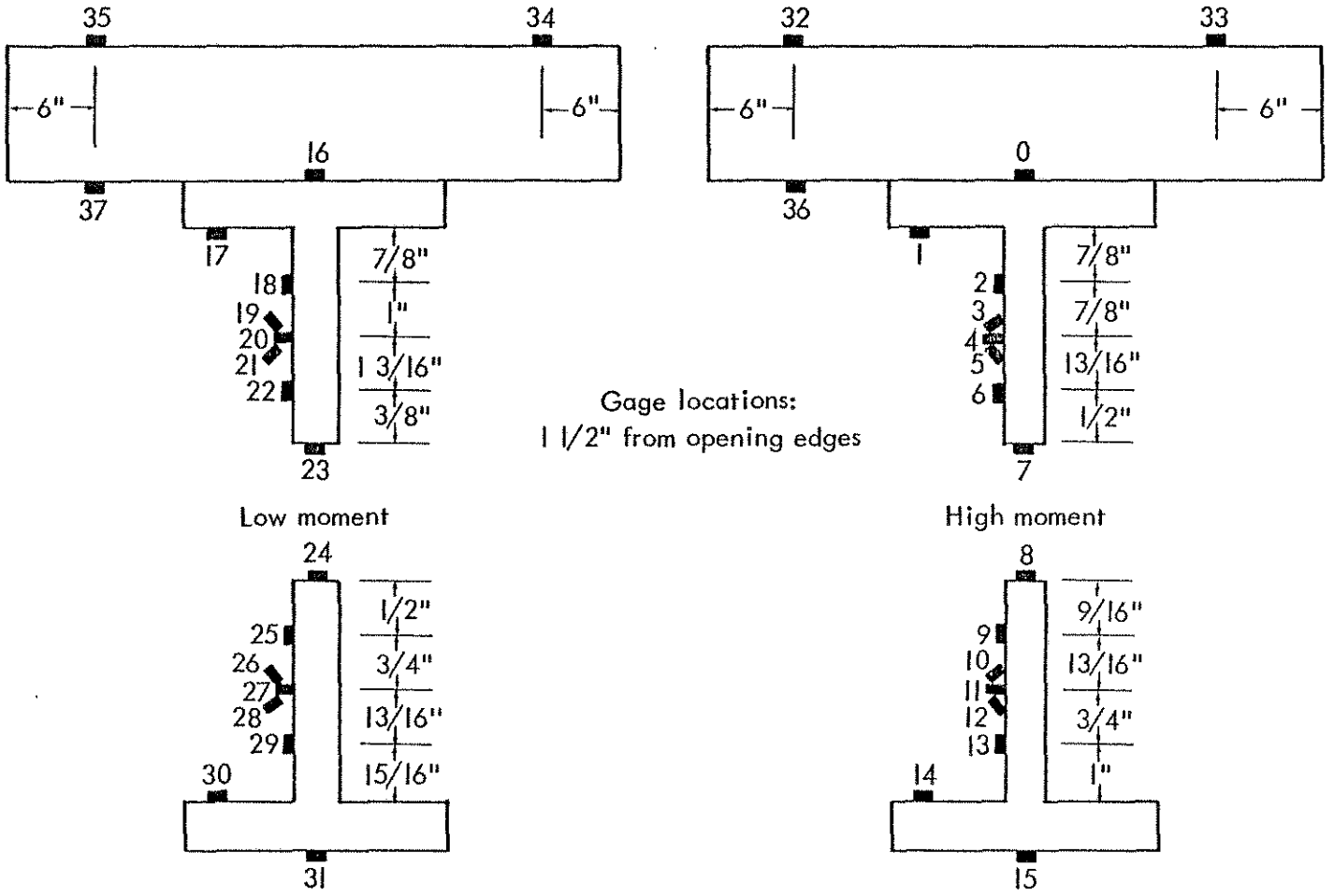

Fig. 2.14 Strain Gage Locations for Beam No. 5

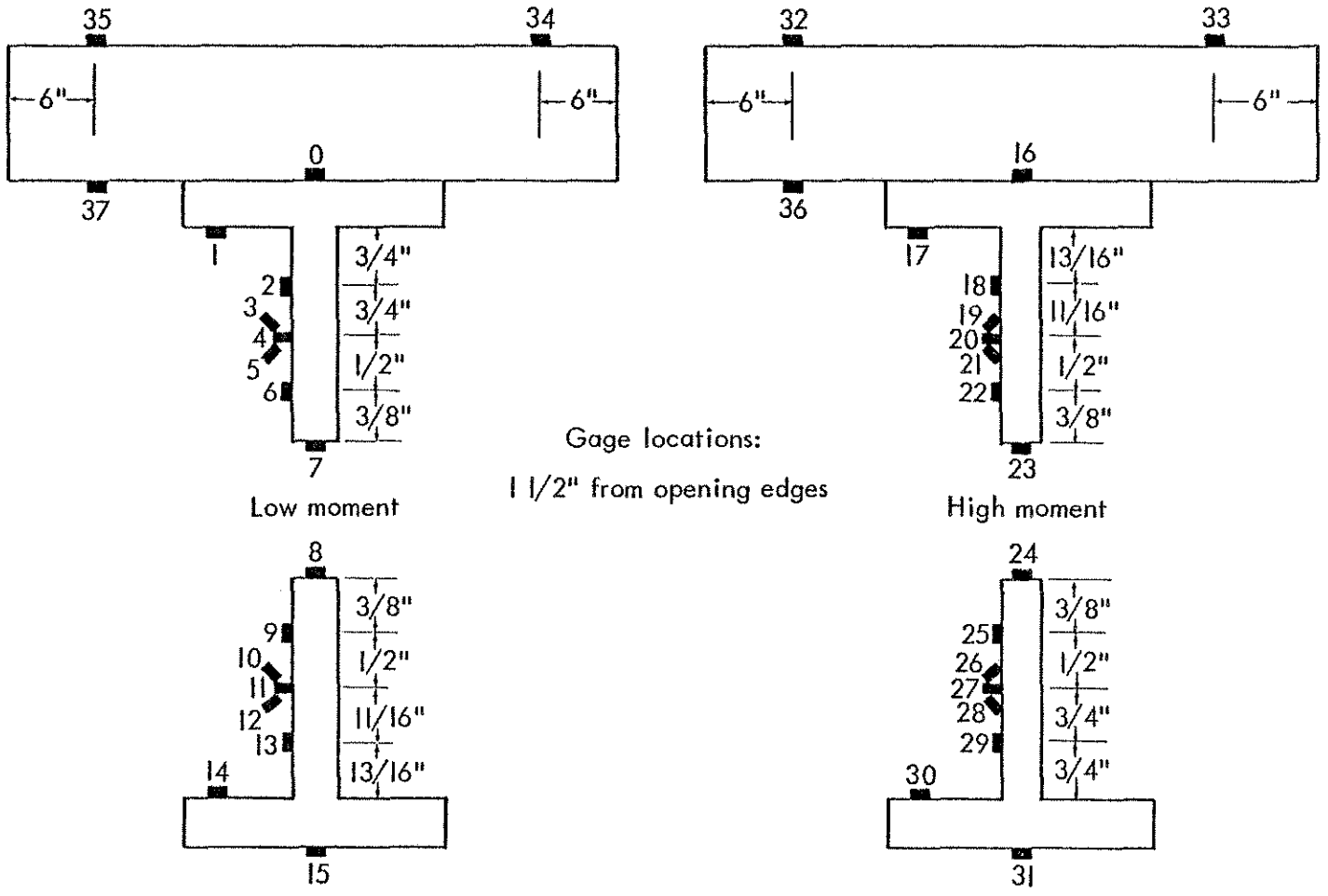

Fig. 2.15 Strain Gage Locations for Beam No. 6

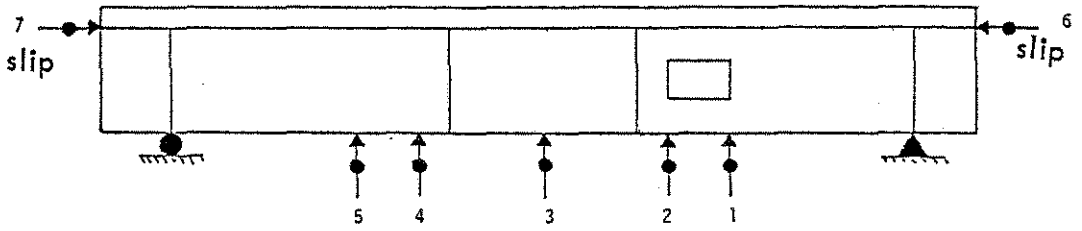

Beam No. 1

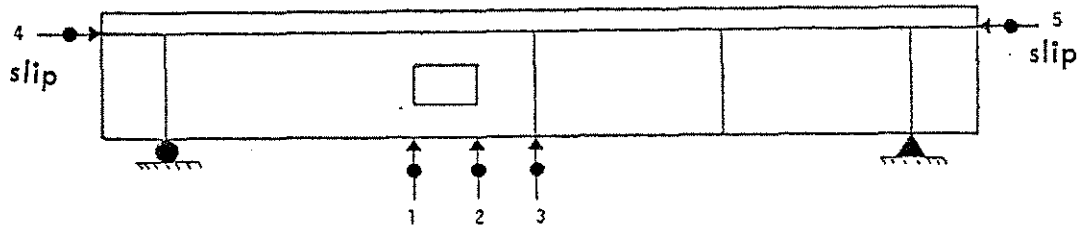

Beam No. 2

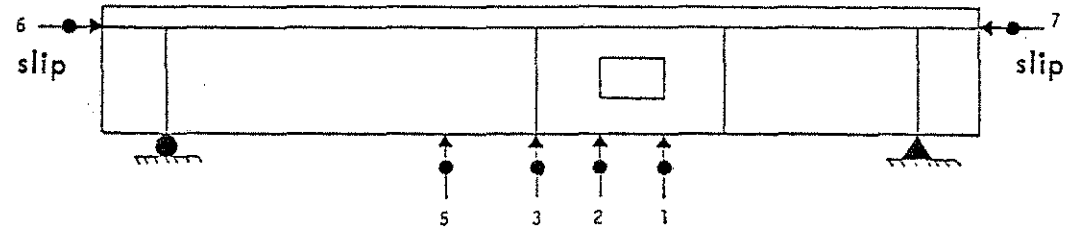

Beam No. 3

Fig. 2.16 Deflection Gage Locations for Beams No. 1, 2, and 3

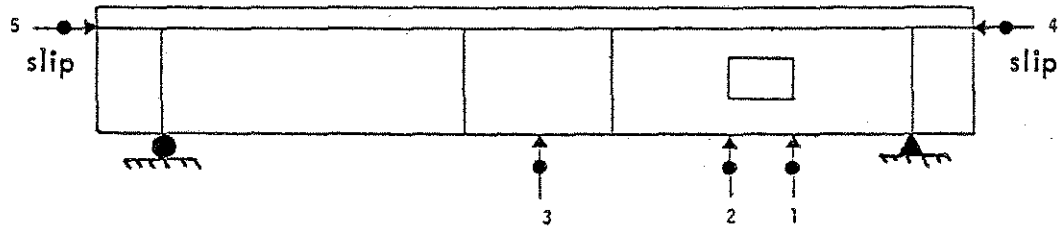

Beam No. 4

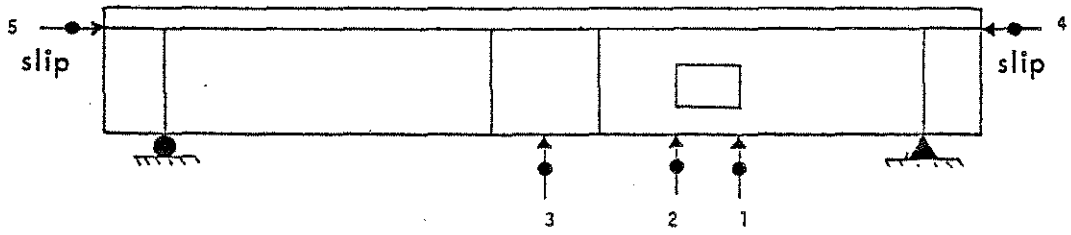

Beam No. 5

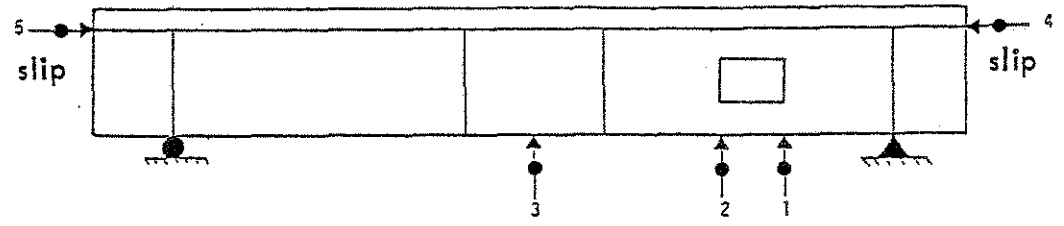

Beam No. 6

Fig. 2.17 Deflection Gage Locations for Beams No. 4, 5, and 6

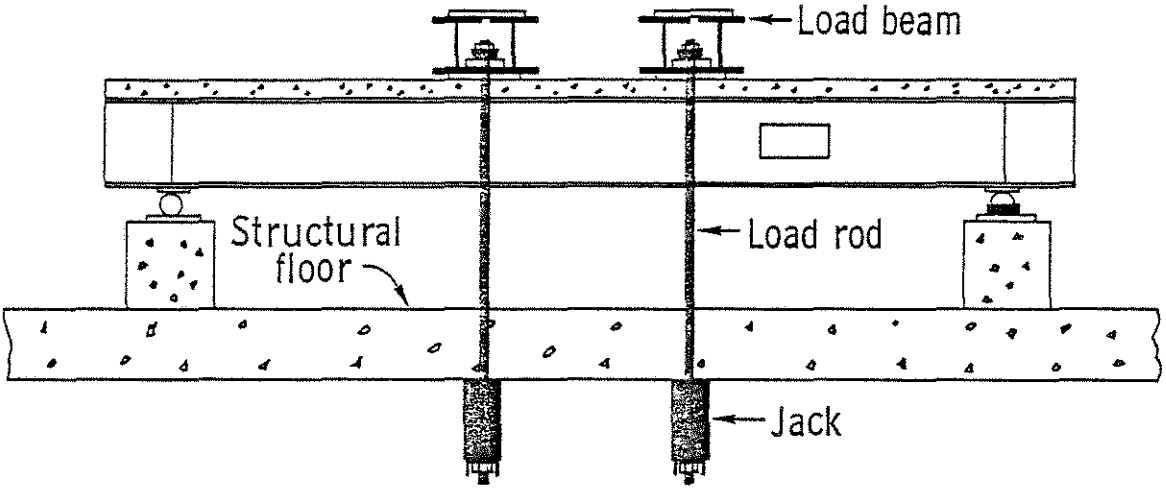

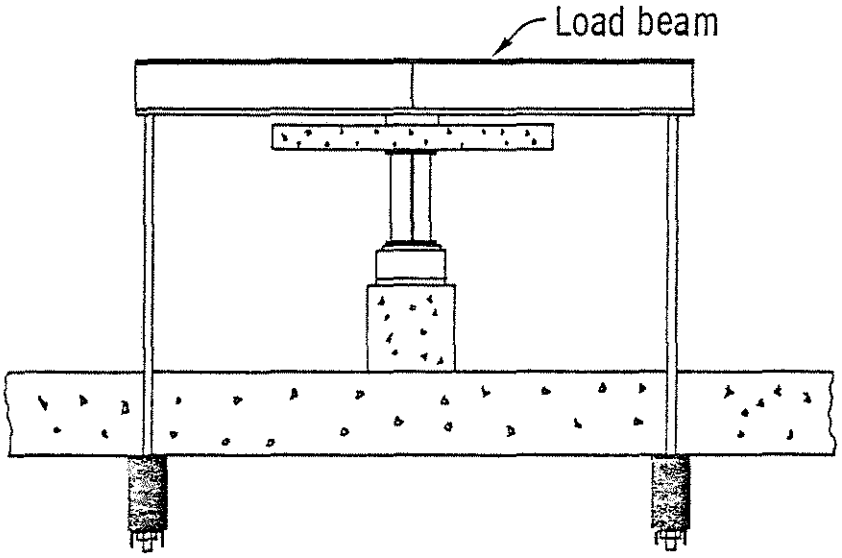

Fig. 2.18 Load System

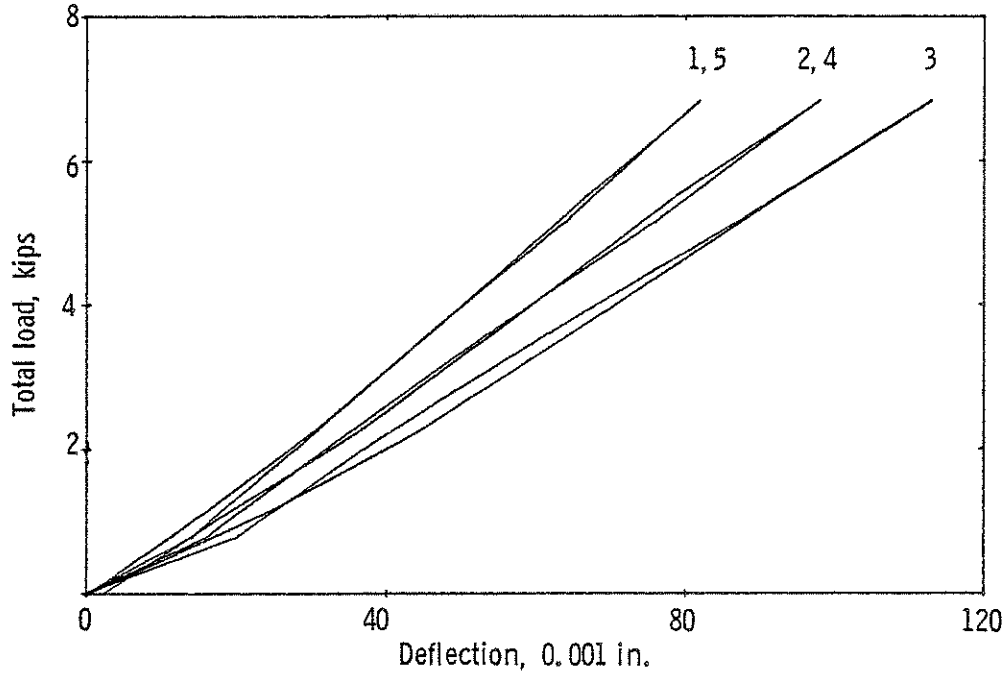

Fig. 3.1 Elastic Load-Deflection Curves for Beam No. 1

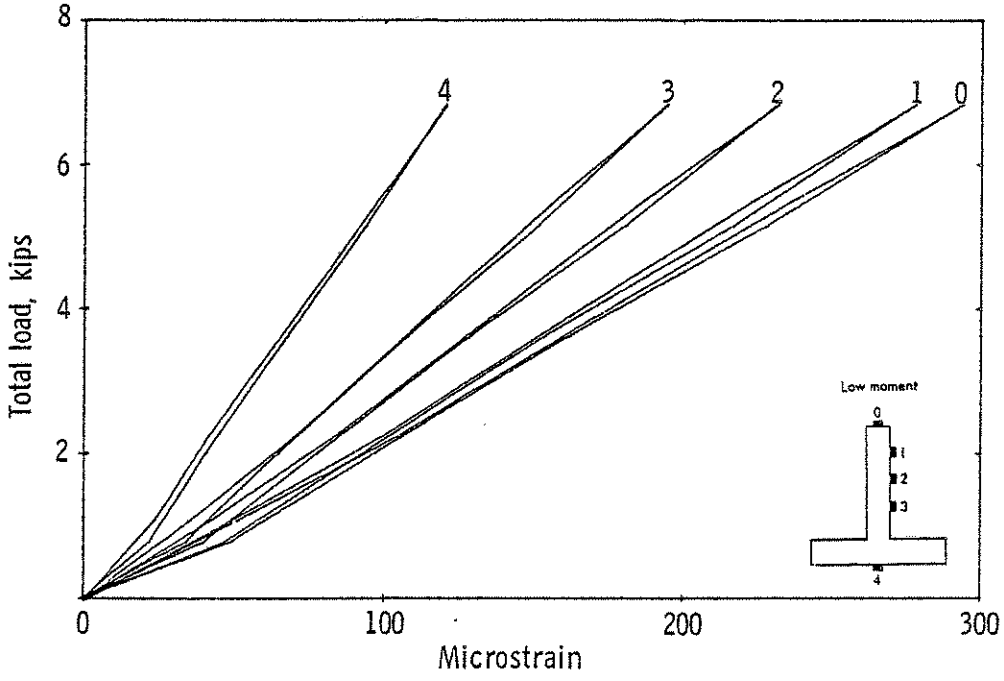

Fig. 3.2 Elastic Load-Strain Curves for Beam No. 1

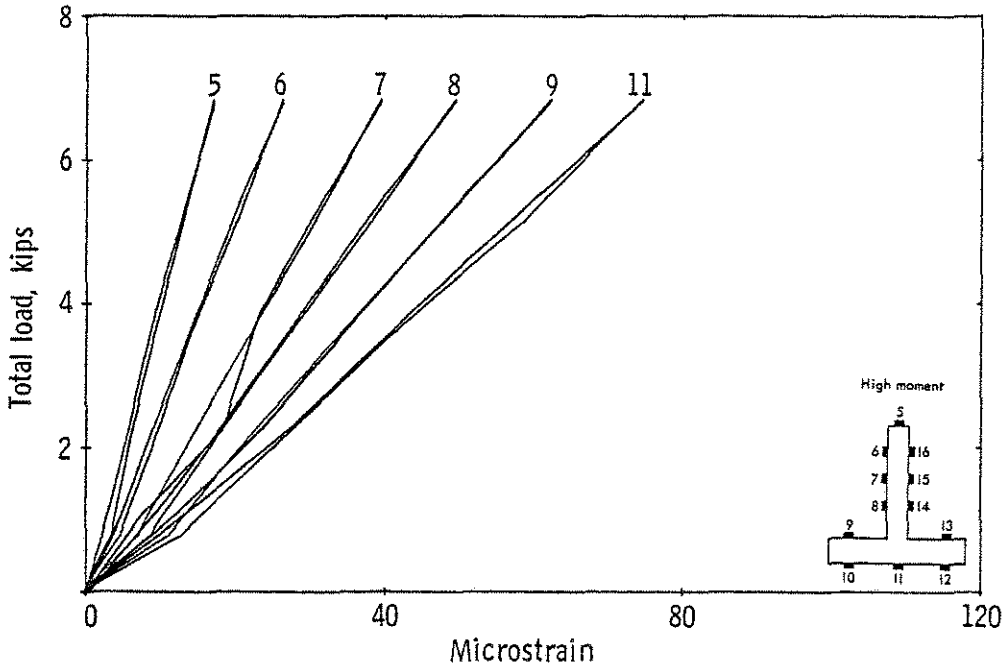

Fig. 3.2 Elastic Load-Strain Curves for Beam No. 1 (cont'd)

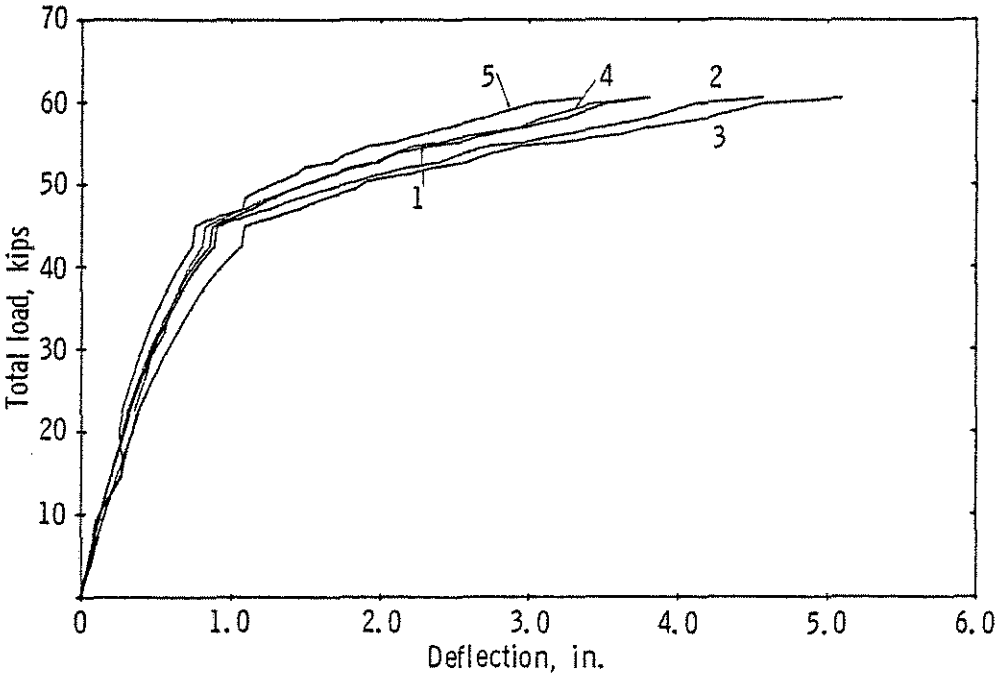

Fig. 3.3 Ultimate Load-Deflection Curves for Beam No. 1

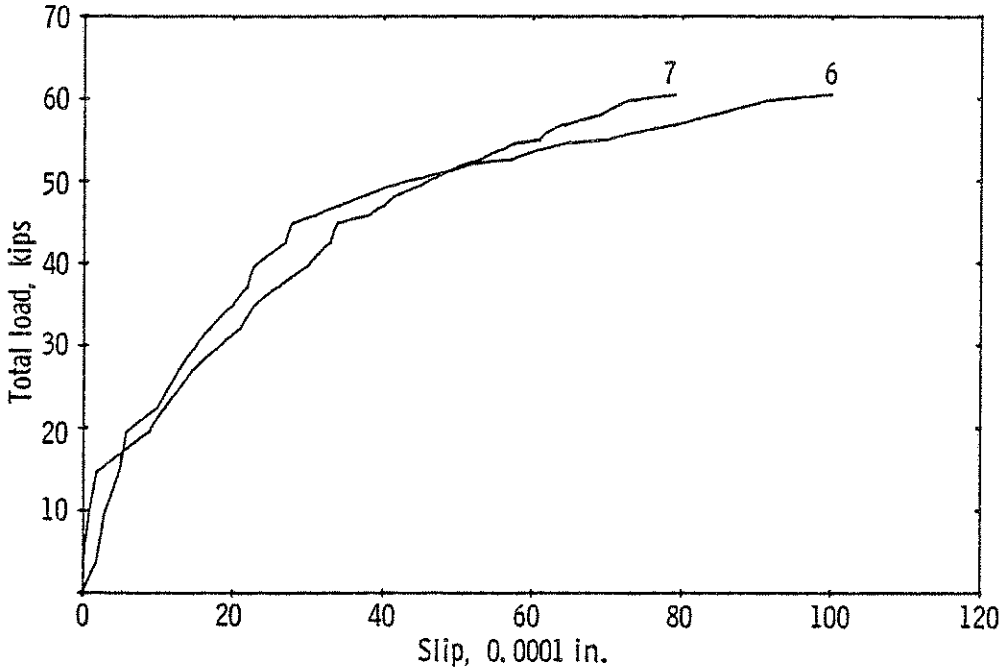

Fig. 3.4 Load-Slip Curves for Beam No. 1

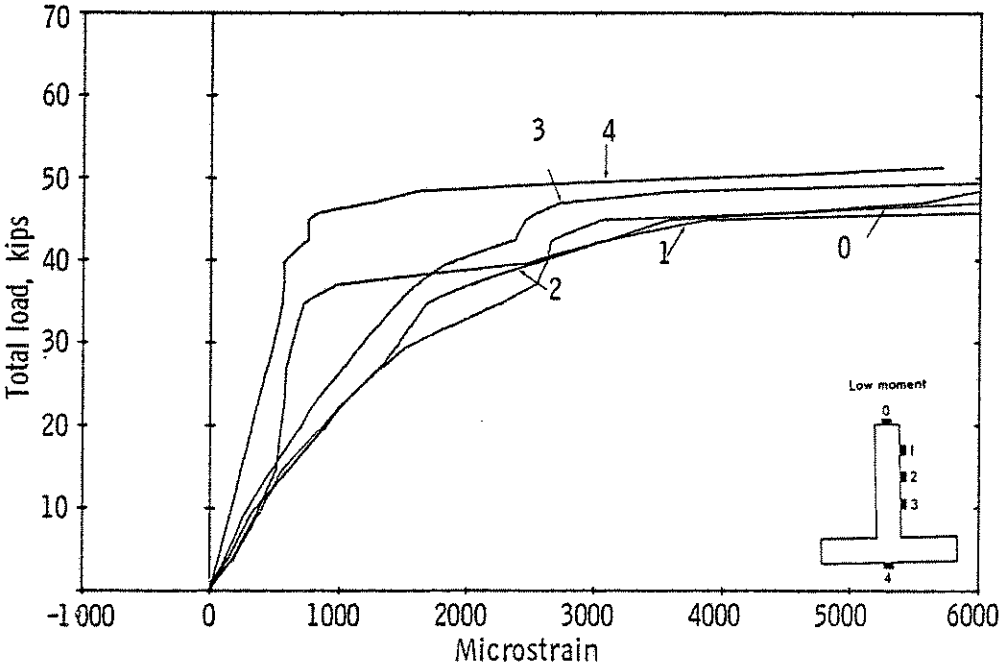

Fig. 3.5 Ultimate Load-Strain Curves for Beam No. 1

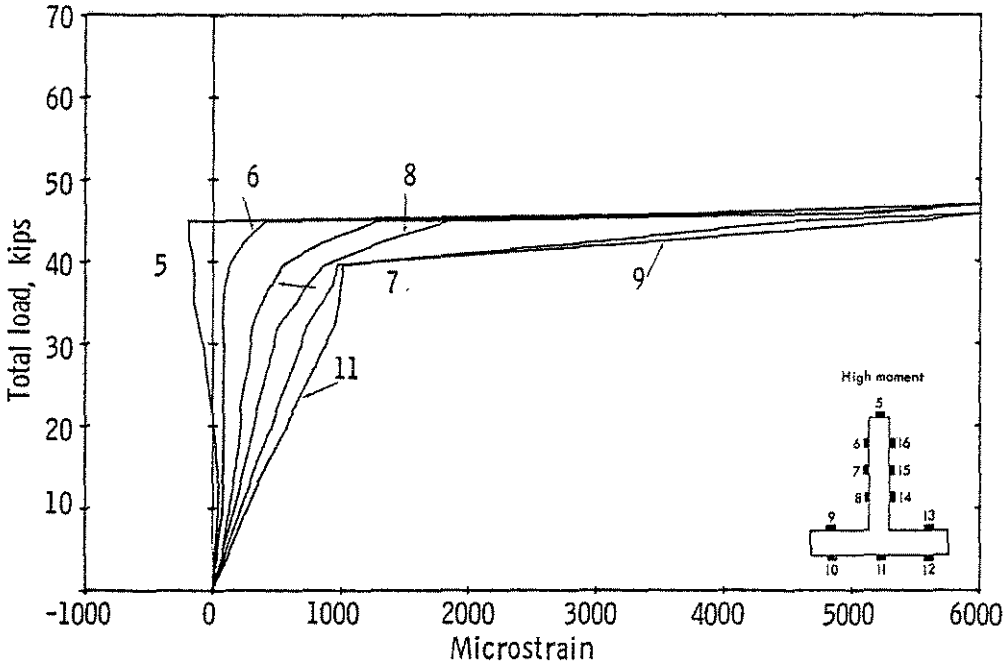

Fig. 3.5 Ultimate Load-Strain Curves for Beam No. 1 (cont'd)

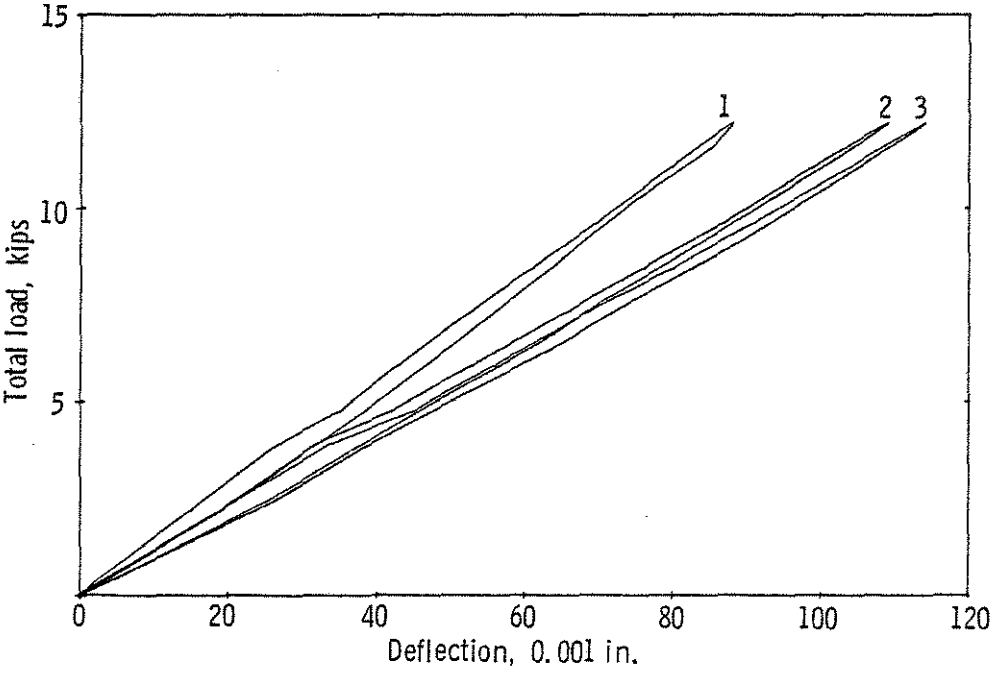

Fig. 3.6 Elastic Load-Deflection Curves for Beam No. 2

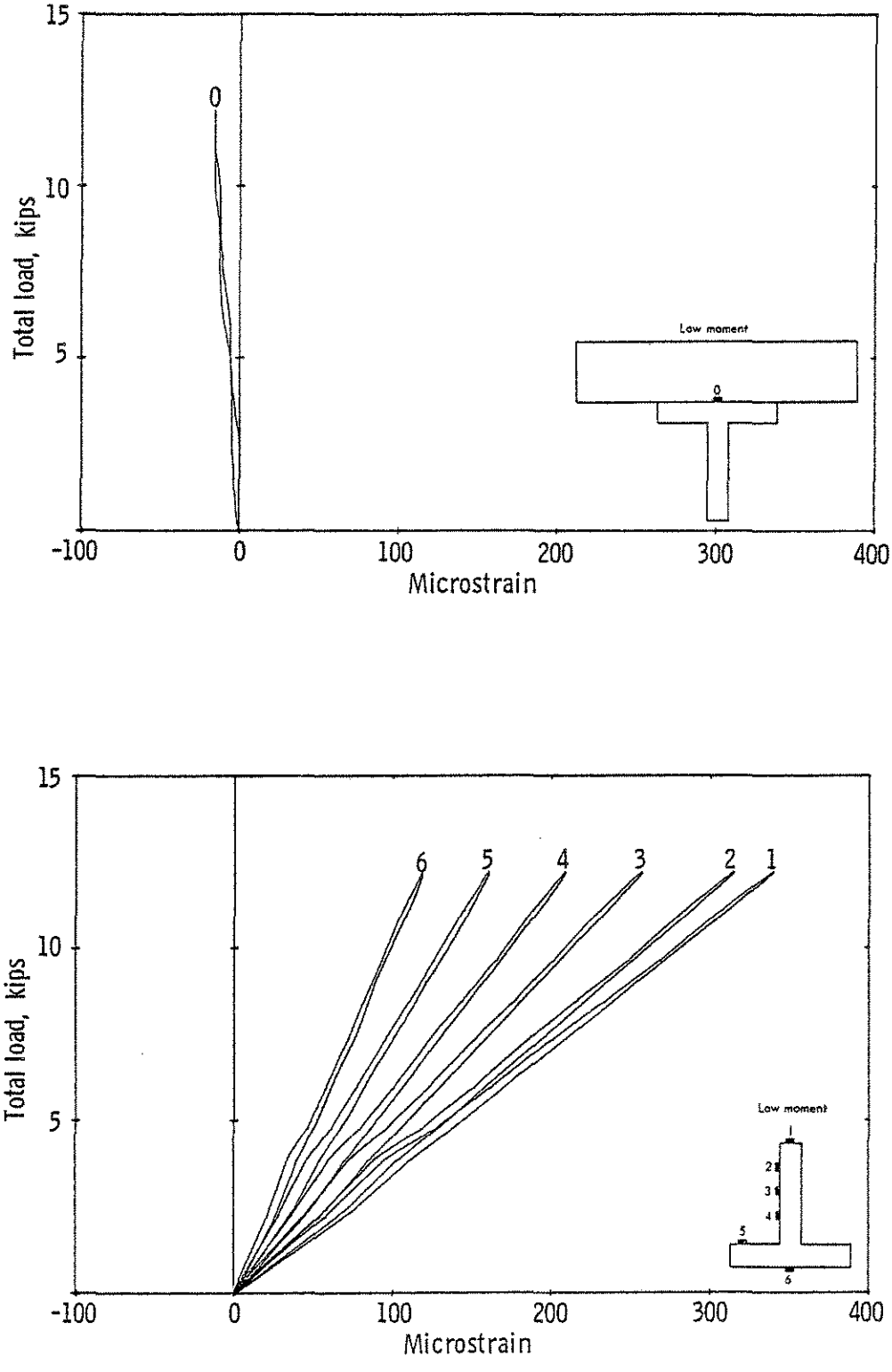

Fig. 3.7 Elastic Load-Strain Curves for Beam No. 2

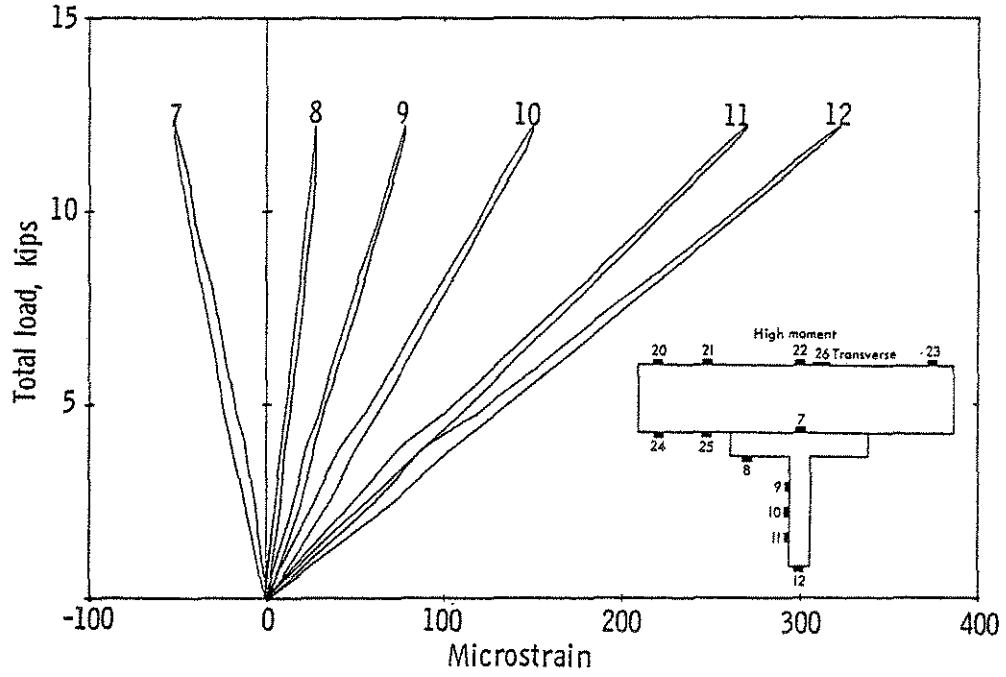

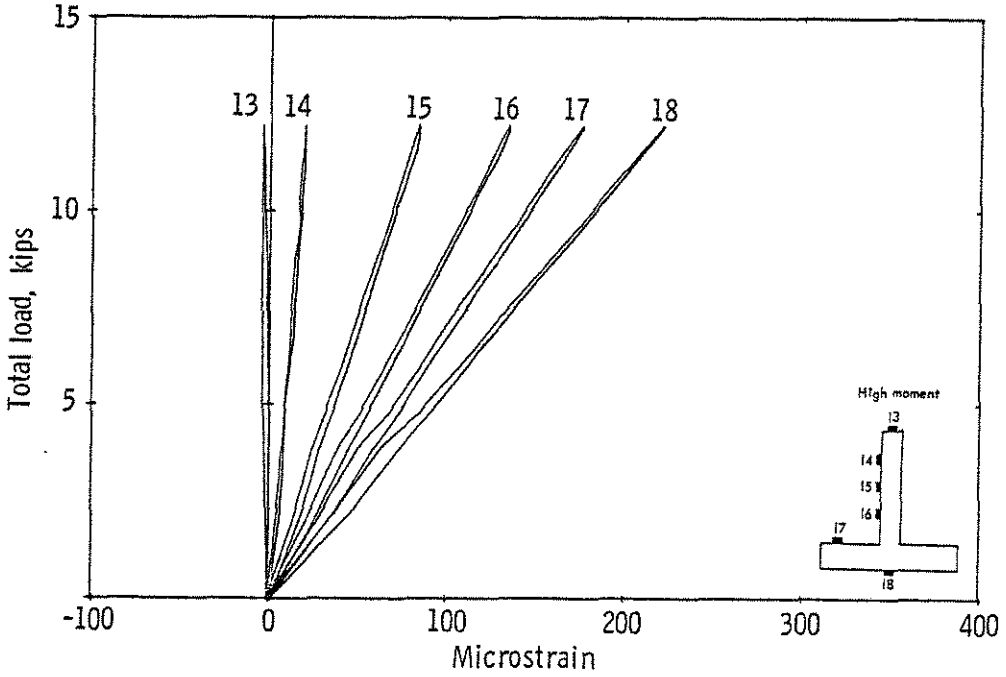

Fig. 3.7 Elastic Load-Strain Curves for Beam No. 2 (cont'd)

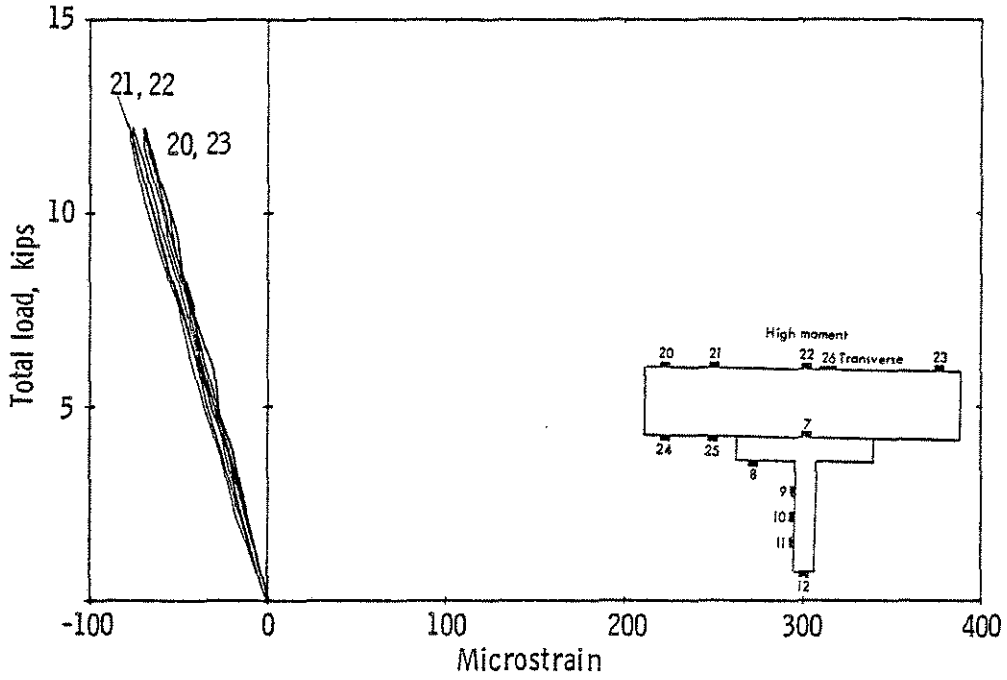

Fig. 3.7 Elastic Load-Strain Curves for Beam No. 2 (cont'd)

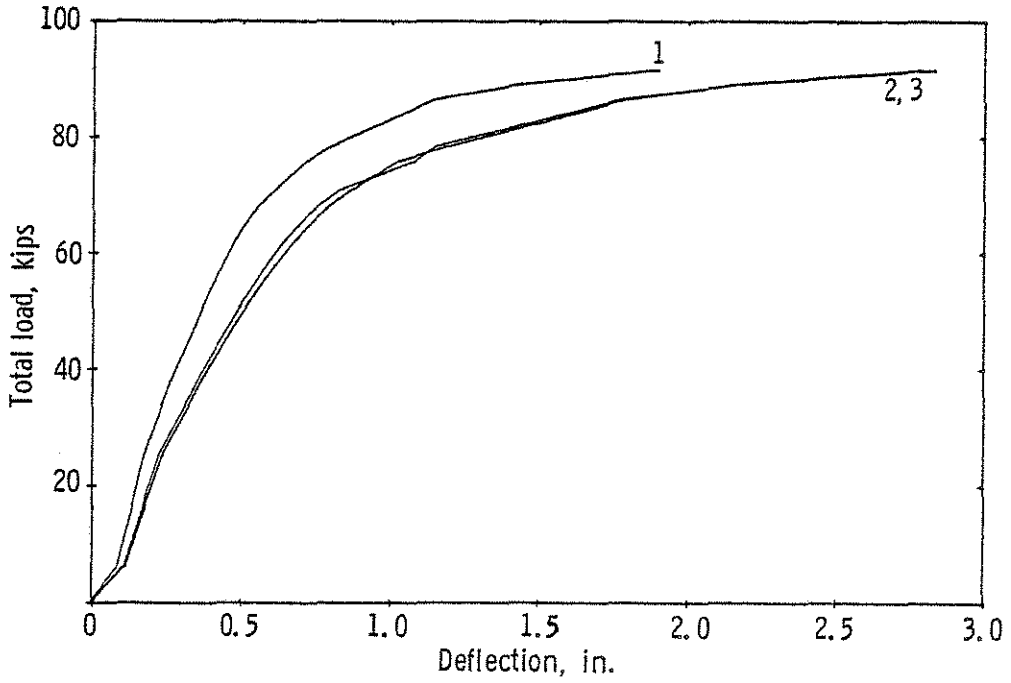

Fig. 3.8 Ultimate Load-Deflection Curves for Beam No. 2

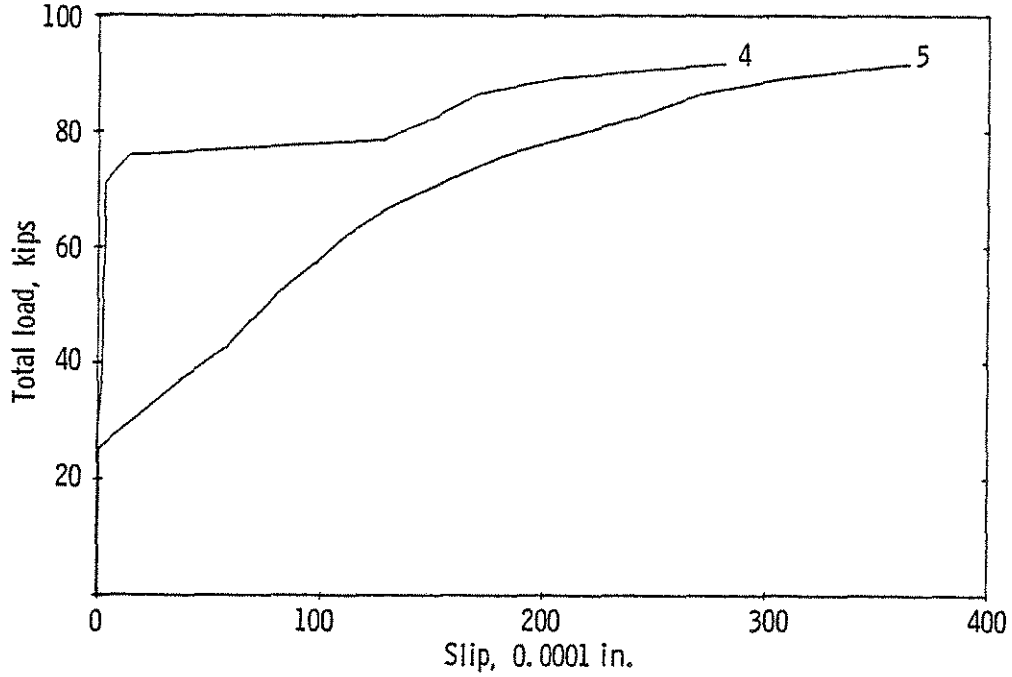

Fig. 3.9 Load-Slip Curves for Beam No. 2

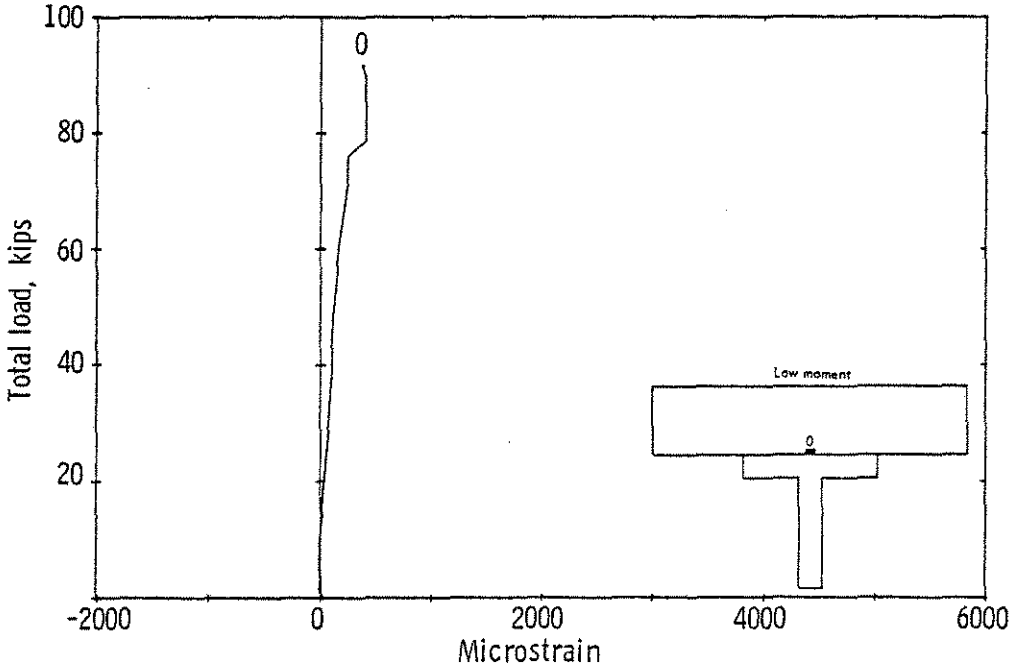

Fig. 3.10 Ultimate Load-Strain Curves for Beam No. 2

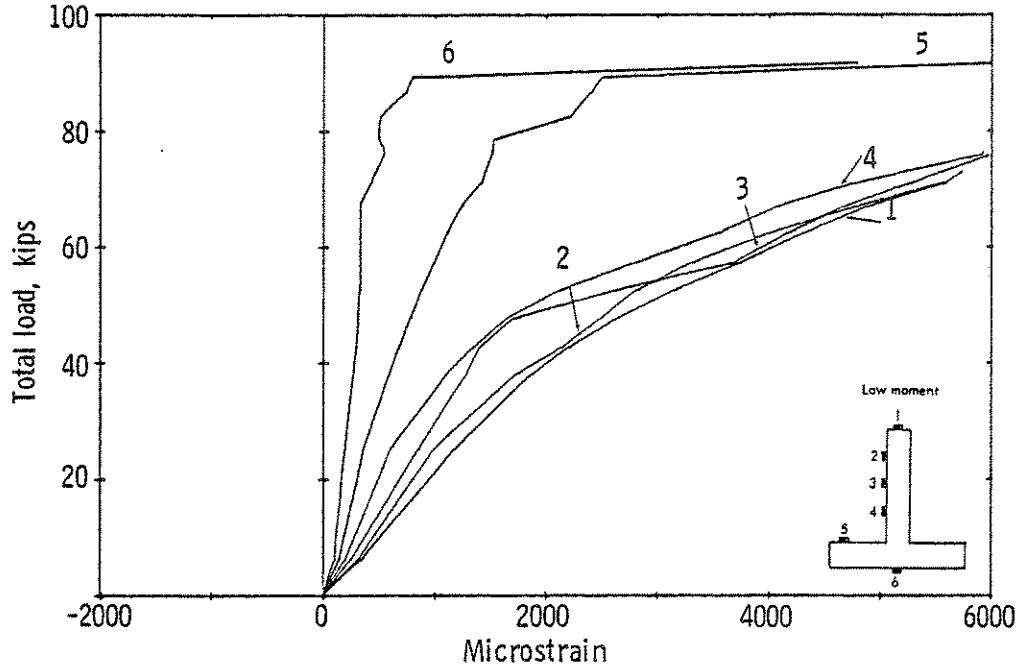

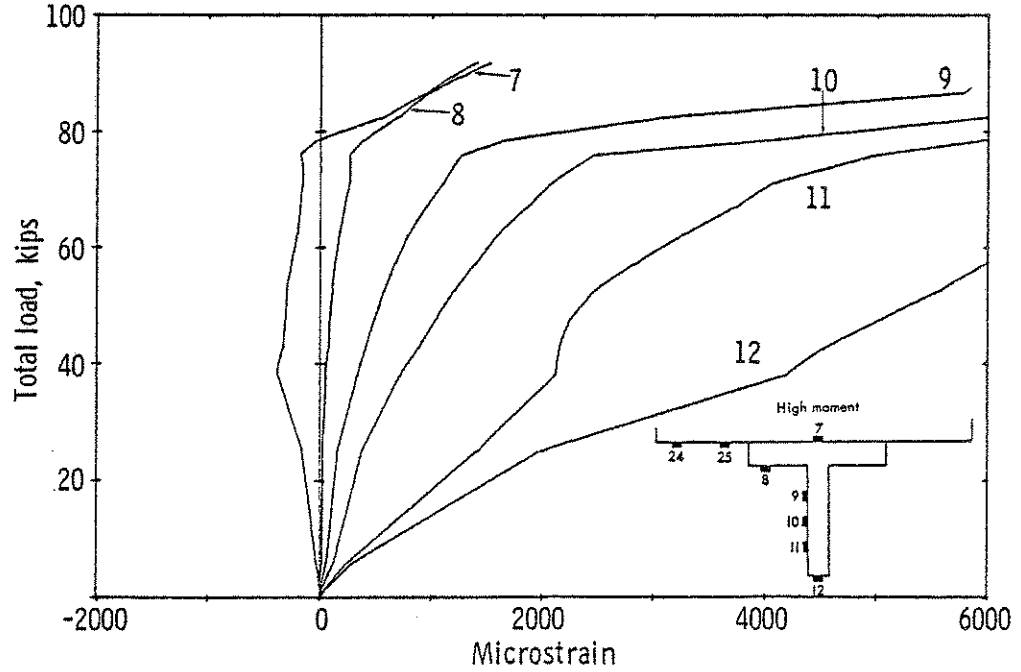

Fig. 3.10 Ultimate Load-Strain Curves for Beam No. 2 (cont'd)

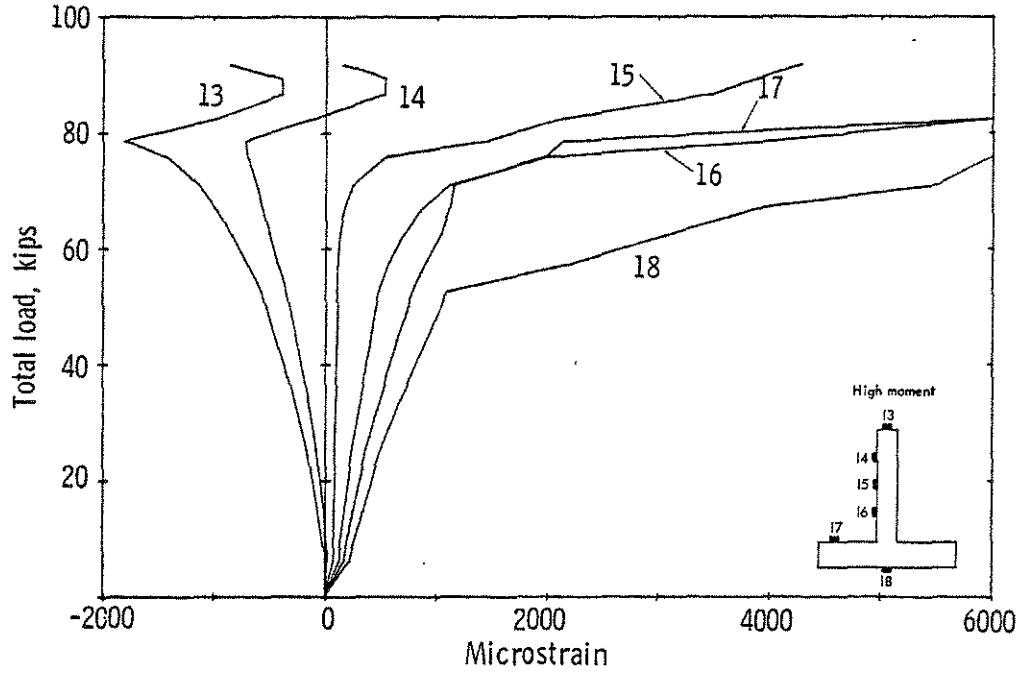

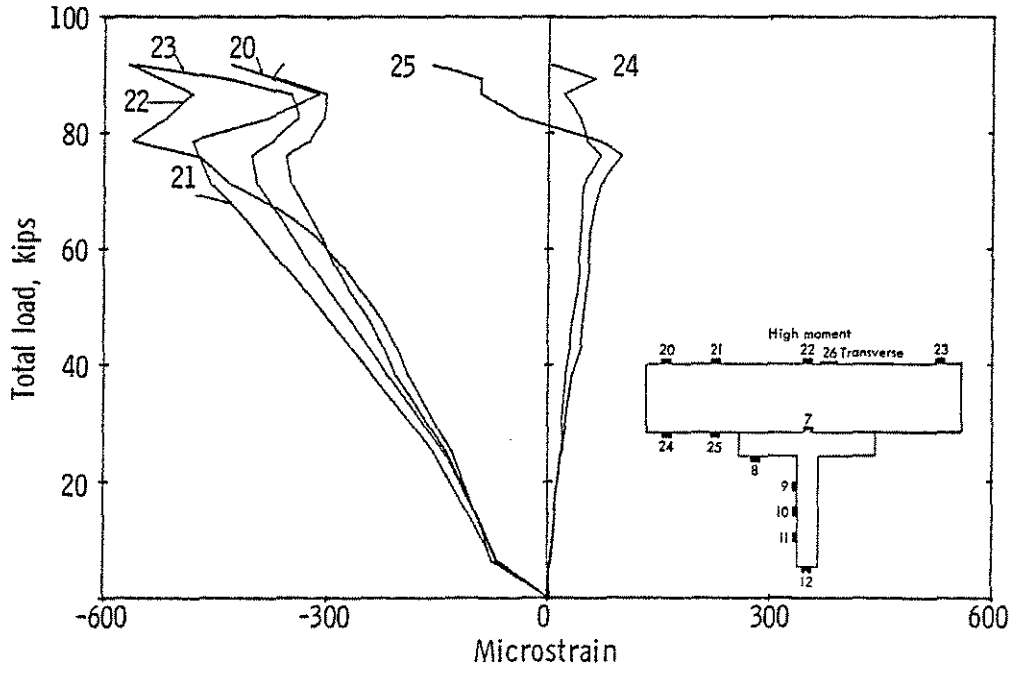

Fig. 3.10 Ultimate Load-Strain Curves for Beam No. 2 (cont'd)

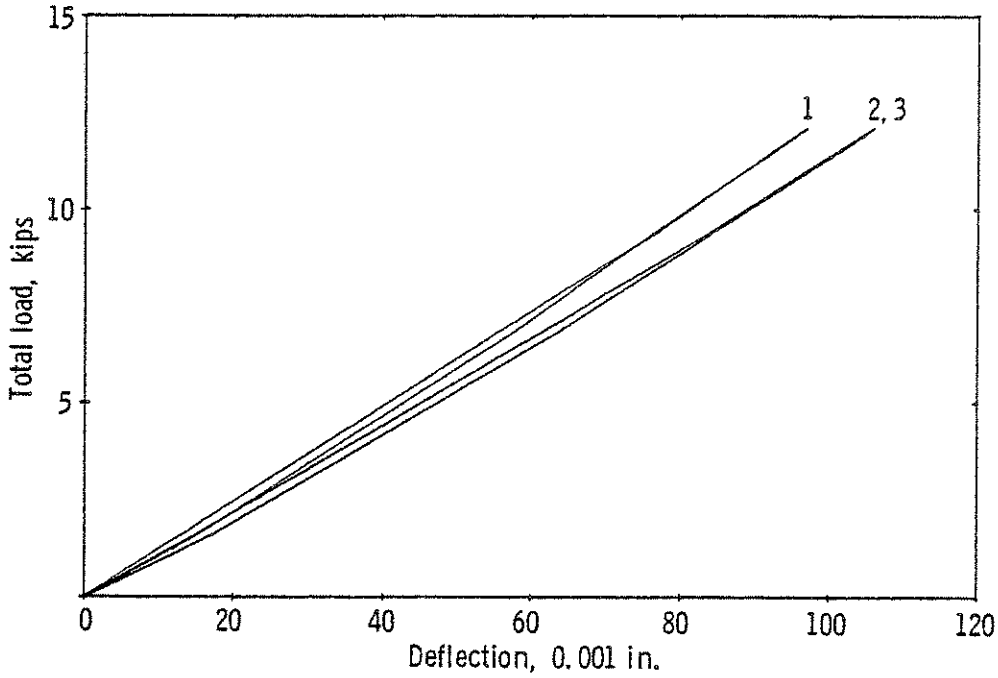

Fig. 3.11 Elastic Load-Deflection Curves for Beam No. 3

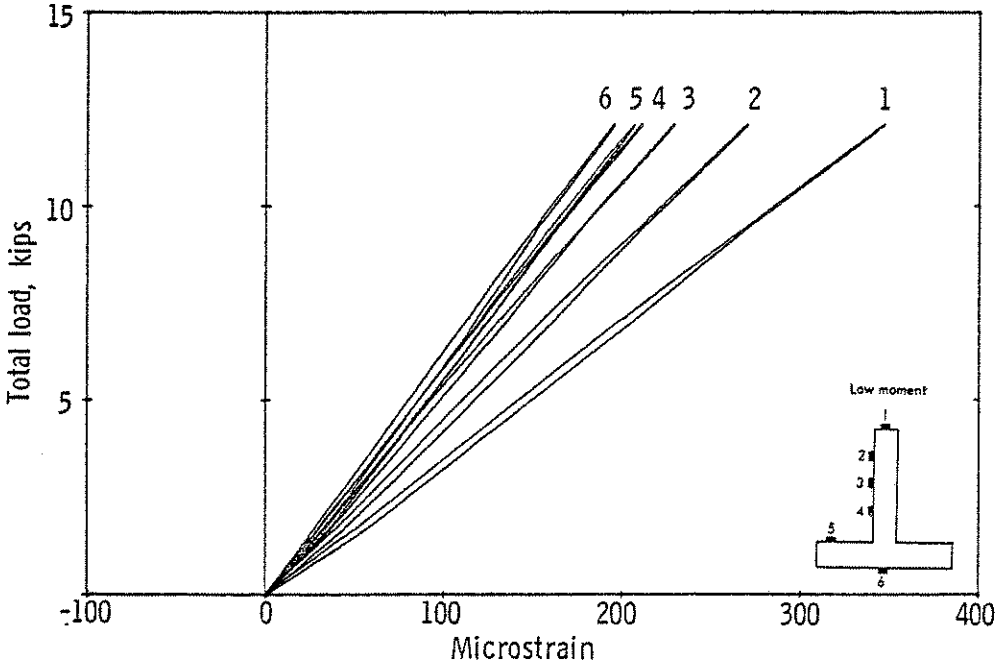

Fig. 3.12 Elastic Load-Strain Curves for Beam No. 3

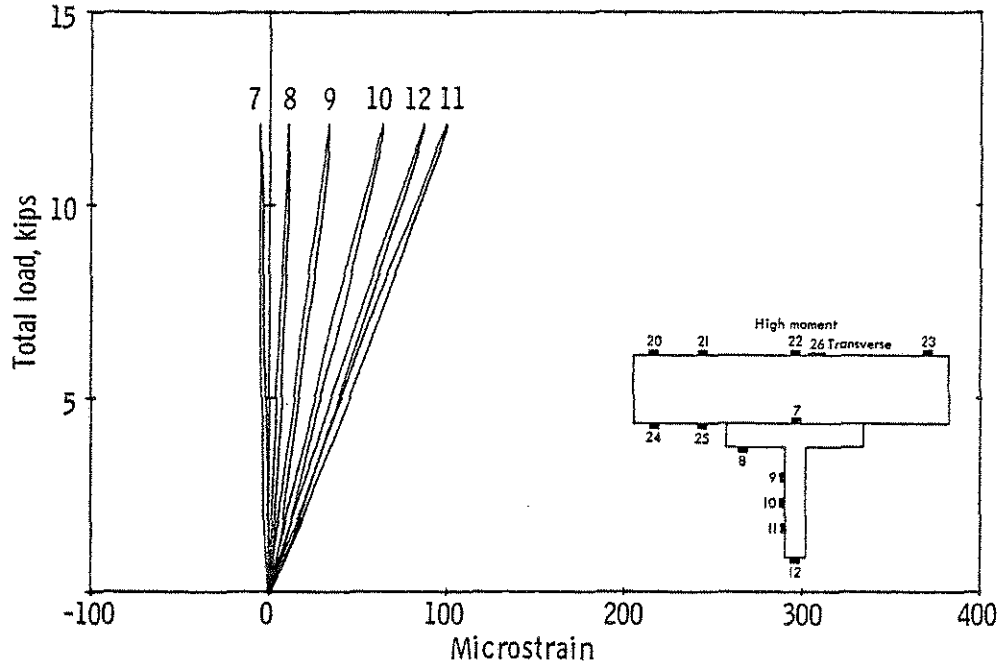

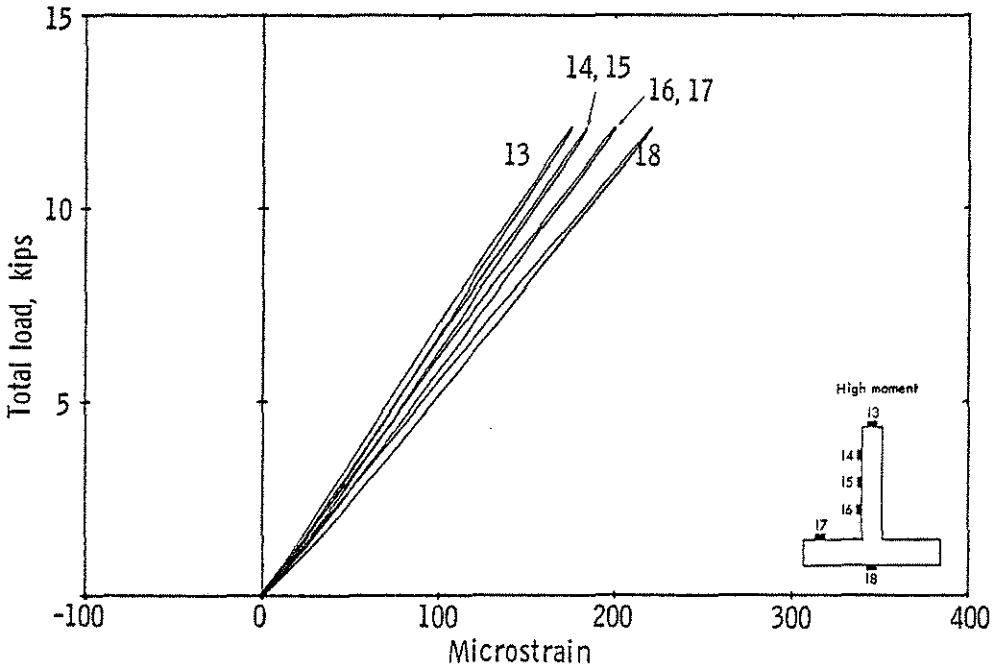

Fig. 3.12 Elastic Load-Strain Curves for Beam No. 3 (cont'd)

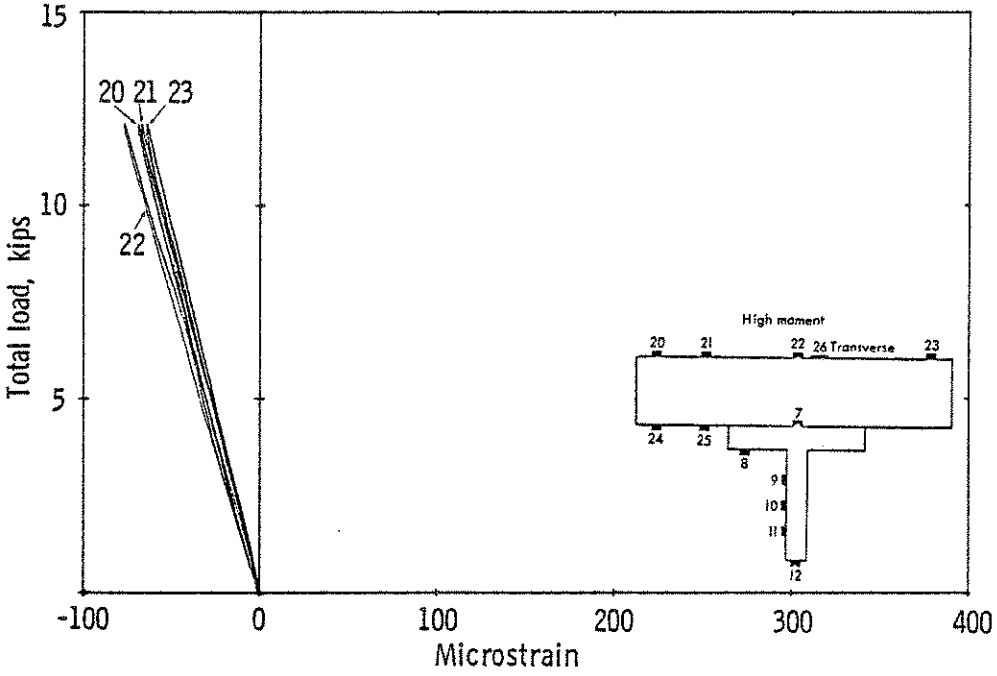

Fig. 3.12 Elastic Load-Strain Curves for Beam No. 3 (cont'd)

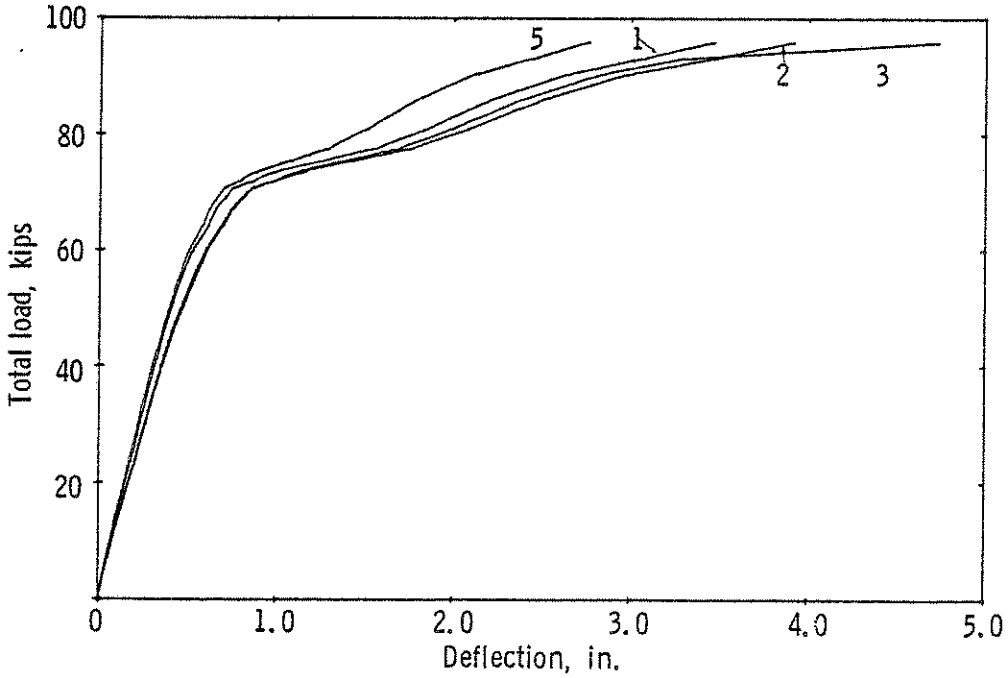

Fig. 3.13 Ultimate Load-Deflection Curves for Beam No. 3

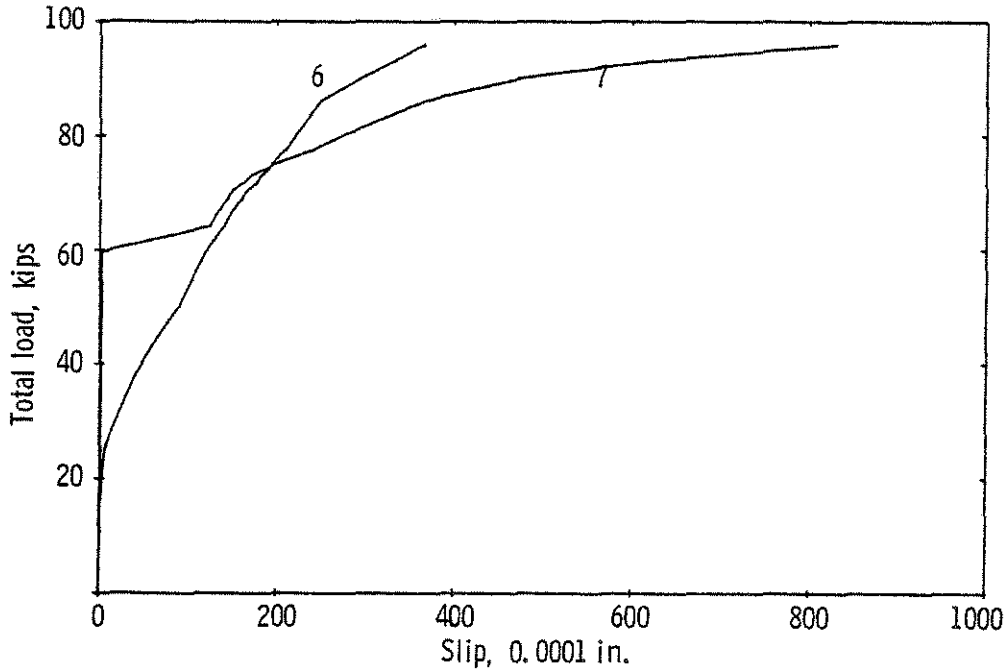

Fig. 3.14 Load-Slip Curves for Beam No. 3

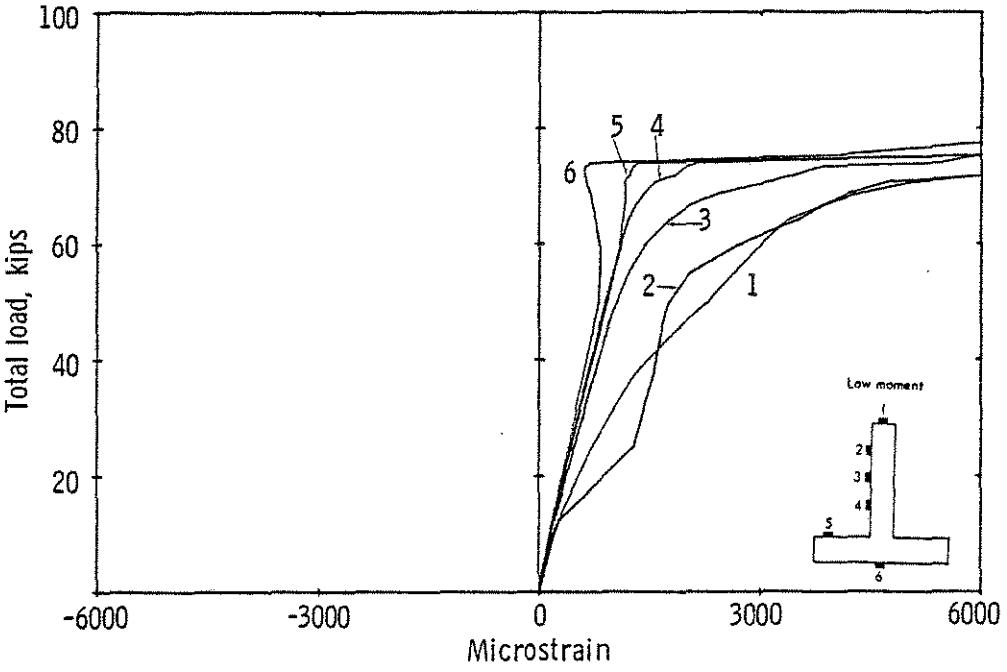

Fig. 3.15 Ultimate Load-Strain Curves for Beam No. 3

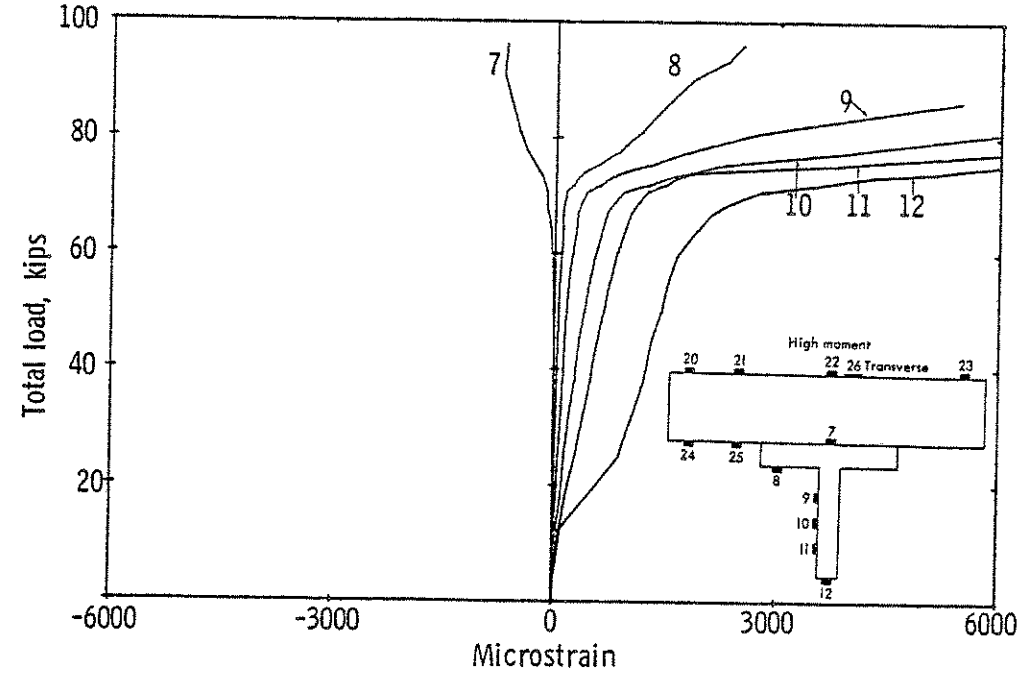

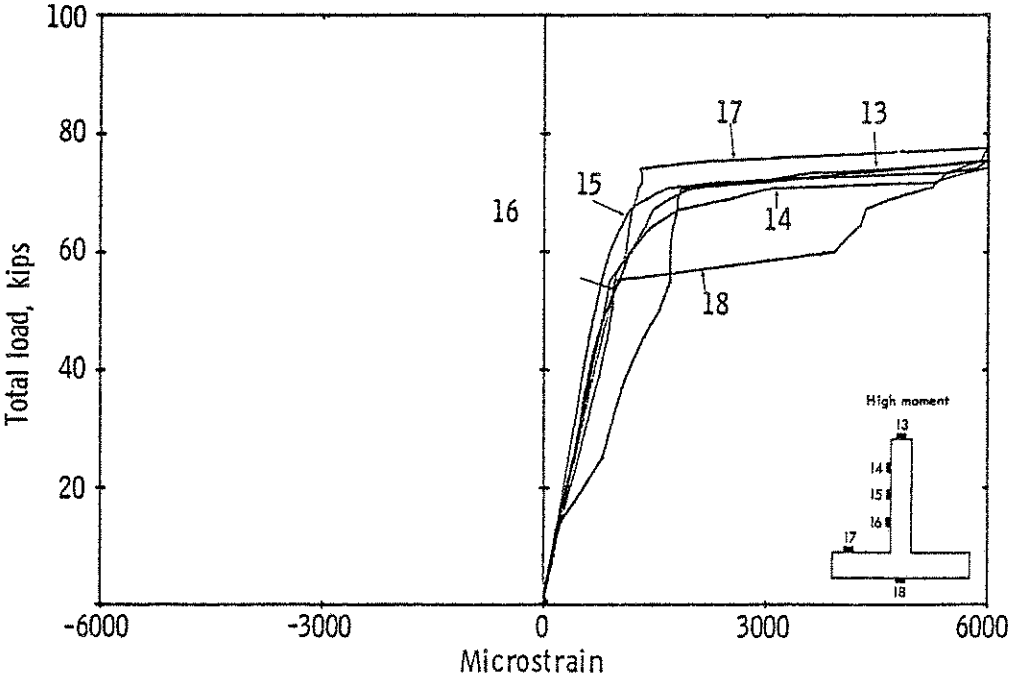

Fig. 3.15 Ultimate Load-Strain Curves for Beam No. 3 (cont'd)

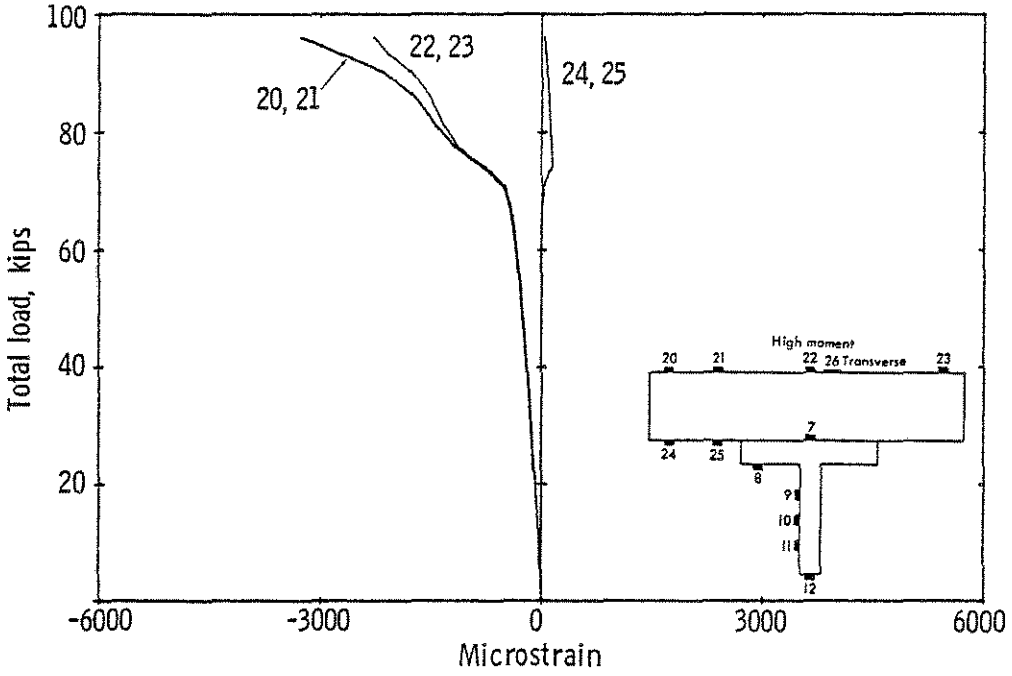

Fig. 3.15 Ultimate Load-Strain Curves for Beam No. 3 (cont'd)

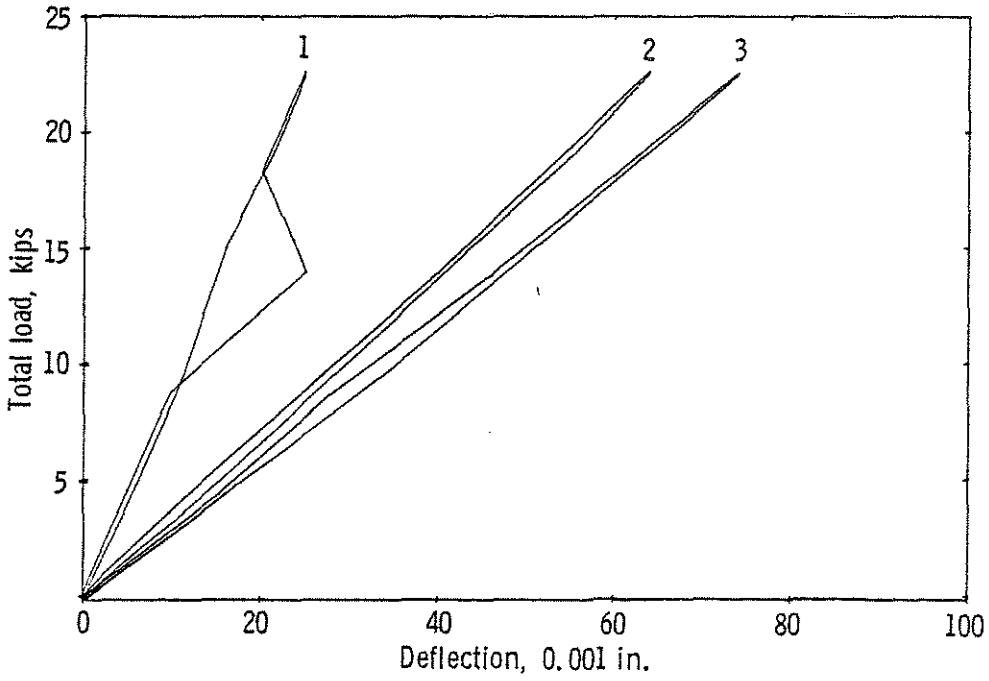

Fig. 3.16 Elastic Load-Deflection Curves for Beam No. 4

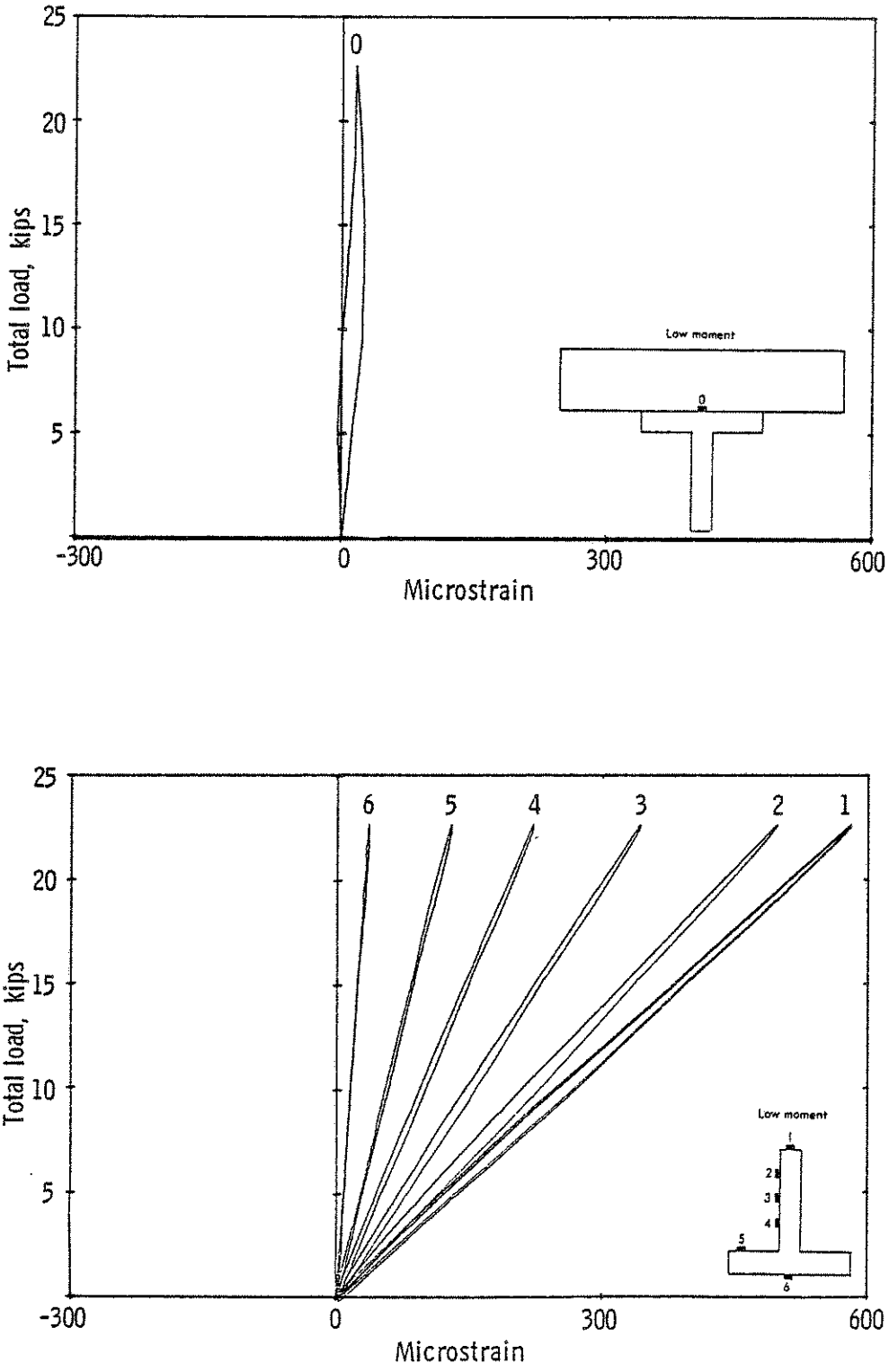

Fig. 3.17 Elastic Load-Strain Curves for Beam No. 4

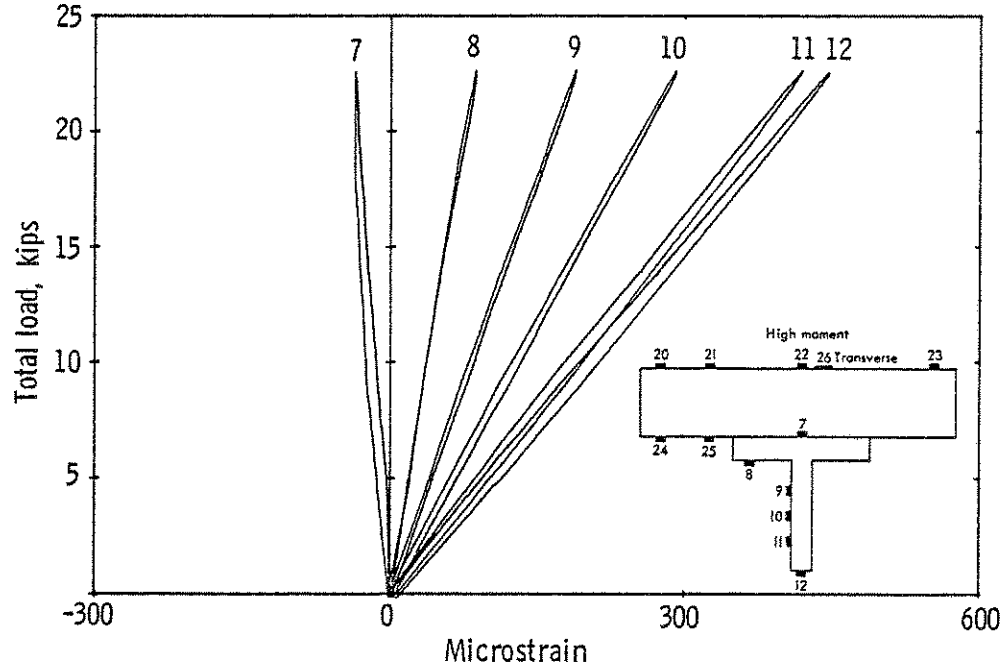

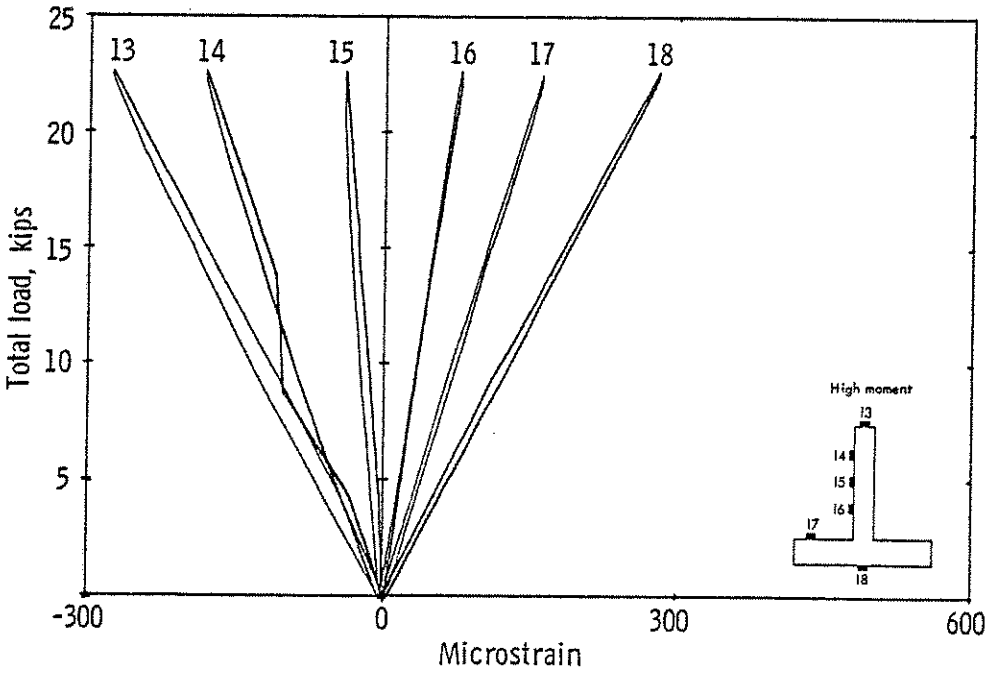

Fig. 3.17 Elastic Load-Strain Curves for Beam No. 4 (cont'd)

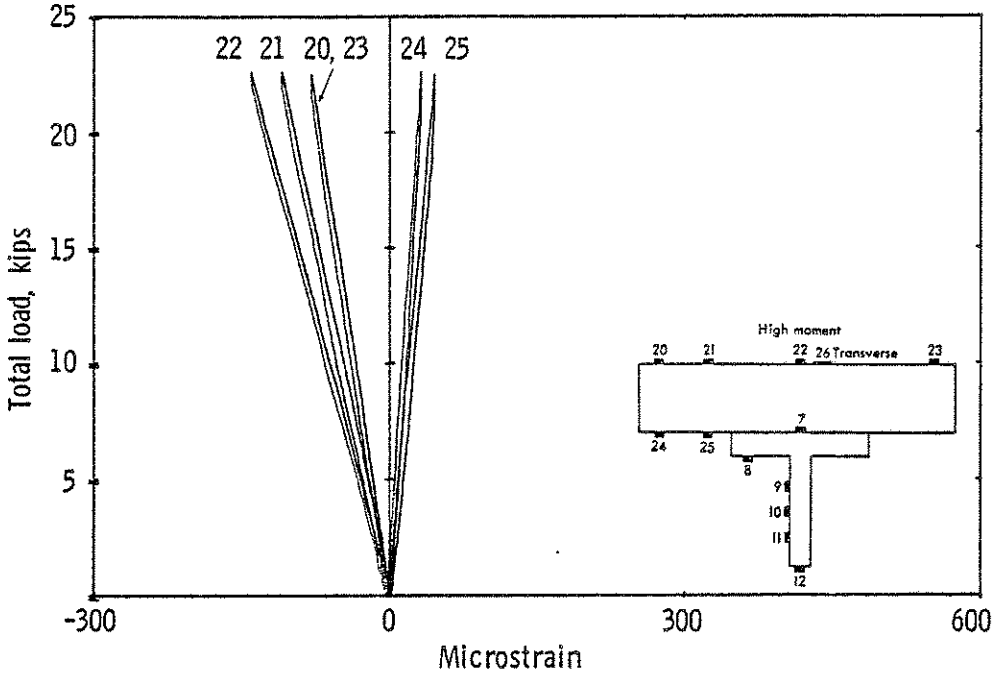

Fig. 3.17 Elastic Load-Strain Curves for Beam No. 4 (cont'd)

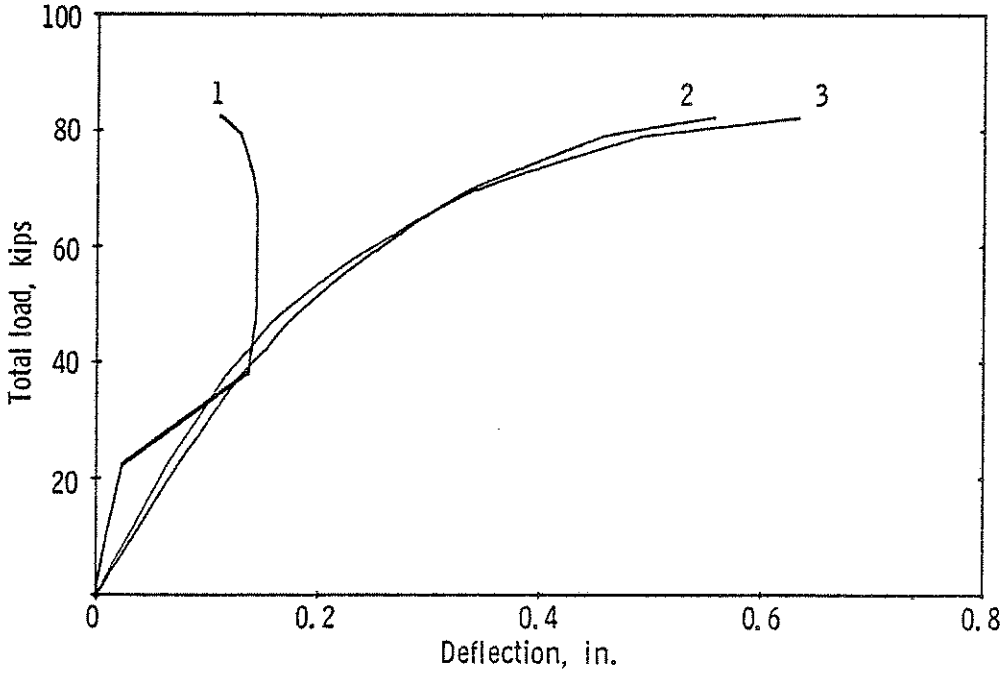

Fig. 3.18 Ultimate Load-Deflection Curves for Beam No. 4

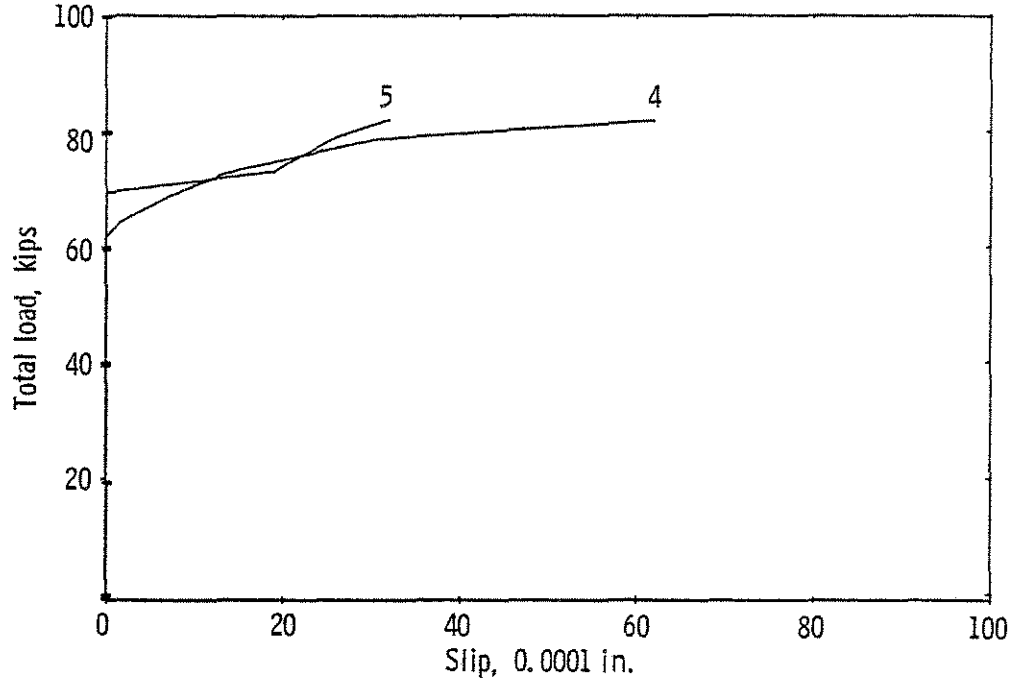

Fig. 3.19 Load-Slip Curves for Beam No. 4

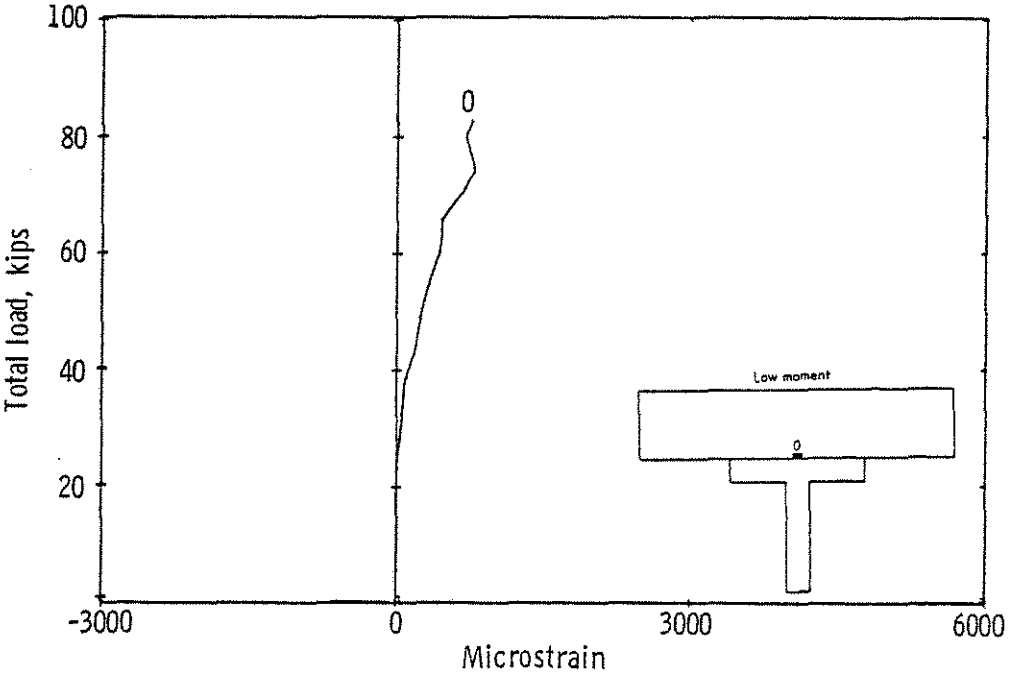

Fig. 3.20 Ultimate Load-Strain Curves for Beam No. 4

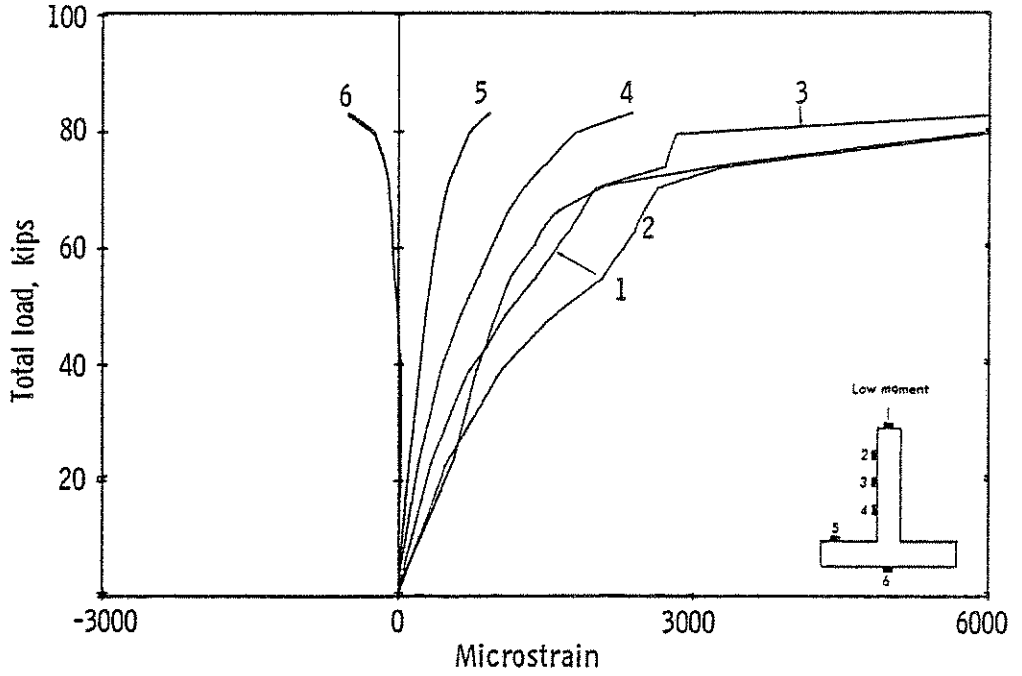

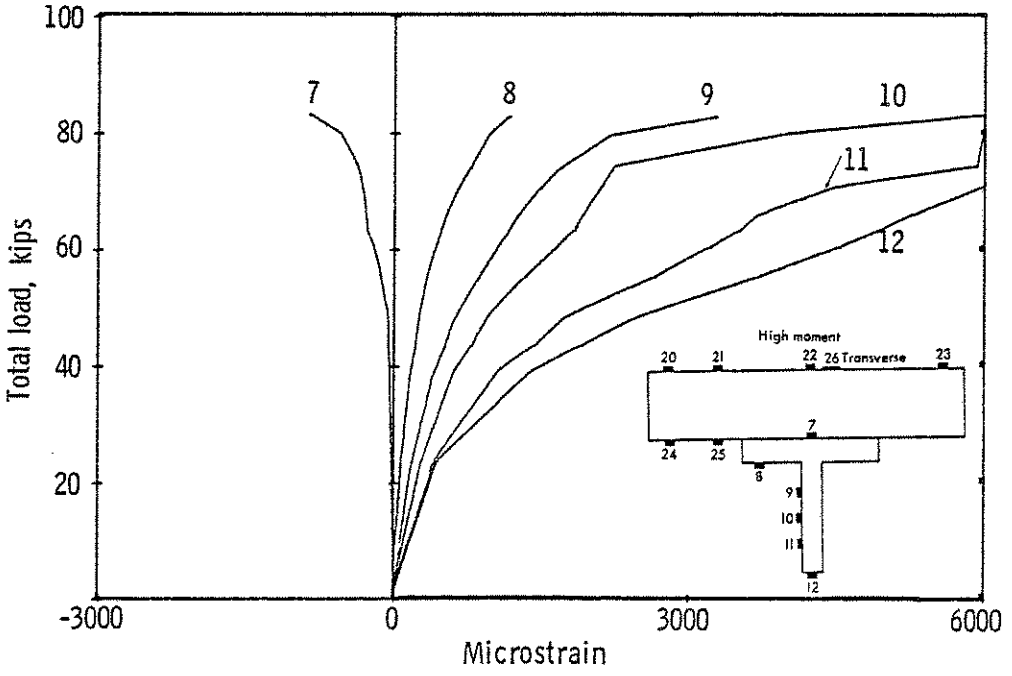

Fig. 3.20 Ultimate Load-Strain Curves for Beam No. 4 (cont'd)

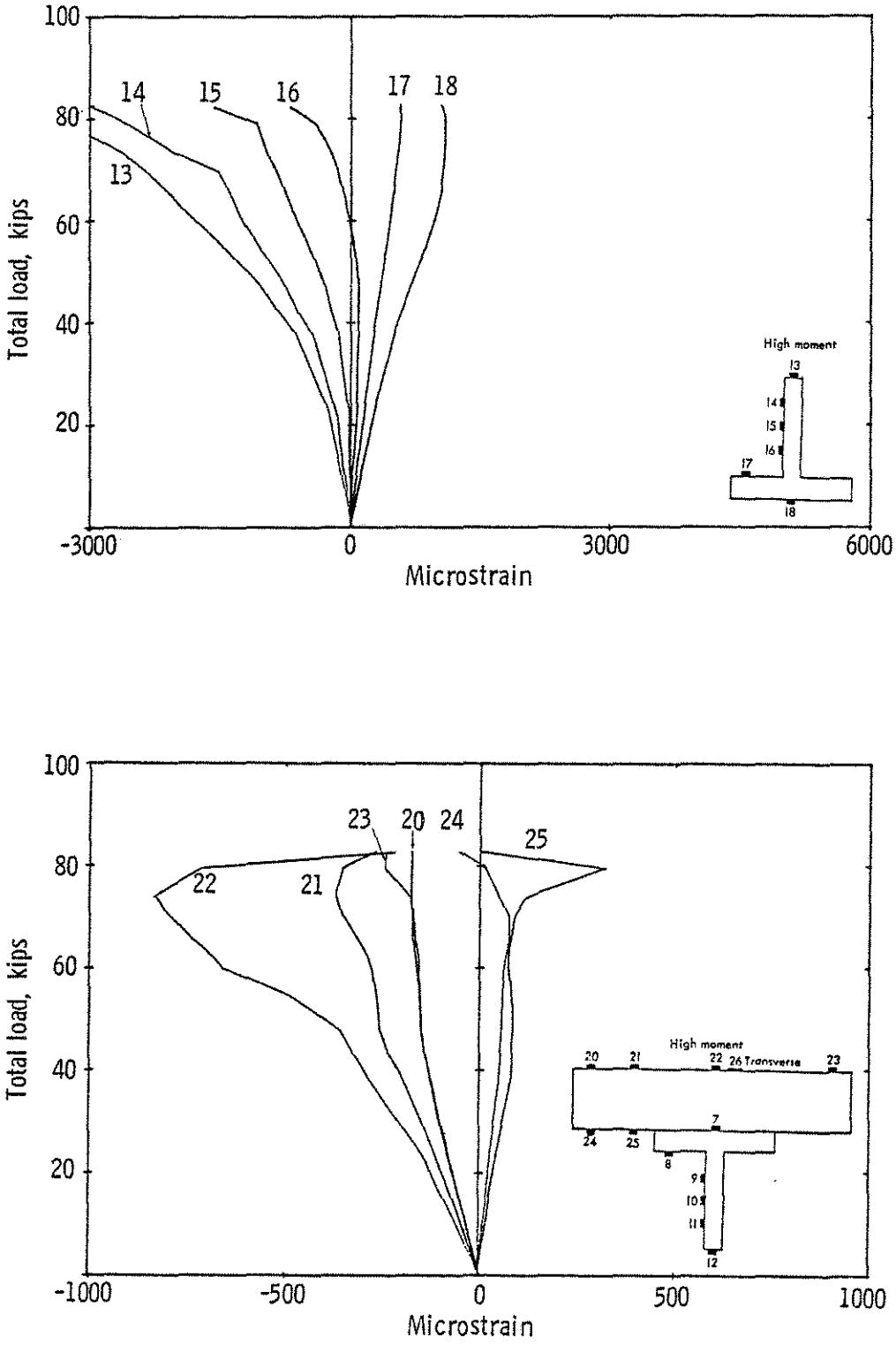

Fig. 3.20 Ultimate Load-Strain Curves for Beam No. 4 (cont'd)

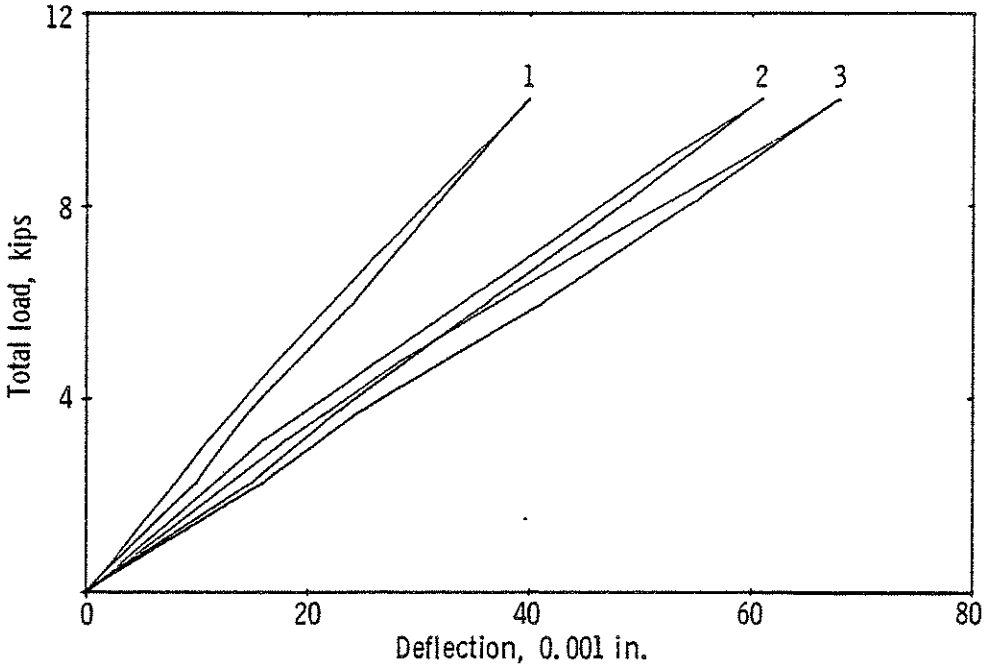

Fig. 3.21 Elastic Load-Deflection Curves for Beam No. 5

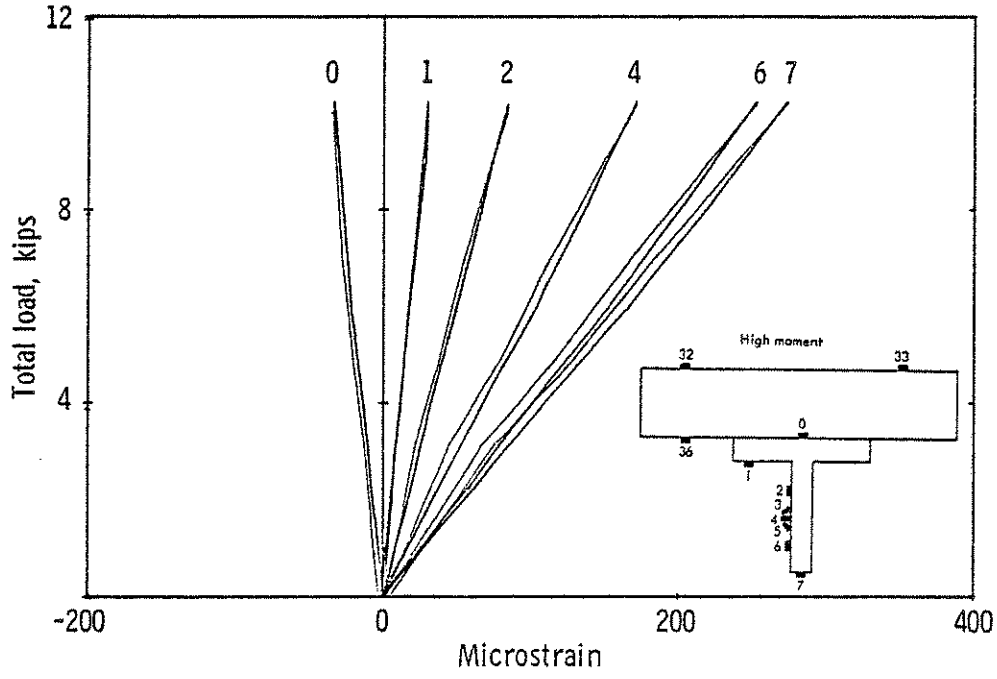

Fig. 3.22 Elastic Load-Strain Curves for Beam No. 5

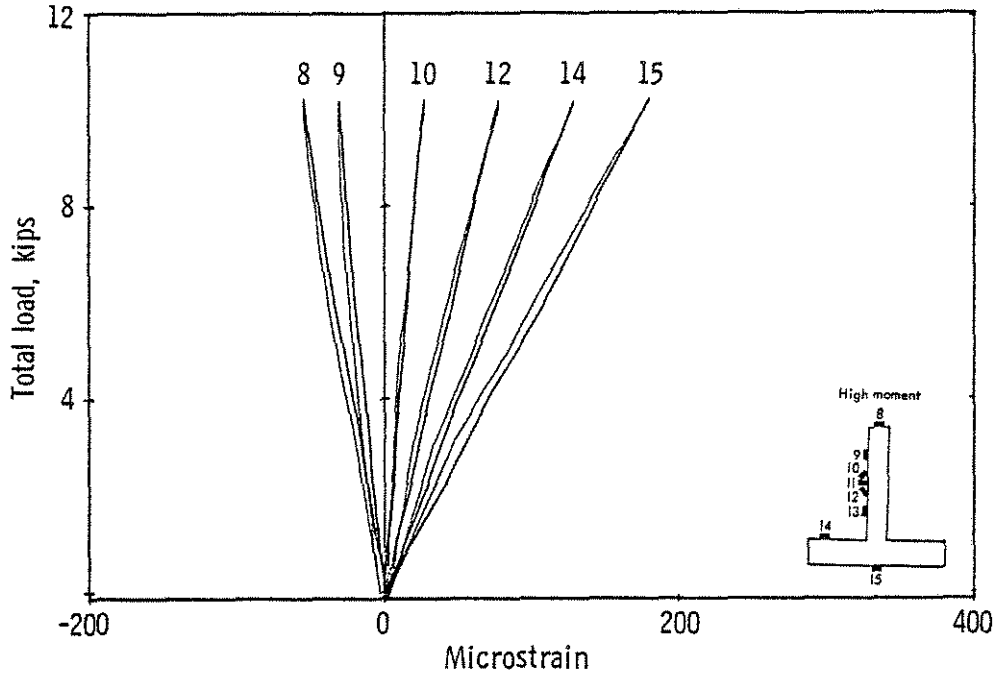

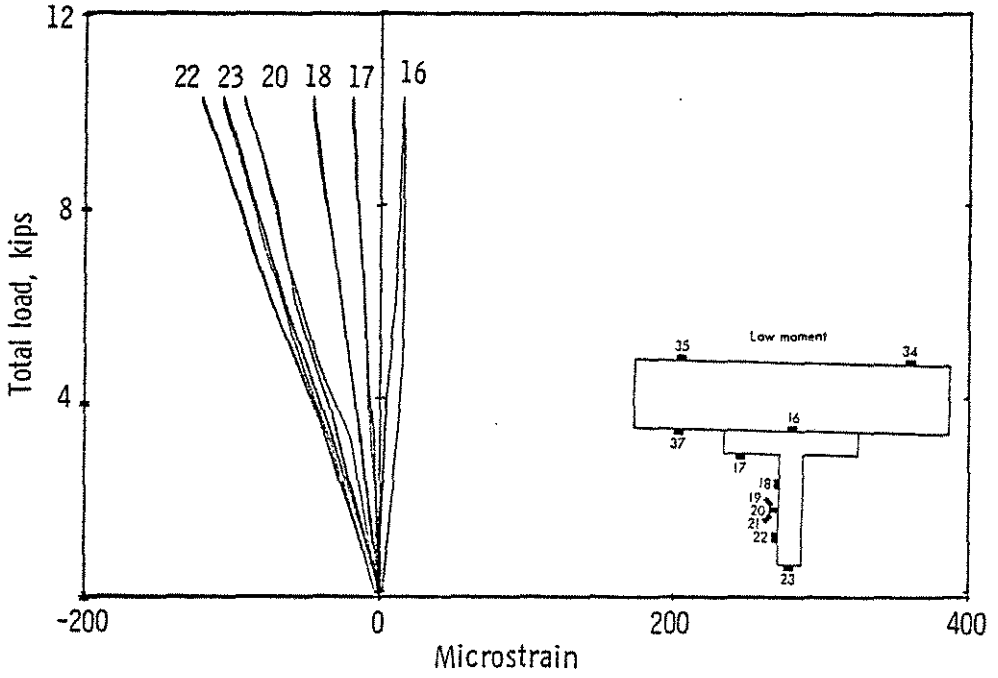

Fig. 3.22 Elastic Load-Strain Curves for Beam No. 5 (cont'd)

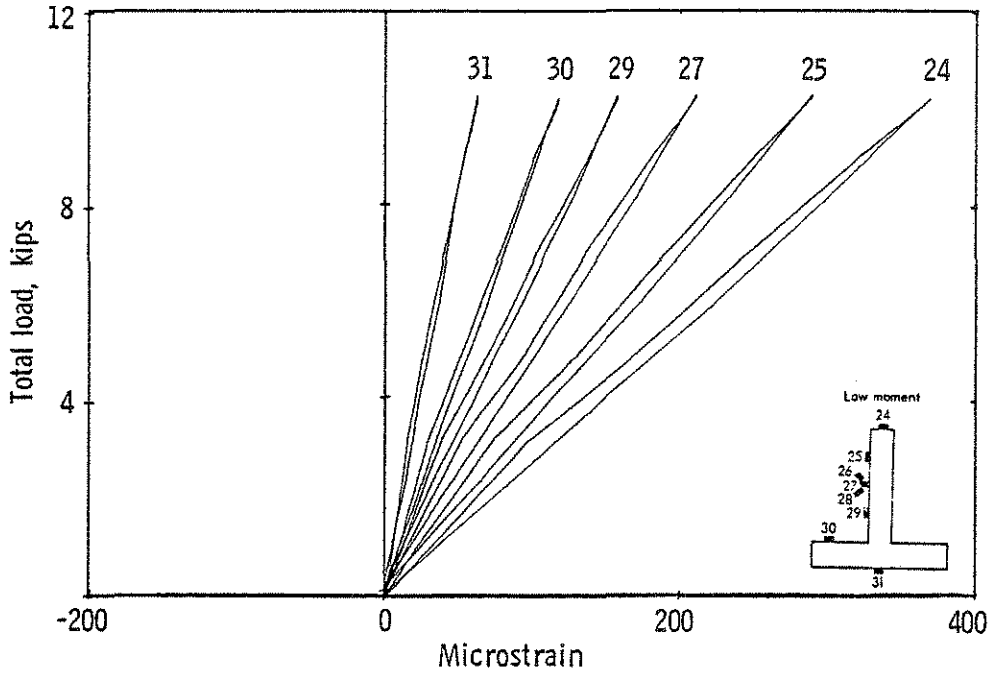

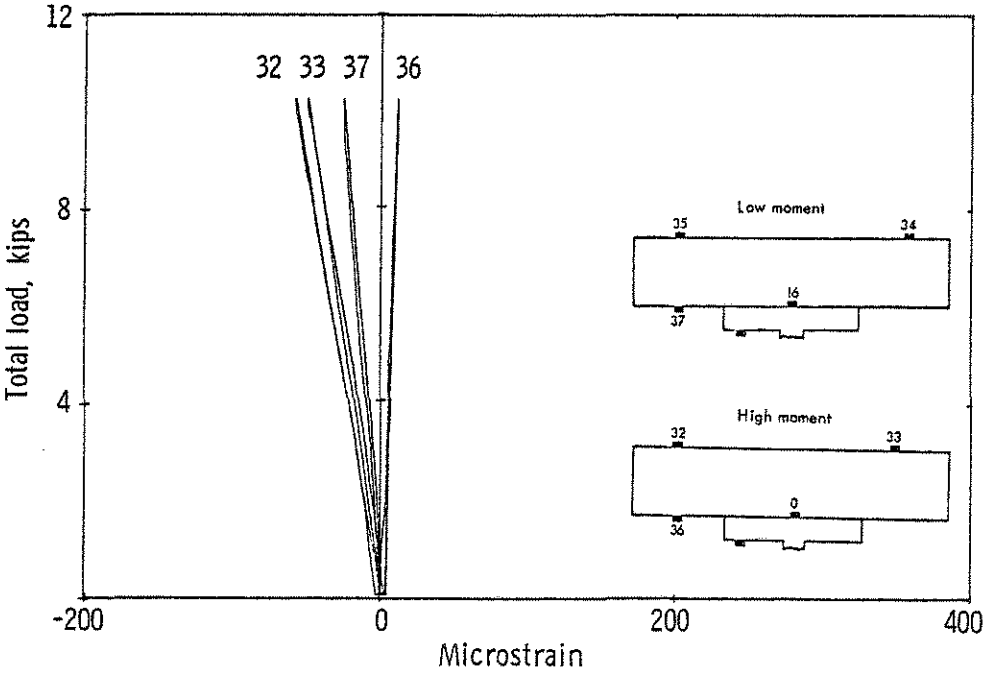

Fig. 3.22 Elastic Load-Strain Curves for Beam No. 5 (cont'd)

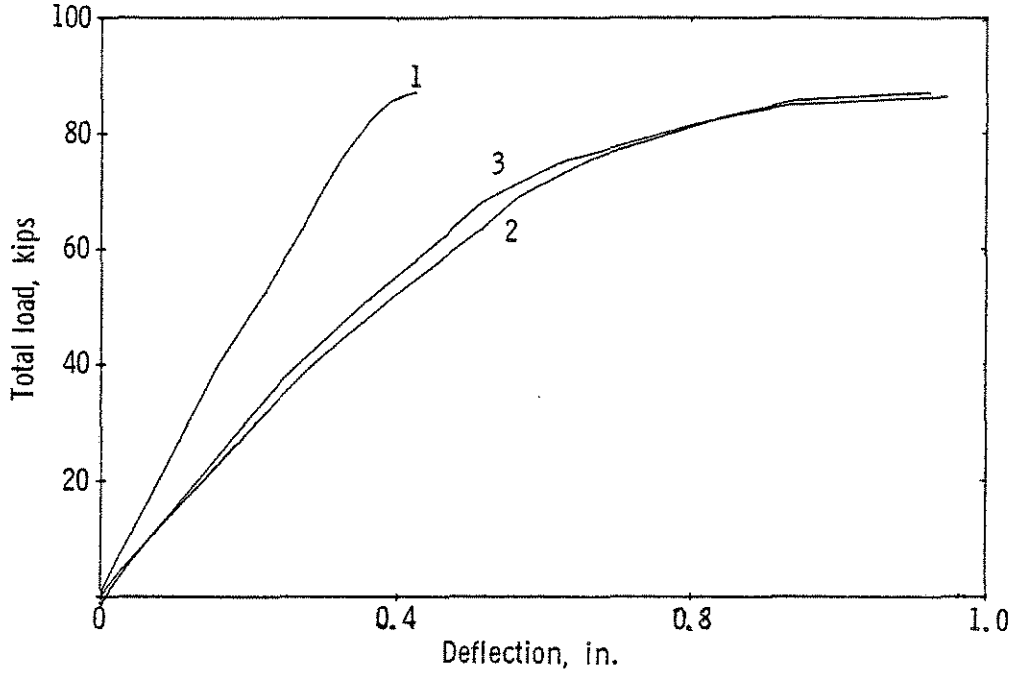

Fig. 3.23 Ultimate Load-Deflection Curves for Beam No. 5

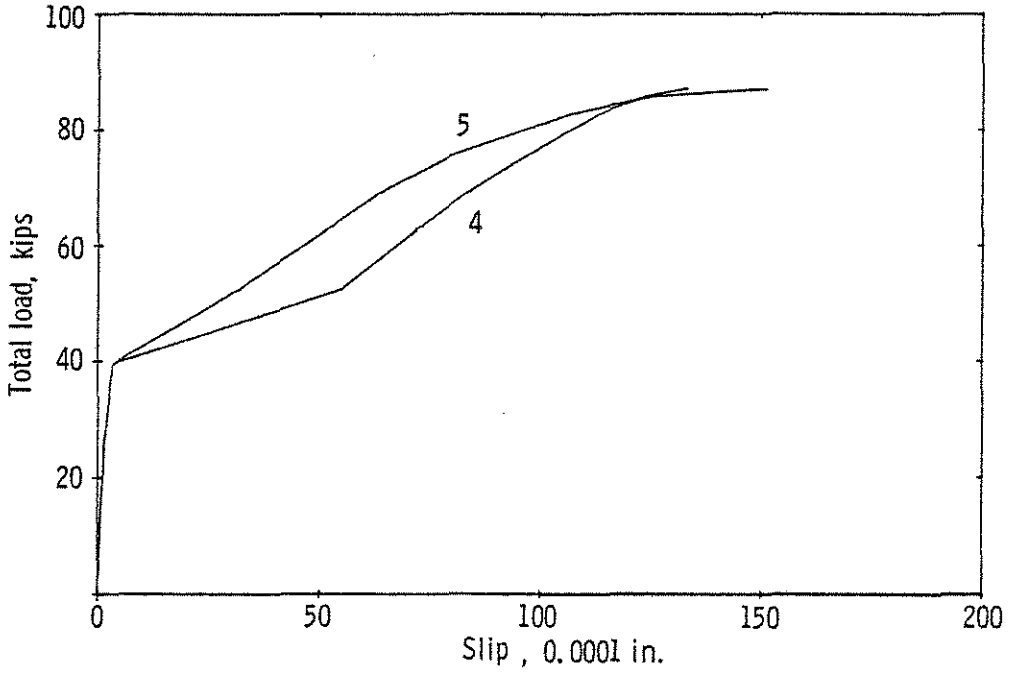

Fig. 3.24 Load-Slip Surves for Beam No. 5

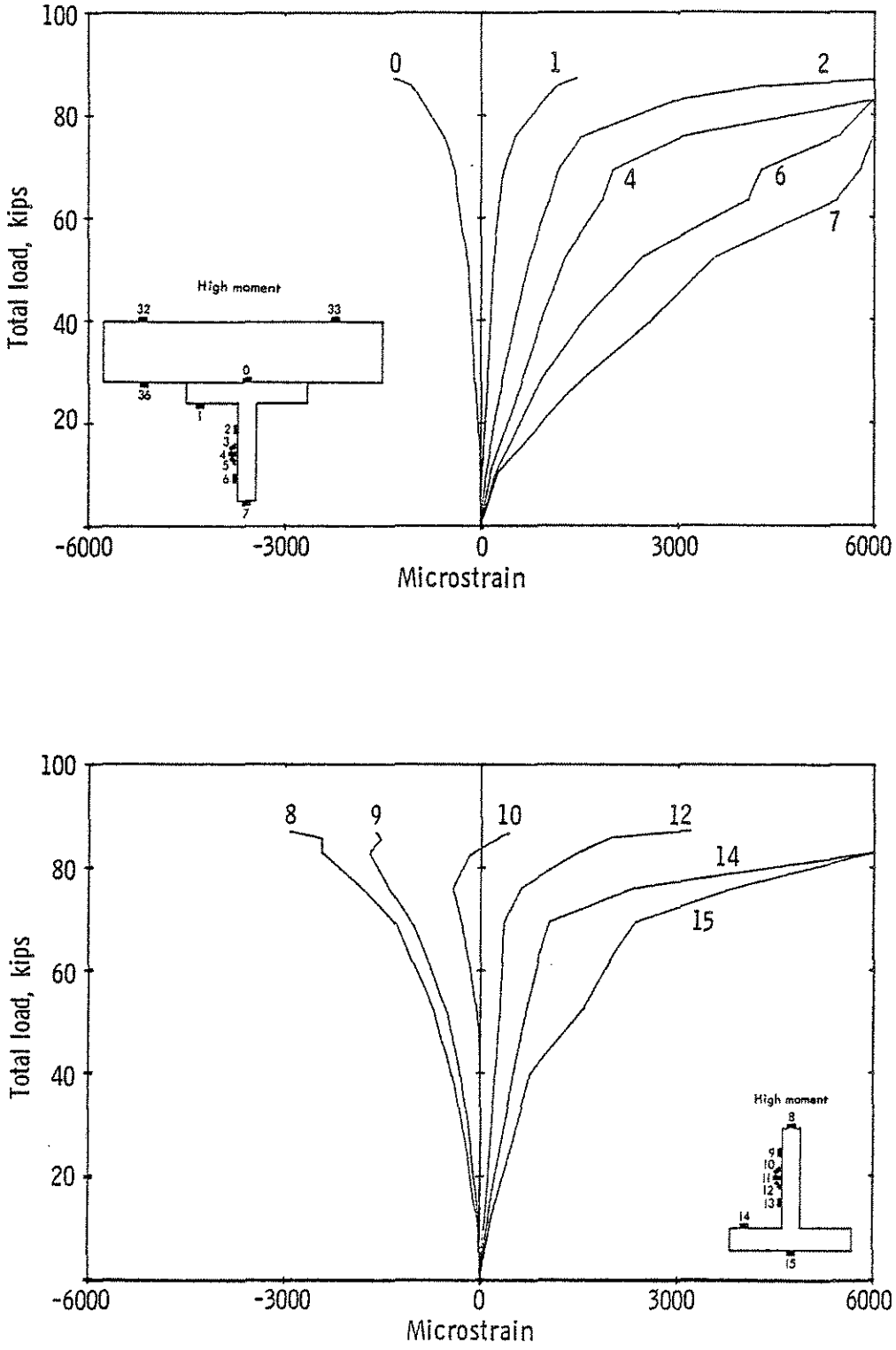

Fig. 3.25 Ultimate Load-Strain Curves for Beam No. 5

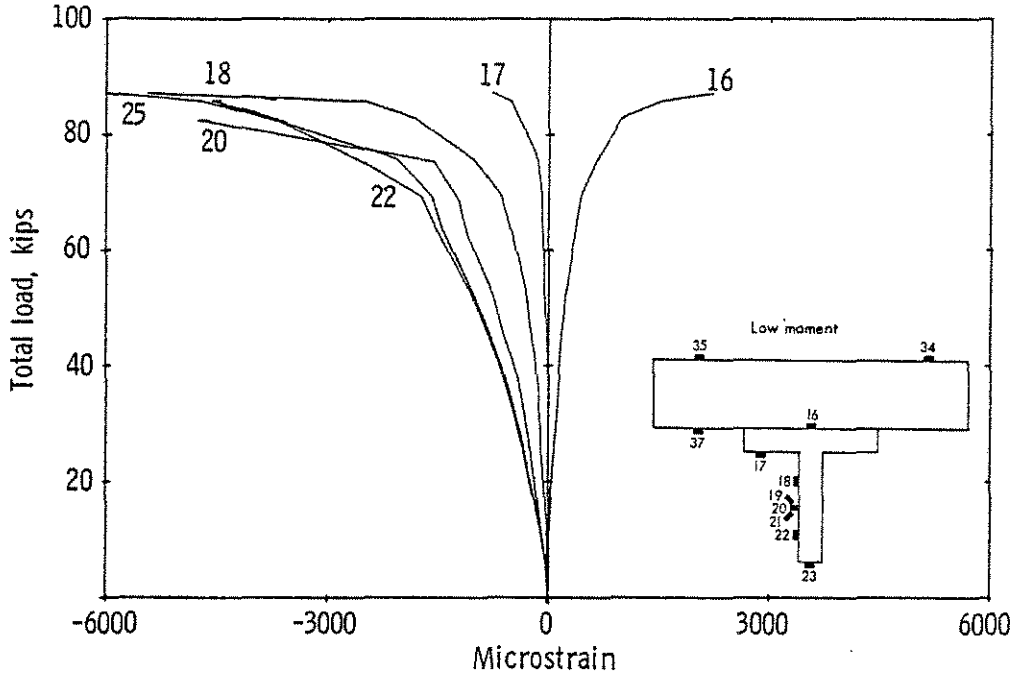

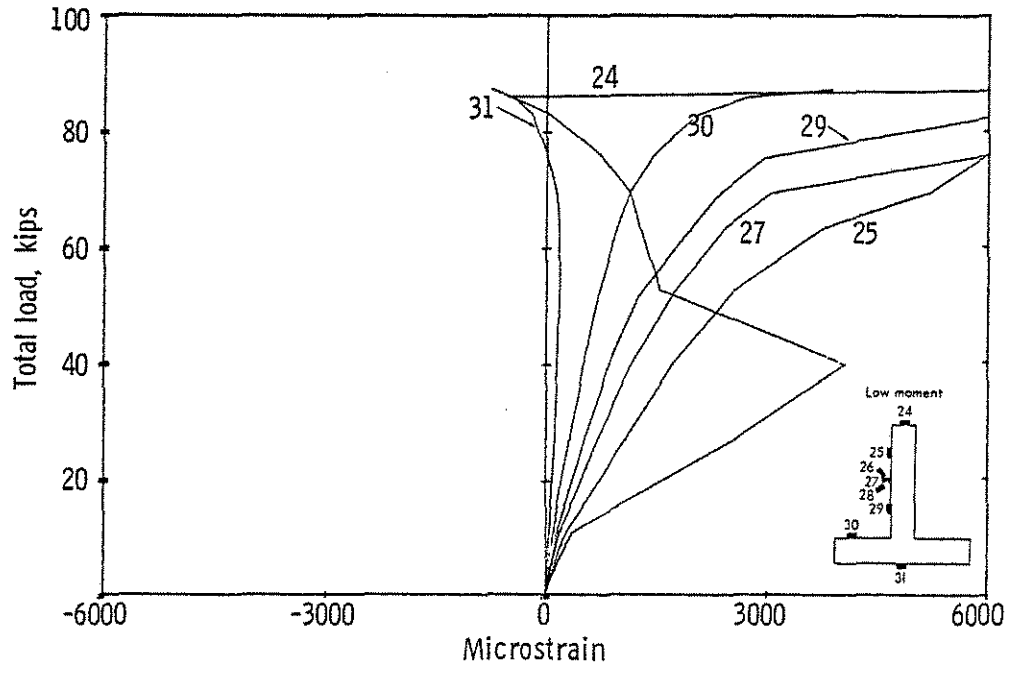

Fig. 3.25 Ultimate Load-Strain Curves for Beam No. 5 (cont'd)

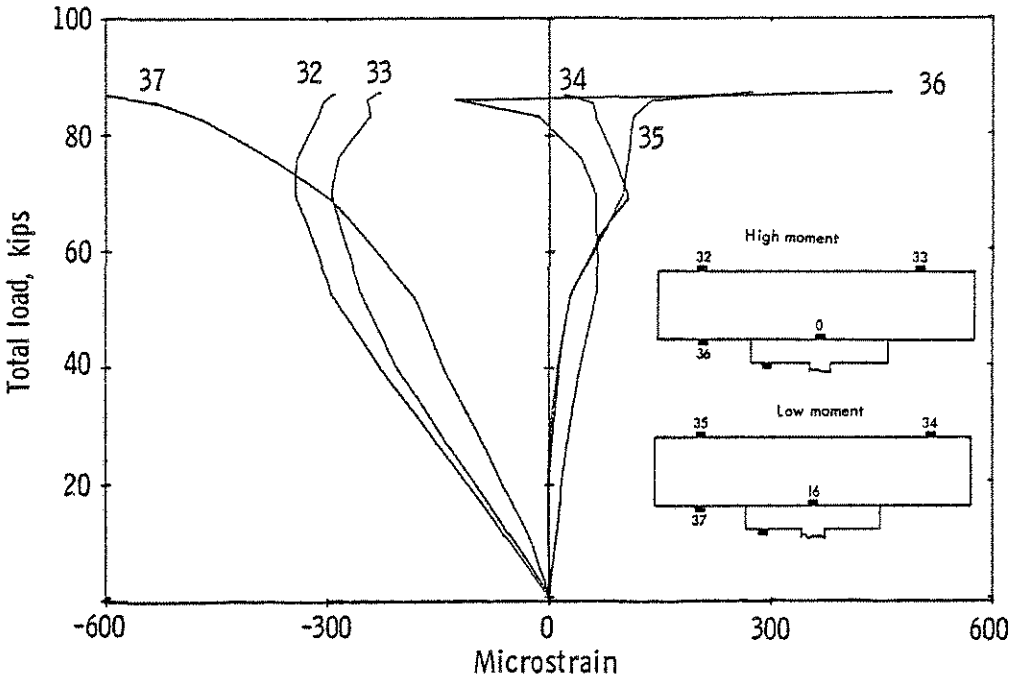

Fig. 3.25 Ultimate Load-Strain Curves for Beam No. 5 (cont'd)

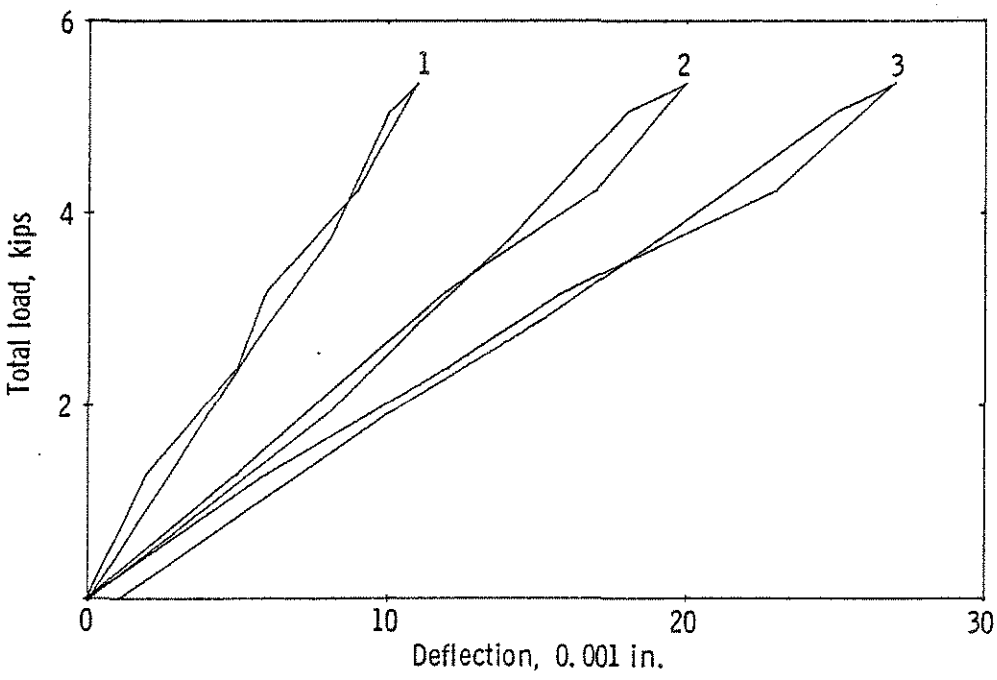

Fig. 3.26 Elastic Load-Deflection Curves for Beam No. 6

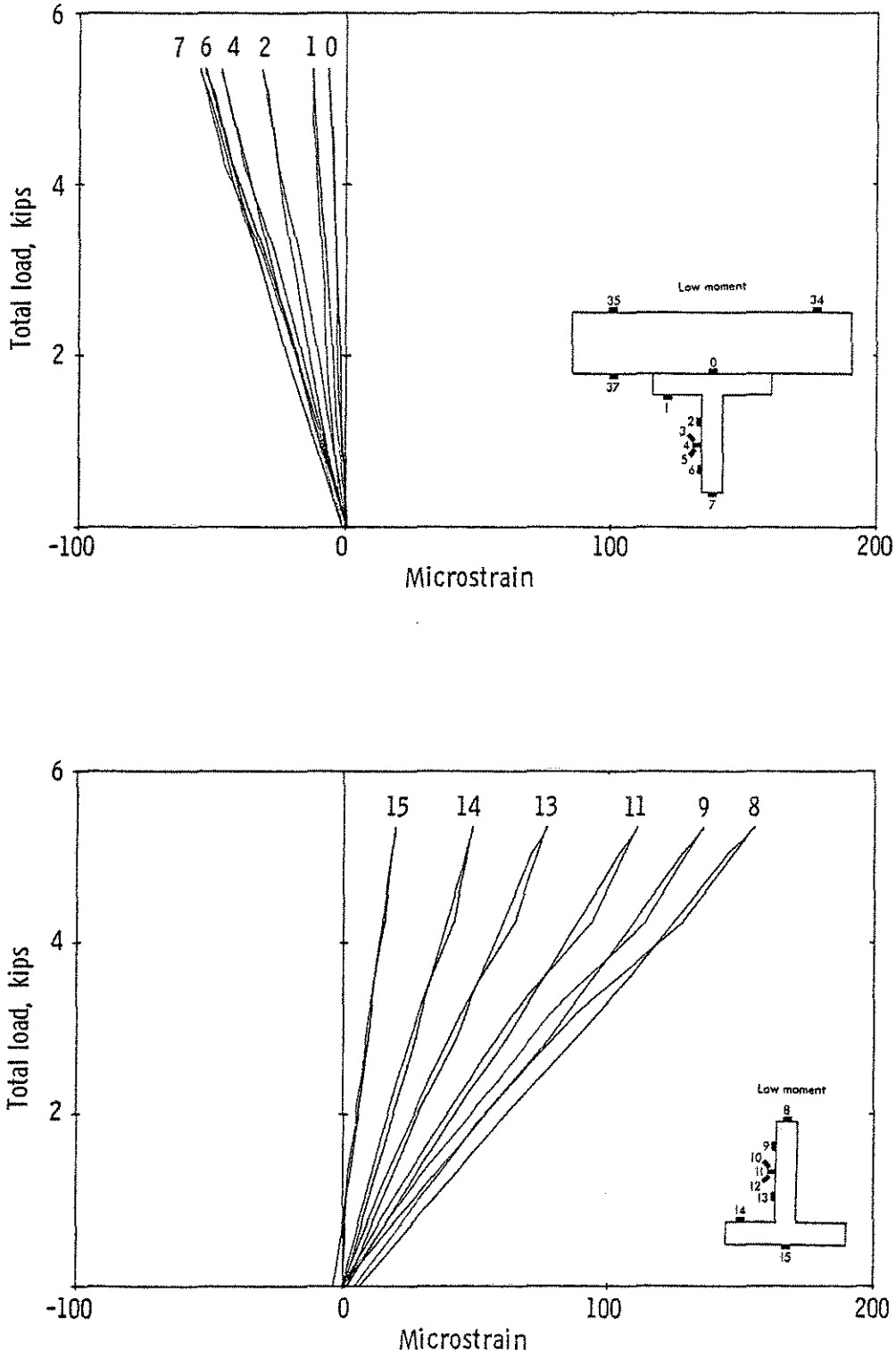

Fig. 3.27 Elastic Load-Strain Curves for Beam No. 6

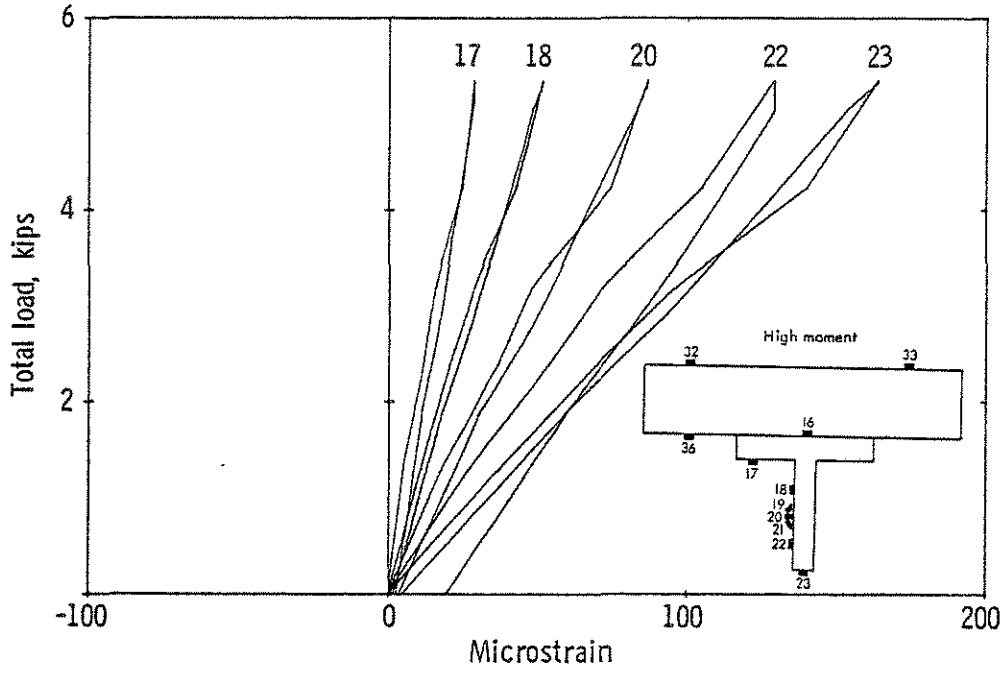

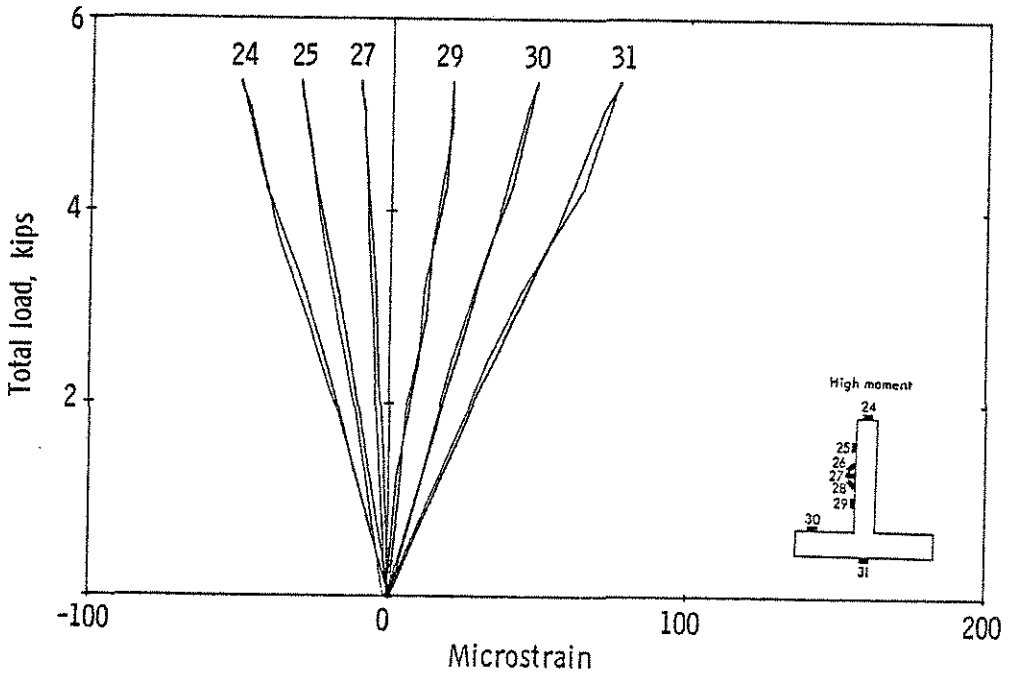

Fig. 3.27 Elastic Load-Strain Curves for Beam No. 6 (cont'd)

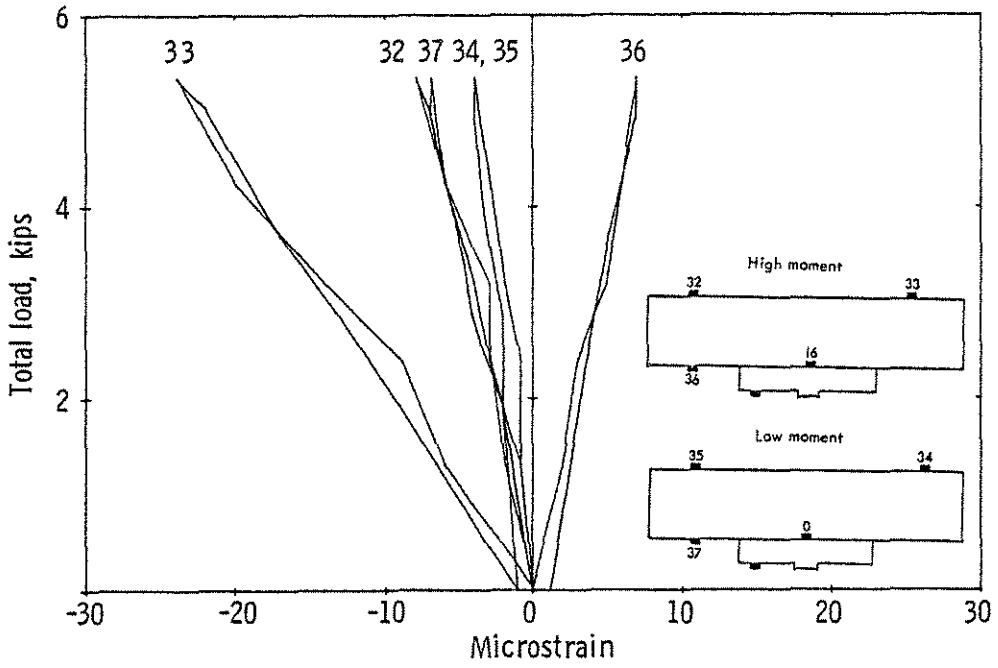

Fig. 3.27 Elastic Load-Strain Curves for Beam No. 6 (cont'd)

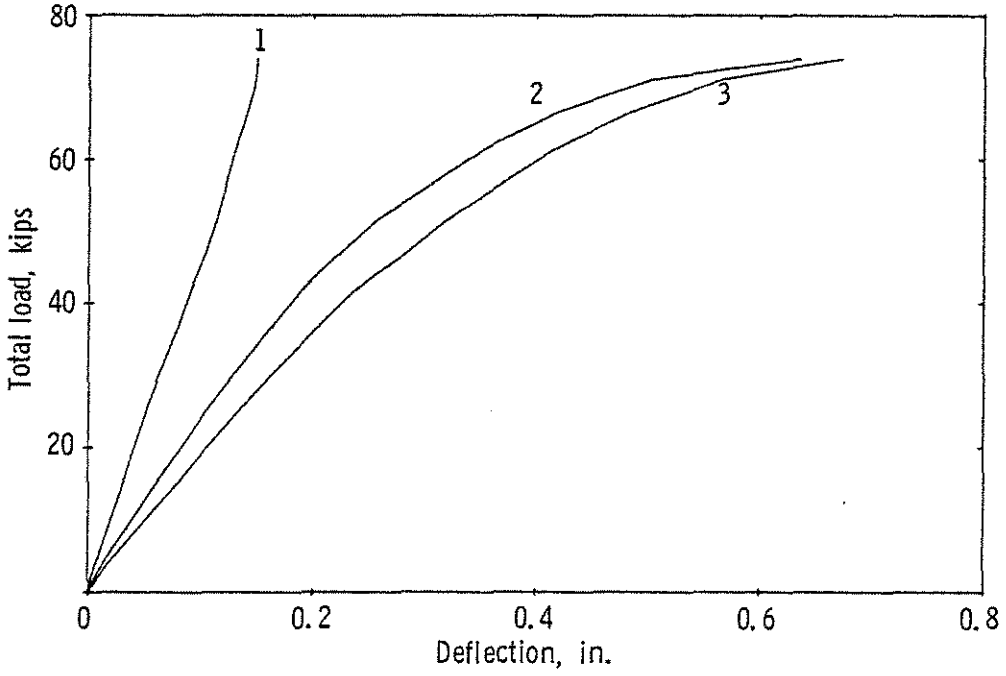

Fig. 3.28 Ultimate Load-Deflection Curves for Beam No. 6

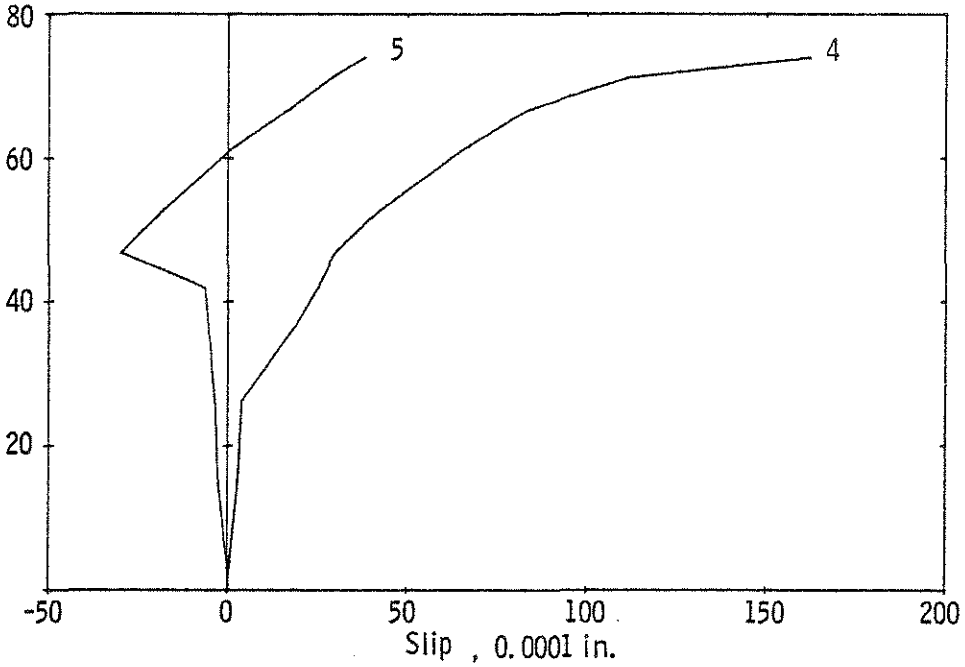

Fig. 3.29 Load-Slip Curves for Beam No. 6

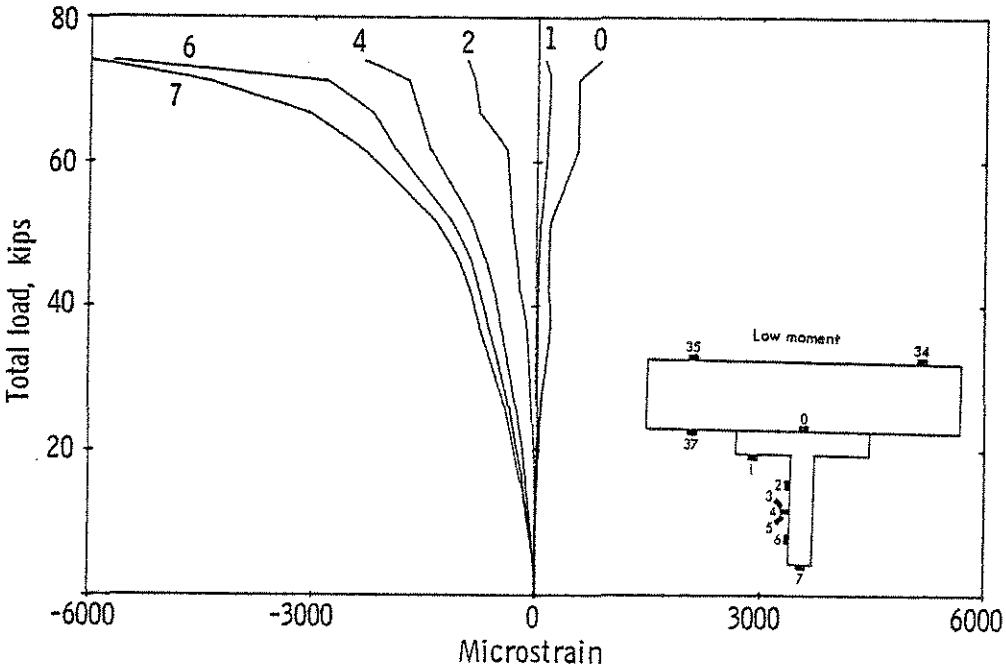

Fig. 3.30 Ultimate Load-Strain Curves for Beam No. 6

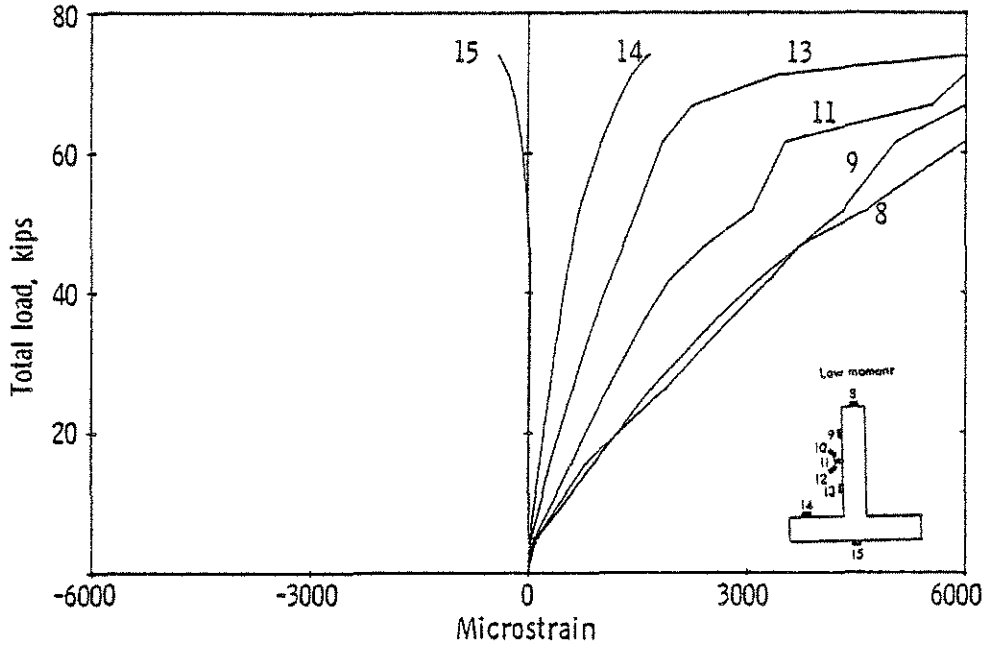

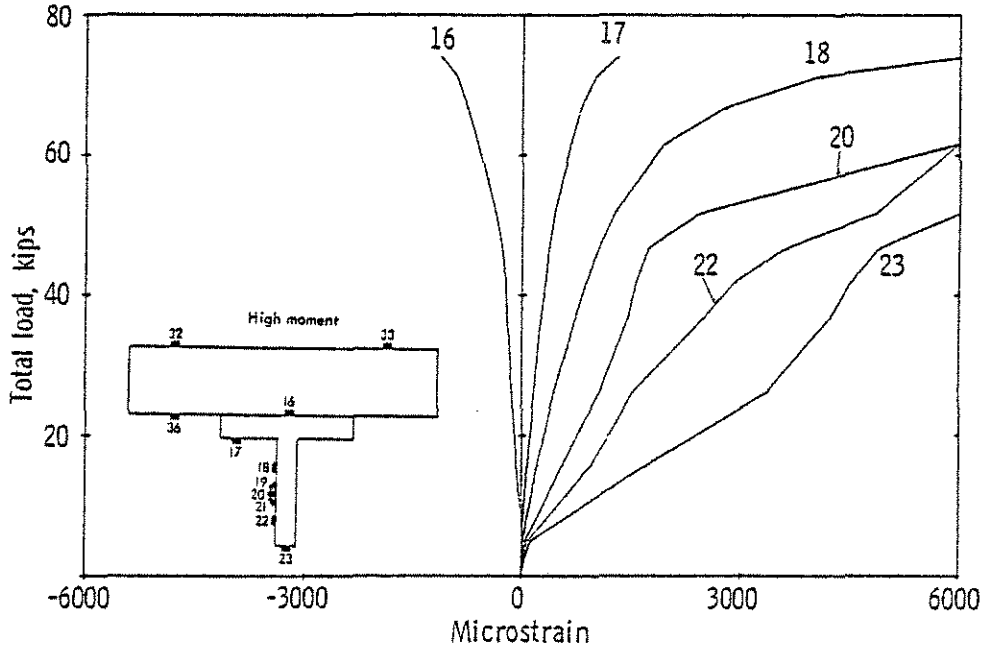

Fig. 3.30 Ultimate Load-Strain Curves for Beam No. 6 (cont'd)

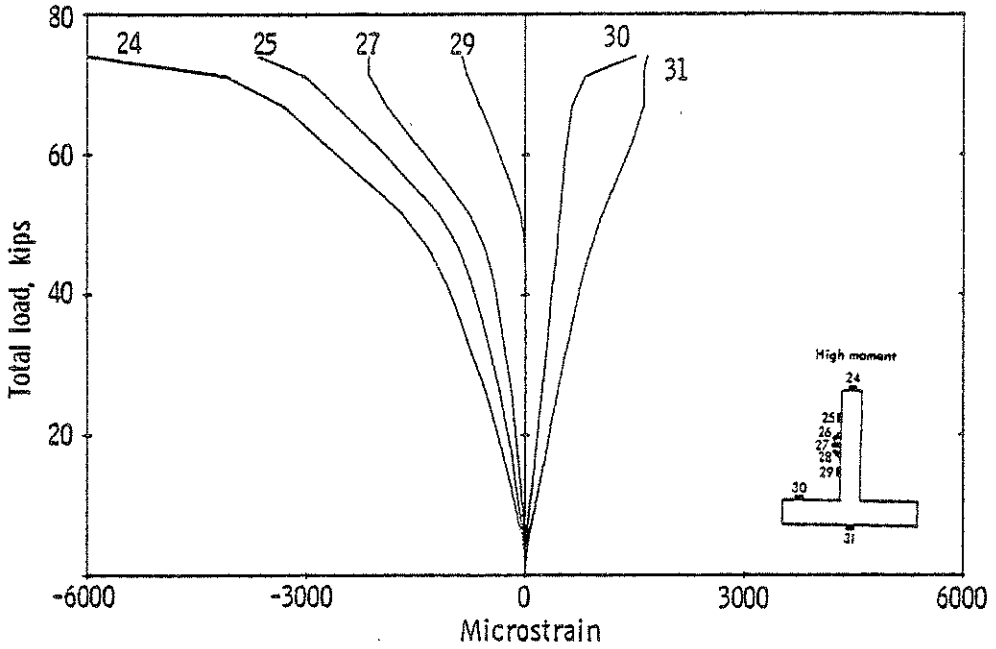

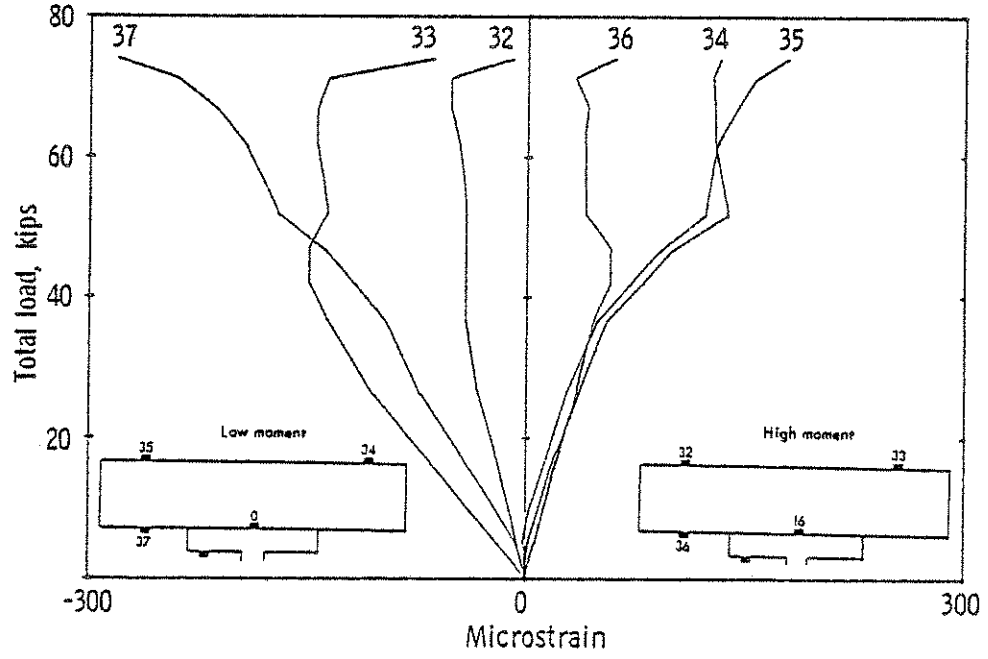

Fig. 3.30 Ultimate Load-Strain Curves for Beam No. 6 (cont'd)

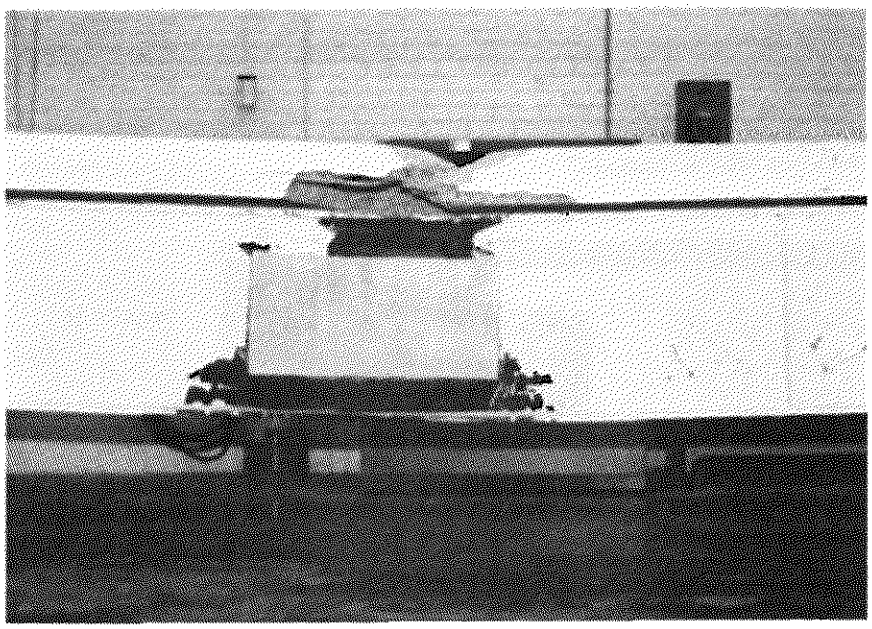

Beam No. 3

Fig. 3.31 Failure in Beam with High Moment-shear Ratio

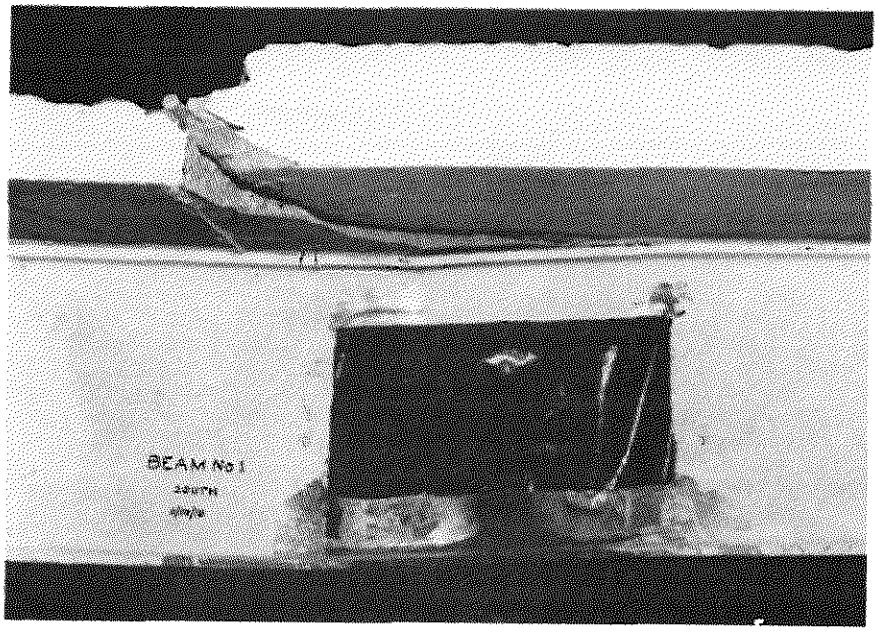

Beam No. 1

Fig. 3.32 Failure in Beams with Medium and Low Moment-shear Ratios

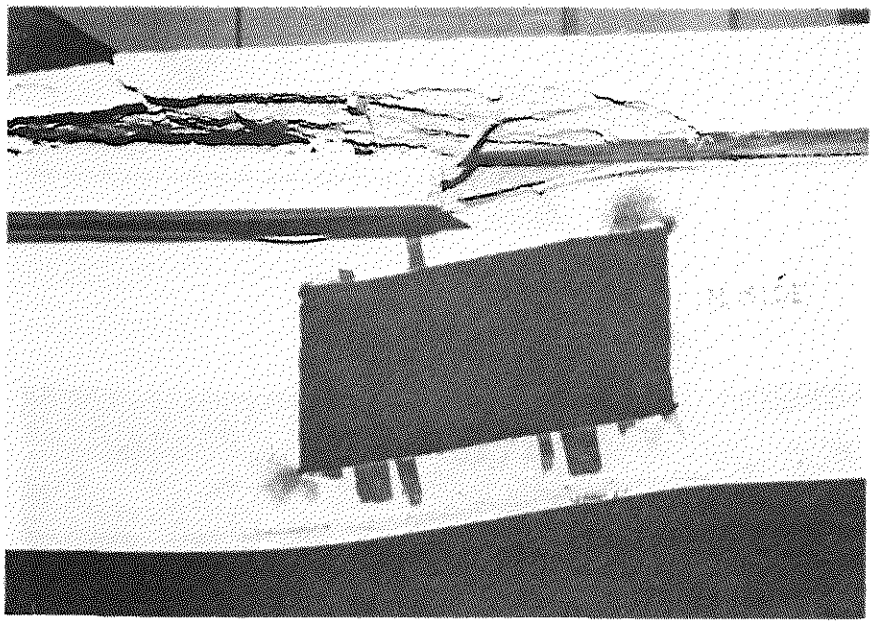

Beam No. 2

Fig. 3.32 Failure in Beams with Medium and Low Moment-shear Ratios (cont'd)

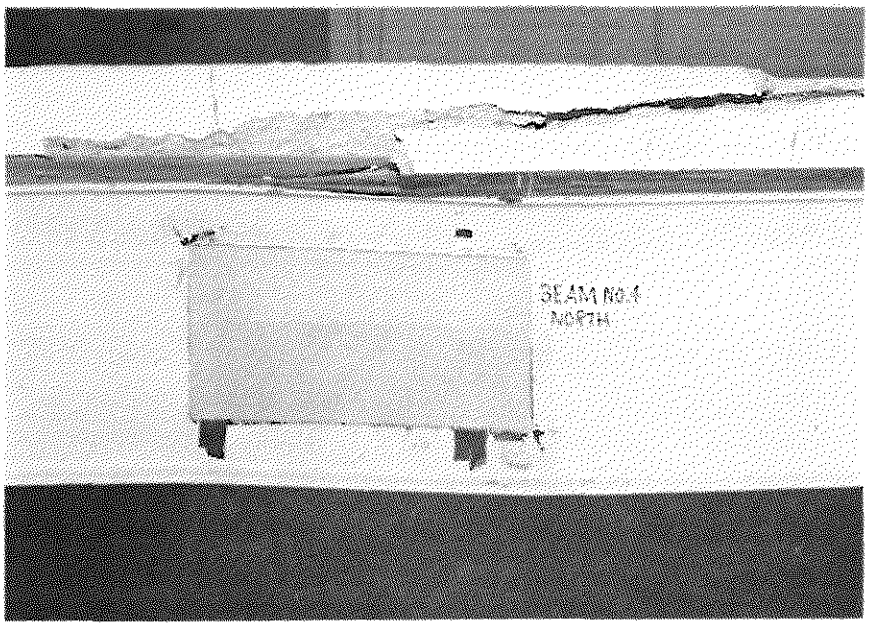

Beam No. 4

Fig. 3.32 Failure in Beams with Medium and Low Moment-shear Ratios (cont'd)

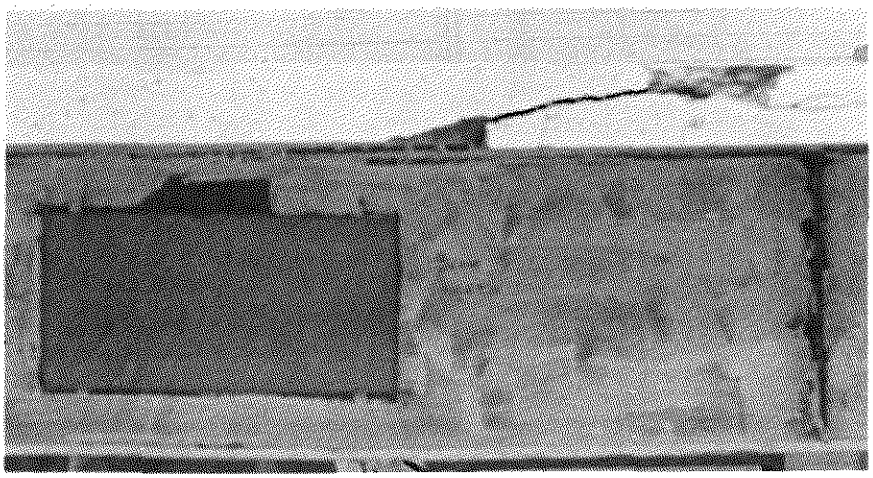

Beam No. 5

Fig. 3.32 Failure in Beams with Medium and Low Moment-shear Ratios (cont'd)

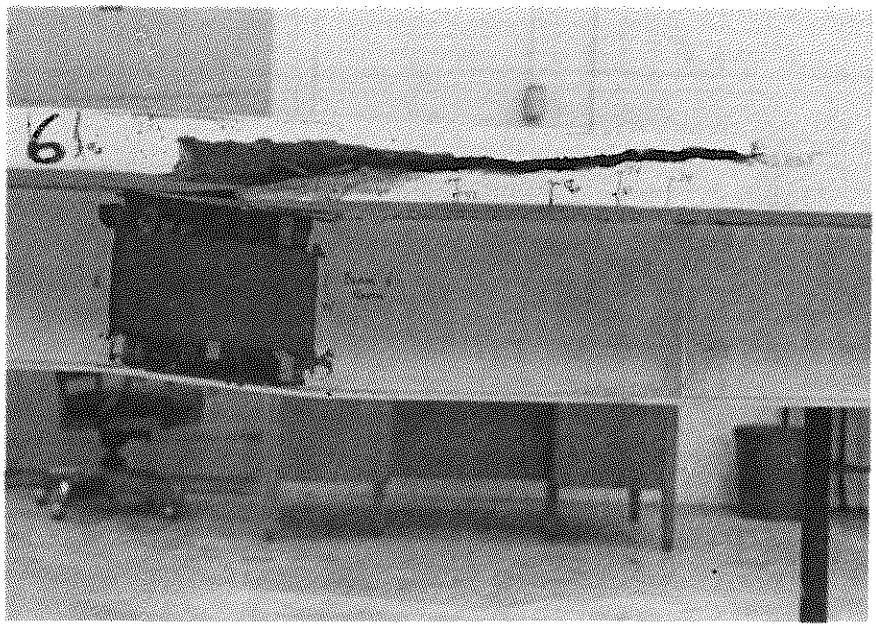

Beam No. 6

Fig. 3.32 Failure in Beams with Medium and Low Moment-shear Ratios (cont'd)

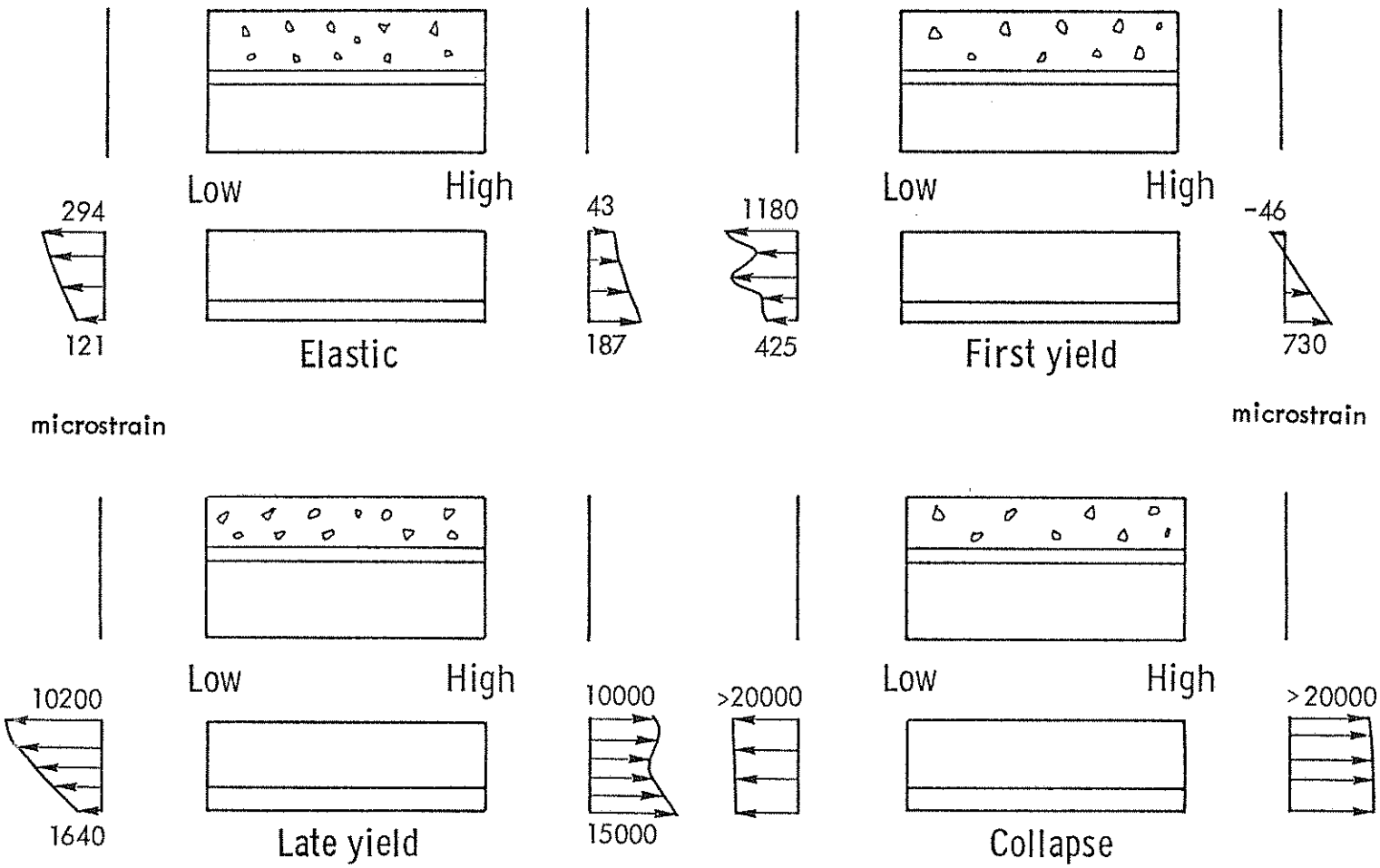

Fig. 3.33 Strain Distribution in Beam No. 1

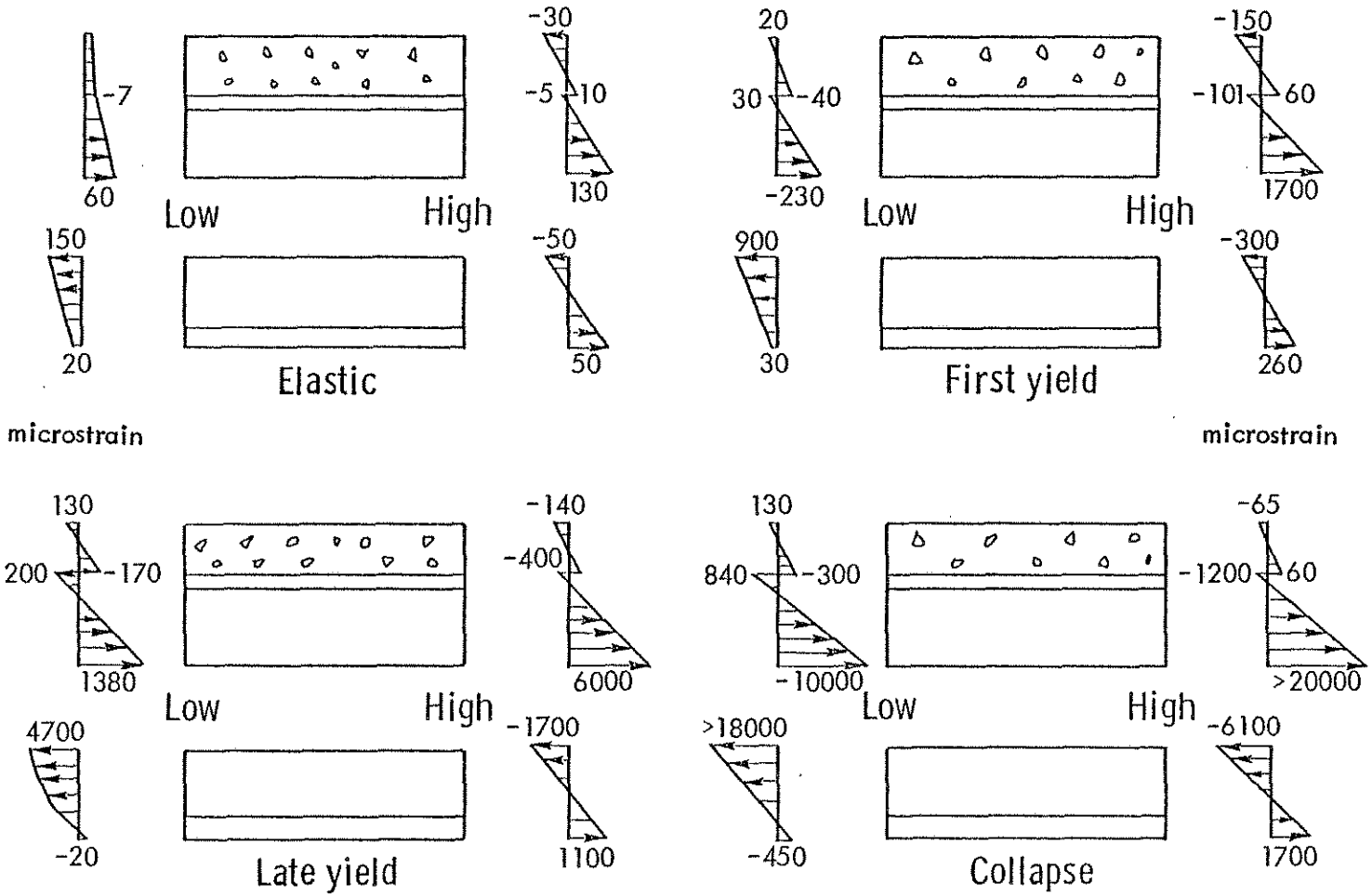

Fig. 3.34 Strain Distribution in Beam No. 6

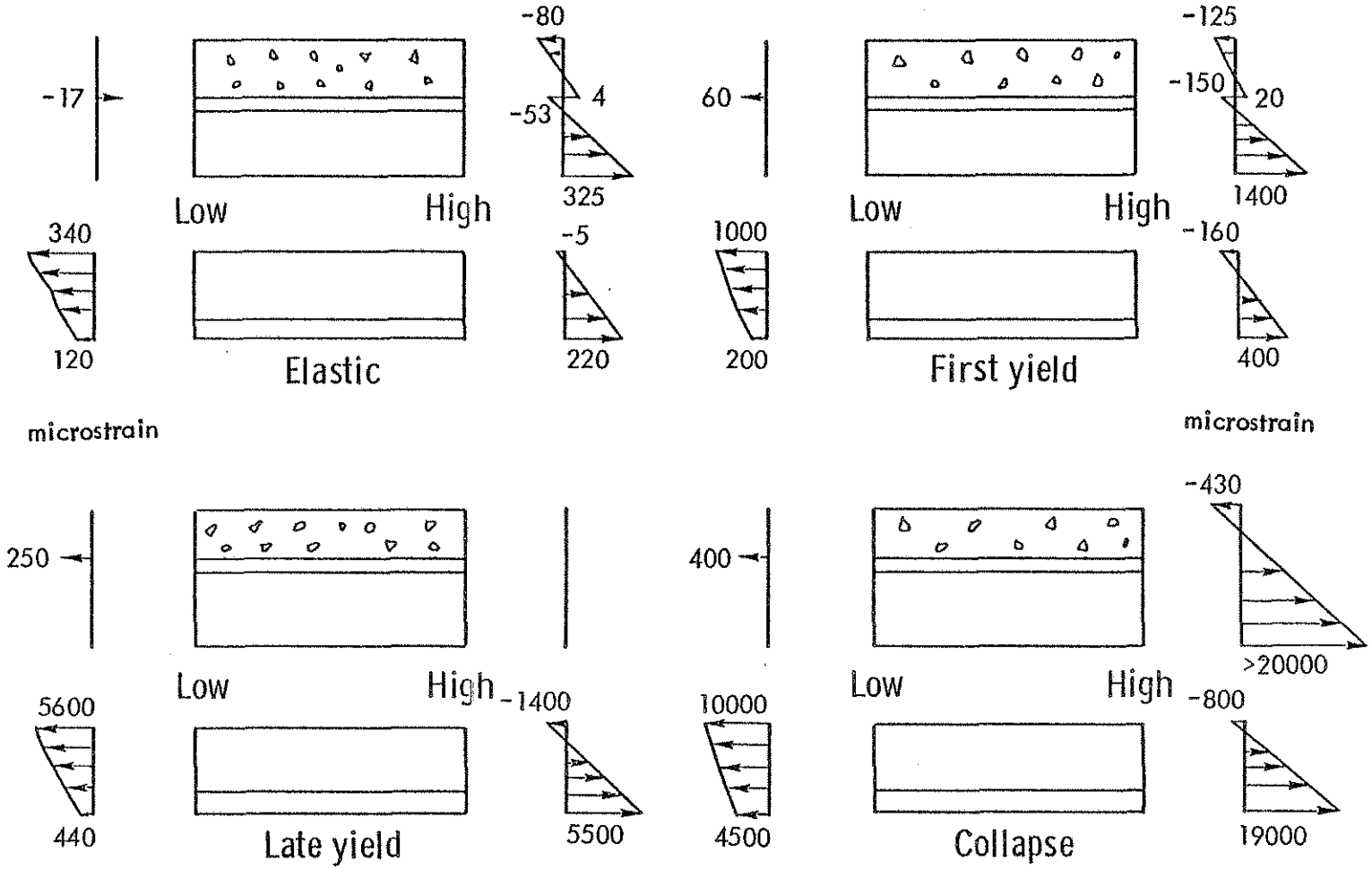

Fig. 3.35 Strain Distribution in Beam No. 2

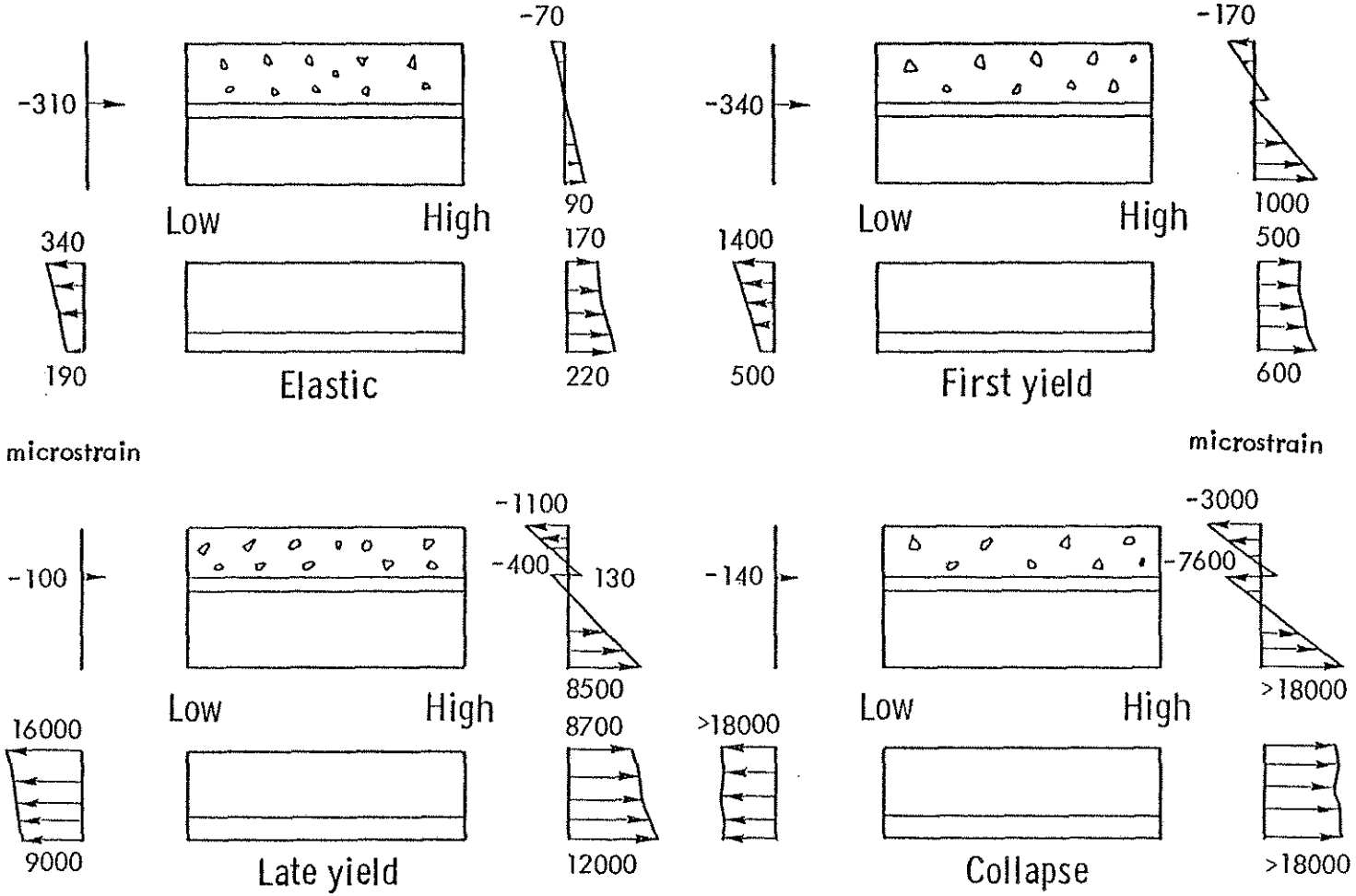

Fig. 3.36 Strain Distribution in Beam No. 3

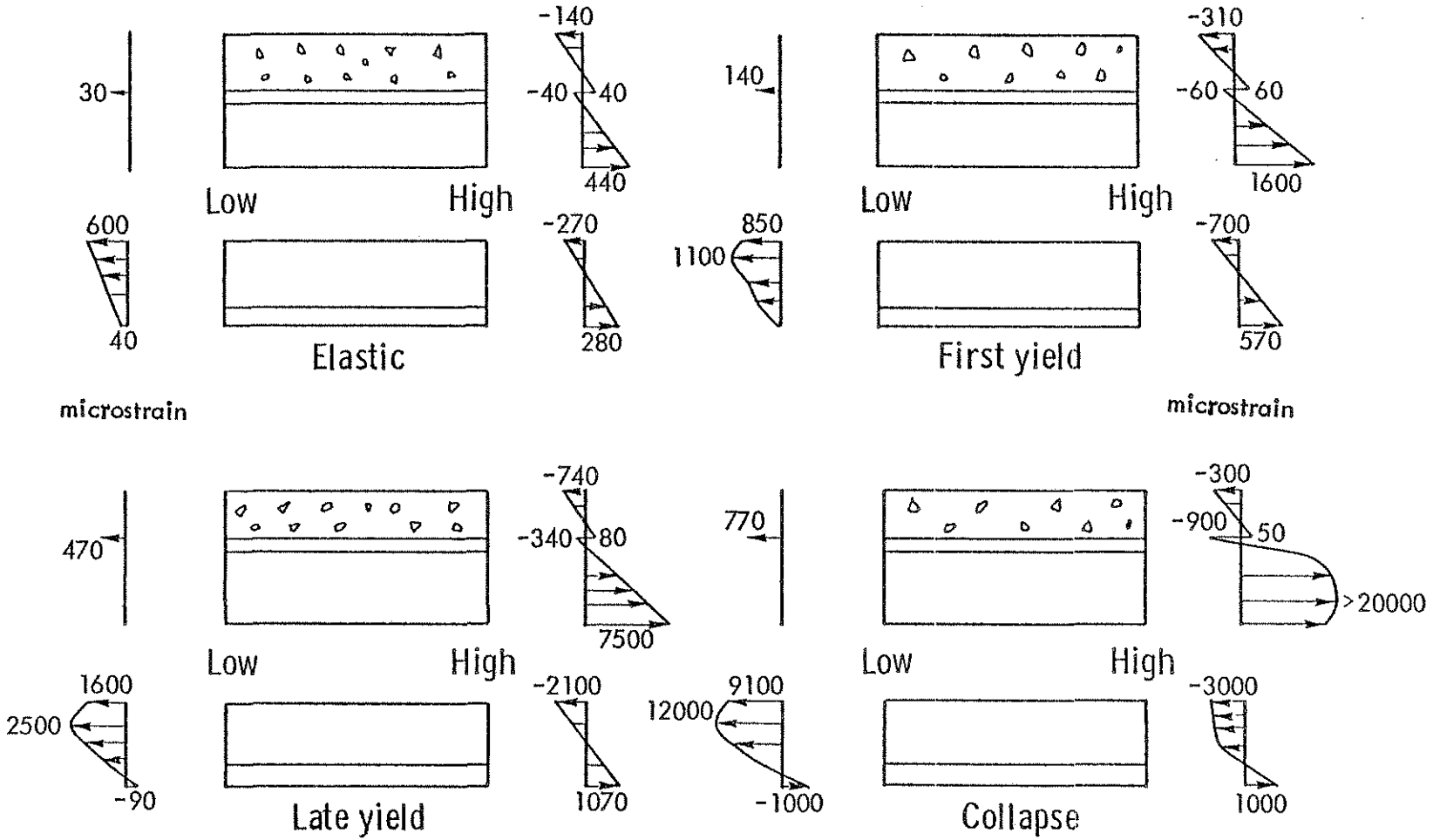

Fig. 3.37 Strain Distribution in Beam No. 4

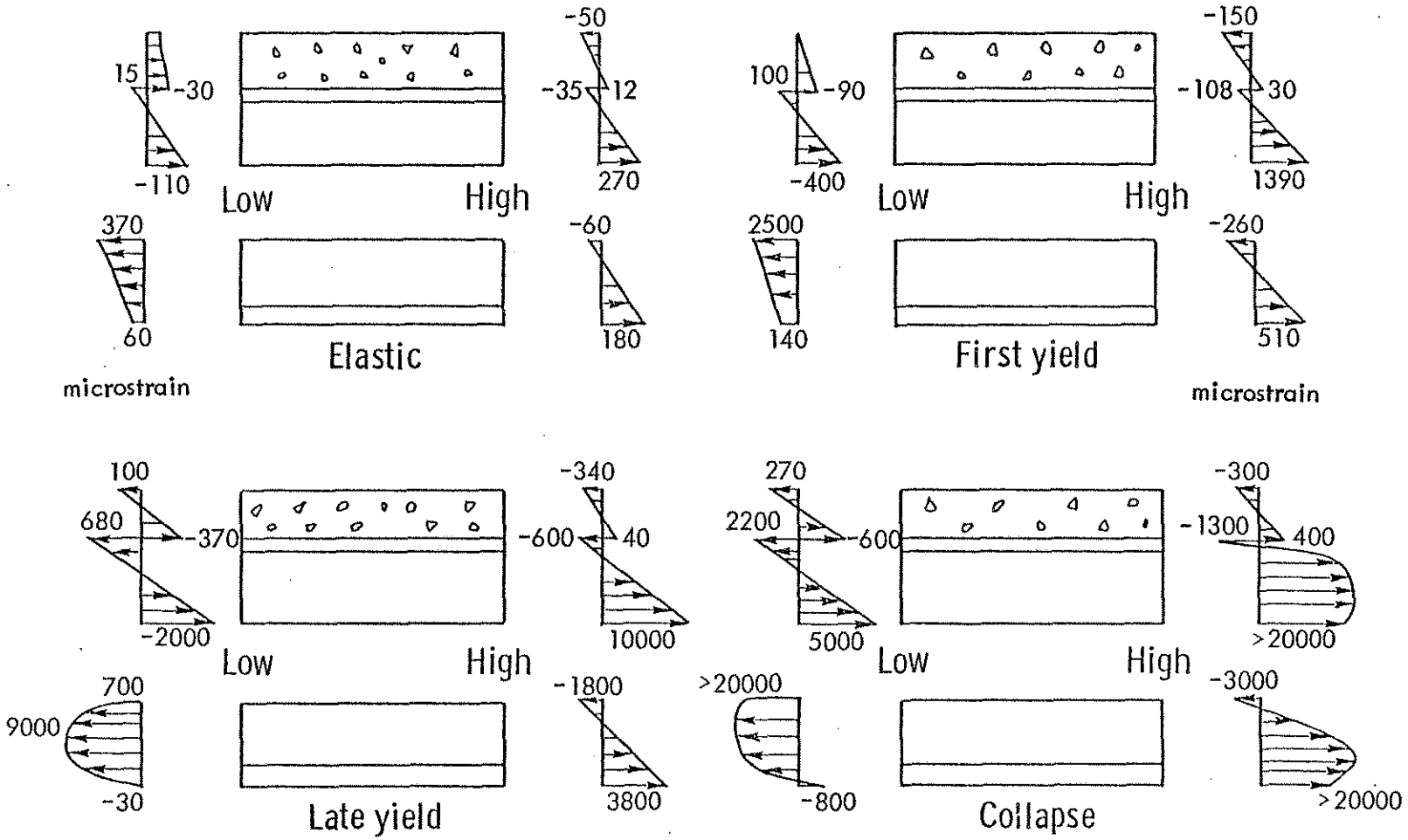

Fig. 3.38 Strain Distribution in Beam No. 5

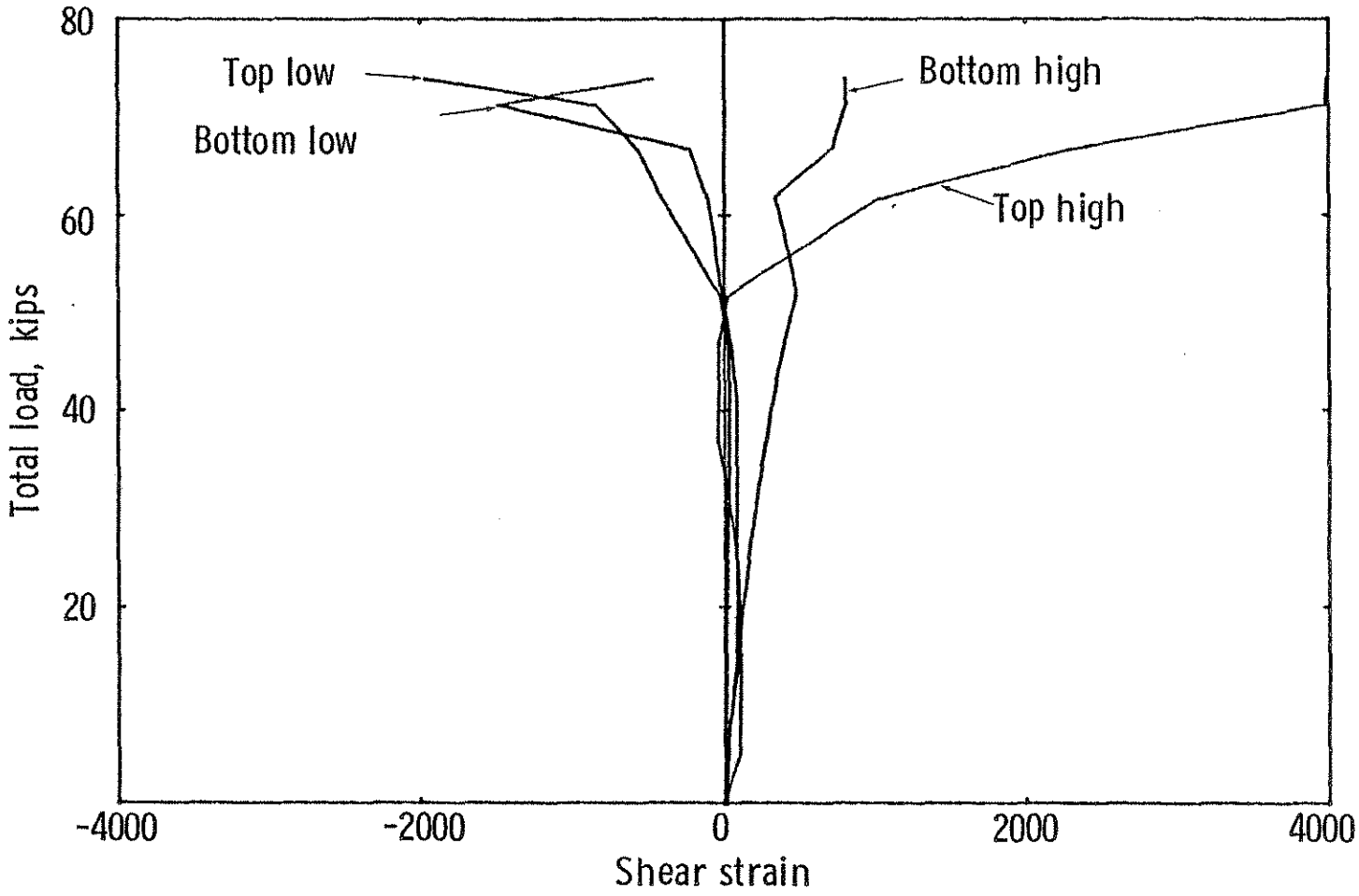

Fig. 3.39 Load-Shear Strain Curves for Beam No. 6

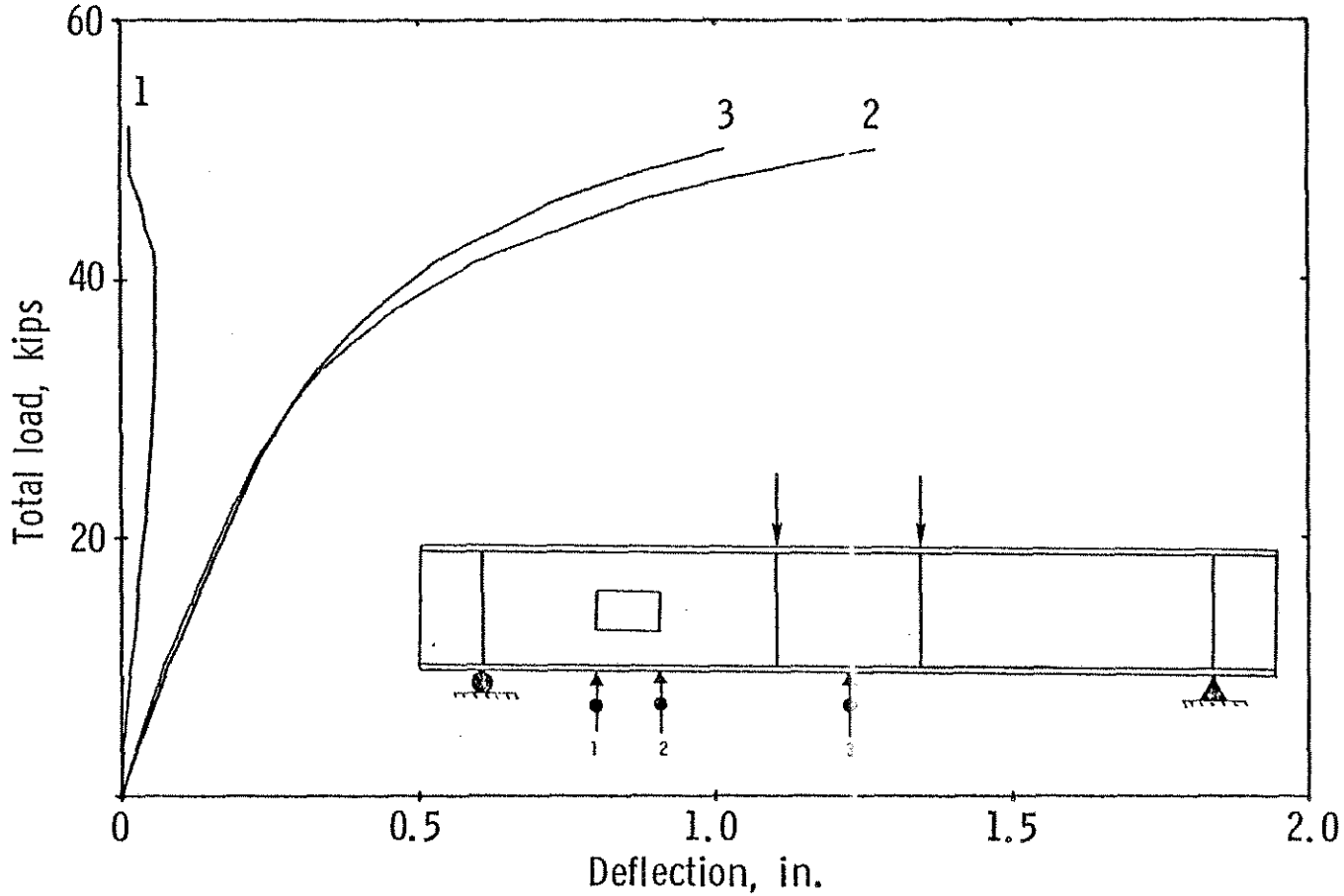

Fig. 3.40 Load-Deflection Curves for Beam No. 4B

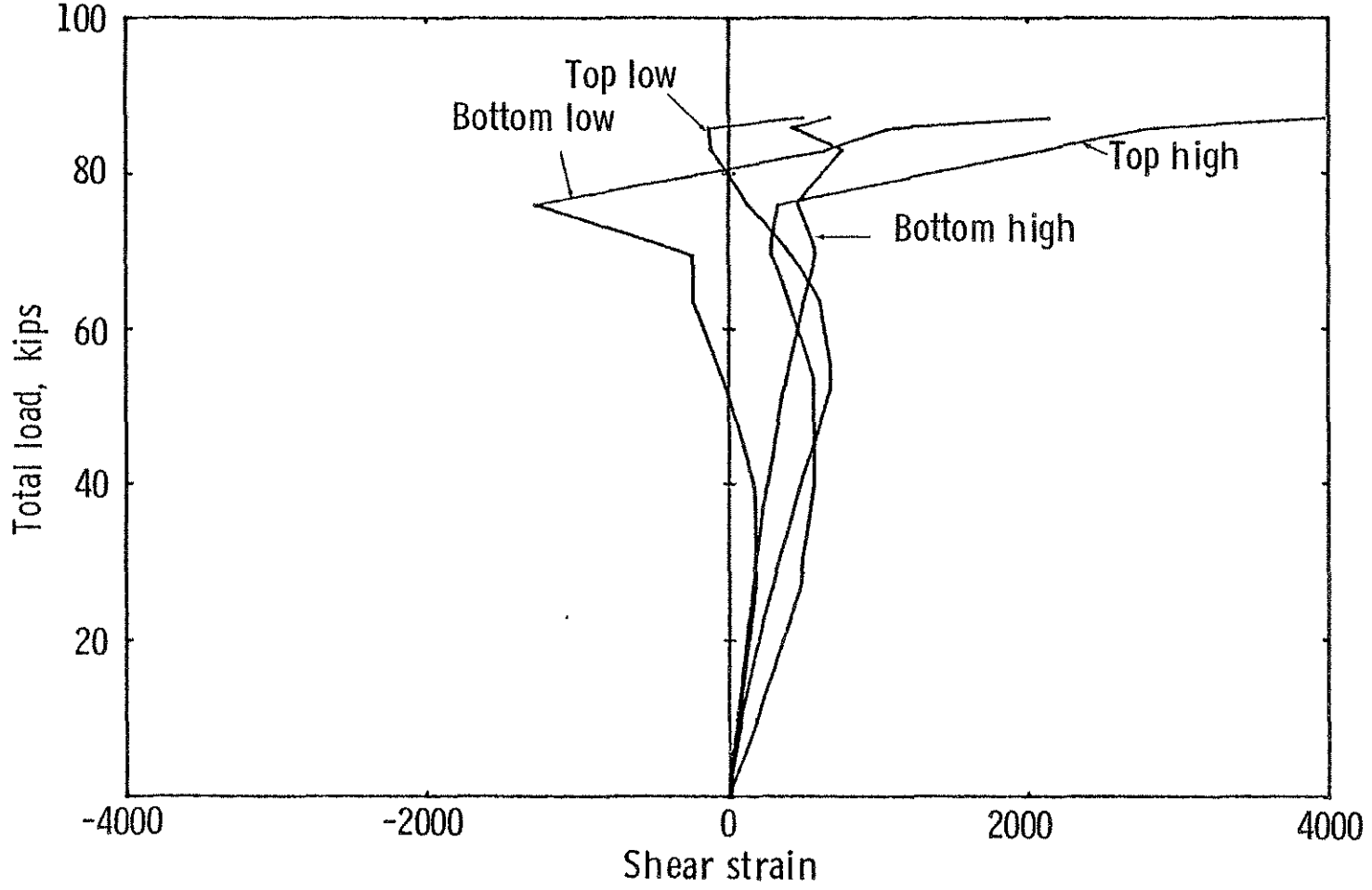

Fig. 3.41 Load-Shear Strain Curves for Beam No. 5

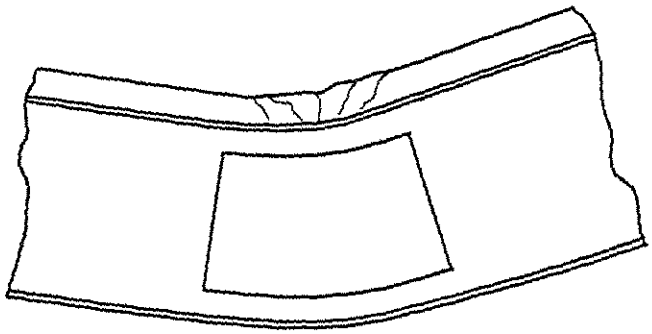

Fig. 4.1 Pure Bending Failure at Opening

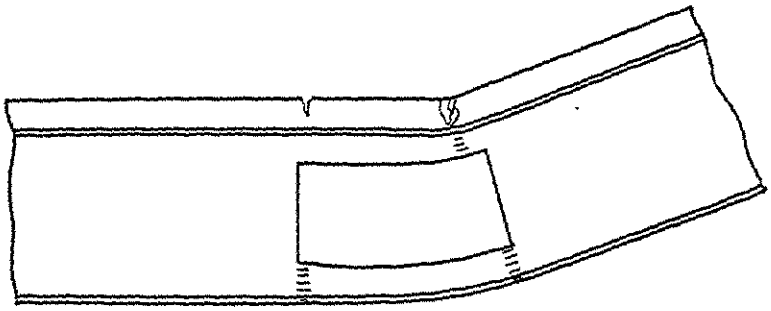

Fig. 4.2 "Mechanism" Failure with Combined Moment and Shear

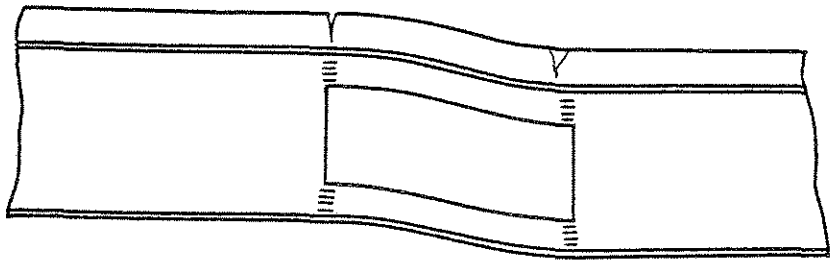

Fig. 4.3 "Mechanism" Failure in Pure Shear

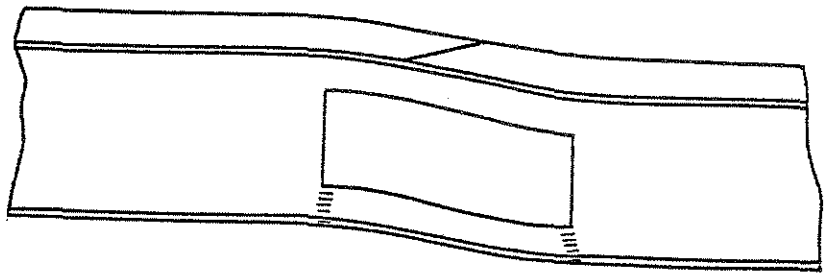

Fig. 4.4 "Shear" Failure in Top Tee

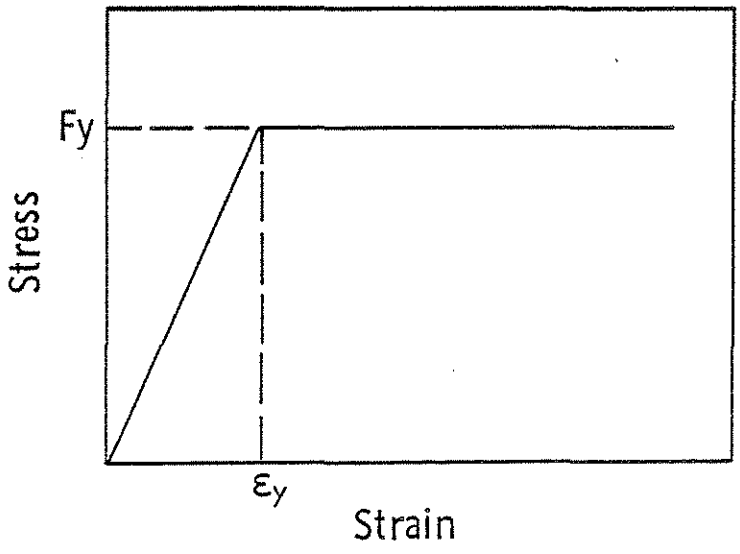

Fig. 4.5 Idealized Stress-Strain Diagram for Steel

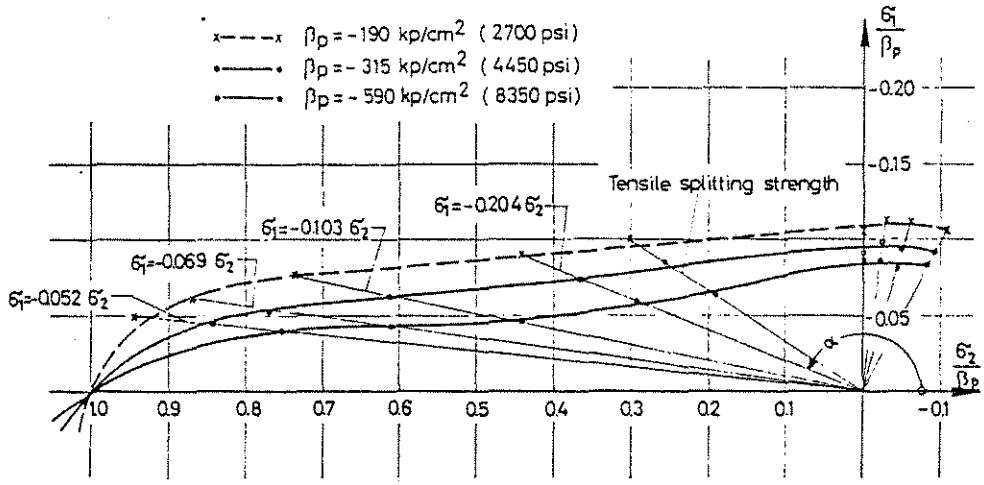

Fig. 4.6 Experimental Results for the Strength of Concrete Under Combined Tension and Compression (19)

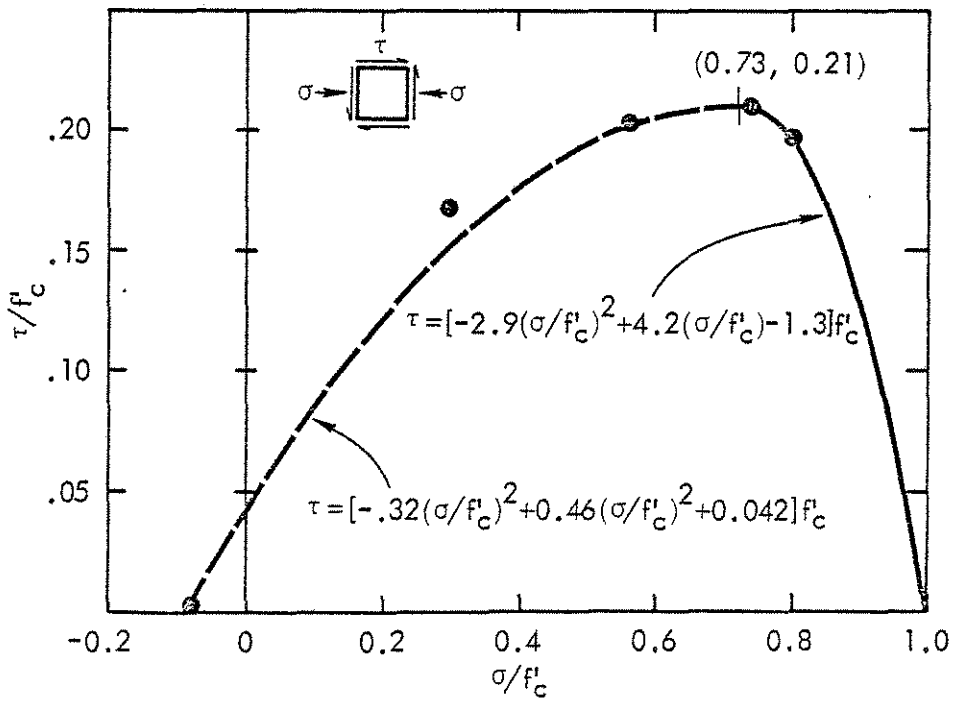

Fig. 4.7 Concrete Strength Under Combined Shear and Normal Stress

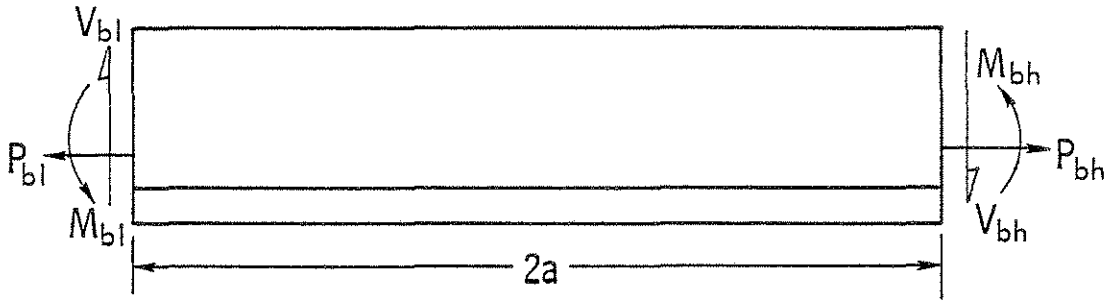

Fig. 4.8 Forces Acting on Bottom Tee

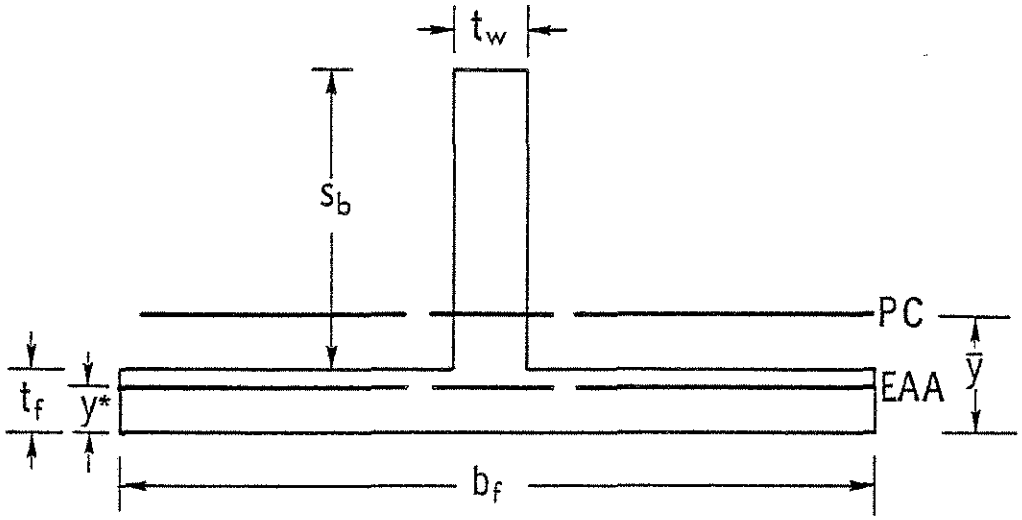

Fig. 4.9 Bottom Tee Cross-Section

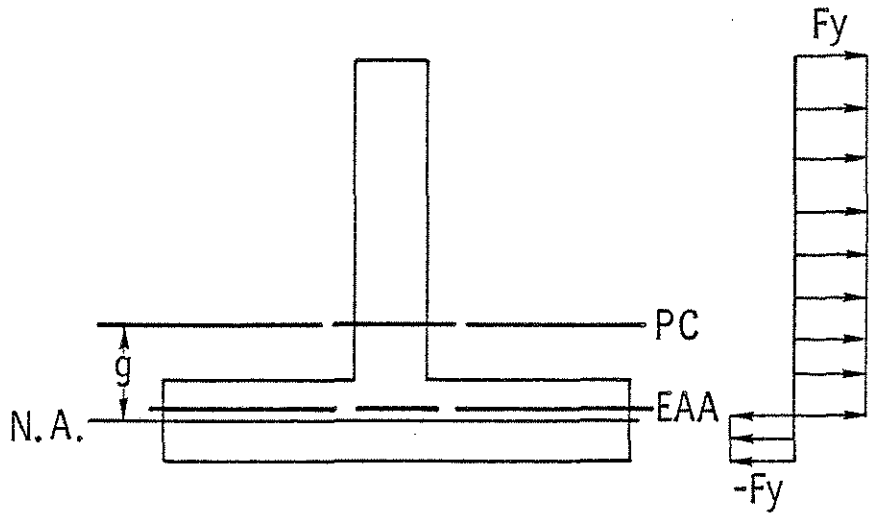

Fig. 4.10 Stress Distribution at Low Moment End of Bottom Tee

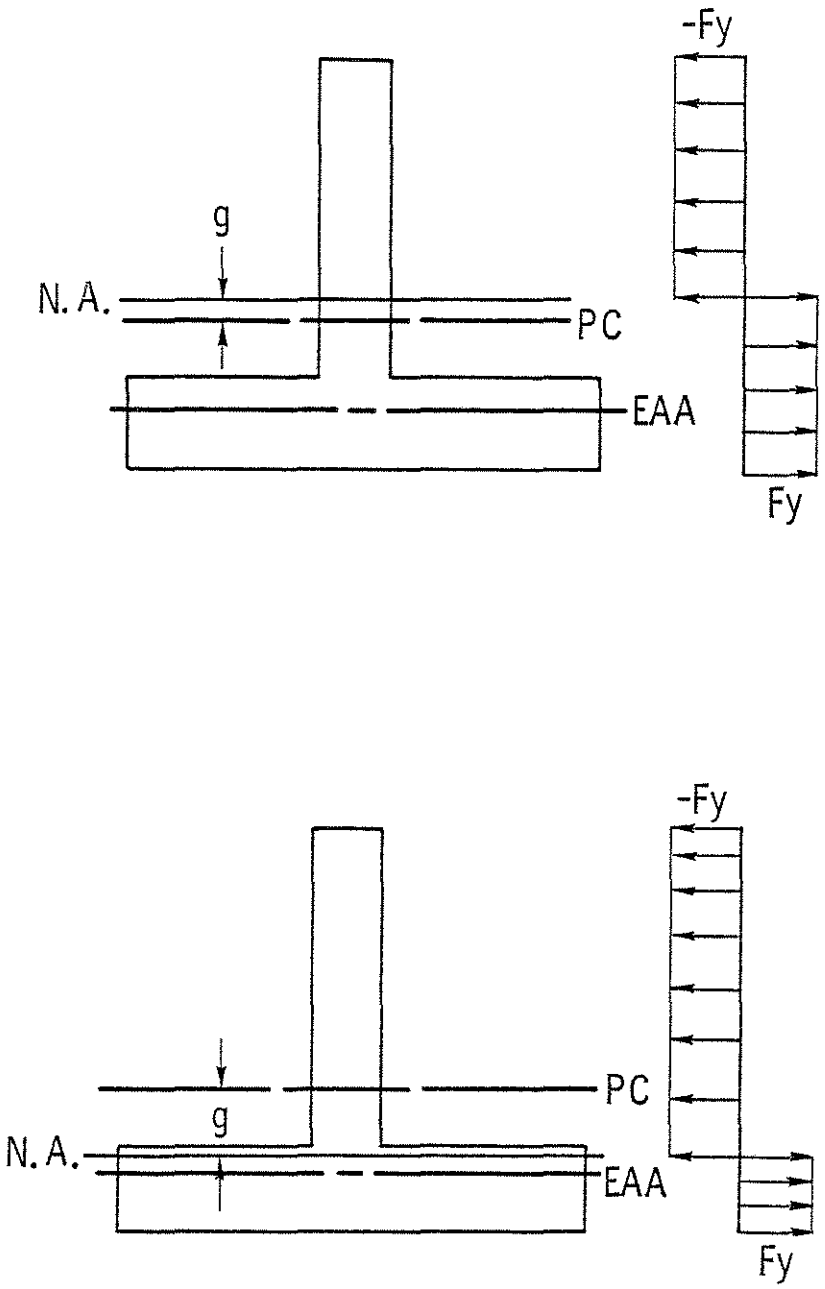

Fig. 4.11 Stress Distributions at High Moment End of Bottom Tee

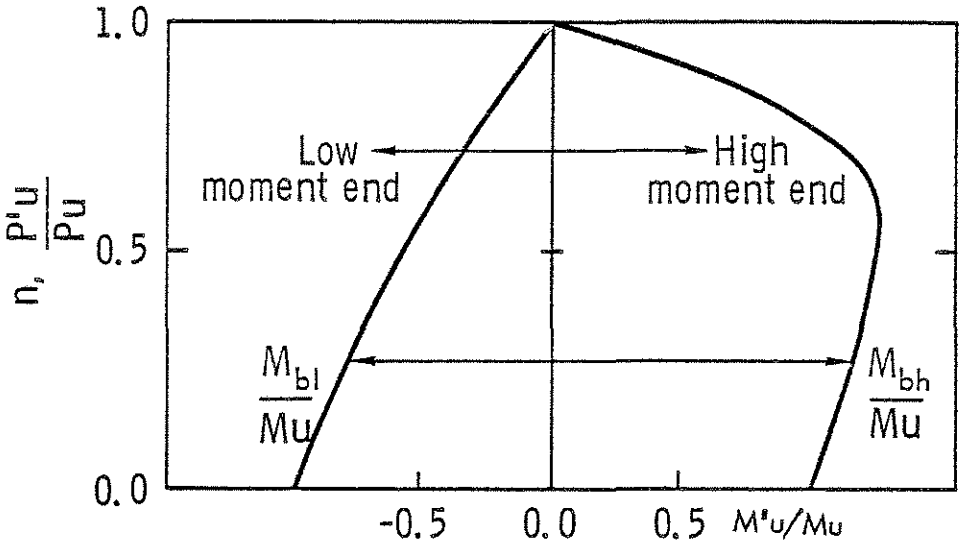

Fig. 4.12a Moment-Axial Force Interaction Curves for Bottom Tee

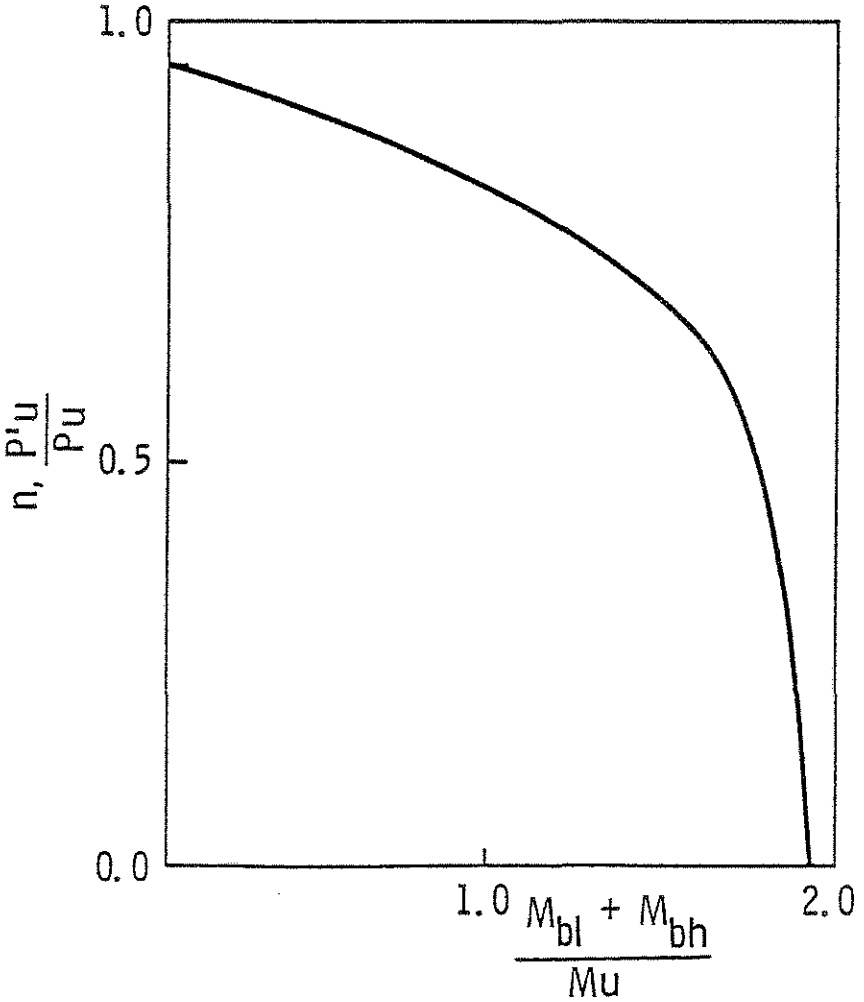

Fig. 4.12b Total Secondary Moment-Axial Force Interaction Curves for Bottom Tee

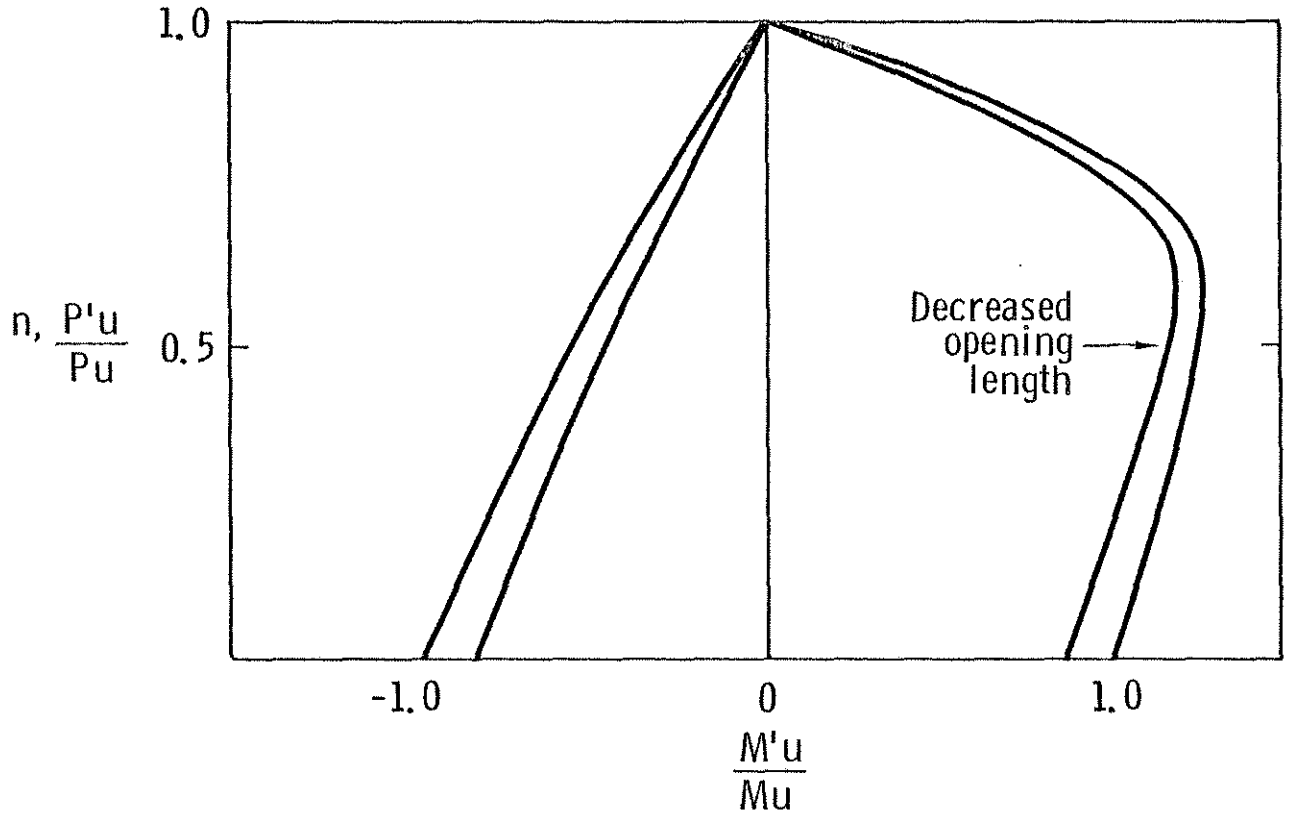

Fig. 4.13 Effect of Opening Length on Bottom Tee Moment-Axial Force Interaction

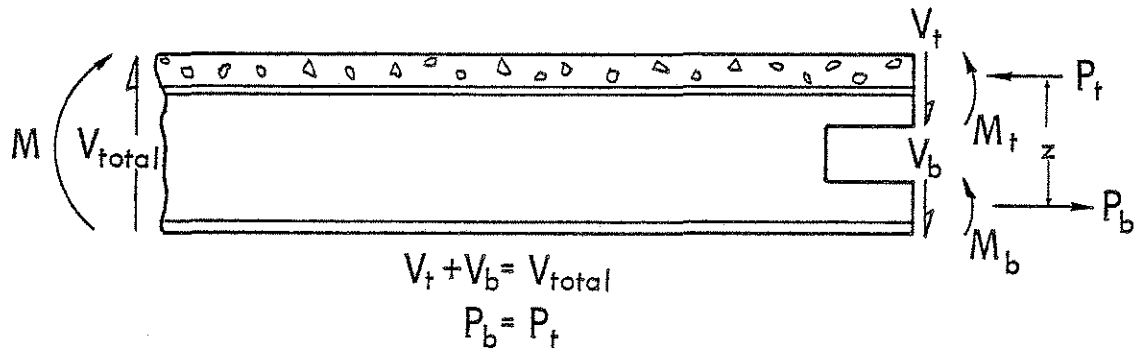

Fig. 4.14 Forces Acting on Top and Bottom Tees

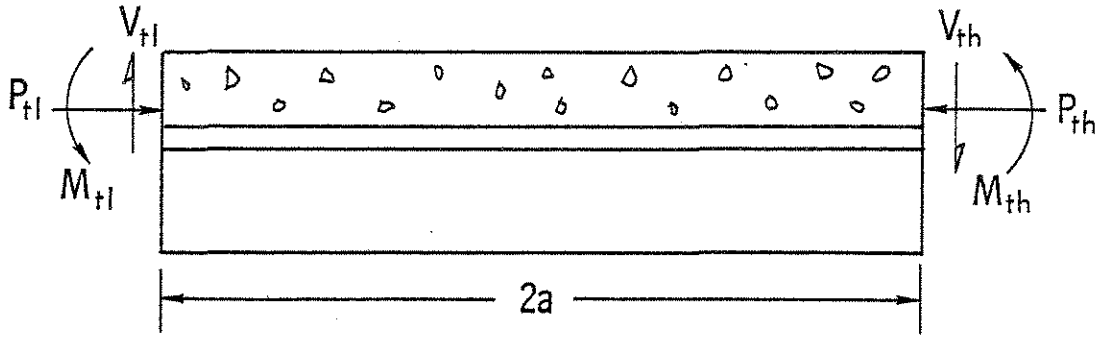

Fig. 4.15 Forces Acting on Top Tee

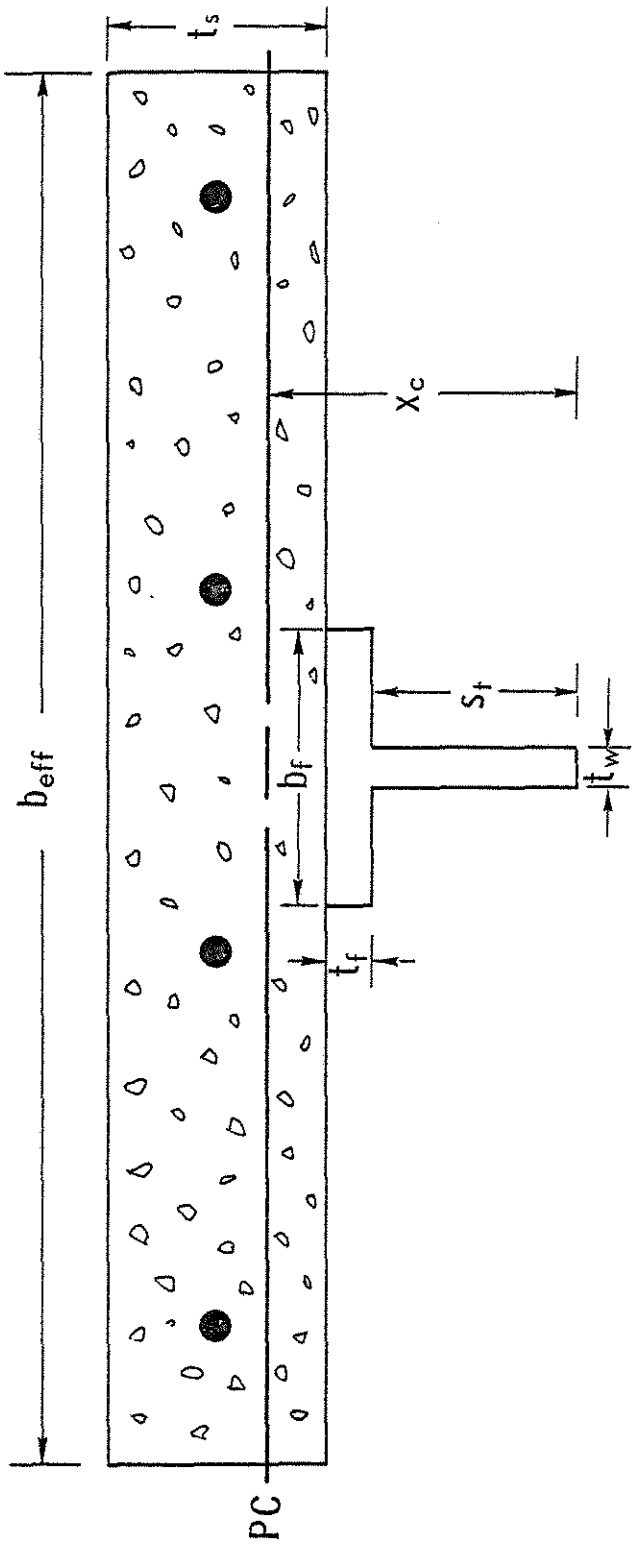

Fig. 4.16 Top Tee Cross-Section

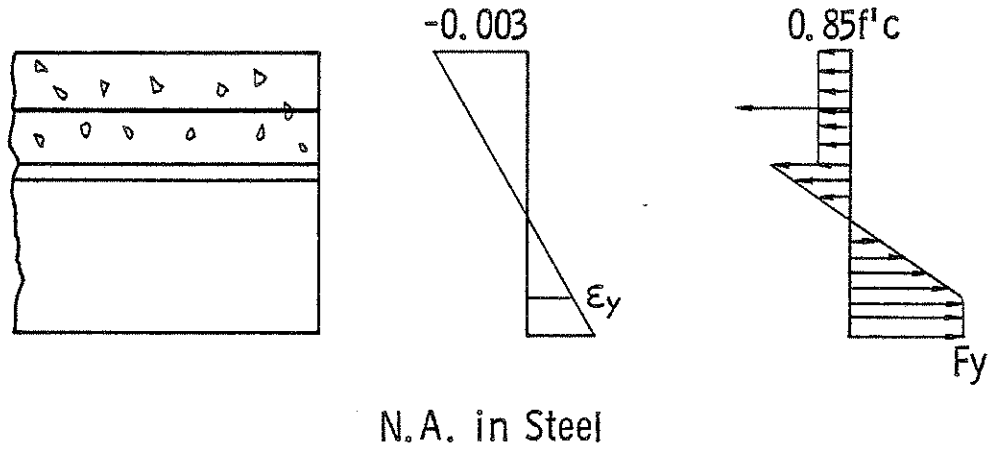

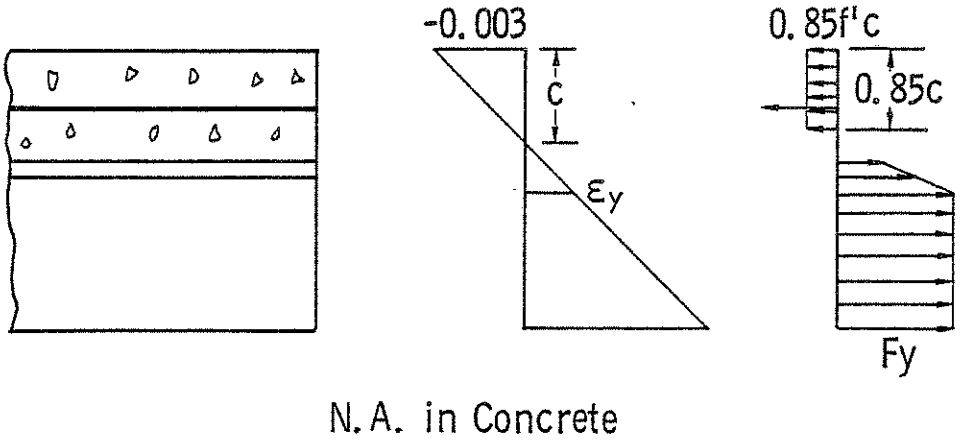

Fig. 4.17 Strain and Stress Distributions for Different Neutral Axis Locations at High Moment End of Top Tee

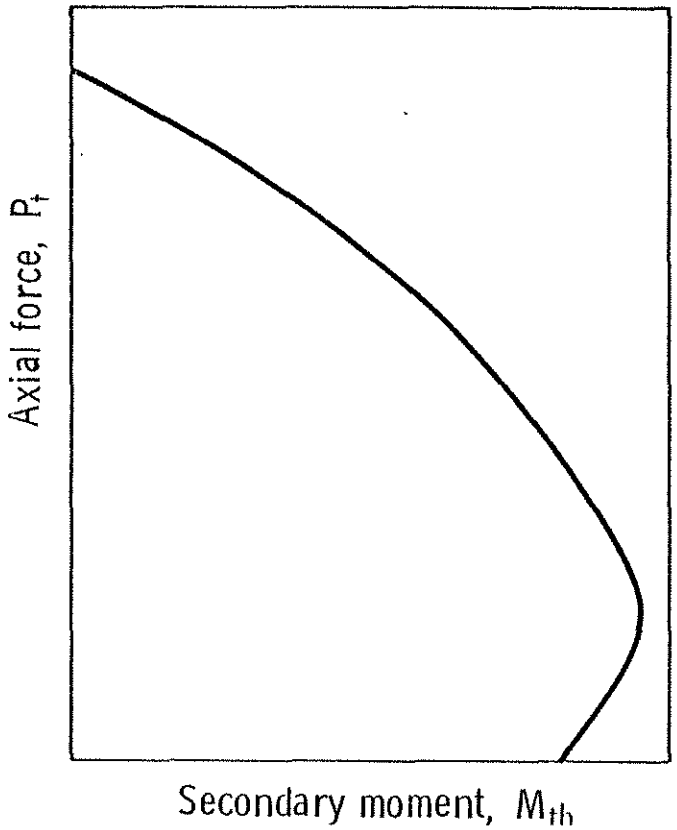

Fig. 4.18 Moment-Axial Force Interaction Curve for High Moment End of Top Tee

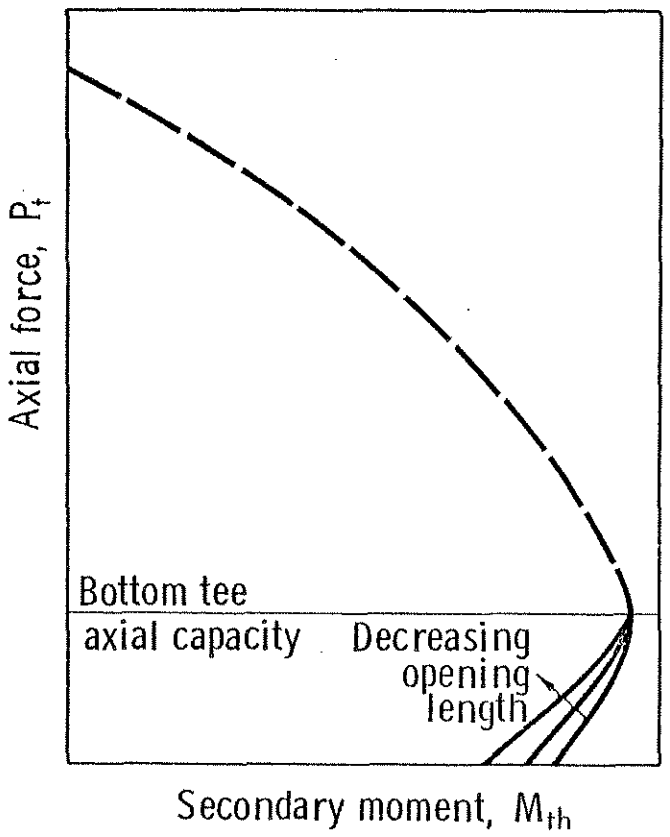

Fig. 4.19 Moment-Axial Force Interaction Curve for High Moment End of Top Tee with Shear Reduction

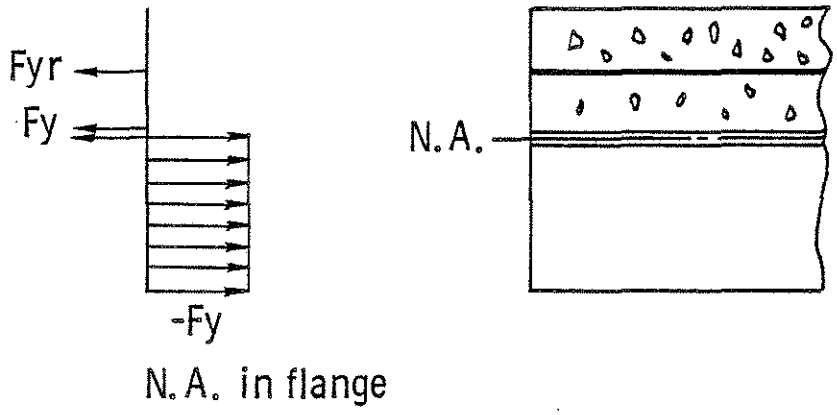

Fig. 4.20a Stress Distribution for Low Moment End of Top Tee with Neutral Axis in Flange

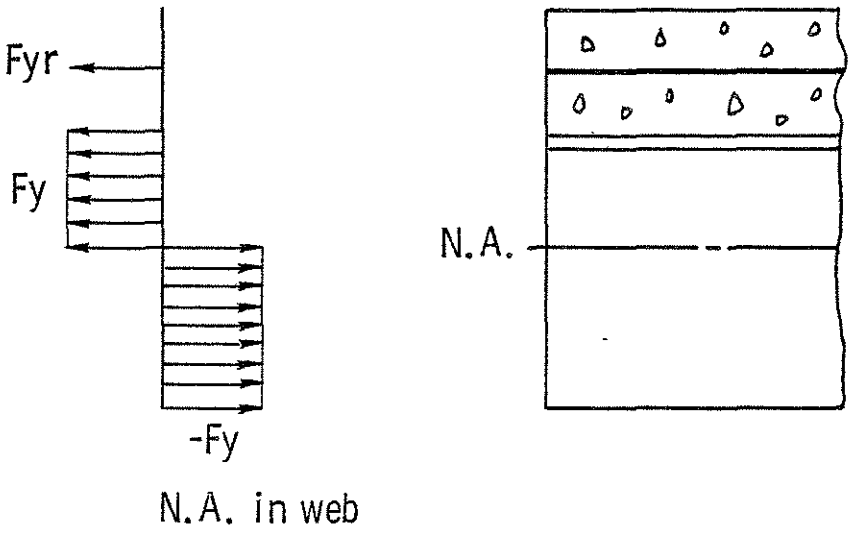

Fig. 4.20b Stress Distribution for Low Moment End of Top Tee with Neutral Axis in Web

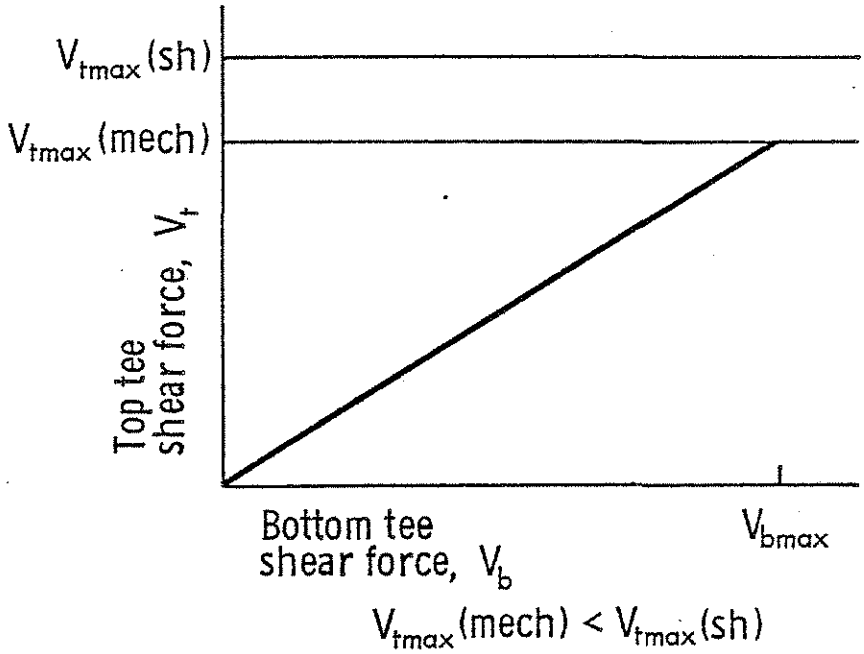

Fig. 4.21 Shear Force Distribution to Top and Bottom Tees with V_{tmax}(mech) Controlling

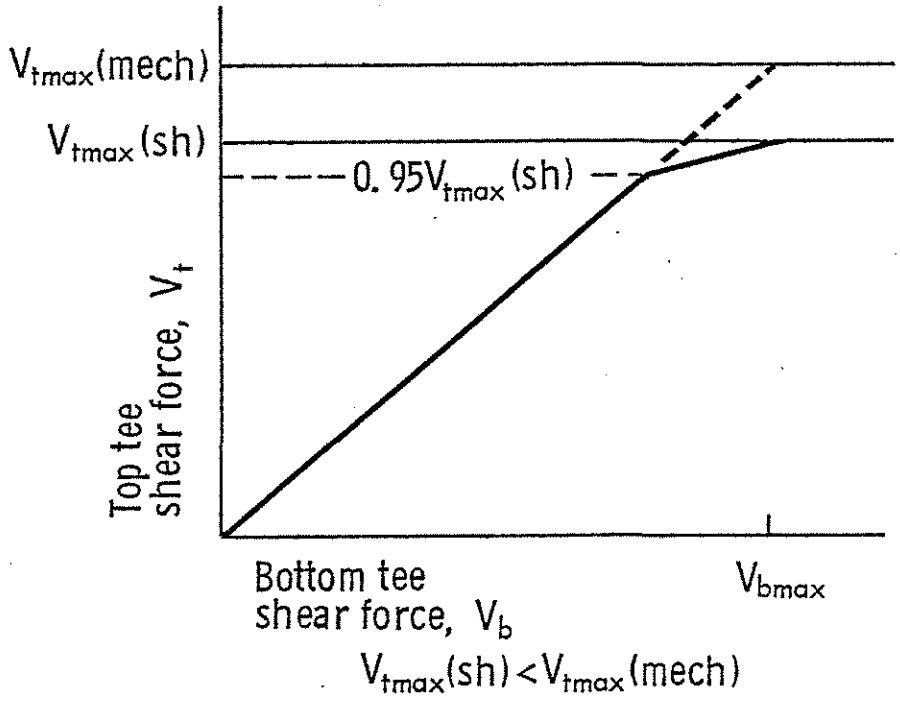

Fig. 4.22 Shear Force Distribution to Top and Bottom Tees with V_{tmax}(sh) Controlling

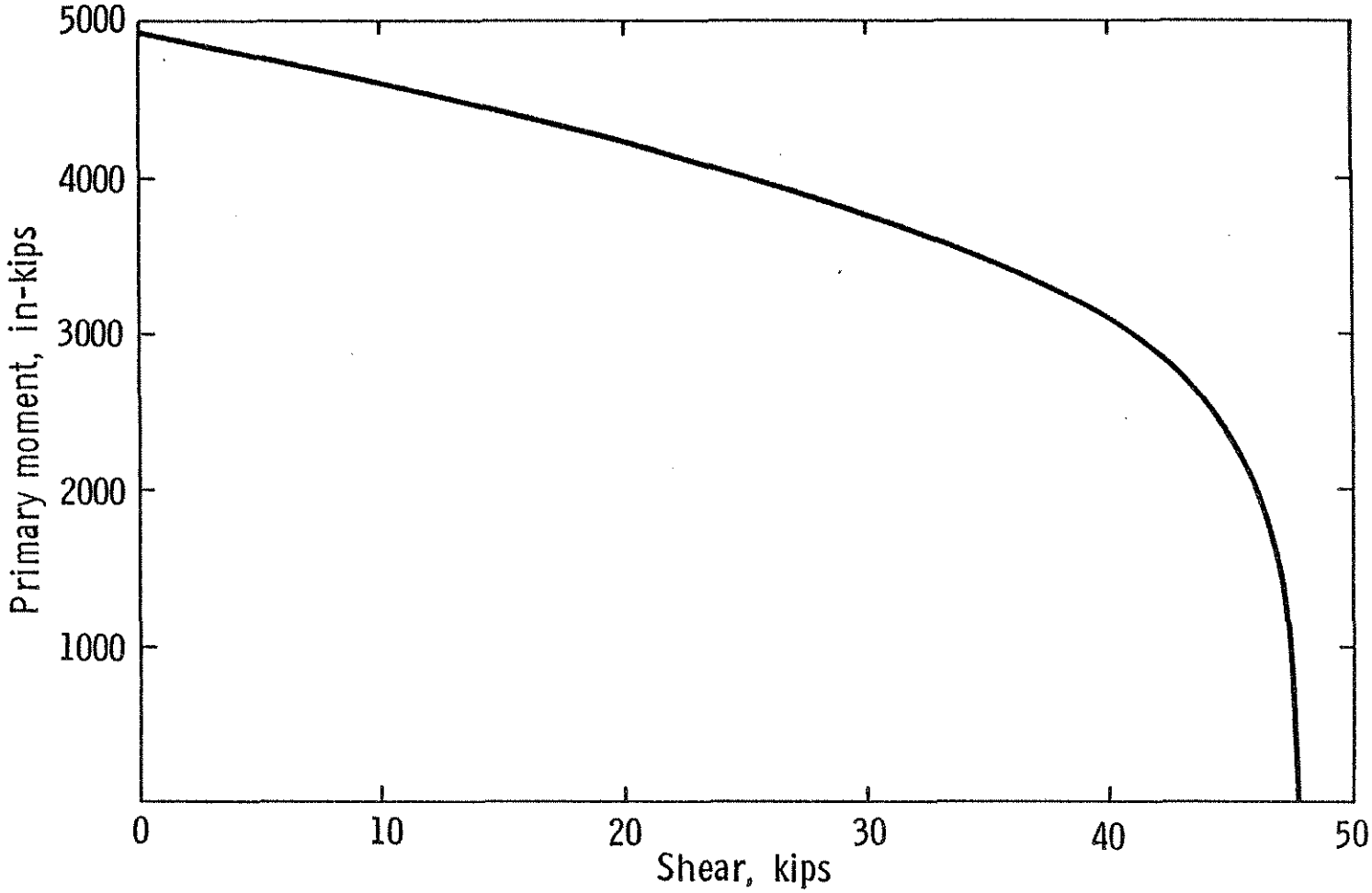

Fig. 4.23 Moment-Shear Interaction at a Web Opening with a "Mechanism" Failure Controlling

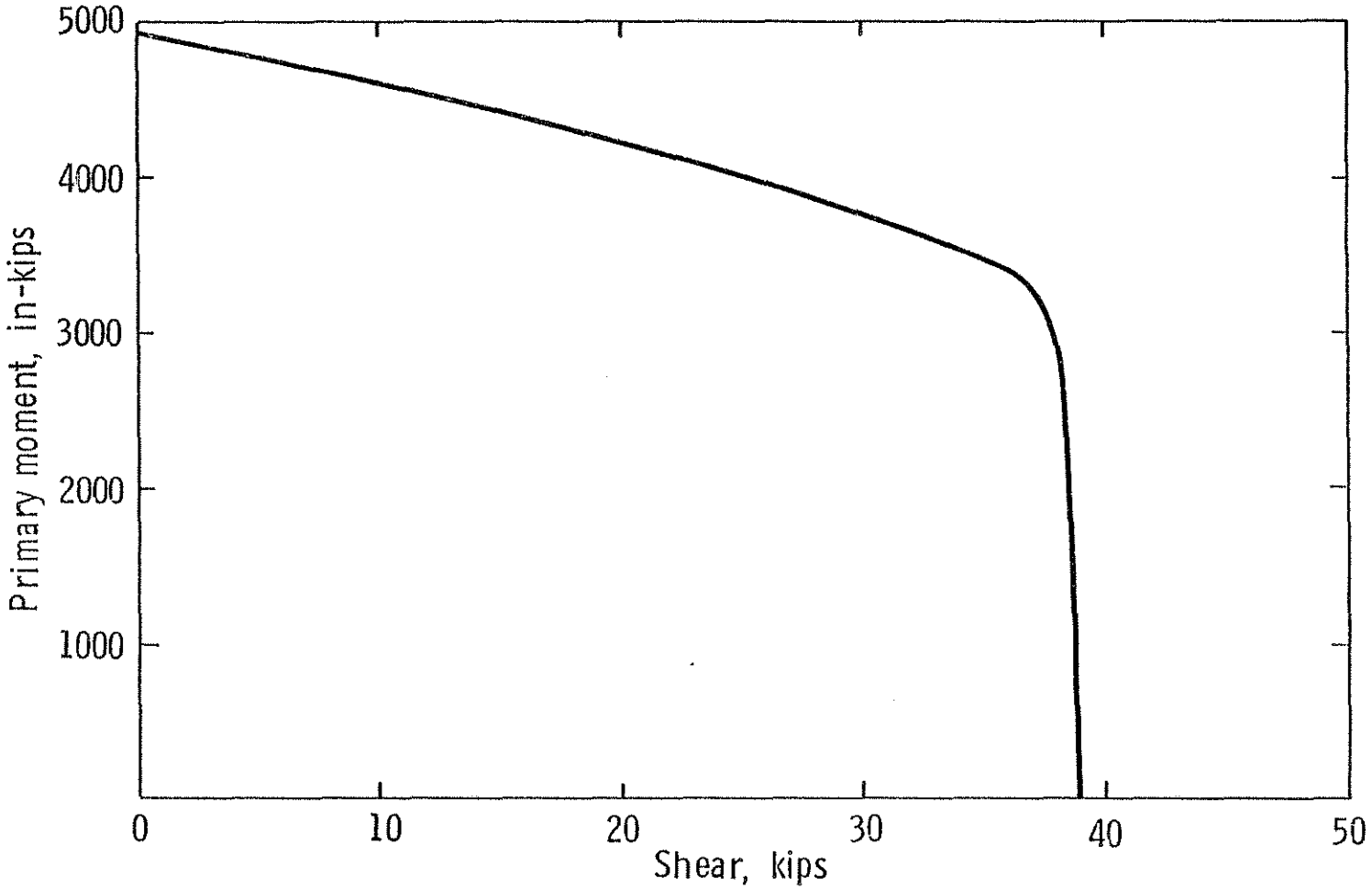

Fig. 4.24 Moment-Shear Interaction at a Web Opening with a "Shear" Failure Controlling

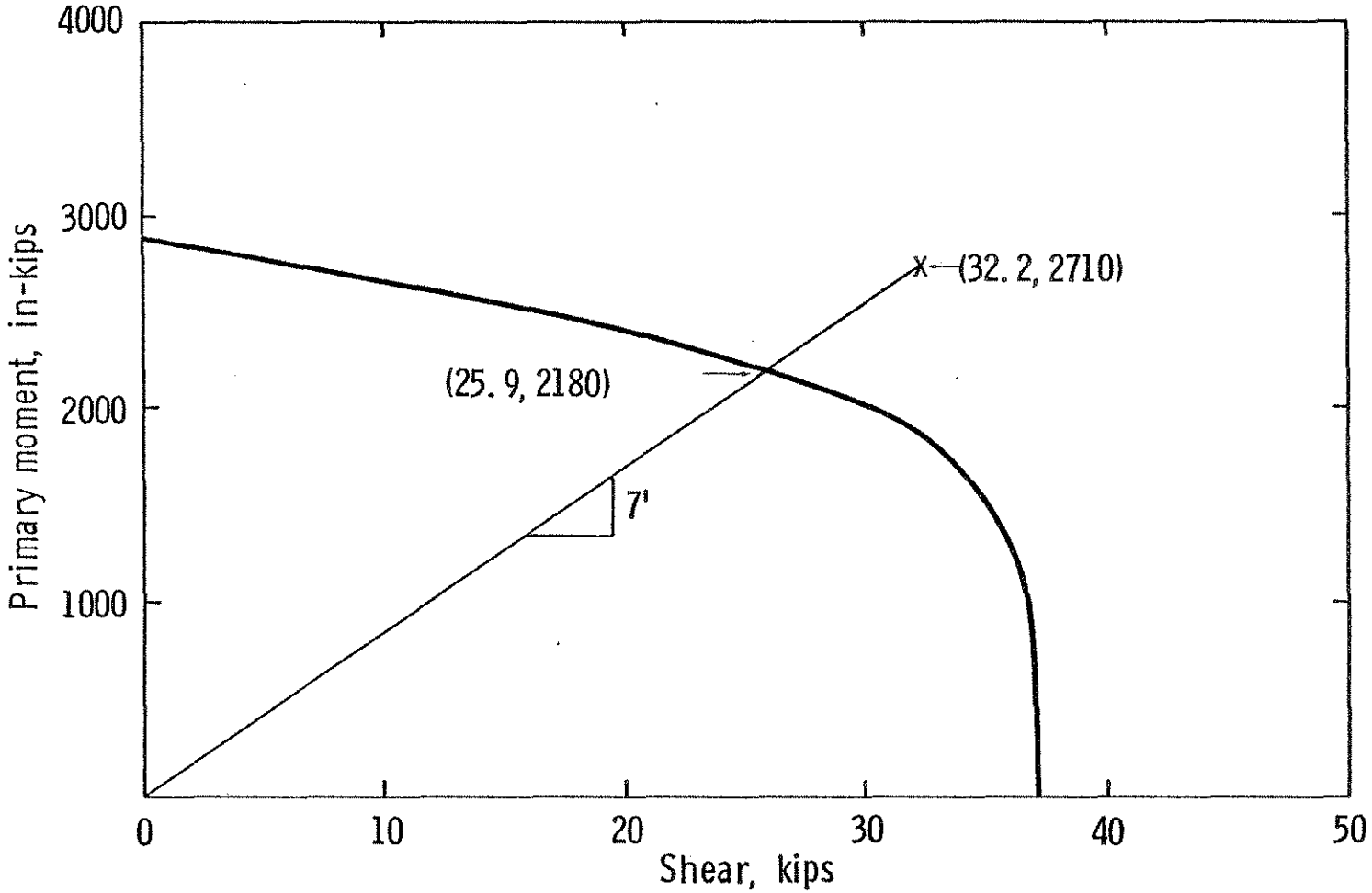

Fig. 5.1 Moment-Shear Interaction Curve for Beam No. 1

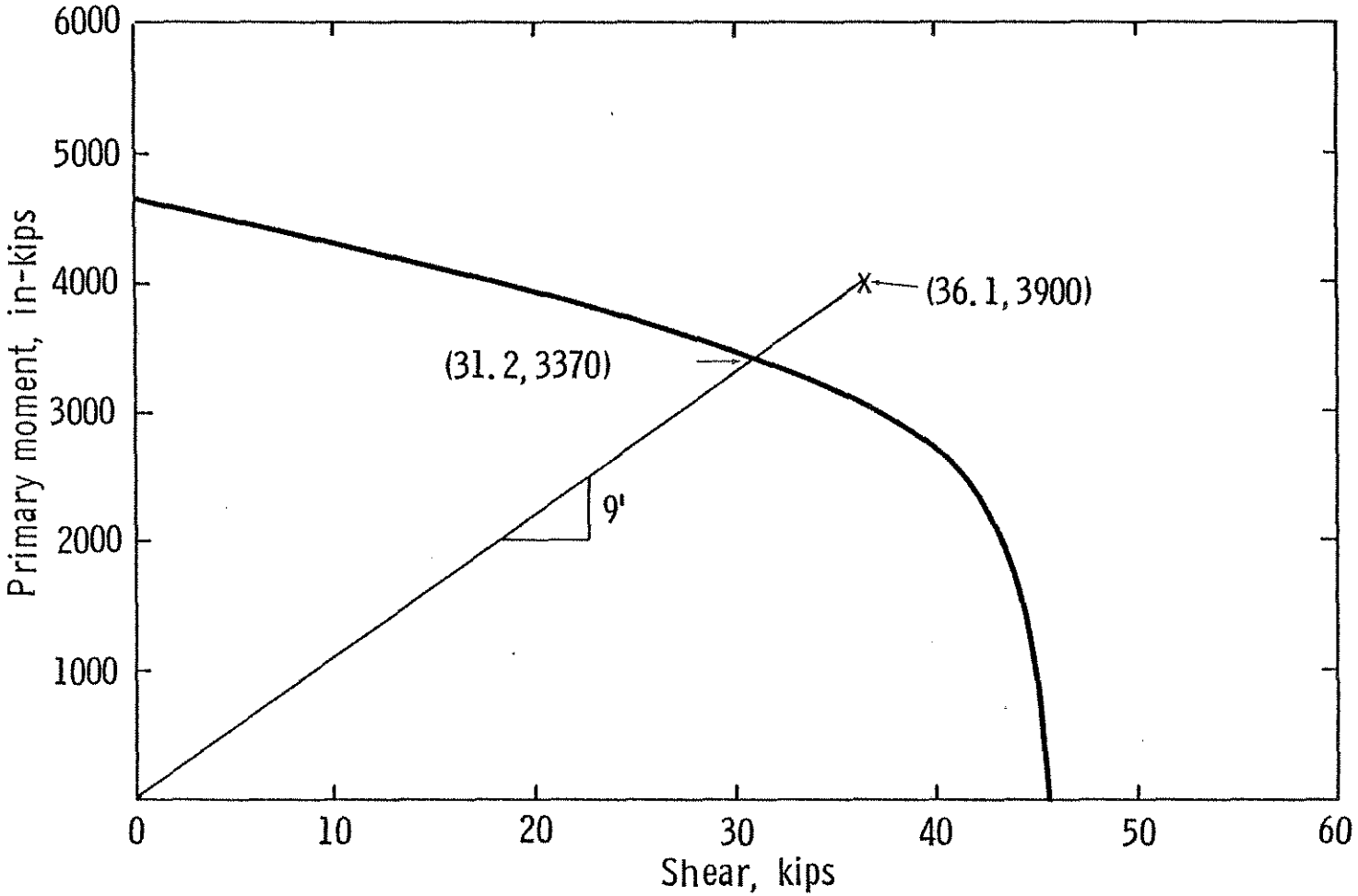

Fig. 5.2 Moment-Shear Interaction Curve for Beam No. 2

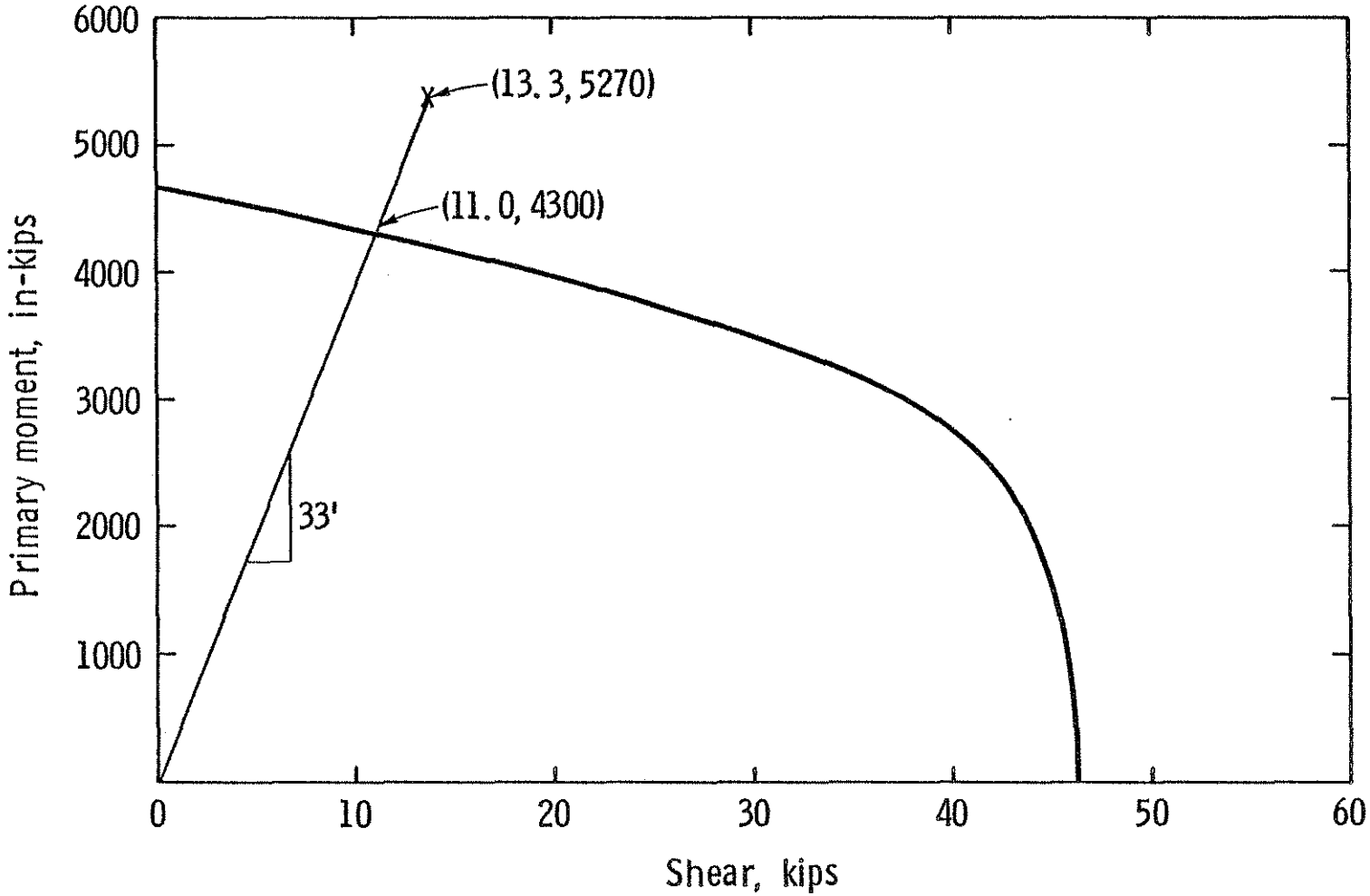

Fig. 5.3 Moment-Shear Interaction Curve for Beam No. 3

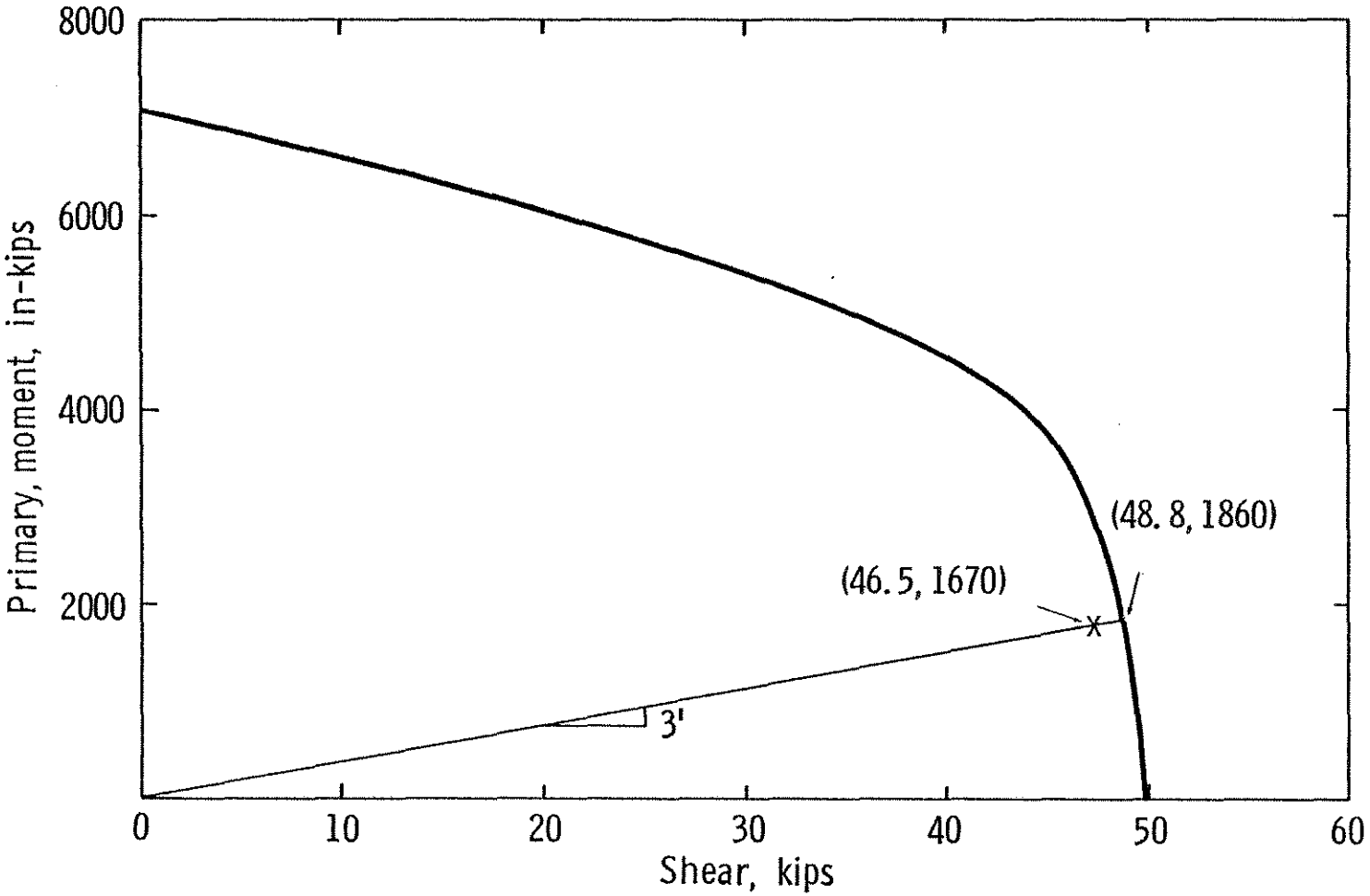

Fig. 5.4 Moment-Shear Interaction Curve for Beam No. 4

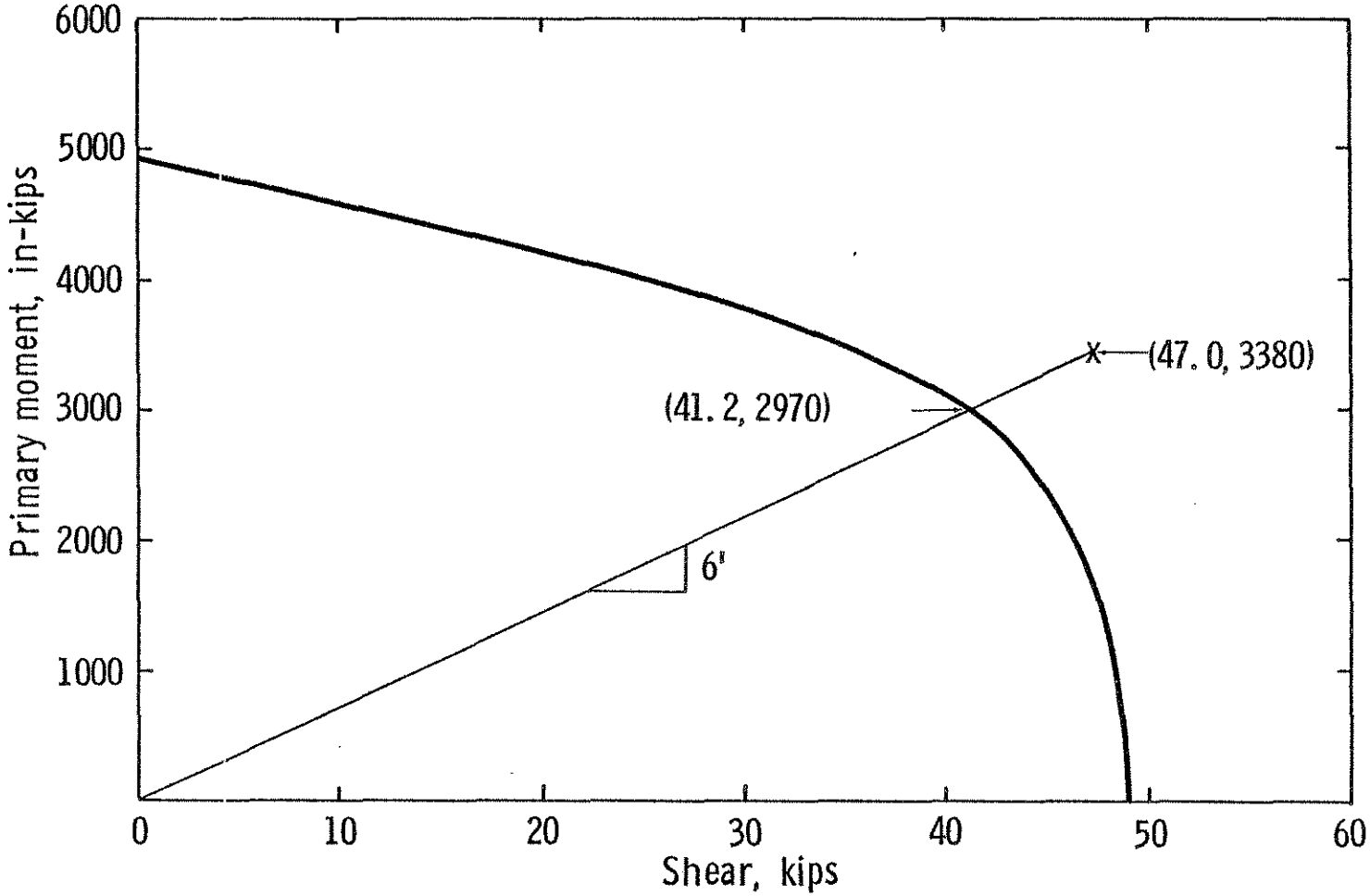

Fig. 5.5 Moment-Shear Interaction Curve for Beam No. 5

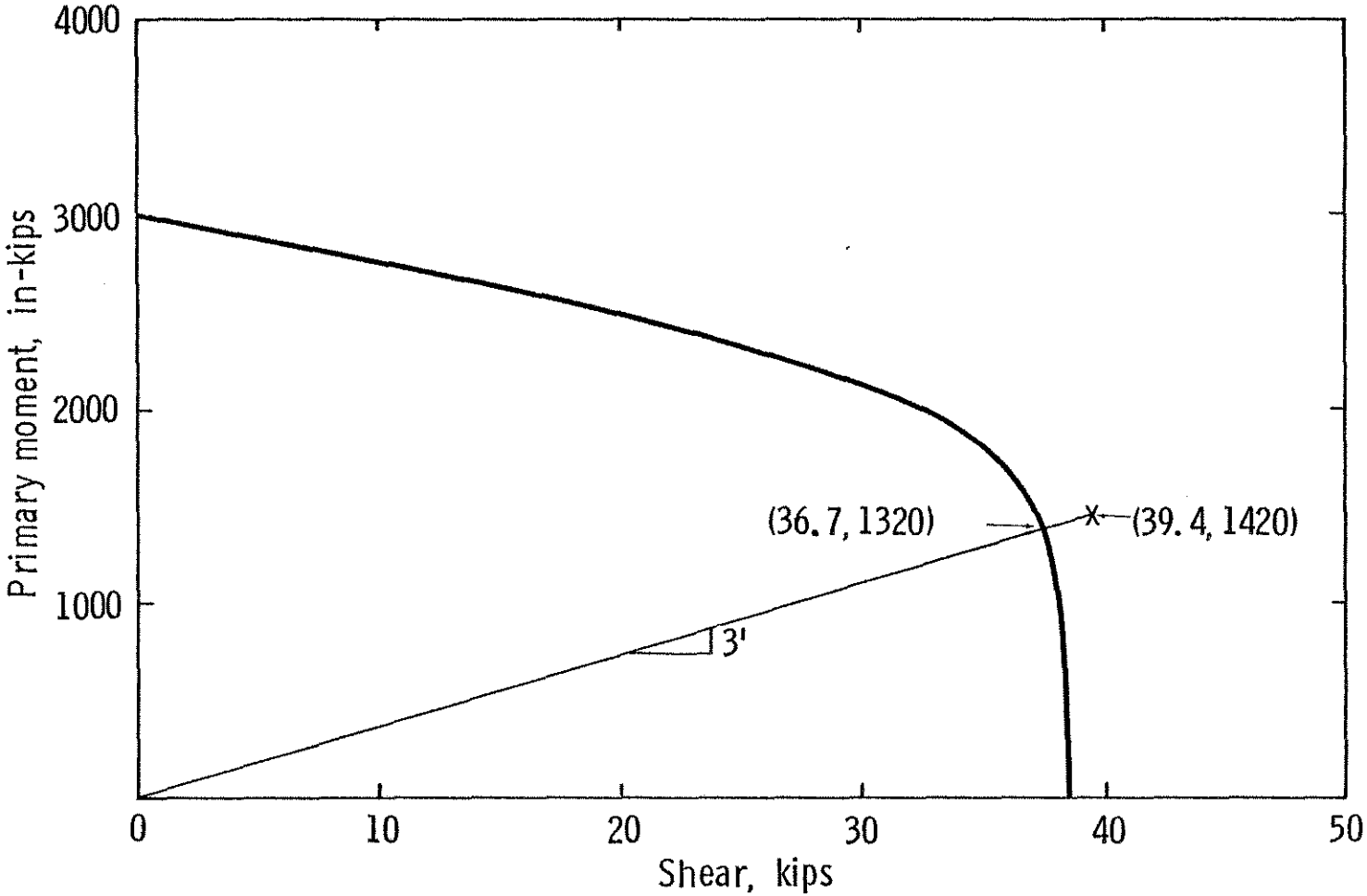

Fig. 5.6 Moment-Shear Interaction Curve for Beam No. 6

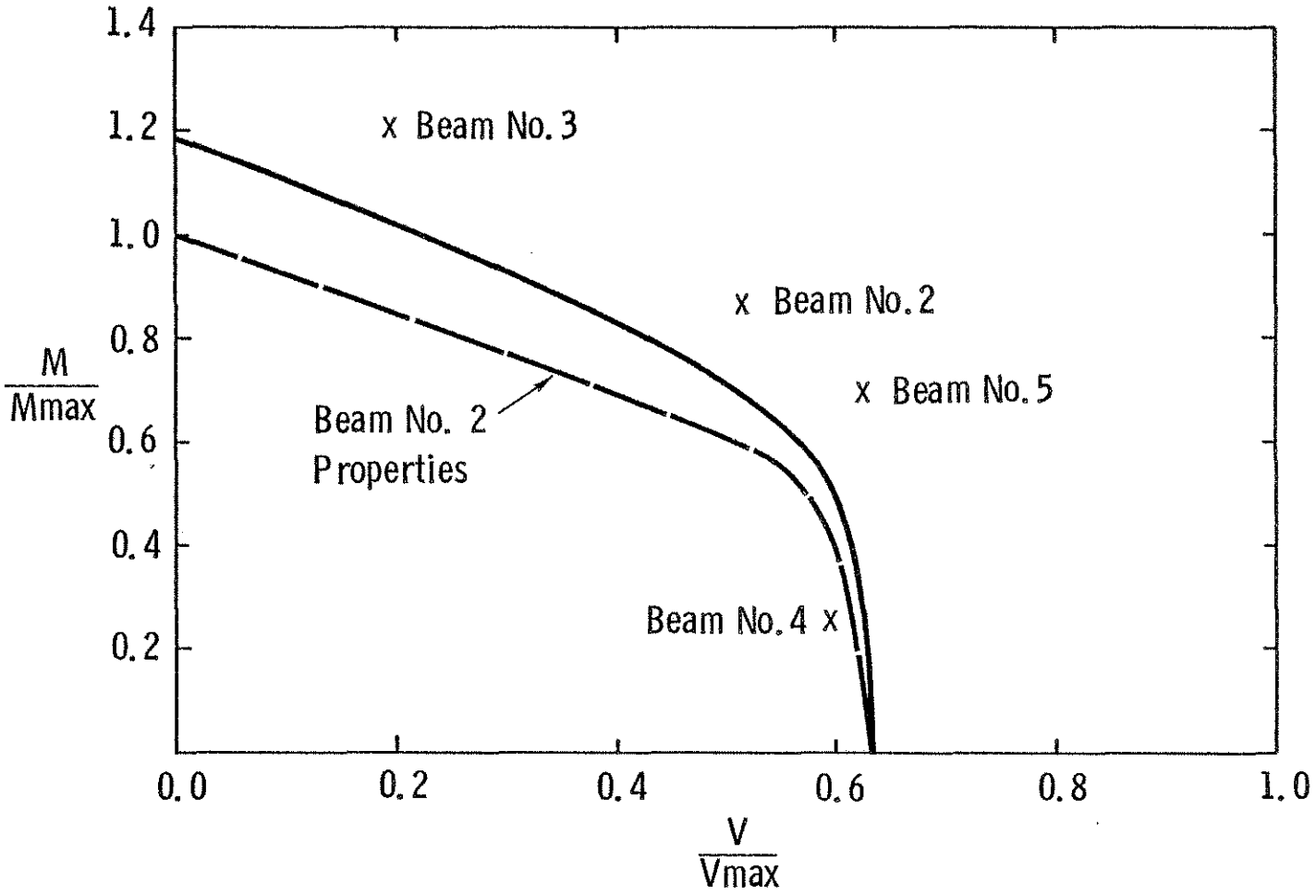

Fig. 5.7 Effect of Increasing Yield Stress in Steel to Represent Strain Hardening

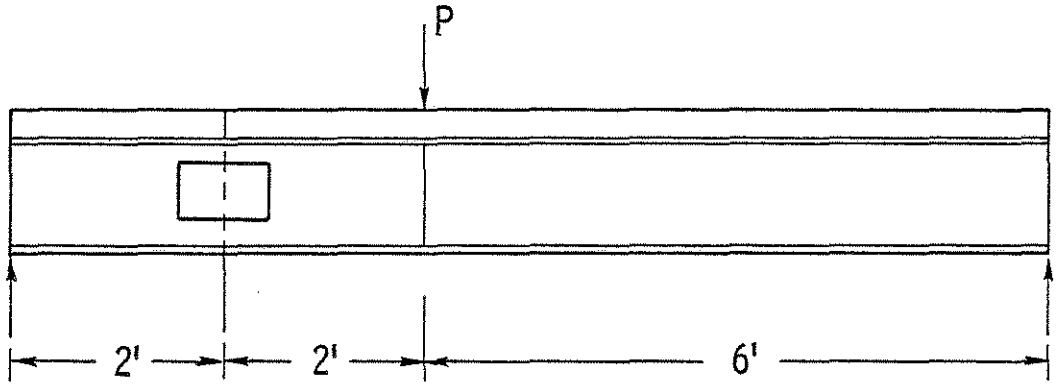

Beam No. 1

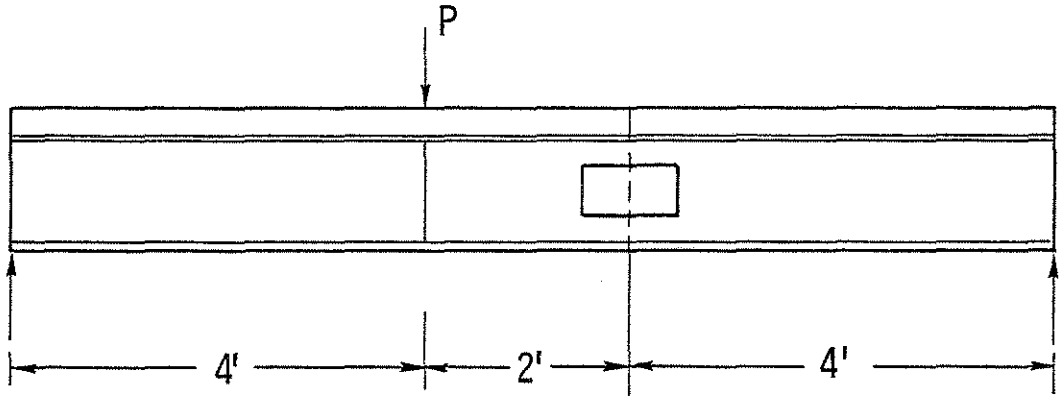

Beam No. 2

Fig. 5.8 Granade's Beams

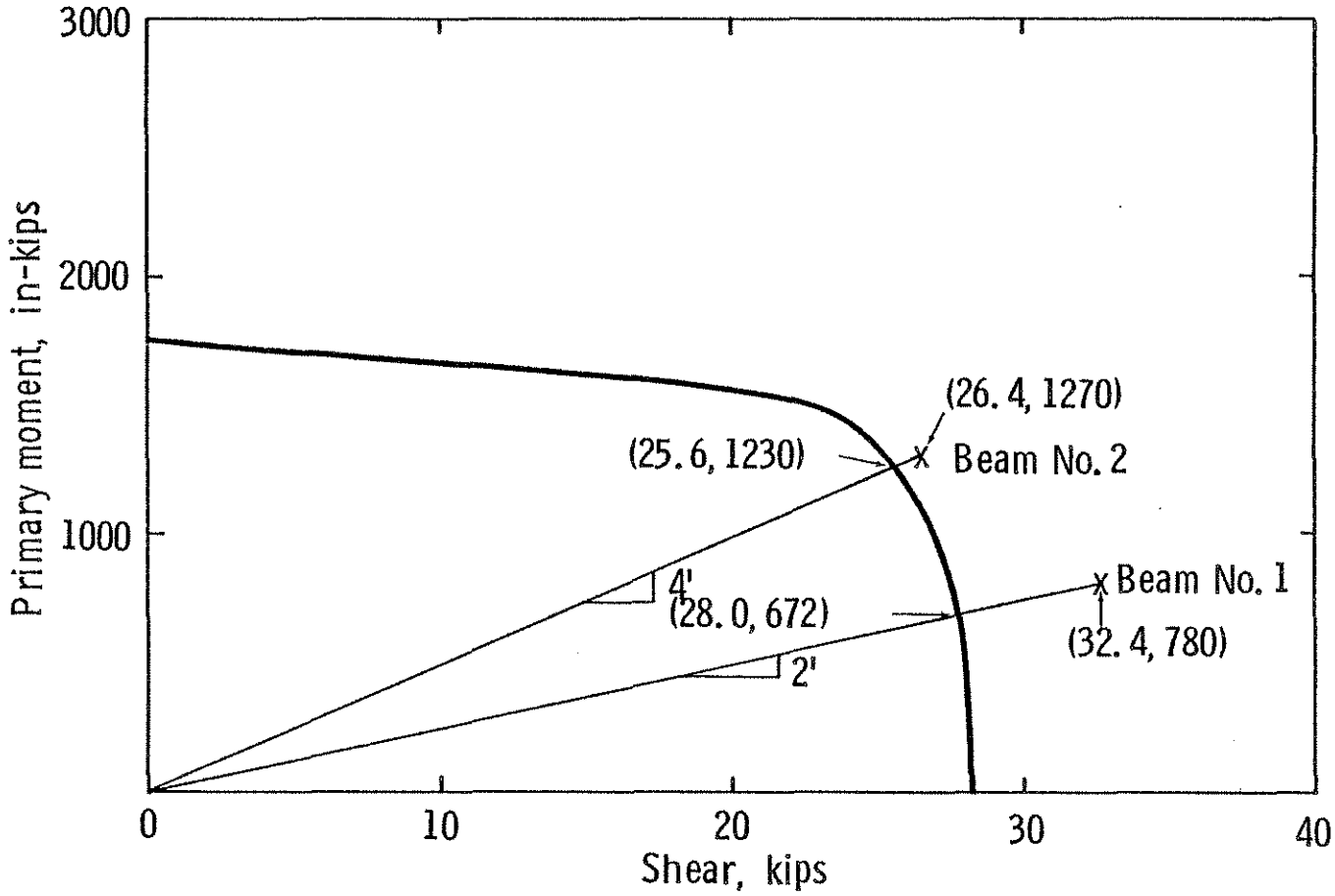

Fig. 5.9 Moment-Shear Interaction Curve for Granade's Beams

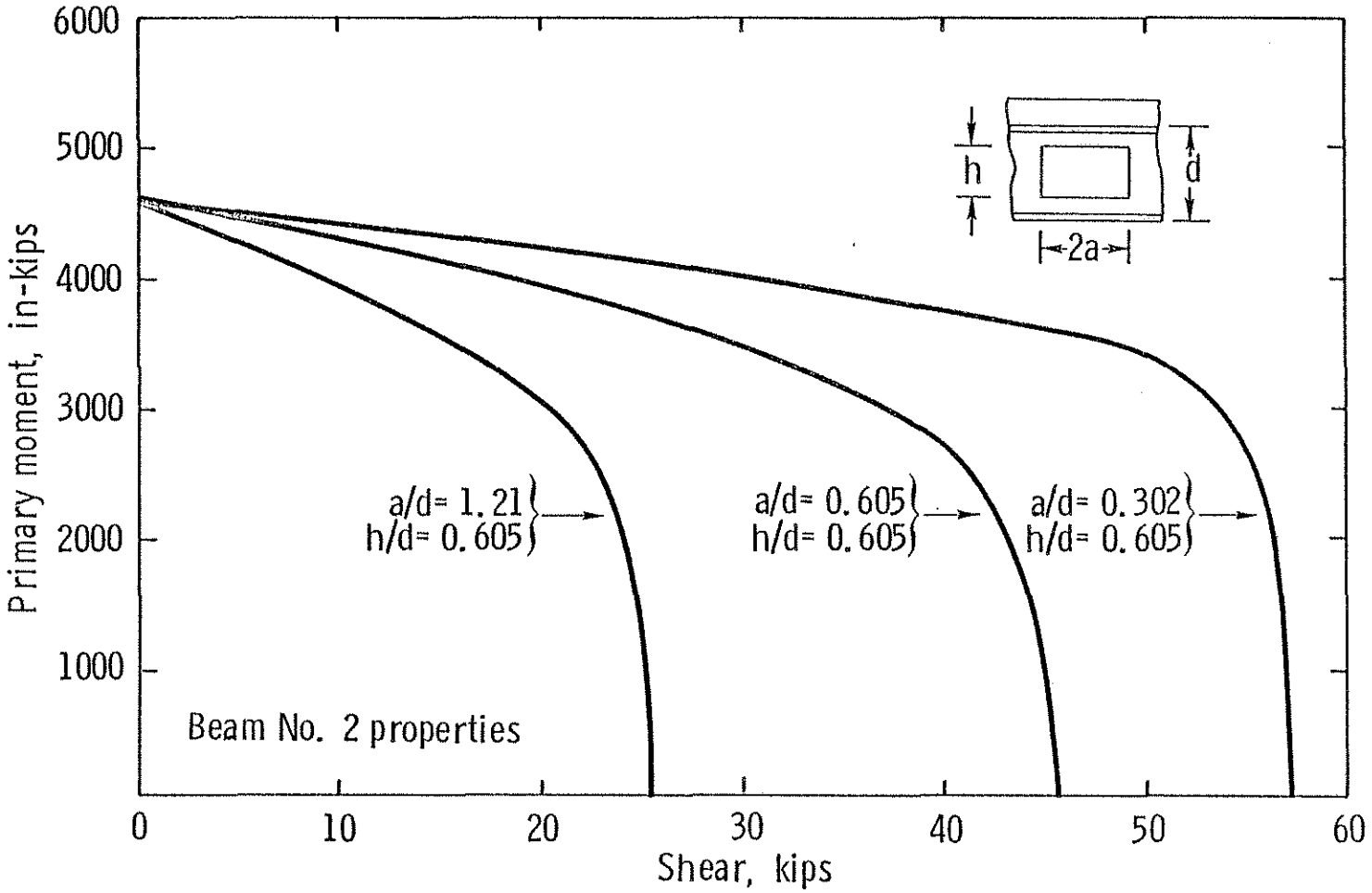

Fig. 5.10 Effect of Opening Length on Moment-Shear Interaction at Web Openings.

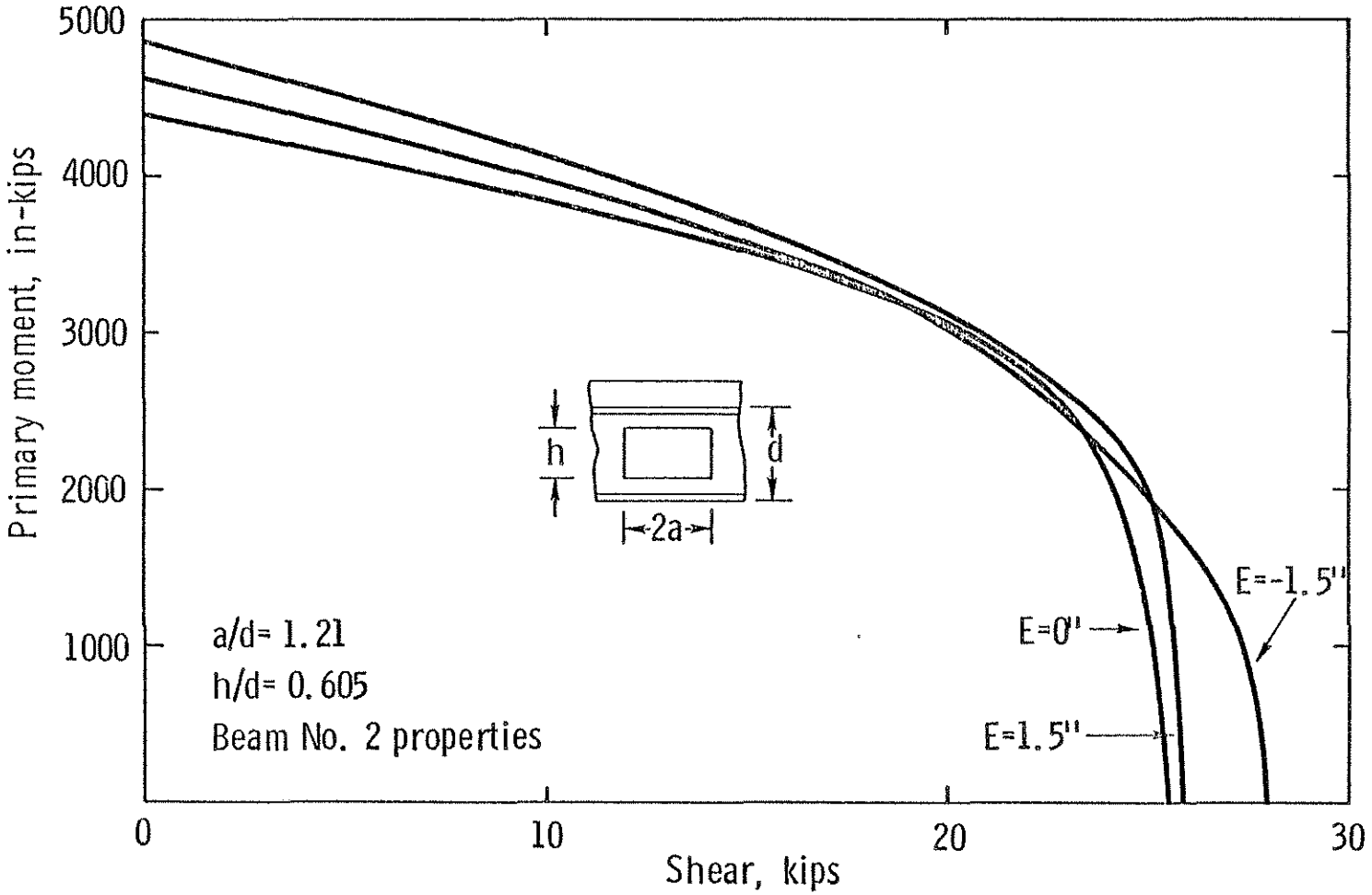

Fig. 5.11 Effect of Eccentricity on Moment-Shear Interaction at Web Openings with "Mechanism" Failure

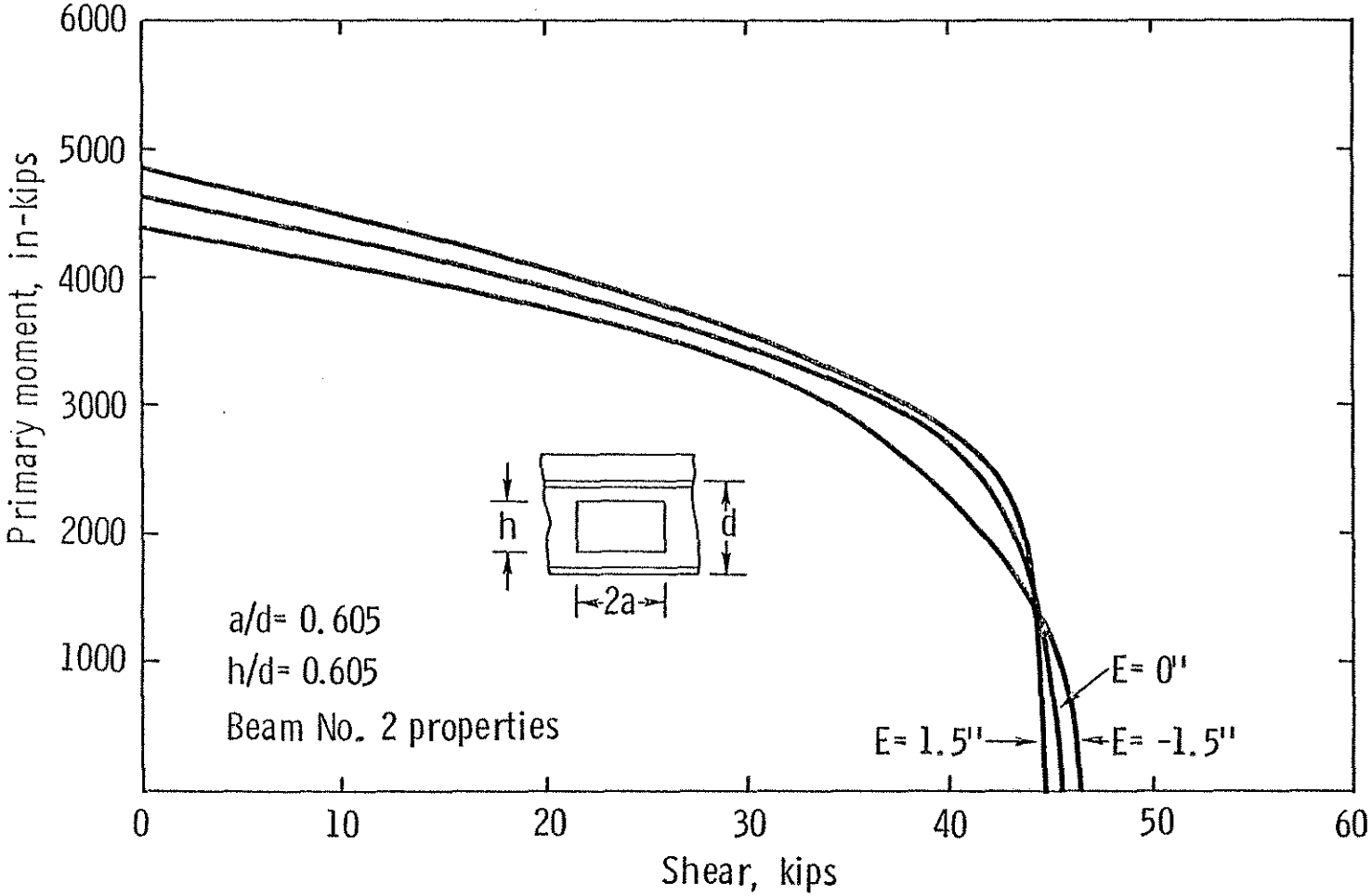

Fig. 5.12 Effect of Eccentricity on Moment-Shear Interaction at Web Openings with "Shear" Failure

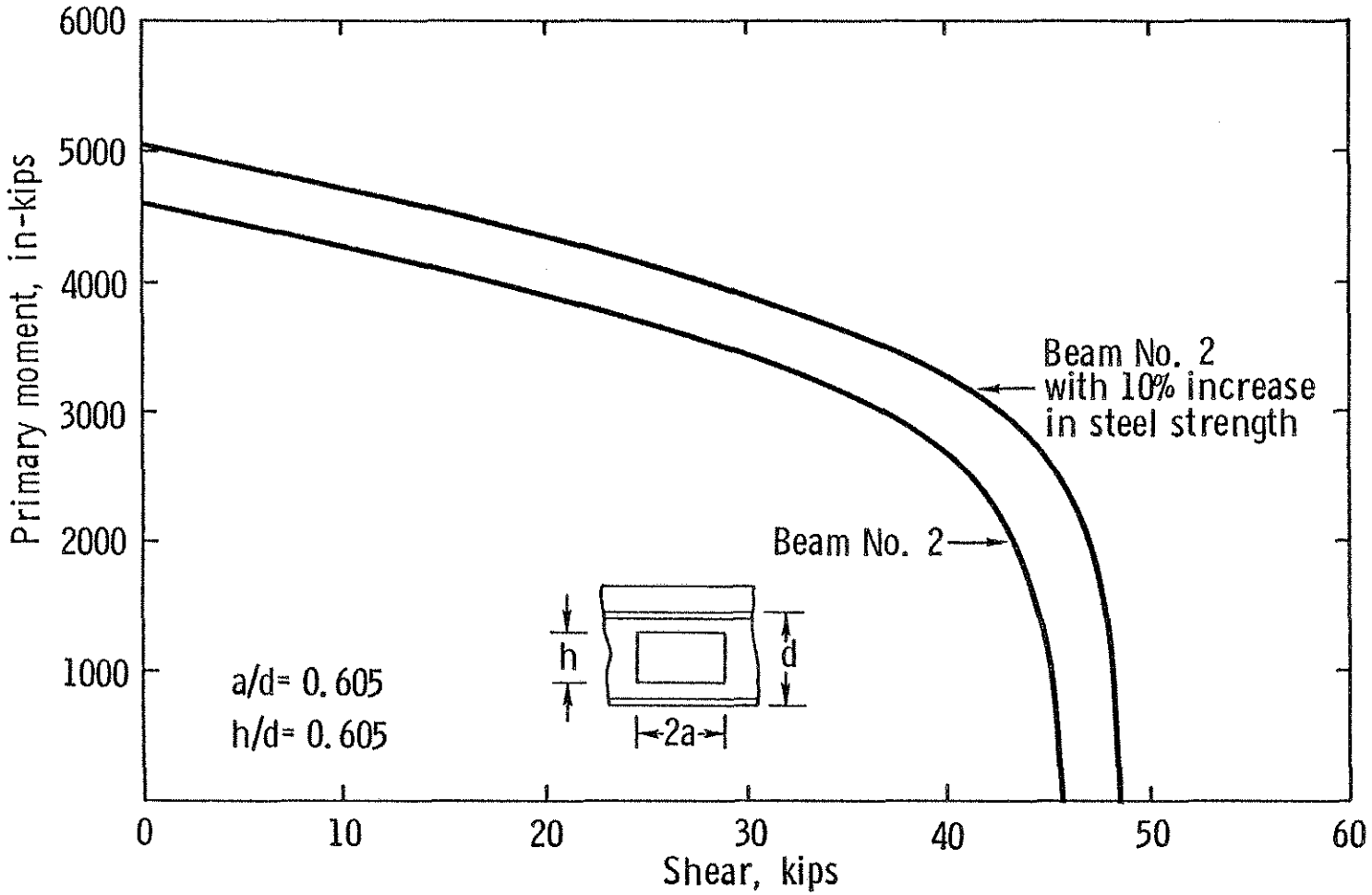

Fig. 5.13 Effect of Steel Strength on Moment-Chear Interation at Web Opening

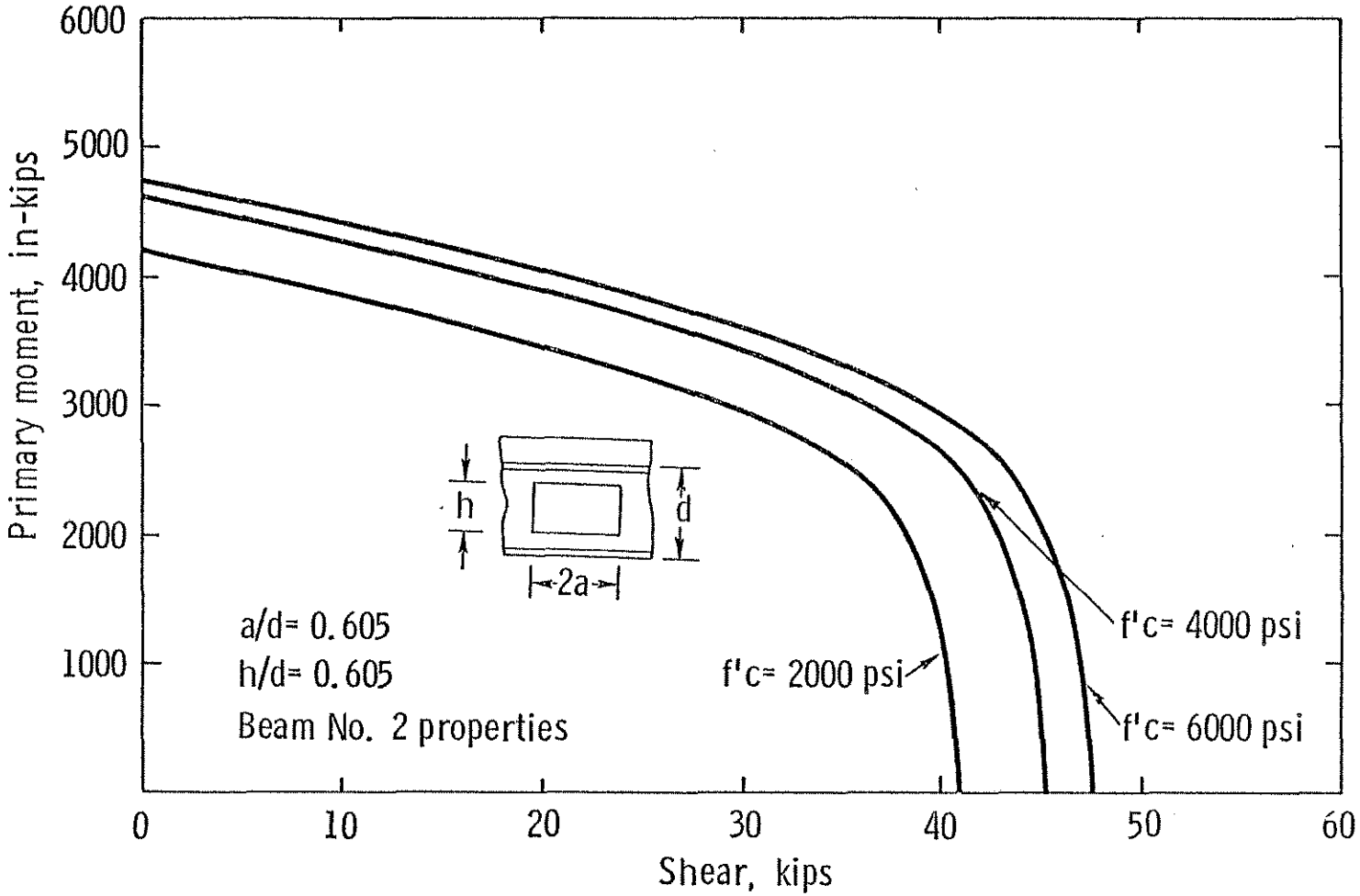

Fig. 5.14 Effect of Concrete Strength on Moment-Shear Interaction at Web Opening

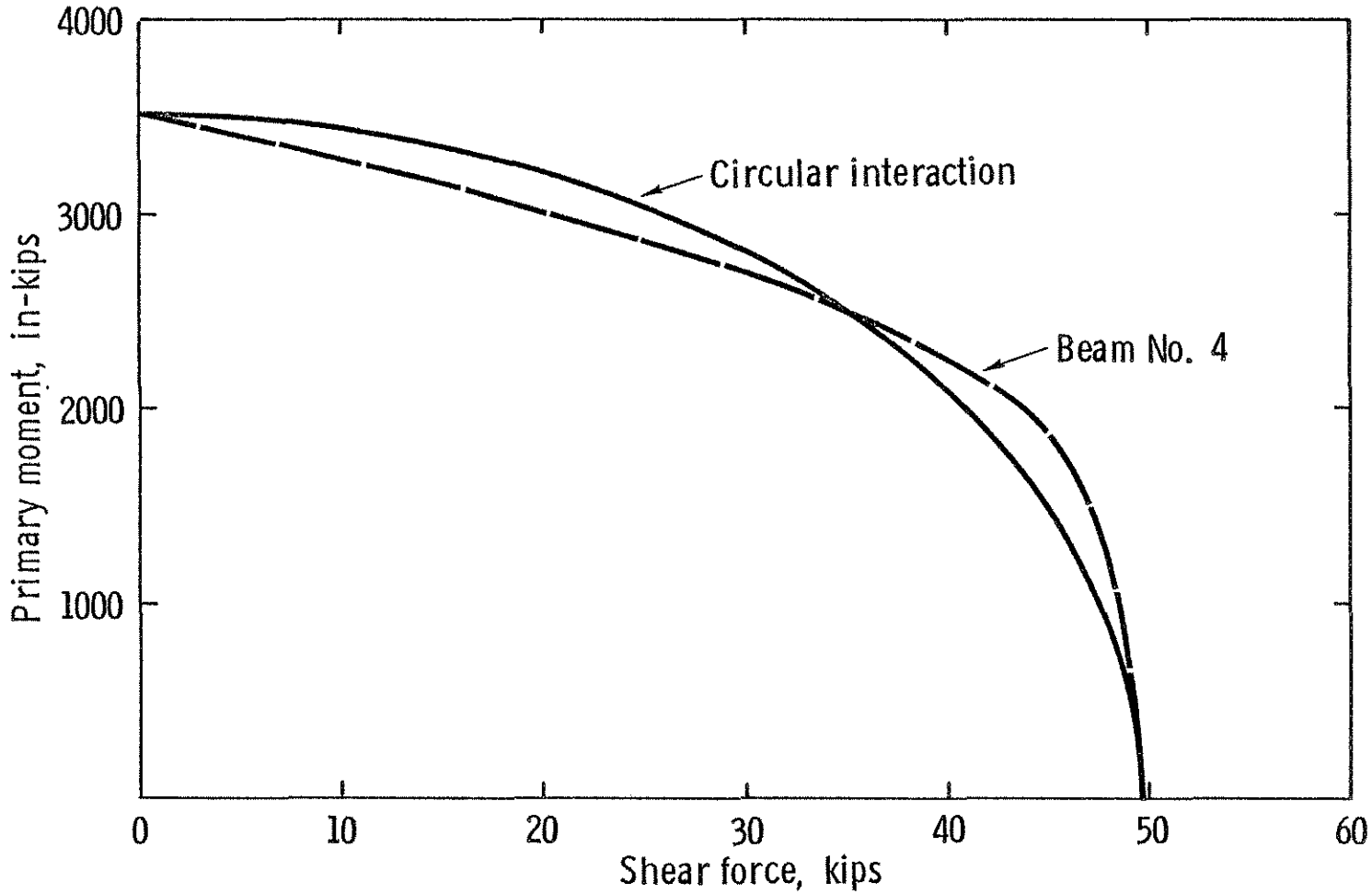

Fig. 6.1 Comparison of Circular and Proposed Ultimate Strength Model Moment-Shear Interaction at a Web Opening

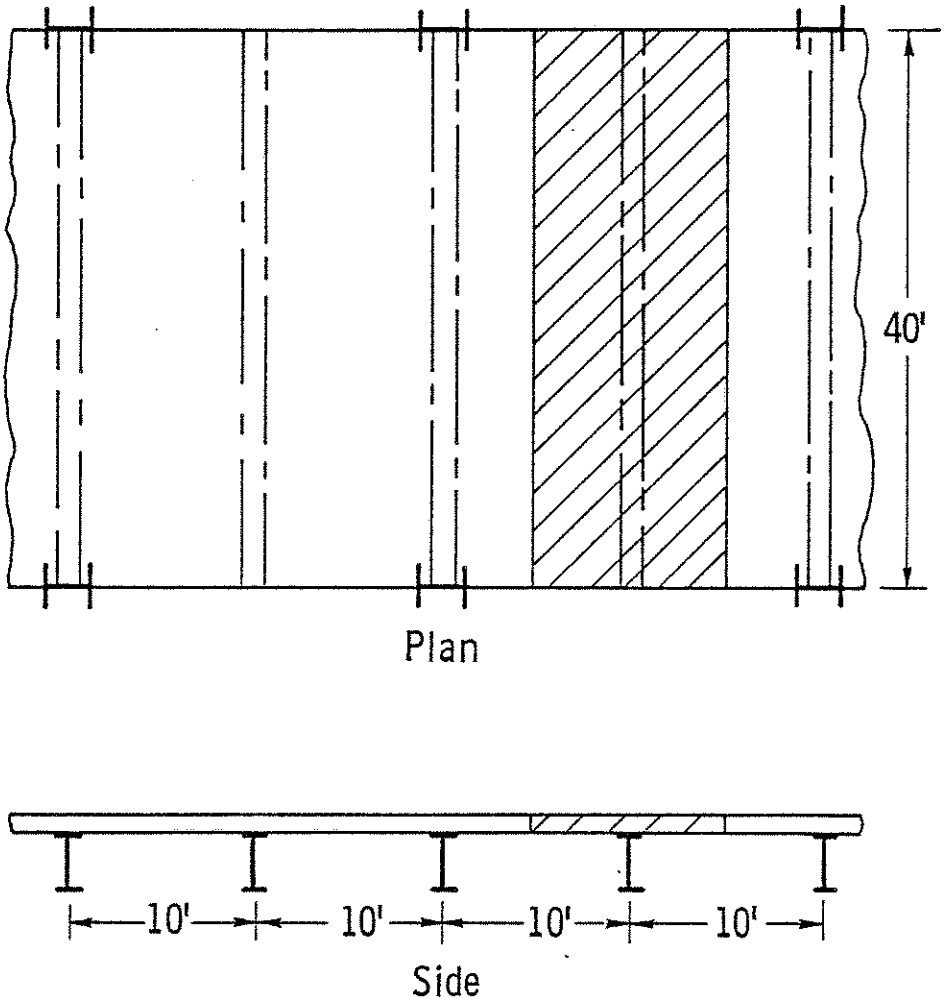

Fig. 6.2 Composite Beam in Floor System

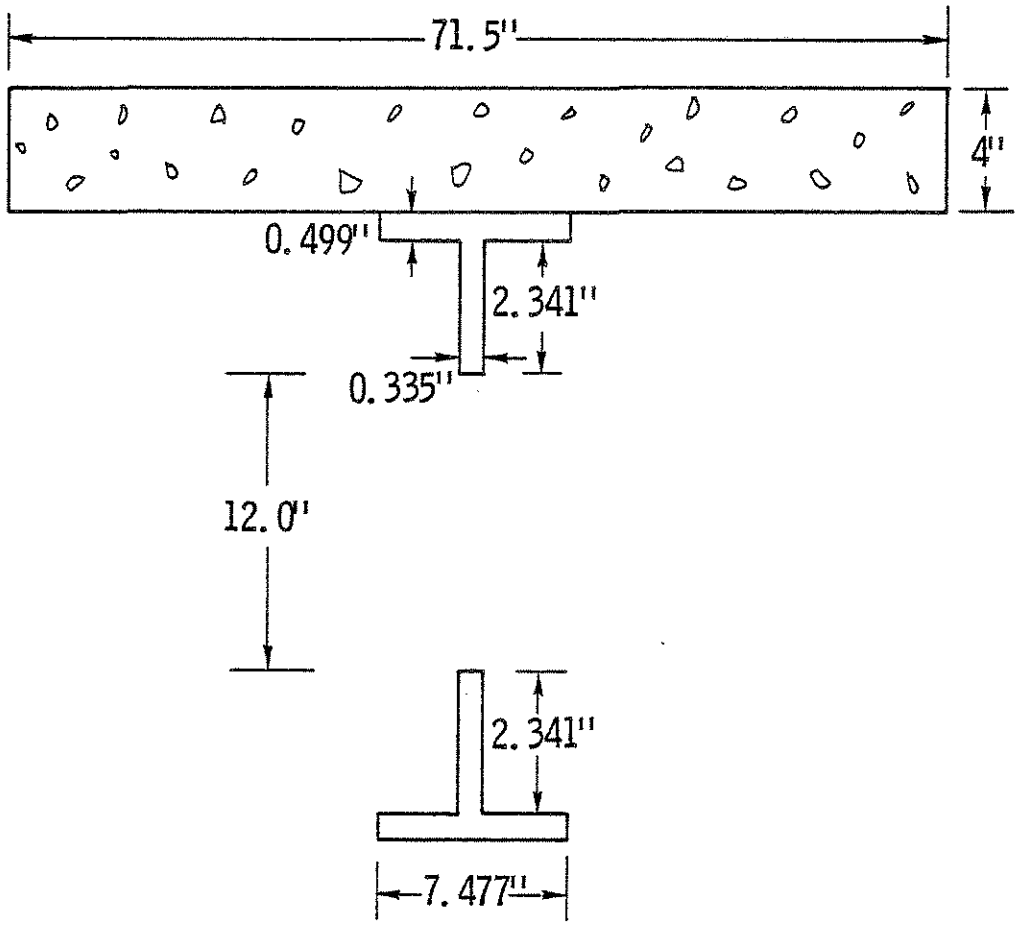

Fig. 6.3 Cross-Section of Composite Beam in Design Example

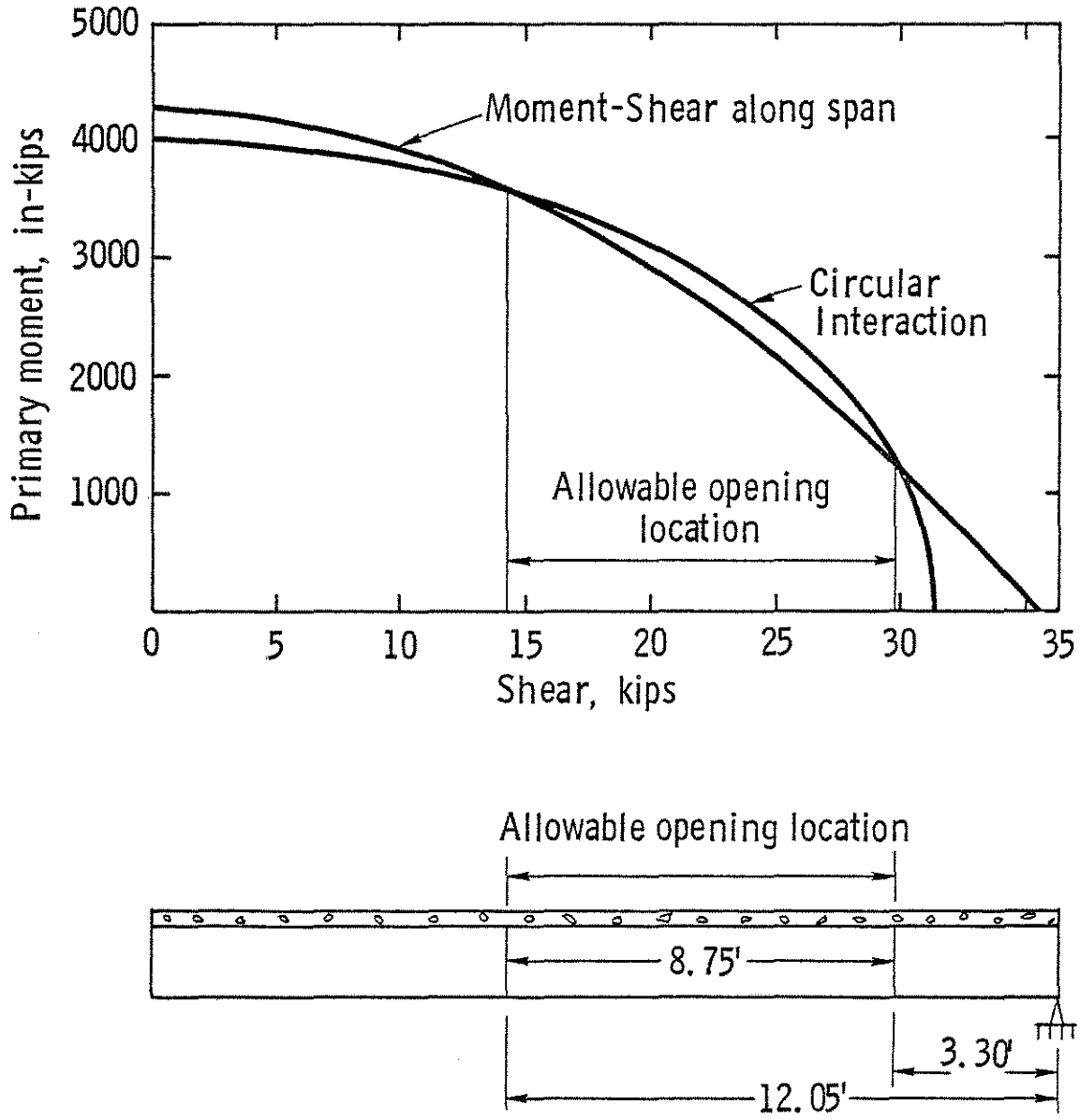

Fig. 6.4 Circular Moment-Shear Interaction and Moment-Shear Values Along Span

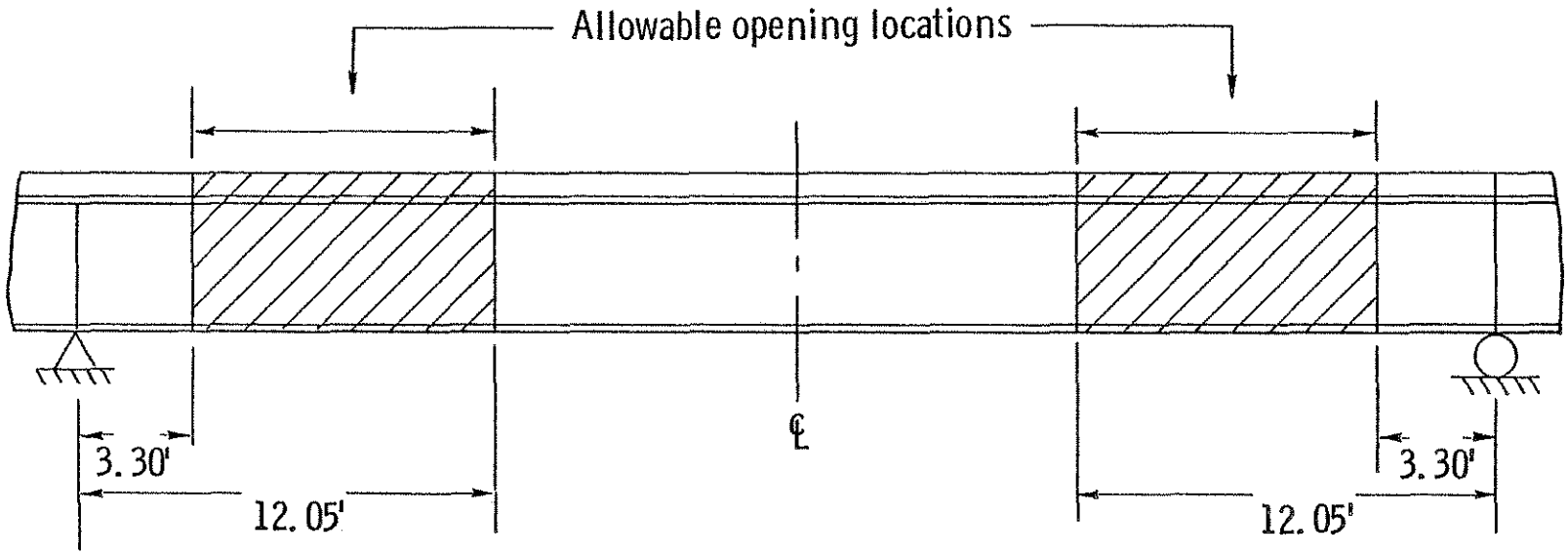

Fig. 6.5 Allowable Opening Locations for Design Example

APPENDIX A

NOMENCLATURE

a	one-half of the opening length
A_c	area of the effective concrete slab
A_f	area of a steel flange
A_r	area of the longitudinal reinforcing steel in the effective slab width
A_w	area of the steel web or stub
b_{eff}	effective width of concrete slab
b_f	steel flange width
c	depth to neutral axis from the top of the slab at the high moment end of the top tee
C_i	constants in bottom tee moment-axial force equations
C'_c	axial capacity of effective slab
E	opening eccentricity from the centerline of the steel beam
EAA	equal area axis
f	normal stress
f'_c	nominal compressive concrete strength obtained from 6" diameter cylinder tests
f_r	concrete modulus of rupture obtained from 6" x 6" x 21" flexure specimens
F_y	yield stress of steel
F_{yf}	yield stress of steel flange
F_{yfr}	reduced yield stress of steel flange
F_{yr}	yield stress of reinforcing steel
F_{yw}	yield stess of steel web
F_{ywr}	reduced yield stress of steel web
g	location of neutral axis in bottom tee
h	opening depth

h_r	height of reinforcing steel above top flange
L	span length
M	primary moment at the centerline of the opening
M_{bh}	secondary moment at the high moment end of the bottom tee
M_{bl}	secondary moment at the low moment end of the bottom tee
M_{max}	maximum primary moment capacity at an opening
$M_{primary}$	primary moment at the centerline of an opening
M_{th}	secondary moment at the high moment end of the top tee
M_{tl}	secondary moment at the low moment end of the top tee
n	P'_u/P_u ratio for the bottom tee
P_{bh}	axial force at the high moment end of the bottom tee
P_{bl}	axial force at the low moment end of the bottom tee
PC	plastic centroid
$P_{1,2}$	total load per load point
P_{1y}	total load at first yield
P'_u	maximum axial capacity in bottom tee with secondary moment
P_{th}	axial force at the high moment end of the top tee
P_{tl}	axial force at the low moment end of the top tee
P_u	maximum axial capacity of bottom tee
P_{ult}	total load at failure
r	F_{yw}/F_{yf} ratio for bottom and top tees
R	ratio of observed to predicted strength
s_b	bottom tee stub length
s_t	top tee stub length
T'	axial capacity steel beam
V	shear force at the centerline of the opening
V_b	bottom tee shear force

V_{hc}	shear assigned to the concrete at the high moment end of the top tee
V_{max}	maximum shear capacity at an opening
$V_{max\ a=0}$	maximum shear capacity at an opening with length equal to zero
V_s	shear assigned to the steel at the high moment end of the top tee
$V_{tmax}(mech)$	maximum shear capacity of top tee with "mechanism" failure
$V_{tmax}(sh)$	maximum shear capacity of top tee with "shear" failure
V_{total}	shear forces at the centerline of an opening
V_{wmax}	web stub shear capacity
x_c	location of plastic centroid in top tee
$\bar{y}$	location of plastic centroid in bottom tee
y^*	location of equal area axis in bottom tee
y_1	location of neutral axis in flange at low moment end of top tee
y_2	location of neutral axis in web at low moment end of top tee
z	distance between the plastic centroids of the top and bottom tees
Z_i	constants in bottom tee moment-axial force equations
$\bar{\delta}$	δ_r/δ_c ratio
δ_c	centerline deflection
δ_r	relative vertical displacement between the low and high moment ends of the opening at failure
ε_{sh}	shearing strain
ε_{+45}	strain reading from rosette gage oriented at +45°
ε_{-45}	strain reading from rosette gage oriented at -45°
τ	shear stress
τ_b	shear stress in the web stub in the bottom tee

τ_c shear stress in the concrete at the high moment end of the top tee

τ_s shear stress in the steel web stub at the high moment end of the top tee

APPENDIX B

STRAIN GAGE APPLICATION

The strain gages used on the steel were two varieties. The single gages were 120Ω, 1/4" gage length gages produced by Micro-Measurements (EA-06-250BG-120). The 3-gage rosettes were composed of 120Ω, 1/8" gage length gages also produced by Micro-Measurements (EA-06-125-RA-120).

The steel surfaces were prepared by grinding away the scale and imperfections until the surface was smooth. This was done with a pneumatic grinder with a coarse abrasive disk. The surface was sprayed with a degreaser and wiped clean with gauze sponges until it was clean. An acidic cleaning solution was added to the steel surface and was sanded with emory paper to further smooth the surface. Sanding was completed using a find grade of emory paper. The surface was wiped clean and a neutralizing solution was added using a cotton swab. This solution was removed using a gauze sponge, leaving a clear surface ready for strain gage application.

The strain gage was placed on a clean surface and a terminal strip was placed at the end of the gage near the gage terminals. Cellophane tape was applied to the gage and terminal and gently peeled back with the gage attached to the tape. The tape was then applied to the desired location on the beam. The tape was peeled back until the gage and terminal were revealed. A thin coat of adhesive catlyst was applied to the bottom of the gage and allowed to dry for at least 1 minute. The adhesive was applied to the steel surface, and the tape was pressed down with the thumb, maintaining pressure on the gage for 2-3 minutes. The

tape was left on the gage to protect it temporarily. All steel gages were attached in this manner, leaving the tape on the gages until the lead wires were ready to be soldered to the gages.

Small 3-wire tabs were soldered to the terminals with small single strands soldered to the gages. One wire was soldered to one terminal tab, and 2 wires were soldered to the other. The wiring was completed by soldering 3-wire shielded cables to the tabs. The steel strain gages were moisture-proofed using 2 different methods. Gages under the concrete were protected using MCOAT-G and MCOAT-D which are epoxy and rubber-based materials, respectively, both produced by Micro-Measurements. Other steel gages were protected with a lacquer-type coating called MCOAT-200, also produced by Micro-Measurements.

The concrete strain gages were 120Ω, paper-backed gages. Primarily, strain gages for the concrete were produced by Precision (W240), although a few BLH gages were used.

Since the concrete contains moisture, it was necessary to allow the concrete to dry several days before instrumenting. The surface of the concrete was rough, and it was necessary to grind the surface slightly. After grinding, the surface was blown clean using compressed air. The surface was sealed using a thin coat of DUCO cement which was allowed to dry for about 15 minutes. The bottom of the gage was coated with DUCO cement and placed at the desired locations. A thin sheet of plastic was placed on the top surface of the gage, and the gage was pressed firmly to the concrete surface using the thumb. The plastic sheet was removed, and the gage was allowed to dry. Curing of the DUCO cement was usually complete in 24 hours. The gages were not moisture-

proofed because moisture could migrate from the concrete and be trapped under the coating and affect the gage reliability. Three-wire shielded cables were connected to the gages.

APPENDIX C

EXPERIMENTAL DATA

BEAM NO. 1 ELASTIC TEST

Load No.	P_1	P_2	P_T *	D.G.1 d	D.G.2	D.G.3	D.G.4	D.G.5	D.G.6 s	D.G.7
0	0.0	0.0	0.0	0	0	0	0	0	0	0
1	0.37	0.40	0.77	14½	16½	20	16½	14½	0	0
2	0.94	1.06	2.00	28	32	37	31½	29	1	0
3	1.73	1.89	3.61	46	54	62	53	48	3	0
4	2.48	2.66	5.14	64	76	87	76	69	4	0
5	3.32	3.51	6.83	82	98	113	94	84	4	0
6	2.69	2.85	5.54	67	79	93	79	68	2	0
7	1.88	2.02	3.90	49	58	69	57	49	1	0
8	1.05	1.20	2.24	30½	36	44	36	30	0	0
9	0.52	0.56	1.08	15	18	23	19	16	0	0
10	0.0	0.0	0.0	1½	2	1½	2	1	0	0

Load No.	S.G.0 t	S.G.1	S.G.2	S.G.3	S.G.6	S.G.5	S.G.6	S.G.7	S.G.8	S.G.9
0	0	0	0	0	0	0	0	0	0	0
1	49	47	40	34	22	9	12	18	22	28
2	97	93	78	65	41	15	23	34	42	52
3	162	154	129	108	68	24	36	56	69	86
4	228	217	181	152	94	33	51	77	96	120
5	294	278	232	195	121	43	66	99	124	156
6	238	225	188	158	98	34	52	80	100	127
7	171	162	136	114	70	23	37	58	72	92
8	104	99	83	70	41	14	22	45	44	58
9	51	49	42	35	23	7	12	19	23	30
10	-1	1	1	-1	1	-1	0	2	1	1

Load No.	S.G.10	S.G.11	S.G.12	S.G.13	S.G.14	S.G.15	S.G.16	S.G.17	S.G.18	S.G.19
0	0	0	0	0	0	0	0	0	0	0
1	31	32	32	27	19	17	12	0	-9	-9
2	60	63	64	54	42	32	23	0	-18	-18
3	98	104	105	88	68	52	37	0	-30	-30
4	139	147	148	125	97	74	52	0	-43	-43
5	179	187	187	158	123	94	66	0	-54	-55
6	146	152	151	127	99	77	52	0	-44	-44
7	106	109	107	90	71	54	37	0	-32	-32
8	66	67	65	55	44	34	22	0	-19	-20
9	31	33	31	27	22	17	12	0	-10	-10
10	1	1	1	1	0	0	0	0	0	0

* P forces expressed in kips

d deflection readings expressed in 0.001"

s slip readings expressed in 0.0001"

t strain readings expressed in microstrain

BEAM NO. 1 ULTIMATE TEST

Load No.	P_1	P_2	P_T	D.G.1	D.G.2	D.G.3	D.G.4	D.G.5	D.G.6	D.G.7
0	0.0	0.0	0.0	0	0	0	0	0	0	0
1	1.73	1.92	3.64	50	61	72	59	53	2	0
2	4.50	4.73	9.23	110	134	157	128	115	3	1
3	7.21	7.39	14.60	273	210	246	200	279	5	2
4	9.72	9.84	19.56	341	292	343	281	248	6	9
5	11.24	11.11	22.35	375	336	395	324	284	10	11
6	13.59	13.51	27.10	453	432	510	418	364	13	15
7	14.79	14.78	29.57	493	482	571	466	408	15	18
8	15.94	16.01	31.95	536	537	643	522	456	17	21
9	17.35	17.44	34.79	596	613	732	594	518	20	23
10	18.40	18.67	37.06	650	680	811	660	575	22	26
11	19.75	19.84	39.59	719	767	923	742	648	23	30
12	21.11	21.33	42.44	816	892	1072	863	748	27	33
13	22.32	22.60	44.92	834	915	1096	882	766	28	34
14	22.68	23.13	45.81	938	1046	1245	993	861	31	38
15	23.36	23.61	46.97	1083	1240	1438	1138	1077	34	40
16	23.73	24.68	48.40	1252	1453	1640	1282	1098	38	42
17	24.20	25.26	49.46	1403	1641	1826	1411	1210	41	45
18	24.67	25.74	50.40	1551	1834	1910	1546	1321	45	47
19	25.08	26.21	51.30	1691	2012	2194	1686	1434	49	49
20	25.71	26.43	52.14	1840	2206	2389	1810	1501	52	51
21	26.08	26.54	52.62	1984	2393	2580	1964	1664	57	53
22	26.60	27.23	53.83	2126	2575	2776	2106	1800	61	56
23	27.02	27.71	54.73	2370	2758	2976	2249	1950	65	58
24	27.18	27.87	55.05	2523	2953	3196	2398	2082	70	61
25	27.65	28.35	55.99	2727	3212	3595	2632	2262	74	62
26	28.07	28.77	56.84	2929	3468	3797	2951	2447	79	64
27	28.59	29.41	58.00	3088	3799	4190	3244	2690	84	69
28	29.53	30.31	59.85	3448	4131	4588	3542	3039	92	73
29	29.74	30.74	60.48	3773	4562	5087	3808	3346	100	79
30	30.86	31.86	62.72							

Load No.	S.G.0	S.G.1	S.G.2	S.G.3	S.G.4	S.G.5	S.G.6	S.G.7	S.G.8	S.G.9
0	0	0	0	0	0	0	0	0	0	0
1	186	176	147	124	76	27	41	82	78	98
2	390	371	328	276	165	55	87	134	170	215
3	568	521	618	487	249	37	100	185	251	336
4	867	556	893	701	334	-5	95	226	327	456
5	1014	582	1026	809	375	-22	95	226	365	514
6	1351	604	1338	1050	455	-70	86	284	439	630
7	1542	641	1460	1172	495	-90	85	304	476	687
8	1869	683	1564	1307	531	-118	77	320	511	740
9	2269	736	1699	1462	565	-161	81	369	648	857
10	2549	1001	2030	1613	577	-160	105	456	739	941
11	2629	2451	2530	1853	558	-152	145	556	888	984
12	2669	3101	3100	2372	763	-200	255	878	1341	3501
13	3069	3881	3590	2462	758	-204	423	1296	1865	5501
14	4599	6011	4530	2562	858	3672	3990	5202	5022	9641
15	-	7871	5540	2742	1255	10412	9850	7922	8322	14161
16	10289	9861	8600	3682	1637	-	10350	8312	8822	15411
17	11689	10711	11220	8512	2911	-	-	8412	8992	15741
18	12959	12051	12250	-	4561	-	-	-	9132	15981
19	-	14011	-	-	5701	-	-	-	9272	16181
20	17289	13061	-	-	6651	-	-	-	9422	16281
21	19459	13241	-	-	7961	-	-	-	9602	16501
22	-	13221	-	-	9241	-	-	-	9782	16781
23	-	12781	-	-	10411	-	-	-	9962	-
24	-	12121	-	-	11541	-	-	-	10252	-
25	-	-	-	-	12291	-	-	-	10512	-
26	-	-	-	-	13291	-	-	-	10962	-
27	-	-	-	-	14051	-	-	-	11462	-
28	-	-	-	-	15151	-	-	-	12192	-
29	-	-	-	-	15761	-	-	-	12502	-

Load No.	S.G.10	S.G.11	S.G.12	S.G.13	S.G.14	S.G.15	S.G.16	S.G.17	S.G.18	S.G.19
0	0	0	0	0	0	0	0	0	0	0
1	114	119	120	101	79	60	42	0	-34	-34
2	250	260	259	271	171	129	88	1	-75	-75
3	398	413	409	336	252	176	100	0	-117	-118
4	548	571	562	455	327	213	96	1	-168	-165
5	621	648	639	516	365	233	97	2	-195	-192
6	767	804	797	638	438	266	88	11	-256	-249
7	838	880	876	700	475	284	87	25	-288	-279
8	909	957	958	764	511	299	79	25	-324	-313
9	1056	991	1163	910	668	380	100	40	-376	-360
10	1130	1004	1217	1005	776	456	133	53	-421	-402
11	1160	1025	1285	1131	941	570	200	71	-475	-451
12	1390	3051	1304	1223	1519	1012	406	91	-551	-527
13	3952	4601	1461	1344	2202	1517	712	93	-593	-582
14	8212	7781	4202	3402	6242	5092	4832	112	-639	-633
15	13292	11711	6382	5592	8652	8142	7752	130	-677	-678
16	15082	13091	8342	6962	8922	8352	8072	150	-714	-727
17	15712	13711	9822	8042	9082	8452	8152	170	-750	-779
18	16152	14401	11182	9212	9302	8602	8232	196	-790	-835
19	16502	15071	12212	10162	9552	8752	8282	224	-830	-905
20	16702	15541	12952	10752	9772	8862	8312	258	-868	-965
21	17202	16061	13872	11472	9932	8942	8332	293	-906	-1019
22	17642	16531	14652	12002	10072	9022	8362	335	-957	-1074
23	-	-	15512	12552	10222	9122	8402	376	-1016	-1140
24	-	-	-	13532	10472	9292	8442	448	-1083	-1221
25	-	-	-	14252	10712	9472	8602	543	-1159	-1304
26	-	-	-	15182	11112	9862	8692	579	-1256	-1424
27	-	-	-	16022	11602	10332	9202	656	-1356	-1560
28	-	-	-	17432	12322	10892	9962	746	-1462	-1694
29	-	-	-	18112	12652	11082	12142	802	-1540	-1785

Load No.	S.G.12	S.G.13	S.G.14	S.G.15	S.G.16	S.G.17	S.G.18	S.G.19	S.G.20	S.G.21
0	000	000	000	000	000	000	000	000	000	000
1	055	001	005	016	025	033	040	036	-015	-014
2	119	000	009	033	051	067	083	075	-026	-029
3	189	-002	012	050	080	104	131	118	-039	-045
4	257	-003	017	068	108	140	177	159	-057	-061
5	324	-004	021	085	137	176	222	200	-069	-077
6	257	-004	017	066	108	140	176	158	-052	-060
7	193	-003	012	050	081	105	132	119	-038	-045
8	122	-001	008	032	052	067	084	076	-025	-029
9	053	000	004	015	024	030	037	033	-011	-013
10	000	000	000	000	000	000	000	000	000	000

Load No.	S.G.22	S.G.23	S.G.24	S.G.25	S.G.26
0	000	000	000	000	000
1	-016	-014	000	000	-003
2	-031	-026	001	001	-002
3	-048	-041	002	001	-001
4	-064	-055	002	003	002
5	-081	-070	002	004	003
6	-063	-055	002	002	003
7	-046	-042	000	002	002
8	-030	-026	001	002	001
9	-013	-012	000	000	000
10	000	000	000	000	000

BEAM NO. 2 ELASTIC TEST

Load No.	P_1	P_2	P_T	D.G.1	D.G.2	D.G.3	D.G.4	D.G.5	S.G.0	S.G.1
0	0.0	0.0	0.0	0	0	0	0	0	000	000
1	1.135	1.141	2.28	17	21	20	0	-1	-003	059
2	2.354	2.335	4.689	35	43	43	0	-1	-006	127
3	3.574	3.688	7.262	53	65	67	0	0	-010	198
4	4.793	4.802	9.675	70	86	91	0	0	-015	270
5	6.035	6.235	12.27	88	109	113	0	0	-019	339
6	4.740	4.856	9.596	70	87	91	0	-1	-014	269
7	3.574	3.635	7.209	53	67	69	0	-1	-012	202
8	2.304	2.282	4.586	35	44	44	0	-1	-007	129
9	0.930	0.982	1.912	15	20	19	0	-1	-003	056
10	0.0	0.0	0.0	0	0	0	0	0	000	000

Load No.	S.G.2	S.G.3	S.G.4	S.G.5	S.G.6	S.G.7	S.G.8	S.G.9	S.G.10	S.G.11
0	000	000	000	000	000	000	000	000	000	000
1	053	046	036	029	020	-007	006	014	026	047
2	117	097	078	061	045	-017	011	030	056	100
3	182	151	122	094	069	-028	018	046	088	158
4	249	205	166	128	094	-040	024	062	119	215
5	313	257	208	161	117	-051	030	079	151	271
6	249	204	166	128	094	-041	024	061	118	215
7	186	152	124	096	070	-030	018	045	089	161
8	119	097	079	062	046	-019	012	029	056	102
9	051	042	035	027	020	-007	006	012	024	044
10	000	000	000	000	000	000	000	000	000	000

BEAM NO. 2 ULTIMATE TEST

Load No.	P_1	P_2	P_T	D.G.1	D.G.2	D.G.3	D.G.4	D.G.5
0	0.0	0.0	0.0	0	0	0	0	0
1	6.005	6.209	12.21	90	111	115	-1	0
2	12.259	12.657	25.016	179	229	241	0	1
3	18.758	19.105	37.863	270	358	371	3	41
4	20.985	21.440	42.425	308	408	425	3	58
5	23.474	23.988	47.462	349	463	483	3	70
6	25.935	26.429	52.364	391	520	544	3	83
7	28.294	28.704	52.364	436	581	610	4	98
8	30.808	31.364	62.172	486	651	685	4	113
9	33.140	33.646	62.172	542	732	771	4	132
10	35.394	35.342	70.336	619	837	876	4	154
11	37.776	37.838	75.614	719	1082	1027	15	183
12	38.891	39.351	78.242	807	1158	1201	128	206
13	40.782	41.314	82.096	969	1461	1495	152	242
14	43.112	43.118	86.230	1154	1778	1798	173	272
15	44.331	44.604	88.935	1459	2197	2189	209	310
16	45.600	45.692	91.292	1901	2835	2783	281	364
17			94.400	-	-	-	-	-

Load No.	S.G.0	S.G.1	S.G.2	S.G.3	S.G.4	S.G.5	S.G.6	S.G.7	S.G.8	S.G.9
0	000	000	000	000	000	000	000	000	000	000
1	-016	345	319	260	212	163	119	-047	030	084
2	080	1189	997	859	612	373	211	-176	040	181
3	121	1883	1746	1298	1119	601	283	-389	076	346
4	126	2210	2149	1415	1352	691	306	-321	092	421
5	139	2650	2499	1723	1662	791	326	-294	109	501
6	157	3170	2829	2649	2139	894	343	-281	129	588
7	174	3750	3319	3689	2819	1006	336	-240	154	688
8	201	4330	4019	4189	3559	1131	330	-189	194	814
9	230	4900	4799	4689	4099	1257	328	-160	234	965
10	257	5580	5549	5279	4779	1428	438	-140	278	1120
11	264	7010	6679	6219	5909	1531	553	-185	271	1287
12	409	9050	8479	7889	7439	1549	484	-014	401	1702
13	403	10810	10439	9649	9139	2219	515	579	711	3150
14	418	12500	12299	11399	10799	2409	749	960	987	5770
15	402	16400	15719	14259	13089	2519	812	1184	1270	7590
16	365	-	-	10149	19459	9129	4780	1406	1530	10770
17	-	-	-	-	-	-	-	-	-	-

Load No.	S.G.10	S.G.11	S.G.12	S.G.13	S.G.14	S.G.15	S.G.16	S.G.17	S.G.18	S.G.19
0	000	000	000	000	000	000	000	000	000	000
1	152	274	328	-006	020	086	138	178	226	202
2	391	1430	2000	-181	-095	102	252	371	502	409
3	733	2131	4189	-358	-212	117	364	564	778	619
4	893	2171	4529	-432	-261	120	405	637	884	698
5	1055	2261	5049	-515	-318	119	446	714	997	782
6	1224	2481	5569	-594	-372	120	489	793	1111	867
7	1413	2851	6059	-719	-443	127	580	905	2199	945
8	1629	3301	6589	-865	-520	148	715	1049	3099	1030
9	1882	3751	7149	-1005	-582	192	890	1137	3919	1096
10	2090	4071	7459	-1157	-640	261	1134	1176	5509	1154
11	2480	5001	8139	-1451	-722	555	2039	1979	6519	1218
12	4110	7391	10169	-1821	-738	1445	4019	2149	7579	1244
13	7860	10931	14159	-967	-098	2140	6869	7429	11329	1300
14	11188	14761	17759	-385	530	3480	8439	12019	15069	1368
15	14270	18411	17039	-408	547	3880	9139	13369	16939	1424
16	18840	-	16849	-868	151	4280	10569	15069	19819	1467
17	-	-	-	-	-	-	-	-	-	-

Load No.	S.G.20	S.G.21	S.G.22	S.G.23	S.G.24	S.G.25	S.G.26
0	000	000	000	000	000	000	000
1	-069	-075	-076	-068	004	005	009
2	-140	-158	-133	-144	020	021	001
3	-208	-240	-192	-219	025	034	009
4	-224	-267	-207	-244	031	045	021
5	-245	-298	-227	-270	035	049	026
6	-271	-338	-256	-298	041	052	019
7	-291	-362	-283	-325	044	057	013
8	-311	-395	-320	-351	045	058	-008
9	-332	-426	-371	-374	047	064	-054
0	-350	-457	-430	-396	049	072	-085
1	-357	-475	-475	-404	072	101	-166
2	-323	-484	-563	-373	050	070	2319
3	-303	-381	-517	-339	040	-037	-
4	-299	-310	-488	-350	019	-093	-
5	-369	-375	-526	-437	063	-094	-
6	-430	-359	-568	-559	003	-158	-
7	-	-	-	-	-	-	-

BEAM NO. 3 ELASTIC TEST

Load No.	P_1	P_2	P_T	D.G.1	D.G.2	D.G.3	D.G.5	D.G.6	D.G.7
0	0.0	0.0	0.0	0	0	0	0	0	0
1	0.89	0.88	1.76	14.0	16.0	16.0	14.0	-1	0
2	2.14	2.23	4.37	36.0	39.5	39.5	34.5	-1	0
3	3.53	3.55	7.08	58.0	64.0	6.40	54.0	1	1
4	4.71	4.69	9.40	76.5	83.5	84.0	72.0	1	1
5	6.06	6.07	12.14	97.0	106.5	107.5	91.0	1	1
6	4.71	4.77	9.48	77.0	85.0	85.0	72.0	1	1
7	3.42	3.47	6.90	58.0	64.0	64.0	54.0	1	1
8	2.06	2.15	4.21	36.0	40.0	40.0	34.0	1	0
9	0.78	0.85	1.63	15.0	17.0	17.0	14.5	1	0
10	0.0	0.0	0.0	0	0	0	0	0	0

Load No.	S.G.0	S.G.1	S.G.2	S.G.3	S.G.4	S.G.5	S.G.6	S.G.7	S.G.8	S.G.9
0	000	000	000	000	000	000	000	000	000	000
1	082	051	040	033	031	030	028	000	002	005
2	279	126	098	082	076	076	071	-002	004	013
3	290	201	157	133	123	122	114	-004	006	019
4	261	268	209	177	163	160	151	-004	009	026
5	686	347	270	229	211	207	196	-006	011	034
6	260	271	212	178	164	163	153	-006	010	028
7	335	202	158	132	122	122	115	-005	007	020
8	211	126	099	082	076	077	072	-003	005	013
9	-065	053	041	034	031	033	030	-002	002	006
10	000	000	000	000	000	000	000	000	000	000

Load No.	S.G.10	S.G.11	S.G.12	S.G.13	S.G.14	S.G.15	S.G.16	S.G.17	S.G.18	S.G.19
0	000	000	000	000	000	000	000	000	000	000
1	009	015	012	026	028	027	029	030	032	029
2	023	036	031	064	068	068	073	076	081	074
3	036	057	050	102	108	107	116	121	129	118
4	049	077	067	136	144	144	156	161	172	157
5	064	100	087	176	185	185	201	206	222	203
6	051	079	069	138	146	145	158	162	175	159
7	038	059	051	102	108	107	117	121	130	118
8	023	037	032	064	068	067	073	076	082	074
9	010	015	014	026	028	028	030	032	034	031
10	000	000	000	000	000	000	000	000	000	000

Load No.	S.G.20	S.G.21	S.G.22	S.G.23	S.G.24	S.G.25	S.G.26
0	000	000	000	000	000	000	000
1	-010	-009	-011	-009	000	+002	+001
2	-025	-025	-028	-024	-001	+001	+002
3	-041	-040	-045	-038	-002	+001	+003
4	-054	-053	-061	-051	-002	+001	+004
5	-070	-068	-078	-065	-002	+002	+006
6	-055	-055	-061	-053	-002	000	+005
7	-040	-041	-045	-040	-002	+001	+003
8	-025	-027	-028	-025	-002	+001	+002
9	-010	-011	-011	-011	-001	000	+001
10	000	000	000	000	000	000	000

BEAM NO. 3 ULTIMATE TEST

Load No.	P_1	P_2	P_T	D.G.1	D.G.2	D.G.3	D.G.5	D.G.6	D.G.7
0	0.0	0.0	0.0	0.0	0.0	0.0	0.0	0	0
1	6.17	6.23	12.4	100.5	109.5	110.0	93.5	0	1
2	12.34	12.57	24.91	200.0	221.0	225.0	188.0	7	2
3	18.71	19.04	37.75	304.0	338.0	344.0	290.0	40	2
4	22.69	22.72	45.41	372.0	415.0	424.5	360.0	70	3
5	24.75	25.11	49.86	418.5	470.0	482.0	406.5	90	3
6	27.26	27.5	54.76	471.0	530.5	544.0	456.0	105	3
7	29.69	29.99	59.68	531.0	599.5	613.5	512.5	121	4
8	31.86	32.27	64.13	621.0	695.5	706.0	586.0	141	125
9	33.35	33.68	67.03	666.0	750.0	761.0	628.5	151	136
10	34.21	34.55	68.76	711.0	801.0	813.0	668.0	160	144
11	35.18	35.53	70.71	763.0	867.5	875.5	717.0	169	153
12	35.68	36.06	71.74	861.5	976.0	975.0	790.5	177	163
13	36.51	36.83	73.34	979.0	1140.0	1099.0	879.0	184	174
14	36.81	37.17	73.98	1054.0	1199.0	1175.0	935.0	189	183
15	37.48	37.84	75.32	1253.5	1419.0	1378.0	1078.0	196	202
16	38.53	38.95	77.48	1555.5	1756.0	1686.0	1292.5	209	238
17	40.17	40.70	80.87	1849.0	2086.5	1991.0	1511.5	224	285
18	42.96	43.25	86.21	2236.5	2527.0	2408.0	1813.5	250	368
19	45.03	45.26	90.29	2634.5	2975.0	2828.0	2120.5	297	482
20	46.26	46.80	93.06	3063.0	3462.0	3288.0	2449.5	331	623
21	47.67	48.21	95.88	3465.0	3915.0	4734.0	2761.5	364	829
22	49.23	49.80	99.03 (104.7)	-	-	-	-	-	-

Load No.	S.G.0	S.G.1	S.G.2	S.G.3	S.G.4	S.G.5	S.G.6	S.G.7	S.G.8	S.G.9
0	000	000	000	000	000	000	000	000	000	000
1	-340	297	283	241	220	215	202	-006	013	035
2	-351	1287	723	490	451	442	410	-018	037	077
3	-356	1576	1331	777	699	681	621	-007	054	130
4	-398	1629	1901	948	847	826	748	-021	064	160
5	-408	1783	2300	1078	951	926	830	-034	074	187
6	-416	2050	2650	1226	1031	1018	840	-044	084	212
7	-393	2700	3010	1445	1127	1114	828	-058	102	255
8	-352	3520	3390	1786	1231	1151	750	-077	119	301
9	-302	3930	3930	2110	1339	1182	701	-116	111	316
10	-210	4220	4390	2470	1439	1169	674	-128	135	365
11	-135	4760	5130	3148	1584	1148	614	-141	171	438
12	-115	8320	7060	3440	1836	1228	596	-161	253	599
13	+009	11860	9800	3860	2000	1284	617	-209	331	787
14	-089	13350	12510	5440	2150	1346	706	-237	389	920
15	-140	14190	15390	12220	8360	10279	4099	-306	567	1289
16	-104	15710	16790	14890	12370	11049	9629	-413	851	1785
17	+211	18310	19120	15760	13410	11219	10959	-512	1162	2769
18	+004	-	-	18720	15720	12659	13199	-621	1546	5459
19	+020	-	-	-	18130	15509	15699	-722	1887	6449
20	-007	-	-	-	-	18419	18349	-700	2310	7689
21	-269	-	-	-	-	-	-	-690	2520	8119
22	-139	-	-	-	-	-	-	-7620	-3710	1669

Load No.	S.G.10	S.G.11	S.G.12	S.G.13	S.G.14	S.G.15	S.G.16	S.G.17	S.G.18	S.G.19
0	000	000	000	000	000	000	000	000	000	000
1	066	102	114	180	184	191	210	214	232	211
2	166	307	896	804	416	349	413	435	483	421
3	286	493	1228	1106	593	520	626	663	746	642
4	352	591	1335	1358	733	626	751	803	883	782
5	411	675	1455	1570	863	704	833	901	950	888
6	465	745	1534	1719	1041	785	907	979	987	979
7	552	845	1669	1708	1175	903	1185	1123	3920	1078
8	647	967	1939	1760	1461	1053	1377	1169	4270	1169
9	705	1046	2139	1808	1828	1179	1487	1210	4360	1224
10	804	1136	2389	1812	2480	1378	1698	1254	4710	1267
11	945	1263	2779	1867	3070	1683	2010	1290	5250	1307
12	1244	1469	3469	2970	5310	2430	2860	1332	5310	1334
13	1598	1696	4289	4310	5449	5430	3680	1303	5760	1359
14	1826	1887	5059	4810	5830	5600	4870	1280	6230	1371
15	2270	3799	6779	6650	6970	5900	7780	2299	9630	1388
16	3880	6019	8529	8690	9470	7970	10380	6019	12410	1416
17	6860	7209	10799	10430	11660	10170	12140	11029	13800	1479
18	8890	9439	13029	12450	13480	11680	14020	13819	16240	1572
19	10820	11319	15029	14320	15490	13800	16100	16199	18630	1653
20	12670	13219	17139	16570	17770	16000	18470	18749	-	1760
21	13598	14319	18619	18460	19680	17830	-	-	-	1960
22	9550	11919	17929	17670	19750	18960	-	-	-	0620

Load No.	S.G.20	S.G.21	S.G.22	S.G.23	S.G.24	S.G.25	S.G.26
0	000	000	000	000	000	000	000
1	-072	-071	-081	-067	-002	+002	+005
2	-143	-138	-129	-136	-006	001	+008
3	-221	-211	-222	-209	-011	002	+009
4	-267	-256	-268	-253	-014	003	+012
5	-304	-290	-304	-287	-014	010	+014
6	-335	-320	-337	-316	-011	000	+017
7	-378	-361	-380	-357	-005	+007	+018
8	-423	-405	-427	-396	+006	+018	+020
9	-465	-446	-460	-437	+025	+043	+002
10	-502	-480	-495	-469	+040	+057	-003
11	-547	-523	-538	-510	+063	+078	-009
12	-627	-598	-617	-586	+125	+115	-021
13	-740	-707	-721	-689	+163	+089	-034
14	-809	-775	-789	-757	+154	+077	-045
15	-970	-942	-957	-900	+129	+056	-060
16	-1206	-1192	-1168	-1096	+107	+081	-070
17	-1458	-1445	-1346	-1293	+079	+097	-067
18	-1785	-1788	-1571	-1529	+059	+131	-036
19	-2190	-2210	-1820	-1788	+042	+158	+018
20	-2710	-2748	-2099	-2121	+021	+308	+089
21	-3250	-3280	-2299	-2561	000	+190	+149
22	-1300	+240	-649	-2391	-069	+007	-011

BEAM NO 4 ELASTIC TEST

Load No.	P_1	P_2	P_T	D.G.1	D.G.2	D.G.3	D.G.4	D.G.5	S.G.0	S.G.1
0	0.0	0.0	0.0	0	0	0	0	0	0	0
1	2.2	2.2	4.4	5	12	15	-1	-1	-5	108
2	4.4	4.4	8.8	10	25	28	-1	-1	1	218
3	7.0	6.9	13.9	25	40	46	-2	-1	9	354
4	9.1	9.2	18.2	20	52	60	-2	-1	15	465
5	11.3	11.3	22.6	25	64	74	-3	-1	17	581
6	9.5	9.5	19.0	21	55	63	-3	-1	23	494
7	7.6	7.6	15.2	16	44	51	-2	-1	26	396
8	4.7	4.8	9.5	11	28	33	-2	0	22	255
9	2.5	2.4	4.9	6	15	17	-1	0	10	132
10	0.0	0.0	0.0	0	0	1	0	0	0	3

Load No.	S.G.2	S.G.3	S.G.4	S.G.5	S.G.6	S.G.7	S.G.8	S.G.9	S.G.10	S.G.11
0	0	0	0	0	0	0	0	0	0	0
1	91	65	42	26	9	-4	19	37	55	78
2	186	130	85	51	15	-14	34	72	110	157
3	302	210	136	80	23	-24	53	115	177	256
4	398	275	179	104	30	-32	69	152	233	335
5	498	344	224	131	37	-38	88	190	292	420
6	423	292	189	110	30	-37	72	160	246	357
7	339	233	150	86	22	-31	55	126	197	288
8	219	150	96	55	13	-23	33	80	125	186
9	113	78	49	27	6	-12	16	41	65	99
10	3	2	1	0	-1	-1	0	1	2	5

Load No.	S.G.12	S.G.13	S.G.14	S.G.15	S.G.16	S.G.17	S.G.18	S.G.19	S.G.20	S.G.21
0	0	0	0	0	0	0	0	0	0	0
1	82	-47	-32	-6	16	31	54	52	-16	-21
2	168	-102	-104	-15	31	61	106	99	-31	-42
3	273	-169	-112	-26	49	99	172	158	-49	-67
4	358	-223	-147	-34	63	130	225	205	-65	-89
5	447	-278	-184	-43	79	162	281	257	-81	-111
6	381	-240	-159	-39	65	136	237	215	-69	-95
7	308	-195	-130	-33	51	108	190	172	-55	-75
8	200	-128	-86	-22	31	68	121	108	-35	-49
9	107	-67	-46	-12	16	35	63	56	-18	-25
10	5	-3	-3	-1	0	0	2	1	0	-1

Load No.	S.G.22	S.G.23	S.G.24	S.G.25	S.G.26
0	0	0	0	0	0
1	-28	-15	6	9	-12
2	-54	-29	12	17	-26
3	-86	-47	20	29	-45
4	-114	-62	27	38	-60
5	-142	-78	33	47	-76
6	-120	-66	28	41	-66
7	-95	-53	22	33	-54
8	-60	-33	14	21	-35
9	-30	-17	7	11	-18
10	-1	0	0	0	-1

BEAM NO. 4 ULTIMATE TEST

Load No.	P_1	P_2	P_T	D.G.1	D.G.2	D.G.3	D.G.4	D.G.5	S.G.0	S.G.1
0	0.0	0.0	0.0	0	0	0	0	0	0	0
1	11.2	11.4	22.7	25	65	74	-3	-1	18	584
2	19.2	19.2	38.4	138	119	132	-5	-1	105	818
3	21.4	21.3	42.7	141	139	154	-5	-1	186	911
4	23.9	23.9	47.8	145	161	176	-5	-1	239	1016
5	27.3	27.2	54.5	146	204	216	-5	-1	338	1172
6	29.8	29.8	59.7	146	243	252	0	0	441	1392
7	31.3	31.2	62.5	146	268	273	0	0	468	1476
8	32.6	32.8	65.4	146	292	294	2	0	473	1608
9	35.1	35.1	70.2	142	342	337	8	0	678	2123
10	37.1	36.7	73.8	137	397	383	14	19	795	3343
11	39.7	39.7	79.5	128	494	460	31	26	687	6553
12	40.9	41.7	82.6	110	633	557	62	32	770	9103
13	45.2	46.0	91.1							

Load No.	S.G.2	S.G.3	S.G.4	S.G.5	S.G.6	S.G.7	S.G.8	S.G.9	S.G.10	S.G.11
0	0	0	0	0	0	0	0	0	0	0
1	500	345	225	131	36	-39	89	191	293	423
2	1045	725	450	230	23	-62	183	416	636	1083
3	1275	910	549	258	-9	-71	228	530	810	1443
4	1558	1093	653	292	-27	-82	269	637	976	1778
5	2073	1398	833	346	-63	-150	342	861	1349	2656
6	2303	1621	972	391	-80	-225	431	1060	1674	3216
7	2413	1748	1053	419	-89	-290	492	1177	1844	3516
8	2483	1848	1134	452	-94	-305	550	1276	1276	1947
9	2653	2015	1314	524	-116	-341	673	1495	2134	2134
10	3313	2715	1504	605	-154	-392	794	1711	2274	5926
11	6063	2845	1837	746	-266	-569	984	2230	4064	9876
12	12033	12165	2380	938	-518	-866	1193	3277	9024	14376
13										

Load No.	S.G.12	S.G.13	S.G.14	S.G.15	S.G.16	S.G.17	S.G.18	S.G.19	S.G.20	S.G.21
0	0	0	0	0	0	0	0	0	0	0
1	451	-281	-185	-44	80	165	282	258	-82	-111
2	1422	-668	-464	-163	100	283	527	433	-131	-203
3	1917	-877	-620	-242	88	318	621	484	-144	-235
4	2515	-1089	-776	-321	79	361	723	541	-154	-261
5	3695	-1457	-1038	-477	33	422	875	615	-160	-271
6	4525	-1773	-1230	-614	-25	465	982	669	-165	-282
7	4925	-1957	-1322	-688	-63	487	1027	696	-169	-297
8	5285	-2106	-1396	-762	-93	510	1067	730	-177	-319
9	7495	-2396	-1541	-876	-168	545	1098	777	-177	-358
10	11405	-2686	-2037	-990	-246	568	1113	812	-179	-374
11	15295	-3336	-2597	-1109	-434	593	1097	863	-175	-351
12	19915	-2956	-2957	-1570	-699	600	1049	889	-178	-271
13										

Load No.	S.G.22	S.G.23	S.G.24	S.G.25	S.G.26
0	0	0	0	0	0
1	-144	-78	33	47	-77
2	-292	-127	55	85	-134
3	-326	-144	59	86	-128
4	-364	-155	61	90	-103
5	-494	-158	63	80	-8
6	-658	-159	67	72	11
7	-693	-162	72	75	47
8	-737	-170	78	82	82
9	-802	-176	72	94	365
10	-835	-180	47	123	1109
11	-708	-247	11	323	-
12	-221	-242	-56	4	-
13					

BEAM NO. 5 ELASTIC TEST

Load No.	P_1	P_2	P_T	D.G.1	D.G.2	D.G.3	D.G.4	D.G.5	S.G.0	S.G.1
0	0	0	0	0	0	0	0	0	0	0
1	1.148	1.098	2.246	10	15	16	0	0	-9	7
2	1.923	1.848	3.771	15	23	25	0	0	-14	12
3	2.991	2.946	5.937	24	36	41	0	0	-23	18
4	4.086	4.017	8.103	32	49	55	0	0	-29	25
5	5.154	5.061	10.215	40	61	68	0	1	-35	31
6	4.593	4.499	9.092	35	53	60	0	1	-32	28
7	3.525	3.454	6.980	26	40	44	0	1	-27	20
8	2.430	2.330	4.760	17	26	28	0	0	-19	12
9	1.629	1.526	3.155	11	16	18	0	0	-12	7
10	.427	.348	.775	1	1	1	0	0	-2	0

Load No.	S.G.2	S.G.3	S.G.4	S.G.5	S.G.6	S.G.7	S.G.8	S.G.9	S.G.10	S.G.11
0	0	0	0	0	0	0	0	0	0	0
1	19	45	39	-4	59	63	-13	-9	7	14
2	31	73	65	-6	96	104	-21	-13	10	23
3	50	117	104	-10	153	166	-35	-21	16	36
4	68	157	139	-14	204	222	-46	-27	21	46
5	85	196	172	-18	253	274	-56	-32	28	58
6	73	169	150	-15	222	241	-51	-30	22	50
7	53	125	112	-9	167	183	-42	-26	16	37
8	35	82	76	-4	112	124	-30	-19	8	25
9	20	47	44	-2	67	75	-19	-14	5	15
10	0	0	1	0	2	3	-2	-2	0	0

Load No.	S.G.12	S.G.13	S.G.14	S.G.15	S.G.16	S.G.17	S.G.18	S.G.19	S.G.20	S.G.21
0	0	0	0	0	0	0	0	0	0	0
1	18	-4	29	43	3	-5	-11	-23	-22	0
2	29	-5	47	68	5	-9	-18	-37	-35	0
3	47	-7	76	109	11	-12	-28	-57	-59	0
4	62	-9	103	145	14	-17	-38	-76	-73	0
5	79	-11	129	181	16	-21	-47	-95	-94	-3
6	67	-10	111	157	17	-18	-42	-82	-80	0
7	49	-8	83	118	17	-12	-30	-59	-64	-2
8	31	-7	54	78	14	-8	-20	-39	-41	-2
9	18	-4	32	47	10	-3	-12	-23	-19	-2
10	1	0	1	1	1	0	3	0	1	0

Load No.	S.G.22	S.G.23	S.G.24	S.G.25	S.G.26	S.G.27	S.G.28	S.G.29	S.G.30	S.G.31
0	0	0	0	0	0	0	0	0	0	0
1	-29	-24	84	67	7	48	28	35	27	16
2	-44	-40	140	110	16	81	48	60	44	24
3	-75	-66	222	175	25	127	75	95	71	39
4	-98	-87	298	235	36	172	103	129	95	50
5	-122	-108	370	290	44	212	127	159	119	64
6	-107	-96	323	254	39	184	111	140	102	54
7	-85	-76	243	191	28	136	82	101	77	40
8	-57	-53	162	127	20	92	56	68	49	25
9	-35	-33	96	75	10	53	32	39	29	15
10	-2	-2	1	1	1	0	1	1	0	1

Load No.	S.G.32	S.G.33	S.G.34	S.G.35	S.G.36	S.G.37
0	0	0	0	0	0	0
1	-14	-11	0	0	5	-4
2	-22	-18	-1	0	6	-8
3	-35	-30	-2	-2	8	-15
4	-47	-40	-2	-3	10	-21
5	-59	-51	-3	-5	12	-27
6	-52	-43	-2	-5	10	-24
7	-39	-31	-1	-3	8	-18
8	-26	-18	1	-2	6	-12
9	-16	-10	1	-1	4	-6
10	-2	4	3	0	3	1

BEAM NO. 5 ULTIMATE TEST

Load No.	P_1	P_2	P_T	D.G.1	D.G.2	D.G.3	D.G.4	D.G.5	S.G.0	S.G.1
0	0	0	0	0	0	0	0	0	0	0
1	5.448	5.356	10.804	44	66	74	1	1	-37	35
2	13.353	13.202	26.555	108	168	189	2	2	-108	108
3	19.896	19.682	39.578	160	255	285	4	4	-165	173
4	26.358	26.055	52.413	224	363	403	32	55	-253	224
5	31.780	31.518	63.298	274	467	516	53	73	-381	305
6	34.957	34.357	69.314	298	520	570	64	84	-428	364
7	38.242	37.651	75.893	329	623	671	81	98	-591	526
8	41.580	41.292	82.872	369	817	844	108	114	-950	966
9	43.236	42.605	85.841	395	934	944	126	124	-1096	1190
10	43.583	43.515	87.098	425	1145	1123	151	133	-1341	1418

Load No.	S.G.2	S.G.3	S.G.4	S.G.5	S.G.6	S.G.7	S.G.8	S.G.9	S.G.10	S.G.11
0	0	0	0	0	0	0	0	0	0	0
1	93	210	185	-20	272	295	-62	-35	27	62
2	314	535	600	49	852	1379	-255	-175	16	140
3	518	751	935	172	1558	2570	-450	-321	-13	206
4	748	899	1298	318	2480	3580	-738	-543	-84	276
5	1049	1018	1866	630	4080	5430	-1124	-867	-227	346
6	1180	998	2020	720	4290	5800	-1324	-1037	-313	392
7	1528	1360	3110	1015	5470	10030	-1835	-1418	-447	666
8	2940	4810	11060	2720	14610	17190	-2460	-1743	-158	1069
9	4290	6160	14150	3340	16730	18890	-2460	-1548	230	1159
10	7380	8060	18300	4090	-	-	-2940	-1640	420	1570

Load No.	S.G.12	S.G.13	S.G.14	S.G.15	S.G.16	S.G.17	S.G.18	S.G.19	S.G.20	S.G.21
0	0	0	0	0	0	0	0	0	0	0
1	85	-11	138	192	19	-23	-52	-104	-106	0
2	186	-37	349	511	103	-28	-124	-294	-281	9
3	260	-69	523	775	181	-36	-198	-476	-467	12
4	323	-111	720	1581	260	-94	-343	-722	-799	-18
5	365	-169	936	1060	393	-103	-532	-799	-1133	-199
6	382	-201	1071	2380	458	-114	-660	-730	-1255	-321
7	632	-216	2340	3870	682	-188	-1074	-582	-1600	-459
8	1504	296	6890	9800	1026	-435	-1870	-1335	-4770	-1466
9	2010	742	10130	11720	1548	-543	-2250	-2320	-7030	-2470
10	3180	890	13020	16230	2220	-770	-5450	-4710	-12530	-4210

Load No.	S.G.22	S.G.23	S.G.24	S.G.25	S.G.26	S.G.27	S.G.28	S.G.29	S.G.30	S.G.31
0	0	0	0	0	0	0	0	0	0	0
1	-133	-119	396	311	49	228	137	173	128	65
2	-402	-382	2550	1099	209	723	409	528	346	140
3	-672	-646	4060	1736	430	1180	597	857	533	189
4	-1090	-1058	1531	2560	822	1776	785	1288	743	215
5	-1542	-1458	1244	3790	1127	2450	877	1959	999	179
6	-1775	-1626	1108	5200	1252	3070	1015	2330	1160	131
7	-2660	-2120	697	8930	2900	7140	1611	2970	1476	-30
8	-3890	-3840	0	14090	3460	13090	4140	8190	2090	-237
9	-4580	-4740	-545	16780	3710	14560	4810	9060	2740	-511
10	-13530	-9830	>20000	-	4450	19010	6590	13900	3860	-760

Load No.	S.G.32	S.G.33	S.G.34	S.G.35	S.G.36	S.G.37
0	0	0	0	0	0	0
1	-61	-56	-3	-5	12	-28
2	-153	-142	5	1	27	-90
3	-230	-209	16	14	44	-143
4	-295	-257	31	33	67	-185
5	-326	-283	71	78	62	-256
6	-345	-296	108	102	62	-297
7	-340	-283	88	110	39	-373
8	-312	-242	62	116	-17	-470
9	-303	-238	57	141	-129	-533
10	-290	-233	20	223	-[illegible]	-[illegible]

BEAM NO. 6 ELASTIC TEST

Load No.	P_1	P_2	P_T	D.G.1	D.G.2	D.G.3	D.G.4	D.G.5	S.G.0	S.G.1
0	0	0	0	0	0	0	0	0	0	0
1	.694	.589	1.283	2	5	6	0	0	-2	-4
2	1.201	1.178	2.379	5	9	12	1	-1	-3	-6
3	1.601	1.580	3.181	6	12	16	1	-1	-4	-8
4	1.922	2.303	4.225	9	17	23	1	-1	-5	-11
5	2.695	2.651	5.346	11	20	27	1	-1	-7	-13
6	2.535	2.517	5.052	10	18	25	1	-1	-6	-13
7	1.868	1.848	3.716	8	14	19	1	-1	-4	-10
8	1.468	1.392	2.860	6	11	15	0	0	-3	-8
9	1.041	.884	1.925	4	8	10	0	0	-3	-7
10	0	0	0	0	0	1	0	0	1	-1

Load No.	S.G.2	S.G.3	S.G.4	S.G.5	S.G.6	S.G.7	S.G.8	S.G.9	S.G.10	S.G.11
0	0	0	0	0	0	0	0	0	0	0
1	-7	-13	-11	2	-13	-12	35	30	5	25
2	-13	-22	-20	3	-22	-23	65	50	12	48
3	-18	-30	-27	4	-31	-32	89	79	16	65
4	-26	-44	-39	5	-43	-46	128	114	23	94
5	-32	-53	-47	6	-53	-55	155	136	26	111
6	-29	-49	-44	6	-49	-51	145	128	--	104
7	-23	-39	-33	4	-38	-39	111	97	18	78
8	-18	-31	-26	4	-30	-30	87	77	15	61
9	-13	-23	-18	3	-21	-21	59	51	9	40
10	-1	-1	-1	0	-1	-1	6	4	1	1

Load No.	S.G.12	S.G.13	S.G.14	S.G.15	S.G.16	S.G.17	S.G.18	S.G.19	S.G.20	S.G.21
0	0	0	0	0	0	0	0	0	0	0
1	15	17	11	2	-2	5	11	21	18	-4
2	29	33	21	7	-3	12	21	44	37	-7
3	37	45	29	10	-4	16	29	59	48	-10
4	52	65	42	16	-3	25	43	86	75	-14
5	60	77	49	20	-5	29	52	100	87	-17
6	57	71	46	18	-7	28	48	93	83	-13
7	43	53	34	12	-11	21	36	68	62	-10
8	36	42	27	9	-10	17	28	52	49	-6
9	26	27	18	5	-6	11	18	32	31	-3
10	6	1	0	-4	-80	2	1	1	3	2

Load No.	S.G.22	S.G.23	S.G.24	S.G.25	S.G.26	S.G.27	S.G.28	S.G.29	S.G.30	S.G.31
0	0	0	0	0	0	0	0	0	0	0
1	27	37	-12	-7	2	-2	-5	3	12	18
2	54	70	-21	-13	5	-4	-8	10	21	33
3	72	96	-29	-18	5	-5	-12	12	29	45
4	105	140	-42	-25	9	-8	-17	19	41	65
5	129	164	-51	-31	8	-11	-21	21	49	77
6	129	153	-47	-29	9	-9	-19	21	45	71
7	102	116	-37	-22	7	-7	-16	14	34	54
8	83	91	-27	-17	6	-5	-12	12	26	41
9	60	60	-17	-11	4	-4	-9	5	17	27
10	19	4	1	-1	1	0	0	0	0	0

Load No.	S.G.32	S.G.33	S.G.34	S.G.35	S.G.36	S.G.37
0	0	0	0	0	0	0
1	-2	-6	-1	0	2	-1
2	-3	-9	-1	-1	3	-3
3	-4	-14	-2	-1	5	-3
4	-6	-20	-3	-3	6	-6
5	-8	-24	-4	-2	7	-7
6	-7	-22	-4	-3	7	-7
7	-5	-17	-3	-1	5	-5
8	-4	-13	-2	-2	4	-4
9	-2	-9	-2	0	3	-2
10	0	-1	-1	0	1	0

BEAM NO. 6 ULTIMATE TEST

Load No.	P_1	P_2	P_T	D.G.1	D.G.2	D.G.3	D.G.4	D.G.5
0	0	0	0	0	0	0	0	0
1	2.484	2.490	4.974	11	19	25	1	-1
2	7.825	7.793	15.617	33	64	83	3	-3
3	13.086	13.068	26.154	55	111	141	4	-4
4	18.347	18.290	36.636	80	164	205	19	-6
5	20.910	20.968	41.878	92	191	238	25	-7
6	23.314	23.351	46.665	105	223	281	30	-30
7	25.824	25.814	51.639	115	258	321	40	-20
8	30.764	30.822	61.587	132	356	419	67	2
9	33.409	33.286	66.694	142	422	487	84	17
10	35.465	35.696	71.160	150	506	568	112	29
11	36.373	37.517	73.889	151	636	673	162	38
12			(77.028)	1	393	973	-8	-144

Load No.	S.G.0	S.G.1	S.G.2	S.G.3	S.G.4	S.G.5	S.G.6	S.G.7	S.G.8	S.G.9
0	0	0	0	0	0	0	0	0	0	0
1	-8	-13	-31	-48	-42	5	-48	-53	141	125
2	32	23	-82	-170	-159	7	-205	-235	927	815
3	88	36	-144	-329	-296	23	-390	-456	1692	1882
4	205	30	-249	-540	-494	33	-648	-764	2630	2820
5	150	40	-290	-630	-590	40	-770	-910	3170	3320
6	170	50	-360	-730	-710	30	-920	-1090	3740	3740
7	202	81	-436	-853	-897	-24	-1169	-1384	4650	4330
8	553	148	-796	-1037	-1461	-299	-1938	-2360	9060	5070
9	545	162	-872	-1029	-1619	-408	-2240	-3090	12210	7300
10	531	171	-976	-905	-1770	-554	-2860	-4480	14420	10840
11	840	86	-2140	-376	-2350	-1078	-5710	-10260	18840	15070

Load No.	S.G.10	S.G.11	S.G.12	S.G.13	S.G.14	S.G.15	S.G.16	S.G.17	S.G.18	S.G.19
0	0	0	0	0	0	0	0	0	0	0
1	26	103	59	73	47	21	17	28	47	95
2	170	613	261	316	175	26	-101	96	222	419
3	351	1102	449	624	309	34	-166	186	459	707
4	555	1641	647	951	452	38	-241	274	755	799
5	650	1950	720	1130	530	40	-260	340	910	840
6	730	2430	760	1320	620	20	-310	390	1070	900
7	844	3088	816	1509	719	-16	-408	459	1284	1221
8	924	3540	800	1859	1024	-118	-645	682	1963	3010
9	1117	5530	874	2250	1214	-204	-783	832	2780	4390
10	3060	10750	1560	3450	1433	-303	-943	1031	4070	6170
11	4380	15740	3910	6640	1665	-449	-1165	1306	6220	8450

Load No.	S.G.20	S.G.21	S.G.22	S.G.23	S.G.24	S.G.25	S.G.26	S.G.27	S.G.28	S.G.29
0	0	0	0	0	0	0	0	0	0	0
1	83	-14	114	151	-49	-31	9	-9	-19	20
2	563	300	960	1695	-292	-190	7	-105	-100	32
3	1094	645	1544	3370	-565	-375	2	-216	-190	39
4	1471	854	2490	4230	-920	-625	-13	-374	-307	23
5	1590	870	2930	4540	-1120	-760	-20	-460	-370	10
6	1750	930	3630	4920	-1360	-940	-40	-580	-450	-20
7	2440	1186	4870	6010	-1720	-1223	-82	-789	-571	-89
8	7130	1978	7610	10410	-2788	-2100	-293	-1527	-917	-438
9	9630	2080	9520	12910	-3310	-2600	-406	-1919	-1136	-639
10	12500	2190	12030	16310	-4130	-3040	-469	-2168	-1293	-807
11	16810	2520	16430	-	-6180	-3670	-392	-2150	-1188	-897

Load No.	S.G.30	S.G.31	S.G.32	S.G.33	S.G.34	S.G.35	S.G.36	S.G.37
0	0	0	0	0	0	0	0	0
1	46	70	-7	-21	3	-3	7	-8
2	147	263	-20	-64	17	12	20	-40
3	246	461	-34	-107	37	28	35	-74
4	350	683	-43	-138	56	50	47	-99
5	400	800	-43	-150	80	72	58	-120
6	450	930	-43	-150	100	92	58	-140
7	497	1984	-42	-137	137	122	40	-171
8	585	1484	-48	-145	128	130	39	-194
9	655	1644	-54	-144	127	143	42	-214
10	857	1619	-54	-136	126	157	32	-242
11	1510	1687	-11	-65	132	178	60	-282